DEVELOPMENT OF LARGE PORE ZEOLITE FROM KAOLINITE CLAYS

BY

AJAYI, OLUSEGUN AYOOLA

MSc. (CHEM. ENGR) 1995

August, 2012

DEVELOPMENT OF LARGE PORE ZEOLITE FROM KAOLINITE CLAYS

BY

AJAYI, OLUSEGUN AYOOLA

MSC (CHEM. ENGR) 1995

Ph.D/ENG./9033/2009-2010

A thesis submitted to the School of Post Graduate Studies, Ahmadu Bello University, Zaria

In partial fulfillment of the requirements for the Award of Doctor of Philosophy in Chemical Engineering, Faculty of Engineering, Ahmadu Bello University, Zaria. Kaduna State, Nigeria.

August, 2012

DECLARATION

I, Ajayi Olusegun Ayoola declare that the work in this thesis title "Development of large pore zeolite from Kaolinite clays" has been performed by me in the Department of Chemical Engineering under the supervision Professor S.S. Adefila, Dr. B.O Aderemi, Prof A.S Ahmed and Prof. M.T. Ityokumbul. The information derived from the literature has been duly acknowledged in the text and a list of references provided. No part of this work has been presented for another degree or diploma at any institution.

Name of student	Signature	Date

CERTIFICATION

This project dissertation titled "Development of large pore zeolite from kaolinite clays" meets the regulations governing the award of the degree of Doctor of Philosophy of the Ahmadu Bello University, and is approved for its contribution to knowledge and literacy presentation.

Chairman, Supervisory Committee Prof. S.S.Adefila	17th October, 2012 Date
Member, Supervisory Committee Dr.B.O.Aderemi	Date
Member, Supervisory Committee Prof. A.S.Ahmed	Date
Member, Supervisory Committee Prof.M.T.Ityokumbul	Nov. 1. 2012 Date
Head of Department Dr.I.A.Muhammed-Dabo	Date
Dean, Postgraduate School Prof. J. Adebayo	Date

ACKNOWLEDGEMENTS

My sincere and heartfelt thanks go to my creator the giver of life and everything, Jehovah God. I acknowledged Him in all my ways but most especially in this quest for synthesis of zeolite from clay. I now know-Jah- what it takes you to get perfect humans - Adam and Eve - from clay. I shall forever appreciate what you have done.

My supervisory teams were the best in the world. I am opportune to work with Prof. S. S. Adefila, Dr. B. O. Aderemi, Prof. A. S. Ahmed, Prof. M. T. Ityokumbul and tangentially with Dr. El-Yaqub Baba. These are not ordinary people in my life, they were mentors, that are sent by God to give my direction, not only in zeolite synthesis but also in my personal life. I thank Prof. S. S. Adefila for financial support rendered from his personal pocket for analyses across the globe. Your assistance is unquantifiable. Dr. B.O. Aderemi, thank you for your academic and zeolitic criticism. I must confess, they are very annoying sometimes but at the end they serve as motivator for knowledge upbuilding. Prof. A. S. Ahmed, my clay "guru", thank you for all your precise and well co-ordinated argument. My Penn state uncle - Prof. Ityokumbul - I say 'msughur' for all your sleepiness night and academic navigation of this thesis. Not to mention, the assess you gave me to international journal and for facilitating some XRD, XRF and SEM analyses, done at Penn State University, USA. To Dr. Baba, I say a big 'sukran' for the assistances rendered in literature and some analyses.

My family had been a strong pillar to me over these years. My wife and children always understood my not being around, even sometimes when I have to sleep in the laboratory. I say thank you for your support and consideration. My triple 'As'' Anu, Ayo and Ade are wonderfully made from clay and I always tell them, that daddy needs to understand how God used clay to make then this nice, as reasons for my sleeping in the laboratory.

The entire families of Ajayi's and Arowosegbe's have been very supportive. God will surely bless them all. It's with heavy heart that I mentioned my father's name- Chief S. A. Ajayi who was not granted longer life to see the conclusion of my doctorate degree program. This was what he longed for and chewed in his mouth continuously. My mother - Mrs. A. A Ajayi -, my brothers (Bode, Wale, Layi and Biodun) and sisters (Shade, Bukky and Lola) along with their families, I extends my appreciation for your silence prayer and contributions. Mike and Peter Arowosegbe, I say a big thanks to you guys.

Dr. A. S. Olawale, a friend, brother, uncle and mentor. Thank you for your sincere concern and I love the way you catalyze my mind. May almighty Allah bless you for your kind heart.

My colleagues and most especially my co-night crawler, Dr. A. Y Atta, Engr. M. S. Olakunle (lakunsmama) and my numerous members of research students, it been very encouraging the ways you assisted, guided and talked to me, especially whenever am about to cave in. My students and host of other Christians brothers and sister - the whole of Jehovah's Witness in Zaria are highly acknowledged. The University Board of Research for the award of ₦250,000.

My acknowldegemnet will never be complete without mentioning the staff of Ashaka Cement under the command of Mr. Okpara, my people in Sokoto Cement, SHETSCO (Kenneth-main man), NAGRL (Cyril, Nura and Oga Abu), Mr. Chagga (NMDC, Jos), Sunday and Ja'oji (CERT), Gbenga (WITS, South Africa), EMDI, Akure (Racheal and others). You guys were great and nice to me anytime I come around for my numerous analyses with so many samples. I highly appreciate the contributions and assistance of Dr. Ogunleye - CERT, Zaria, its only Jah that can pay you back. Host of others forgotten, I pray God remembers you for good.

With all mentioned here, I would be nothing. It is only Jehovah that can reward you all. Thank you all.

ABSTRACT

This thesis is focused on the synthesis of faujasite type NaY zeolite from both Kankara and Elefun kaolinite clays. The raw kaolins were subjected to various treatments, for the purpose of upgrading them and making them useable as an active monomer for zeolite synthesis. The kaolins were beneficiated using wet method, calcined at various temperatures namely; 600,700,750, 800, 850, 900 and 950 degree Celsius. The silica and alumina in kaolin sourced from Elefun was observed to attain it optimal activated state at 850^0C, while that of Kankara was at 900^0C. Sulfuric acid was used to alter the silica-alumina ratio of the optimally calcined metakaolin. A novel approach to dealumination, independent of external source of heating was developed and employed in this work. Furthermore, the synthesis process took place without using any structure directing agent, while parameters such as ageing, seeding, alkalinity (NaOH and pH), dyeing (blanking) were investigated and a reproducibility corrective investigation was done. The transformation stages involved in this work were monitored using X-Ray Flourescence (XRF), X-Ray Diffractograph (XRD), Braunner-Emmett-Teller for surface area analysis (BET), Scanning Electron Microscopy (SEM) and partially Fourier Trace Infrared (FTIR). Faujasite type Y zeolite was synthesized from shelf soluble salts for control reason. Zeolite Y was synthesis from red Kankara kaolin sample aged for 9 days having about 40% NaX and 15% NaY aside other phases and an unnamed zeolite. Post-synthesis aging of this product, for 95 days, established an insitu seeding and formation of more stable phase ZSM3, in company of prominent persistent peak attributed to quartz. Irrespective of the type of kaolin (Kankara or Elefun) 9 days of gel aging was observed to be sufficient for appearance of peak attributeable to zeolite Y. The SEM for the resulting products from aging process indicated increase in crystallinity with aging period, with presence of other highly siliceous phase. Introduction of dye into the gel was observed to suppress nucleation of inherent impurities as well as enhance rate of amorphosity, but with attendant indications that the same dye enveloped

the soluble ingredients from reacting, by increasing their degree of segregation. Both Elefun and Kankara were observed to give zeolite NaY, though at different dye/metakaolin ratio. The gel from Kankara and Elefun with Na_2O/SiO_2 ratio of 7 and 9, were observed to give NaY zeolite peak. Increase in the alkalinity (NaOH and/or pH) gave increased crystallinity though not favourably disposed to the synthesis of zeolite Y. Elefun gel seeded with 1, 1.5, 2.0 and 2.5wt% commercial zeolite Y, were noticed to give zeolite Y with increased crystallinity. NaY zeolite peak were noticed for samples from Kankara seeded with 1.5 and 2.5wt%, respectively. The appearances of highly siliceous zeolite phases along with NaY were blamed either on the inability of NaOH to depolymerise the silica, high level of sulfate salts in the gel and/or low level of reconstitution reaction between the already dissociated silica and alumina. The improvement studies conducted proved successful as highly crystalline NaY zeolite were characterized using XRD analysis. Zeolites belonging to the SSZ, ITQ, ZSM families, were synthesized without the use of templating agent, which gives an insight also of the useability of Nigerian kaolin in an environmental friendly synthetic route.

Keywords: Kankara, Elefun, XRD, XRF, SEM, crystal violet, dealumination, nucleation

TABLE OF CONTENTS

TITLE PAGE ..... **Error! Bookmark not defined.**

DECLARATION iii

CERTIFICATION iv

ACKNOWLEDGEMENTS v

ABSTRACT vii

TABLE OF CONTENTS ix

LIST OF FIGURES xvi

LIST OF FIGURES xxii

LIST OF APPENDICES xxiii

ABBREVIATION, DEFINITIONS, GLOSSARY AND SYMBOLS xxiv

CHAPTER ONE 27

1.0 INTRODUCTION 27

1.1 PROBLEM STATEMENT 30

1.2 AIMS AND OBJECTIVES 31

1.3 JUSTIFICATION 31

1.4 SCOPE 32

1.5 RESEARCH LIMITATIONS 33

CHAPTER TWO 34

2.0 INTRODUCTION 34

2.1 Definition of Clay 34

2.2 Classification of Clay 34

2.3 Kaolin and Kaolinite Clay 35

2.3.1 Structure of kaolinite 37

2.3.2 Formation of kaolinite clay 38

2.3.3 Processing of kaolinite clay 41

2.4 Structure of metakaolin 47

2.4.1 Effect of acidification and alkalination on kaolin and metakaolin 50

2.5. Zeolite, Types, Classifications and Properties 51

2.5.1 Definition 51

2.5.2 Types of zeolitic materials 52

2.5.3 Features of zeolitic materials 53

2.5.4 Catalytic properties of zeolites 56

2.5.5 Structure of zeolites 59

2.5.6 Building zeolites 62

2.5.7 Faujasite type zeolite Y 68

2.6 Applications of zeolites 71

2.7 Synthesis of Zeolites 73

2.7.1 Synthesis of zeolitic material in nature 73

2.7.2 Laboratory synthesis of zeolites 76

2.7.3. Hydrothermal synthesis of zeolites 77

2.7.4 Mechanism of zeolite crystallization 81

2.7.5 Conditions necessary for zeolite crystallization 97

2.7.6 Factors influencing type of zeolites synthesized. 102

2.8 Mechanism of Nucleation and Crystal Growth 138

2.9 Synthesis of Zeolites from Soluble Salts, Clay and other sources. 156

2.9.1 Synthesis of zeolites from soluble salts 156

2.9.2 Synthesis of zeolites from clay and waste materials 156

2.9.3 Application of dyes in zeolite synthesis 157

2.9.4 Characterization of zeolite 162

CHAPTER THREE 170

3.0 INSTRUMENTATION, EQUIPMENT AND METHODOLOGY 170

3.1 Instrumentation and Equipment 170

3.1.1 Clay beneficiation 170

3.1.2 Calcination 170

3.1.3 Dealumination 170

3.1.4 Gel formation 171

3.1.5 Zeolite synthesis 171

3.1.6 Characterization 172

3.2 Methodology 172

3.2.1 Transformation stages of kaolinite clay into Zeolite Y 174

a) Synthesis of zeolite Y from soluble salts 177

b) Synthesis of zeolite Y from pretreated kaolin 178

3.2.2 Characterization technique 182

CHAPTER FOUR 185

4.0 RESULTS AND DISCUSSION 185

4.1 As Mined (Raw) Clay 185

4.1.1 XRF Analysis 185

4.1.2 FTIR Analysis 187

4.1.3 XRD Analysis 188

4.1.4 SEM and BET 188

4.2 Clay Beneficiation 190

4.2.1 XRFAnalysis 190

4.2.2 XRD Analysis 191

4.2.3 SEM and BET 191

4.3 Calcination of Kaolin 193

4.3.1 XRD Analysis 194

4.3.2 XRF Analysis 196

4.3.3 BET and SEM 197

4.4 Dealumination of Metakaolin 200

4.4.1 XRD Analysis 200

4.4.2 XRF Analysis 202

4.4.3 BET and SEM 205

4.4 (a) Novel approach to metakaolin dealumination 206

4.4 (b) Effect of acid quality on rate of metakaolin dealumination 208

4.4 (c) Effect of calcination temperature on rate of metakaolin dealumination 210

4.4(d) Effect of sulphate salts level on extent of dealumination 213

4.5 Gel formation 214

4.5.1 XRD Analysis 214

4.5.2 XRF Analysis 215

4.5.3 BET and SEM 216

4.6. Commercial zeolite 217

4.6.1 XRD Analysis 217

4.6.2 SEM and BET 218

4.7. Zeolite Synthesis-Crystallization Reaction 218

4.7.1 Synthesis of zeolite Y from soluble salts 218

4.7.2 SEM and BET 219

4.8. Synthesis of zeolite Y from pretreated kaolin 220

4.8.1 aging effect 220

4.8.2 blanking agent (dyeing) effect 228

4.8.3 alkali concentration effect 232

4.8.4 pH effect 236

4.8.5 seeding effect 237

4.8.6 crystallization time and temperature 240

4.8.7 process improvement 240

CHAPTER FIVE 245

CONCLUSION AND RECOMMENDATION 245

5.1 CONCLUSION 245

5.2 RECOMMENDATIONS 246

CHAPTER SIX 248

REFERENCES 248

APPENDIX A 270

APPENDIX B 282

APPENDIX C 295

APPENDIX D 302

APPENDIX E 312

APPENDIX F 319

APPENDIX G 322

APPENDIX H 326

LIST OF FIGURES

Figure 2.1. Classification of silicates (adopted from Bailey, 1980 and Rieder *et al.*, 1998) 36

Figure 2.2: Stucture of kaolinite designed by Brindley Nakahra, viewed from the a-axis direction 37

Figure 2.3:Crystallochemical structure of kaolinite 38

Figure 2.4: The change of the tetrahedrical (light) and octahedral (dark) sheets 38

Figure 2.5: Relationship between calcinations temperatures and solubilities of active SiO_2 and Al_2O_3 47

Figure 2.6: Lattice of metakaolinite proposed by Brindley and Nakahira (1957) 48

Figure 2.7: Structure of metakaolin by MacKenzie (1978) 49

Figure 2.8: Representative of some zeolite materials 52

Figure 2.9: Molecular sieve property of type Y zeolite. 54

Figure 2.10: Ion exchange property of zeolitic material. 54

Figure 2.11: Principle of water softening using zeolites. 55

Figure 2.12: Comparison of pore size tolerance of different framework structures. 55

Figure 2.13: The cation sites in the faujasite framework. 56

Figure 2.14: Different types of reaction selectivity imposed by the rigid pore structure of the zeolite. (adopted from Csicseri, 1984.) 58

Figure 2.15: (a) Primary building blocks of zeolites, (b) Simplified surface structure of zeolite 62

Figure 2.16: Perspective view of Y zeolite structure. 64

Figure 2.17: Several representations of the basic building unit of zeolites, the tetrahedron 65

Figure 2.18: Relative sizes of n-rings frequently found in zeolites and related molecular sieves. The scale of the pore aperture is given for the 10-ring to give a sense of scale. 66

Figure 2.19: Two cages frequently found in zeolites. The oxygen and T atoms are depicted in the upper drawings. In the lower half, only the connections between T-atoms are indicated. 66

Figure 2.20: The construction of four different zeolite frameworks with sodalite or h cages. 67

Figure 2.21: The first pictorial depiction of zeolite synthesis "Schematic representation of the formation of zeolite crystal nuclei in a hydrous gel". (Breck, 1974). 68

Figure 2.22: The faujasite framework structure of zeolite Y: the supercage structure (left) and the 12-ring viewed along (111) (right). In the right panel, the larger cycles represent T atoms (Si or Al) linked to each other by shared oxygen atoms (small cycles). 69

Figure 2.23: Silica structure building blocks and materials studied in the MD simulations. 70

Figure 2.24: Formation of zeolite in nature 75

Figure 2.25: Hydrothermal zeolite synthesis. 80

Figure 2.26: Schematic free energy relations between reaction mixtures and various zeolite phases, represented by A, B and C. 83

Figure 2.27: Equilibration of the starting mixture to establish a partly ordered secondary amorphous phase and a characteristic distribution of solution species. (Cundy and Cox, 2005) 86

Figure 2.28: The emergence of order, from the primary amorphous phase (a) through the 87

Figure 2.29: Change of the crystallinity of ZSM-5 materials with synthesis time: (a) X-ray 88

Figure 2.30: Crystallization curves for typical type A and type B syntheses. Redrawn with 89

Figure 2.31: Zeolite crystallization mechanisms: (a) solution mediated process (type A); 91

Figure 2.32: Activation energy requirement for silica stabilization 102

Figure 2.33: Reaction composition diagrams. 107

Figure 2.34: (a)-Effect of alkalinity on the crystallization of zeolite A. (b)- Effect of alkalinity on the particle-size distribution of zeolite A (adopted from Meise and Swochow, 1973) 108

Figure 2.35: Effect of ageing of starting gel on the synthesis of zeolite NaY; wt% of NaY in the solid phase isolated from synthesis gels as a function of heating time for ageing time up to 12 h as determined by powder X-ray diffraction. Adopted from Ginter *et al.,* 1992a 115

Figure 2.36: Effect of pH on the crystallization rate for the synthesis of mordeniete at 300^0C (adopted from Barrer, 1982) 117

Figure 2.37: Correlation between the Si/Al ratio in faujasite-type zeolite and the reaction rate constant k (crystallization temperature of 88^0C). 119

Figure 2.38: Schematic diagram of the structure-making interaction of a sodium cation with water molecules (dotted lines indicate hydrogen bonds) 125

Figure 2.39: Growth rate curves of zeolite NaX at various crystallization temperatures. 131

Figure 2.40: Effect of temperature on the crystallization of MOR. 132

Figure 2.41: Effect of K^+ on the crystallization-field change of zeolite NaX (a) and zeolite NaA (b) at 100^0C. 134

Figure 2.42: Effect of K^+ on the crystallization-field change of zeolite NaY. 135

Figure 2.43: Effect of K^+ on the crystallization-field change of zeolite NaY(100^0C), where SiO_2/Al_2O_3=20-28; H_2O/R_2O=25-40 135

Figure 2.44: Comparative molecular sizes of potassium and sodium. 136

Figure 2.45: The energetics of nucleation, illustrating the concept of a critical nucleus of radius rc; beyond this size, the net energy gain from the resultant (ΔG) of cohesive (ΔGv) and surface (ΔGs) terms is favourable to growth (Mullin, 1993). 139

Figure 2.46: The basic mechanism for the cation-mediated assembly of ordered regions: (a) nomenclature and symbolism; (B) details of in-situ construction process by addition of solution units to a surface site. The same mechanism can be applied to zeolite crystal growth. (Cundy and Cox 2005) 146

Figure 2.47: Proposed reaction scheme for the zeolite growth mechanism in colloidal solution. Adopted from Mintova *et al*., 1999a 152

Figure 2.48: Crystal concentration of zeolite Y after two-stage syntheses. (Li *et al*., 2002). 154

Figure 2.49: Different types of crystal violet 160

Figure 2.50: Mechanism of reaction between potassium salt(s) and crystal violet. 161

Figure 2.51: The XRF Process 163

Figure 4.1: FTIR spectra for the beneficiated Kankara kaolin 187

Figure 4.2: XRD patterns for raw kaolin, (a) Red Kankara (b) Elefun and (c) White Kankara 189

Figure 4.3: A typical SEM showing kaolin morphology for raw sample 190

Figure 4.4: XRD patterns for beneficiated kaolins (a) Red Kankara (b) Elefun (c) White Kankara 192

Figure 4.5: Selected SEM image for beneficiated kaolin 193

Figure 4.6: XRD patterns for metakaolin samples (a) 600^0C (b) 700^0C (c) 800^0C (d) 900^0C 195

Figure 4.7: XRD patterns for metakaolin samples treated at 850^0C (a) Kankara (b) Elefun 197

Figure 4.8: SEM images for metakaolin calcined at (a) 600^0C (b) 700^0C (c) 800^0C (d) 900^0C 199

Figure 4.9: SEM images for metakaolin at 850^0C (a) White Kankara and (b) Elefun 200

Figure 4.10: XRD patterns for dealuminated metakaolinite samples (a) Kankara calcined @ 850^0C (b) Kankara calcined @ 900^0C and (c) Elefun calcined @ 850^0C. 201

Figure 4.11: SEM images of dealuminated samples from kaolin calcined at (a) 700^0C (b) 800^0C (c) 900^0C 205

Figure 4.12: SEM images of dealuminated samples from (a) Kankara and (b) Elefun 206

Figure 4.13: Silica-alumina ratio as a function of sulphuric acid concentrations. 207

Figure 4.14: Comparative silica-alumina ratio for various method of dealumination 207

Figure 4.15: Silica-alumina ratio for different methods of dealumination 209

Figure 4.16: Quantity of alumina extracted for methods of dealumination and type of acid 209

Figure 4.17: Silica-alumina ratio and alumina extracted against calcinations temperature 211

Figure 4.18: Intensity of zeolite Y against calcination temperature 212

Figure 4.19: Metakaolinization temperature and mineral composition effect 212

Figure 4.20: Sulphate salt effect on Si/Al ratio for thermal method (Kankara white) 213

Figure 4.21: Sulphate salt effect on Si/Al ratio for non-thermal method (Kankara white) 213

Figure 4.22: XRD patterns for gels from (a) Kankara and (b) Elefun 215

Figure 4.23: SEM images for gels from (a) Kankara and (b) Elefun 216

Figure 4.24: XRD patterns and SEM for commercial zeolite Y 217

Figure 4.25: XRD pattern and SEM for zeolite synthesized from soluble salts. 218

Figure 4.26: XRD pattern for matrix/composite zeolitic material 221

Figure 4.27: XRD Pattern for Zeolite ZSM3 222

Figure 4.28: XRD patterns for as-synthesized zeolite from Kankara gel aged for 3-11days 224

Figure 4.29: XRD patterns for as-synthesized zeolite from Elefun gel aged for 3-11days 225

Figure 4.30: Scanning Electron Micrographs for (a) zeolite Y and (b) ZSM3 227

Figure 4.31: Scanning Electron Micrographs for zeolite Y from (a) Kankara and (b) Elefun 227

Figure 4.32: XRD patterns for zeolites from Kankara gel with varied dye concentration 229

Figure 4.33:XRD patterns for zeolites from Elefun gel with varied dye concentration 230

Figure 4.34: Scanning Electron Micrograph for zeolite Y (a) Kankara and (b) Elefun 231

Figure 4.35: XRD patterns for zeolite from Kankara with different concentrations of NaOH. 233

Figure 4.36: XRD patterns for zeolite from Elefun with different concentrations of NaOH. 234

Figure 4.37: SEM images for zeolite Y (a) Kankara (NaSi09K) and (b) Elefun (NaSi09E) 236

Figure 4.38: XRD patterns for zeolite from Kankara gel with different amount of seeding agent. 237

Figure 4.39: XRD patterns for zeolite from Elefun gel with different amount of seeding agent. 239

Figure 4.40: SEM images for zeolite formed from (a) Kankara (b) Elefun using seeding material 240

Figure 4.41: XRD patterns for reproduced zeolite from Elefun NaSi09E 241

Figure 4.42 XRD patterns for reproduced zeolite from Kankara dye (Dye/Al_2O_3=0.001) 242

Figure 4.43: XRD patterns for reproduced zeolite from seeded Kankara gel (S03K) 243

Figure 4.44: XRD patterns for reproduced zeolite from seeded Elefun gel (S01E) 243

Figure 4.45: XRD patterns for reproduced zeolite from aged lefun gel (Age9E) 244

LIST OF FIGURES

Table 2.1: Chemical compositions of zeolite X crystallized from K-Na gels 134

Table 2.2: Absorption of Dyes on Zeolites 159

Table 3.1: Decription of the stages involved in zeolite synthesis 173

Table 3.2: Composition of dyes added to the gel 180

Table 4. 1: Compositional analysis for raw and beneficiated Kankara and Elefun kaolinite samples 186

Table 4.2: Compositional analysis for calcinated samples in weight percent 198

Table 4.3a: Chemical composition (in wt%) of the thermally dealuminated samples 202

Table 4.3b: Chemical composition, in weight percentageof the non-thermally dealuminated samples 203

Table 4.3c: Chemical composition (wt %) of the thermally dealuminated samples-use of analytical grade acid 204

Table 4.4: Compositional analysis for dealuminated samples calcined at various temperatures 210

Table 4.5: Compositional analysis for gel from Kankara and Elefun 215

LIST OF APPENDICES

APPENDIX A 270

APPENDIX B 282

APPENDIX C 295

APPENDIX D 302

APPENDIX E 312

APPENDIX F 319

APPENDIX G 322

APPENDIX H 326

ABBREVIATION, DEFINITIONS, GLOSSARY AND SYMBOLS

A – Anatase [TiO_2]

An – Andalusite [$Al_2(SiO_4)OH$]

B – Brookite [TiO_2]

CIT-1- [$Si_{56}O_{112}$]

Cl – Clinochlore

D – Dickite [$Al_2Si_2O_5(OH)_4$]

F – Forsterite [Mg_2SiO_4]

Ge – Goosecreekite [$C_{32}(H_2O)_{101}[Si_{32}A_{14}O_{32}$]

Gi – Gismondine [$Ca_{3.68}(H_2O)_{17.28}$][$Si_{8.8}A_{17.2}O_{32}$]

Go – Gobbinsite [$Na_{26}K_{17}(H_2O)_{1491}$][$Si_{10}A_{16}O_{32}$]

GUS-1 – [$Si_{32}O_{60}$]

H – Halloysite [$Al_2Si_2O_5(OH)_4.2H_2O$]

HAS – Hydrogen Aluminum Silicate [$H_{18,9}Al_{18,9}Si_{173}O_{383}$]

He – Hematite [Fe_2O_3]

He – Heulandite [$K_{8.48}(H_2O)_{181}$][$Si_{26.64}A_{19.36}O_{72}$]

I – Illite [$(K.H_3O)Al_2Si_3A_{10}10(OH)_2$]

K – Kaolin [$Al_2Si_2O_5(OH)_4$]

Ka – Kalsite [$KAlSiO_4$]

K_y – Kyanite [Al_2SiO_5]

La – Laumontite [$Ca_4(H_2O)_{18}$] [$Si_{25.68}Al_{10.32}O_{72}$]

Li – Lithosite [K_{12}][$Al_8Si_{16}O_{52}$]

Ly – Leryne

M – Mica [$KAl_3Si_3O_8$]

Mi – Microcline [$KAl_2Si_3O_8$]

Mo – Mordenite [$Na_2Al_2Si_{13}.3O_3.6+x$]

M_t – Magnetite [Fe_2O_4]

Mu – Muscovite [(K.Na) (Al.Mg.Te)$_2$ (Si_3,$Al_{0,9}$ $O_{10}(OH)_2$]

Ne – Nepheline [$Na_7.11(Al_72Si_88O_{32})$]

NaZ-21 – [$Na_{476.6}(H_2O)_{303.6}$][$Si_{384}Al_{384}O_{1686}$]

Nt – Natrolite [$Na_{16}(H_2O)_{16}$][$Si_{24}Al_{16}O_{80}$]

P – Zeolite Na-P [$Na_{8.92}(H_2O)_{11281}$][$Si_{9.92}Al_{608}O_{32}$]

P_A – Potassium Aluminum Oxide [KAl_5O_8]

Ph – Philipsite [$K_2Ca_{1648}(H_2O)_{121}$[$Si_{107}Al_{53}O_{32}$]

Pl – Potassium Iron Oxide

P_y – Pyrophyllite [$Al_2Si_4O_{10}(OH)_2$]

Q – Quartz [SiO_2]

Q – Alpha Quartz [Si_3O_6]

RUB-10 – [$Si_{35}O_{72}$]

Rub-13 – [$Si_{31}O_{64}$]

RUB-17 – [$K_4Na_{12}(H_2O)_{20.7}$][$Si_{28}Zn_8O_{72}$]

RUB-24 – [$Si_{192}O_{384}$]

S – Smectite

Si – Silhydrite [$Si_3O_5.H_2O$]

SOH – Sodalite Octahydrate [$Na_6(H_2O)_{81}$][$Si_6A_{16}O_{24}$]

St – Stilbite [$Na_{1.76}Ca_4(H_2O)_{29.41}$][$Si_{25.68}Al_{10.32}O_{72}$]

Te – Terranovaite

TNU-9- [$Si_{192}O_{384}$]

Ty – Tridymite – [$Si_{48}O_{96}$]

ZL – Zeolite Linde L [$Na_5K_{4.7}(H_2O)_{20.8}$] [$Si_{27}A_{19}O_{72}$]

L – Lordarite

Am – Amicite – [$Na_{36}K_{376}(H_2O)_{986}$][$Si_8Al_8O_{32}$]

Nt – Natrolite [$Na_{16}(H_2O)_{16}$][$Si_{24}Al_{16}O_{80}$]

Te – Terranovaites

CHAPTER ONE

1.0 INTRODUCTION

Increasing energy demand which calls for processing heavy petroleum feedstock has led to heighten the importance of developing new catalyst systems. Many conventional crude oils from around the world contain 30% residue (which is the fraction of crude oil with boiling point greater than 525^{0}C). As conventional crude oils have become more expensive, interest in processing heavier feeds has increased. These heavier feeds have residue contents of 40% or more, and require further processing in order to find a market. The current motivations for conversion technologies are multifold. The market for heavier fuels is decreasing while that for middle distillate is increasing at a rapid rate. In many parts of the world, light oil production is declining and heavy oil conversion, therefore, becomes increasingly important to maintain economic viability of these regions. Further tightening of environmental regulations has provided incentives to refiners to further reduce sulfur and aromatic levels of the finished products. Additional stringent requirements on the disposal of refinery residues such as coke or residue encourage "minimum-waste" refinery strategies. Zeolites are advantegous materials in meeting these requirements.

Zeolites are commonly, crystalline aluminosilicates with a three dimensional fully crosslinked open framework structures that form uniformly sized pores of molecular dimensions. These crystalline aluminosilicates are made up of corner-sharing SiO_4 and AlO_4 tetrahedra. The pore size of a zeolite plays an important role for adsorbing molecules of different sizes, like a molecular sieve. Therefore, molecules of a certain size are adsorbed by a zeolite and others which are larger than the pore size are not adsorbed. A naturally occurring zeolite called stilbite was discovered by Cronstedt who observed that this mineral started to lose water upon heating, thus the term zeolite (boiling stone) was coined. The replacements of Si^{4+} by Al^{3+} in a framework

of zeolite at many places tend to make the framework carry a net negative charge. However, the negative charge is balanced by a non-framework loosely attached alkali metal cation which sits within the cavities and maintains an overall electroneutrality of the zeolite. These alkali metal cations are capable of ion-exchange with other cations which impart on the potential for reversible reaction with polar molecules. Accordingly, the reaction potentials of zeolites have made them commercially viable for several industrial applications.

The diversification in industrial applications was first realized by R.M. Barrer, in the area of adsorption which triggered the era of synthesized zeolites. The commercially viable synthetic zeolites A, X, and Y were synthesized by R.M. Milton and D.W. Breck in the 1940's and early 1950's. Since then more than 150 types of synthetic zeolites have been synthesized. Many, but not all, find useful industrial applications in the areas of petroleum refining and chemical process industries as selective adsorbents, catalysts and ion-exchangers, thus building an estimated more than two billion dollar industry (Flanigen 2001).

Type Y zeolite, especially, among the Faujasite type zeolites with their large pores (>=8Å), has drawn a lot of attention in the petroleum industry, due to its application in the area of fluidized catalytic cracking (FCC), as about 40% of the gasoline production is obtained through FCC process. Nigeria is richly endowed with huge reserve of oil and gas and kaolin (mineral containing the starting monomers) for zeolites synthesis in varying proportions. The three domestic refineries use imported zeolitic catalysts and other related catalysts, at the cost of US$2000 per ton (Enjugu, 2006), with very short life span in the fluid catalytic cracking unit. The Refineries' annual import of these catalysts is in tune of 500,000 tonnes, at 60% capacity

utilization. The generally used crystal size is in the range of 1-2 micrometer. The pore size of the Y zeolite is sufficient to allow gas oil molecule to enter the pore and react (Scherzer 1989).

The zeolites are normally synthesized through hydrothermal process by reacting silica alumina gels in alkaline solution under mild temperature conditions in the range of $100 - 200^0C$ (Bhatia 1990; Szostak 1998). An expensive structure directing agent (SDA) may or may not be used to get the desired zeolite phase. The solution based synthesis produces wastes at the end of the synthesis process. Also, it takes days to obtain the finished product in a batch process. Many excellent studies have been performed to overcome the challenges of reducing the synthesis time, particle size, and waste production. An effort to change the batch process to a continuous mode is on going. Similarly, in confined space, synthesis from clear solution, microwave heating, parallel processing of batches are some of the examples which are also corrently been investigated (Arafat *et al.,* 1993; Rollmann and Valyocsik 1983; Schmidt *et al.,* 2000; Serrano and Grieken 2001; Valyocsik 1983; Koegler and Yeh 2003; Li *et al*., 2002; Murrell *et al*., 1999; Park *et al*., 2001; Schoeman *et al*., 1994; Slangen *et al*.,1997a).

Major challenges to synthesis of zeolites from synthetic reagents are the requirement for pure and highly reactive starting reagents (silica and alumina) and good passive reactor, to accommodate the expected reaction, without interference. Most of the listed requirements are either difficult or impossible to obtain in developing nations, due to the cost and dearth of analytical grade chemicals.

As mentioned earlier, Nigeria has large and widely distributed reserves of clay (RMRDC,2000), to support the choice of kaolinite clay as a base material for zeolite production. Concurrently this supports government's interest to develop the solid minerals sector (Emofuriefa *et al*., 1992;

Tanko, 1995). Literature presents (Breck, 1974; Barrer 1982; Aderemi, 2000) the production process of zeolite Y to be relatively more sensitive than its family counterparts, through either the use of chemical reagents or mineral ore based monomers. It was further established that, among the family of faujasites, the production of zeolite Y is froth with far greater challenges, such as inhibition resulting by inherent impurities (either from chemical reagents or natural mineral), activity status of the aluminosilicate, difficulty in silica depolymerization, sensitivity of reactors and purity of solvents employed, etc. Subsequently, a decision was taken to focus this work on the production of zeolite Y from mineral ore, in view of its effcetiveness and relative greater ease to production of other zeolites.

Consequently, this work is focused on the development of zeolite Y from kaolinite clay sourced from two different locations in Nigeria, namely: Elefun (Ogun State) and Kankara (Katsina State). The products are to be fully characterized using X-ray flourence (XRF), X-ray diffractograph (XRD), Scanning electron micrograph (SEM) and surface area (BET).

1.1 PROBLEM STATEMENT

The presence of potassium rich mineral phases in some Nigerian kaolinite clay, raw water, sulphuric acid, sodium hydroxide and glassware used in previous attempt to develop zeolite Y was believed to be responsible for unsuccessful synthesis of zeolite Y (Aderemi, 2000). Past attempts to purify the kaolinite clay, water, sodium hydroxide and proper washing of the starting and pretreated materials were not good enough to ensure the successful synthesis of zeolite Y (Ajayi et al, 2011). Conventional method of dealumination desired for partial digestion of alumina and potassium tends to be more favorably disposed towards the digestion of alumina, while some minerals rich in potassium, proved to be stubborn towards the action of the acid

used. Even thorough washing with deionized water after dealumination reaction was unable to achieve the expected reduction of potassium salt(s) formed during the reaction (Ajayi, 2011).

There are contradicting opinions on whether the presence of ferric ion hinders or reduces the rate of nucleation after gel formation. This issue presents an additional challenge to synthesis of zeolite Y.

The attempt to synthesise zeolites from other sources, i.e. lean in potassium and ferric based minerals was not also successful. The structure of silica in the base materials and same resulting from dealumination process was found to be very rigid, hence its depolymerization and/or dissolution was rather difficult, pointing to another factor responsible for unsuccessful synthesis of zeolite Y from natural solid aluminosilicate substrates.

AIMS AND OBJECTIVES

Aim

- To synthesis zeolite Y from soluble salts and selected Nigerian kaolin (i.e. Kankara and Elefun kaolin), while investigating factors (such as seeding, aging, dyeing/masking, concentration of NaOH/pH and crystallization time and temperature) known to affect the types of zeolite synthesized.

Objective

- The objective is to establish optimal conditions for the purpose of synthesizing zeolite Y from Kankara and Elefun kaolinite clay.

1.3 JUSTIFICATION

The following reasons serve as justification for venturing into this work:

- Availability of oil and gases in the Nation

- Harnessing of Nigeria solid mineral deposits for national development
- High demand for zeolite catalyst in processing the available oil and gas in the Nation
- The present FCCU catalysts are imported, with short lifespan and high rate of deactivation.
- Abundant deposits of kaolin in Nigeria- driving factor for national development
- Preserve foreign reserve – when technology is properly developed
- Job creation
- Development of indigenous technology for zeolite synthesis

1.4 SCOPE

The scope is divided into two segments, namely:

To beneficiate and enhance silica and alumina breakdown;

- reduction of potassium, ferric and other ions,oxide or mineral containing such from Kankara and Elefun kaolin, using physical, thermal and chemical method of beneficiation
- enhance depolymerization of silica component during gelation

To develop zeolite Y from Kankara and Elefun kaolinite clay studying the effects of:

- Blanking method with nitrogen based dyes
- Seeding and aging to enhance the rate of the autocatalytic and depolymerization reactions, respectively.
- Depolymerization of silica using pH and concentration of sodium hydroxide
- Crystallization time effect on quality of zeolite Y synthesized
- Use of soluble salts for zeolite Y synthesis (control product).

1.5 RESEARCH LIMITATIONS

- Analytical equipment used in this work were scattered all over the world.
- Difficulty in data handling resulting from different handlers and machine
- Threats of misleading results due to time lag during step-wise analyses

CHAPTER TWO

2.0 INTRODUCTION

2.1 Definition of Clay

The term "clay" is ambiguous and has multiple meaning, depending on the field of interest:

- To a clay mineralogist, a clay mineral is a layer of silicate mineral (also called *Phyllosilicates*) or other mineral, which impart platisticity and hardens upon drying and firing. (Guggenheim *et al.*,1998).
- In practice,"clay" is used to refer to the fine-grained, mineral fraction of earth material, and can include clay silicates as defined in the first bullet, oxide-hydroxide minerals, such as goethite, hematite, manganese oxides and some zeolites.

Since the main thrust of this project is synthesis of zeolite Y from kaolinite clay, it becomes very paramount to have good understanding of its formation, structure and properties of clay.

2.2 Classification of Clay

The classification of clays has not understandably, followed a logical pattern but has depended partly on the use to which the clay is put, partly on general appearance and on geology and location. Two main types of clay, are, however, recognized viz. *residual* and *sedimentary*, according to their geology.

Residual clays are those clays that have not been transported by natural agencies. They are found side-by-side with the altered igneous rocks from which they are formed. They are usually extracted from the parent rock and obtained in comparatively pure state. Example of such clay is

China clay in Cornwall, United Kingdom. On the other hand, the **sedimentary clay**, are those which have been removed from their origin by natural agencies. As a result of this movement, this type of clay is rarely obtained pure, because many impurities (fine-grained in nature) are picked up in transit and are difficult or uneconomical to remove (Worrall, 1986). Kankara and Elefun kaolin are believed to belong to this class, i.e. sedimentary, resulting to its high level of impurities.

Clay minerals are part of a general but important group within the **phyllosilicates** (member of silicates family) that contain large percentages of water trapped between the silicate sheets. Most clays are chemically and structurally analogous to other phyllosilicates but contain various amounts of water and allow more substitution of their cations. There are so many types of clays found in nature, as indicated in Figure 2.1, but out of them only five are important, namely, *kaolinite, montmorillonite*, hydrous mica, *vermiculite* and *allophane*. The first four are crystalline and can be regarded as small sheet-like particles.

2.3 Kaolin and Kaolinite Clay

Kaolin is a soft, lightweight, often chalk-like sedimentary rock that has an earthy odor. Kaolin, commonly referred to as china clay, contains 85–95% of the mineral kaolinite. Beside kaolinite, kaolin usually contains quartz, mica and also, less frequently, feldspar, illite, montmorillonite, ilmenite, anatase, haematite, bauxite, zircon, rutile, kyanite, sillimanite, graphite, attapulgite, and halloysite.

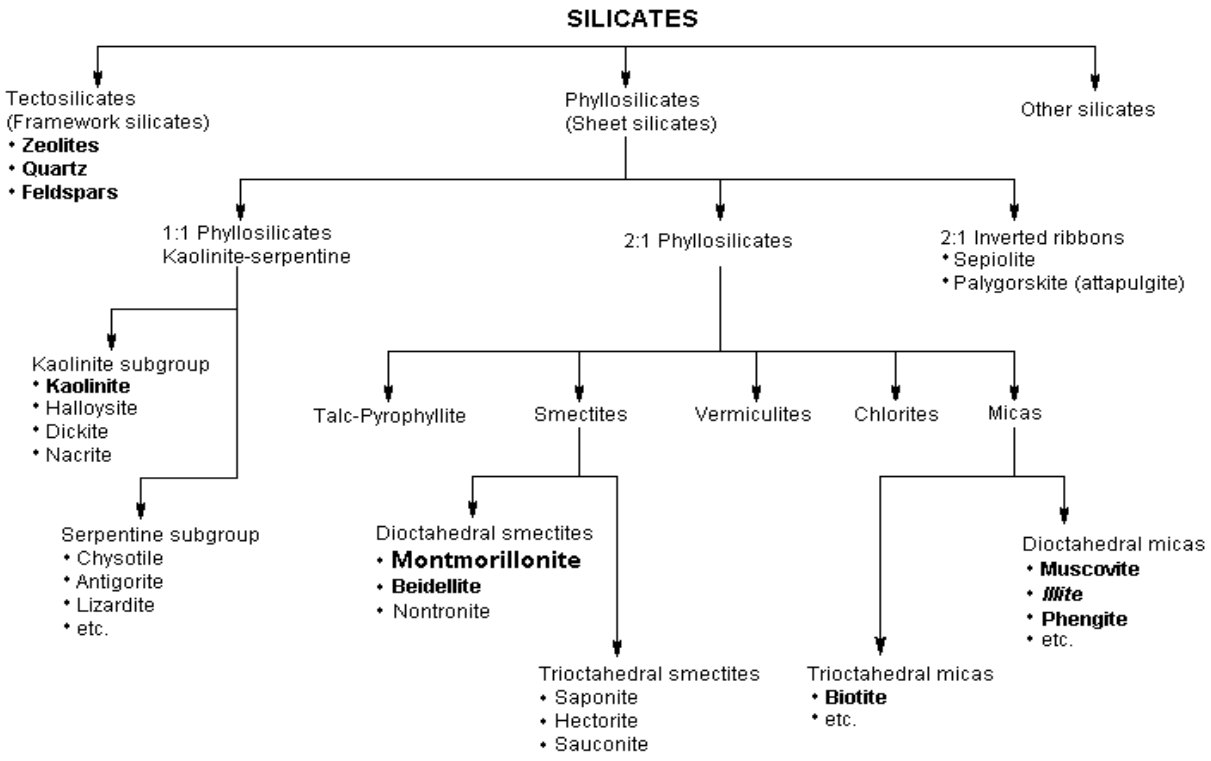


Figure 2.1. Classification of silicates (adopted from Bailey, 1980 and Rieder *et al.*, 1998)

Rocks that are rich in kaolinite are known as **china clay** or simply **kaolin** (Simplified Chinese: 高岭土; pinyin: Gāolǐn tǔ), named after Gaolin ("High Hill") in Jingdezhen, Jiangxi province, China and were traditionally used in the manufacture of porcelain. It was first described as a mineral species in 1867 for an occurrence in the Jari River basin of Brazil **(**Wikipedia, 2004 and www.mindat.org, 2005). Others claimed that, the name "kaolin" is derived from the word Kau-Ling, or high ridge, the name given to a hill near Jau-chau Fu, China, where kaolin was first mined (Sepulveda *et al*., 1983).

2.3.1 Structure of kaolinite

The theoretical formula for kaolinite is $Si_2Al_2O_5(OH)_4$ (other formulae are $Al_2O_3 \cdot 2SiO_2 \cdot 2H_2O$ and $Al_2O_7Si_2.2H_2O$), which has a molecular weight of 258071g/mol. Kaolinite is build up from pseudohexagonal triclinic crystals with diameter 0.2–10μm, thickness 0.7 nm and its density is 2.6 g/cm^3 (www.chemicalland21.com, 2007 and http://www.europa.eu.int, 2007). Kaolinite has a 1:1 sheet structure composed of SiO_4 tetrahedral sheets and $Al(O,OH)_6$ octahedral sheets (or,expressed in another way, $[Si_2O_5]^{2-}$ sheet and $[Al_2(OH)_4]^2$ sheet) with pseudo-hexagonal symmetry (Lee *et al*., 2003). The sheets are created from planes, which are occupied as follows: $O_6 – Si_4 – O_4 – (OH)_2 – Al_4 – (OH)_6$. The morphology of the kaolin crystals is plate-like. The c-axis of the kaolinite crystal is perpendicular to the basal plane. A crystal system of the kaolinite is triclinic, the space group is P1, and lattice parameters are a = 0.515 nm, b = 0.895 nm, c = 0.740 nm, α = 91.68°, β = 104.87°, □ = 89,9°. An ideal cell of the kaolinite is electrically neutral. Its crystalochemical formula is $Al_4Si_4O_{10}(OH)_8$ (Čičel *et al.*, 1981).

Kaolinite, when mixed with water becomes plastic and easy to mold. However, it loses its water of crystallization between 390 and 450 degrees Celsius. It is very soft with a hardness of 2.0-2.5 on the Mohs scales and has a specific gravity of 2.58-2.60. The first model of structure was designed by Brindley and Nakahira (1959a & b), shown in Figures 2.2 and 2.3.

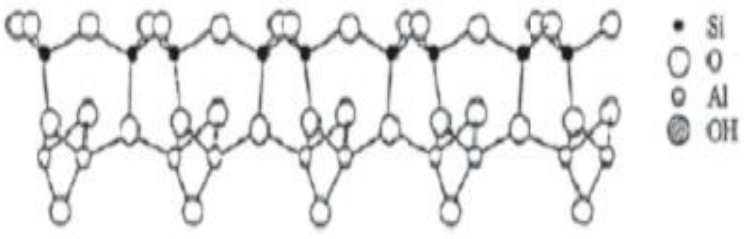


Figure 2.2: Stucture of kaolinite designed by Brindley Nakahra, viewed from the a-axis direction

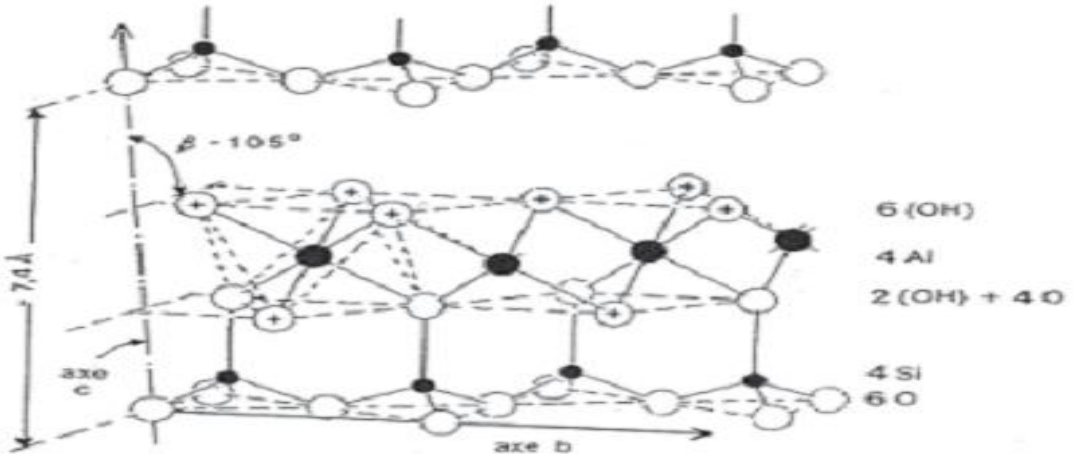


Figure 2.3:Crystallochemical structure of kaolinite

The structure of the lattice layers is shown in Figure 2.4, showing the closeness in layers, thereby disallowing water molecules from getting between the sheets.

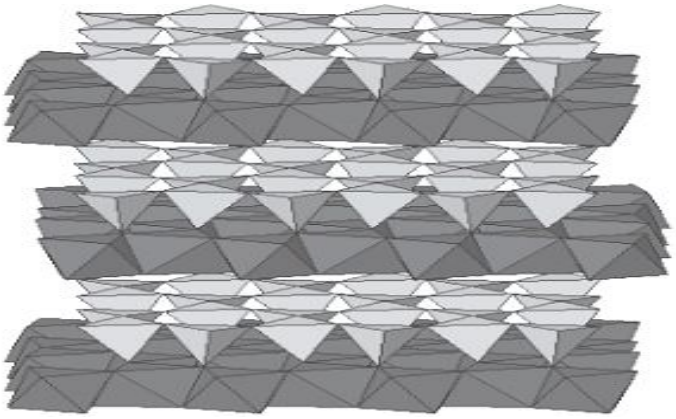


Figure 2.4: The change of the tetrahedrical (light) and octahedral (dark) sheets

2.3.2 Formation of kaolinite clay

Kaolinite is formed by rock weathering and its colour varies from white, greyish-white, or slightly colored. Kaolinite is thought to be formed mainly by decomposition of feldspars (potassium feldspars), granite, and aluminium silicates. The process of kaolin formation is called

kaolinization (Varga,2007). It is also not uncommon to find kaolin deposited together with other minerals (illite, bentonite, halloysite, etc).

Kaolinite formation occurs in three ways:

• crumbling and transformation of rocks due to the effects of climatic factors (Zettlitz type);

• transformation of rocks due to hydrothermal effects (Cornwall type); and

• formation by climatic and hydrothermal effects (mixed type).

Earlier workers' visualization of simple transformation (weather directly) from primary minerals such as feldspars to clay minerals like kaolinite, has been shown to be nonconformant, considering that the structures of these two minerals are so different. For many situations it seems that the primary minerals undergo fairly complete decomposition to simple substances followed by the synthesis of the individual clay minerals. This involves principally the arrangement of the silicon-oxygen tetrahedral and the aluminum octahedral both of which become aligned to form sheet within the clay minerals (Fitzpatrick, 1974). The nature of the weathering environment plays an important role in determining type(s) of mineral that can be formed and extent of purity.

Prolonged leaching of a soil in which montmorillonite has formed can lead to the development of high acidity and conditions favorable for the alteration or breakdown of montmorillonite and the formation of kaolinite. Kaolinite is frequently formed directly from primary minerals in the soils of the humid tropics. Although kaolinite is very stable, it can weather to form gibbsite, $Al(OH)_3$. Kaolin can also be formed by the resilication of aluminum oxide if the weathering zone is invaded by silica-rich waters.

Ironically, noncrystalline or amorphous minerals exist where volcanoes throw ash and cinders into the air, and they solidify before the atoms become organized into crystalline lattices. In the humid tropics, amorphous minerals weather rapidly into crystalline allophane. The soil formed lack discrete mineral particles and are like a gel and feel like mucky soils when wet. Slowly, the allophane clays become more organized or crystalline (Singer & Singer, 1971).

The complex chemical reaction shown in Equation 2.1 is yet not fully understood.

$$2\,KAlSi_3O_8 + 3H_2O \rightarrow Al_2Si_2O_5(OH)_4 + 4SiO_2 + 2KOH \qquad (2.1)$$

2.3.2.1 Kaolinite clay in Nigeria

Past works in this field have listed various locations in Nigeria, where kaolin type of clays are found. Onaji and Ahmed (1995) reported that there are at least, 45 known clay deposits, suitable for local sourcing of industrial raw materials, suitable for application in ceramic industries. RMRDC (2000) also published on her website, information pointing to availability and suitability of kaolin clay in the Country.

According to Sheik (1999), the Nigerian clay deposits are basically of two types - the basement derived or residual clay and the sedimentary or detrital clay. Most Nigerian detrital clay deposits were probably laid down as sedimentary mud in the ancient marine and blackish water environment. This is most likely the reason for the high content of inherent impurities, found in some Nigerian kaolinite clays.

2.3.3 Processing of kaolinite clay

It has been stated earlier, that it is difficult to obtain kaolin in pure form. Accordingly, the accompanying minerals here termed inherent impurities impair the primary characteristics of kaolin and affect its utility for various end applications (Saikia, *et al*., 2003). Deposits of kaolin are usually associated with various impurities like quartz, anatase, rutile, pyrite, siderite, feldspar, etc, depending on the origin and depositional environment (Grimshaw, 1971). One of the most important effects of impurities is that due to fluxing ions, namely Na, K, Ca, and Mg, derived from micas and other associated compounds. These ions, when present, lower the melting point of the system and, in particular, react with silica at, as low as 1000^0C to form viscous liquid, which on cooling does not crystallize but solidifies to form glass, in which the fluxing ions occupy holes in the Si-O network. Sometimes, these impurities are finer than the clay mineral, which therefore, present difficulties in the separation processes (Asmatulu, 2002). In addition, improvement on the properties of kaolin by chemical methods is difficult, because of the high passivity of this material (Belver *et al*., 2002). Despite the aforementioned, various processing methods for mined clay involving both physical and chemical methods have been developed and are in use today.

The processes of kaolin upgradement include sieving, magnetic separation (Asmatulu, 2002; Shoumkov, *et al.*, 1987), selective flocculation (Farhount, 1989), application of ultrasound (Komskaja, *et al*., 1971), leaching with various chemicals like oxalic acid and other organic acids (Veglio *et al*., 1996; Ambikadevi and Lalithambika, 2000) etc. The use of organic acids in the presence of a fermented medium (de Mesquita, *et al*., 1996), lixiviant containing microbially produced oxalic and hydrochloric acid (Groudev, 1999), carbohydrates (Veglio and Toro, 1994), EDTA (Borggaard, 1979), sodium dithionate-H_2SO_4 mixture (Conley and Lloyd, 1970;

Ambikadevi and Gopalakrishna, 1997), etc have been found suitable for removal of most impurities in the mined kaolin. Recently, due to the environmental protection issues, researchers are looking into use of microorganism in pretreating minerals especially kaolin. One of such organisms that has found application in this area is *aspergillus niger*, used to digest iron oxide and co-cultured enzymes for removal of combined oxides in kaolin (Lee, *et al.*, 2002; Hosseini *et al.*, 2007 and Pradhan *et al.*, 2006). Most of the listed methods require pure grade chemicals and enzymes which are pretty expensive and most often not readily available in developing countries. Combination of various methods of beneficiation are applied for kaolin treatment, namely; wet method (i.e. soaking and sieving), deflocculating, thermal and acid treatment. Additionally, most by-products resulting from use of chemical method of purification, as highlighted before, might possess challenges during separation procedure.

2.3.3.1 Effect of heat on kaolinite clay (dehydroxylation)

It is generally accepted, that dehydroxylation begins at about 450 °C, resulting from the mechanical and electrical properties of kaolin. A later finding shows that the beginning of dehydroxylation can be shifted to about 420 °C. A chemical equation of dehydroxylation can be represented by several ways. The chemical equations describing this process are shown in Equations 2.2 a and b.

$$Al_2O_3 \bullet 2SiO_2 \bullet 2H_2O \xrightarrow{450^0C\text{-}600^0C} Al_2O_3 \bullet 2SiO_2 + 2H_2O(g) \qquad 2.2(a)$$

$$\underset{\text{kaolin}}{Al_2Si_5(OH)_4} \xrightarrow{450^0C\text{-}600^0C} \underset{\text{metakaolin}}{Al_2Si_2O_7} + 2H_2O(g) \qquad 2.2(b)$$

It can be considered that in a unit cell there are eight OH groups, which undergo the change, represented in equations 2.3a and b.

$$8\,OH' \rightarrow 4O^{2-} + 4H_2O(g), \qquad 2.3(a)$$

or

$$OH + OH \rightarrow O + H_2O(g) \qquad 2.3(b)$$

The water vapour (in Equation 2.3) carries away about 13.96% of the mass of the stoichiometric kaolinite during dehydroxylation, which occurs primarily on the phase boundary. A mechanism of dehydroxylation includes a transport of OH^- groups to the phase boundary, then the reaction of the groups on the boundary and, finally, transport of the products (molecules H_2O) to the edge of the crystal. The rate of dehydroxylation is determined by the slowest process. It was revealed that this process is diffusion of the water molecules between layers of the kaolinite structure (Kozik *et al.*, 1992; Horvăth, 1976; Toussaint *et al.*, 1963). Accordingly, the dehydroxylation is controlled by diffusion. Activation energy of dehydroxylation for the following degree of the conversion $0 < \alpha < 0.65$ is 140-190 kJ/mol H_2O, depending on size and defects of the kaolinite crystals. The smaller the crystal size and the more the defects, the less activation energy is observed, which can decrease to 100 kJ/mol H_2O (Horvăth and Kranz, 1980). The rate of dehydroxylation is also influenced by the partial pressure of the H_2O vapor (Garn and Anthony, 1969 and Anthony and Garn, 1974).

From a different perspective, there are also experimental evidences for dehydroxylation as a reaction of the first order. Brindley and Nakahira (1957) came to this conclusion through isothermal TGA, and Anthony and Garn (1969 and 1974) by the help of the gas chromatographic analysis. These authors discovered that dehydroxylation may be related to a reaction of the first order if H_2O molecules can escape without obstacles. The first order dehydroxylation kinetics is regarded also in a review (MacKenzie, 1978). Dehydroxylation rate is directly proportional to the surface area of the kaolinite crystals. The precise nature of the first product of dehydration, however, has been a matter of dispute. Formerly believed to be a mixture of amorphous alumina

and silica, the residue has now been shown to possess some definite structural features, some of the original kaolinite structure persisting. Moreover, if the temperature has not been too high, the residue can be rehydrated to kaolinite.

Some authors (MacKenzie, 1978; Hany□ŷ and Kutzendoerfer, 2000) assume that homogeneous and inhomogeneous mechanisms of the dehydroxylation are possible. In the homogeneous process water is formed by reaction between adjacent OH groups and migrates through the crystal. A consequence is the large disruption of the crystal lattice, which resulted in stability of the tetrahedral layer while the octahedral layer was destroyed with decreased distance between these layers. Every crystal cell loses one molecule of H_2O, which is created by the jump of H^+ between two neighbor OH^- groups. In the inhomogeneous process migration of H^+ corresponding counter-migration of Al^{3+} and Si^{4+} between close microscopic regions are assumed. Water is lost from the first regions, which became micropores, and the structural continuity is preserved in the second regions, which became metakaolinte. The mechanism of the dehydroxylation was investigated in detail by Suitch (1986) and it was determined that this mechanism is inhomogeneous for the temperatures lower than 455°C. The inhomogeneous mechanism explains creation of the microporosity well. Liberation of the outer OH groups appears at the temperature 420–600°C, and the liberation of the inner OH groups appear at higher temperatures as far as 850–950 °C (Źivanovič and Janovič, 1978; Freund, 1967).

In kaolinite, the hydroxyl ions are strongly bonded to the aluminosilicate framework structure and can only be eliminated at temperatures above 550 ℃. During the dehydroxylation process, considerable atomic rearrangement occurs (Granizo *et al.*,2000; Madani *et al.*,1990 and Alkan *et al.*,2005). The result is a partly ordered structure that cannot rehydrate in the presence of water (or does so very slowly). Owing to its disordered nature (X-ray amorphous), it has a huge

reactive potential in the presence of an alkali /alkaline earth-containing solution and mineral acid.

At still higher temperatures (say about 925^0C) the metakaolin undergoes further reactions to form crystalline compounds, the end-product being free silica (cristoballite) and mullite, $3Al_2O_3.2SiO_2$ shown in Equation 2.4 to 2.6. Thus, it is clear that there occurs a separation into an alumina-rich compound and free silica, but the precise manner in which this takes place is still a matter of controversy.

Earlier work, based primarily on X-ray diffraction, indicated that at 1000^0C a spinel-type compound was formed, thought to be γ- Al_2O_3. At this temperature, thermal analysis shows an exothermic peak, also thought to be associated with the recrystallisation of Al_2O_3. Other authorities, however, attributed this exothermic peak to the formation of mullite; but this now seems unlikely, since recent X-ray work strongly suggests that mullite is not formed until much higher temperatures are attained, i.e.1150-1300^0C. It has been reported, from experiments with silica-alumina gels, that sillimanite, $Al_2O_3.SiO_2$, a compound structurally similar to mullite, can be formed at temperatures as low as 1000^0C, (see Equation 2.5), but this might be because the silica-alumina gels are much more reactive than metakaolin and moreover may even retain a proportion of their combined water at higher temperature.

More recent accurate measurements of the unit cell dimensions of the spinel compound have shown that it is probably not γ- Al_2O_3 but a silicon-aluminum spinel, of formula $2Al_2O_3.3SiO_2$. This latter compound is then said to lose silica by a progressive diffusion of silica ions from the lattice, forming a mullite-like compound, $Al_2O_3.SiO_2$, as an intermediate stage, and by further loss of silica, true mullite, $3Al_2O_3.2SiO_2$, is formed, as depicted in Equation 2.6.

The entire process may therefore be represented by the following chemical equations:

$$2\left(Al_2O_3.2SiO_2\right) \xrightarrow{925\ ^0C} 2\,Al_2O_3.3SiO_2 + SiO_2 \qquad (2.4)$$

metakaolin *silicon spinel*

$$2\,Al_2O_3.3SiO_2 \xrightarrow{1100\ ^0C} 2\left(Al_2O_3.SiO_2\right) + SiO_2 \qquad (2.5)$$

silicon spinel *pseudo − mullite*

$$3\left(Al_2O_3.SiO_2\right) \xrightarrow{1400\ ^0C} 3\,Al_2O_3.2SiO_2 + SiO_2 \qquad (2.6)$$

pseudo − mullite *mullite* *crystobali te*

The liberated silica, it will be noted, forms cristobalite, but this transformation is commonly believed not to occur below 1350^{0}C. However, the mechanism in Equations 2.4 to 2.6, first proposed by Brindley and Nakahira (1957) is the currently accepted one. There is some evidence that disordered kaolinite behaves in a slightly different manner to that described, because of its lower crystallinity and the presence of ions other than aluminum and silicon in the structure. The other kaolin minerals, halloysite, dickite and nacrite, have all been reported to develop spinel-type phases when heated above 1000^{0}C, but the mechanism of these changes has not been so thoroughly investigated as has that of kaolinite.

The conditions of kaolin calcinations strongly influence the reactivity of the solids obtained; the best conditions for obtaining very reactive metakaolins have been discussed by different authors who reported values between 600 and 800^{0}C (Belver *et al.*, 2002). Only a small part of AlO_6 octahedra is maintained, while the rest are transformed into much more reactive tetra- and pentacoordinated units. This is the reason for the observed semi-amorphuos and semi-crystalline phases noticed in the so called calcined kaolin.

Since the transformation temperature ranges from 600 to 900^{0}C, various authors have declared that the temperature of calcinations affects the rate of dealumination and phase of zeolite formed (Chandrasekhar, 1996; Chandrasekhar and Pramada, 1999; Feng *et al.*, 2009). Another school of thought claimed that most of the inherent impurities in kaolin could be eliminated at very high

temperature, but the problem of having silica in its easily depolymerized form still remain a big challenge.

The work done by Zheng *et al.,*(2002) shed more light on this question, when they investigated the effect of calcinations temperature on the amount of active Al_2O_3 (expressed by acid solubility) and the amount of active SiO_2 (expressed by alkali solubility). Their observation showing the relationship between calcinations temperatures and solubilities of active SiO_2 and Al_2O_3 is presented in Figure 2.5.

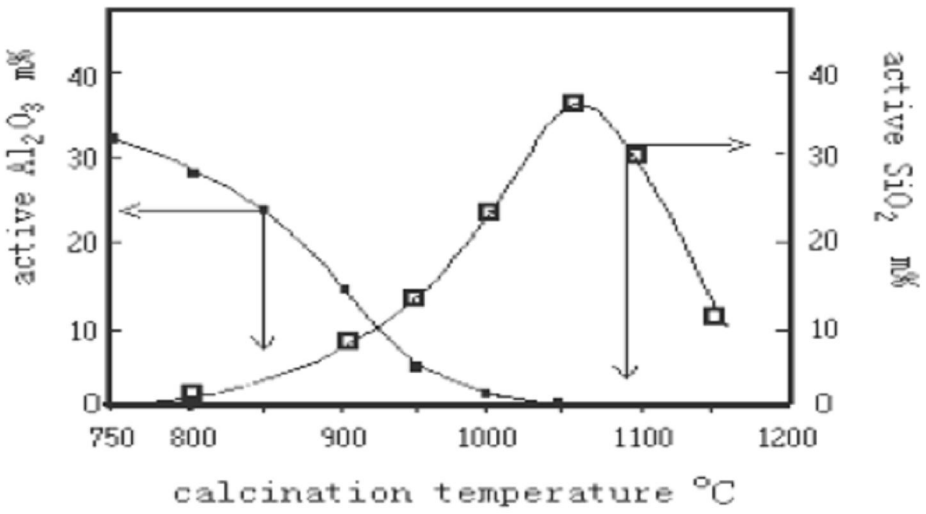


Figure 2.5: Relationship between calcinations temperatures and solubilities of active SiO_2 and Al_2O_3

2.4 Structure of metakaolin

Dehydroxylation is a thermal decomposition of kaolinite crystals to a partially disordered structure. The result of dehydroxylation is a new phase called a metakaolinite. During this reaction, as XRD showed, the higher-order reflections lost their intensity and vanished in the XRD background. This result led to the opinion, that the metakaolinite can be amorphous, now a conception of the short-range order crystalline structure of metakaolinite predominates. The loss

of high-order reflections indicates that dehydroxylation results in structural disturbances through the breaking of unstable bonds. As a result, the degree of ordering became lower than that in kaolinite as dehydroxylation progresses.

The metakaolinite does not collapse but, rather, retains a layered structure. The first attempt to compile a crystallographic model of metakaolinite was made by Brindley and Nakahira (1957 and 1959), who proposed ideal well-ordered lattice presented in Figure 2.6.

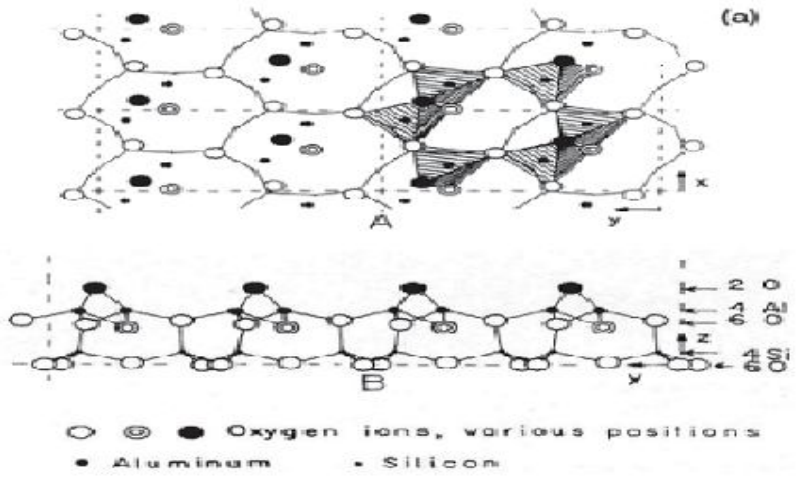


Figure 2.6: Lattice of metakaolinite proposed by Brindley and Nakahira (1957)

Metakaolinite maintains the a and b kaolinite lattice parameters, but c-axis parameter disappears, leading to diffusion of the XRD patterns. Octahedral layer is likely to be changed more than the tetrahedral silica layer during dehydroxylation process. Presumably, the remnant oxygen and vacant anion sites rearrange as a way to lower lattice energy. The structure of metakaolinite allows the kaolinite to collapse to 0.63 nm, in agreement with the measured densities of kaolinite and metakaolinite. Proposed structure of the metakaolinite shows no OH groups. A recent work by Lee and co-workers (Lee *et al.*, 2003) assumes the rearrangement of the oxygen and vacant sites, which gives stability to the layered structure. This rearrangement builds modulations along

the c-axis in metakaolinite with a period of 0.14 nm. If the metakaolinite has a structure shown in Figure 2.6, it means a regular one that should be displayed by XRD reflection. But as it was mentioned before, it is impossible to accurately determine the metakaolinite structure only by XRD analysis. Consequently, the structure of metakaolinite presented in Figure 2.6, must therefore be considered as almost idealized.

A revisited structural model of metakaolinite was proposed by MacKenzie (1978) by computer simulation and nuclear magnetic resonance studies. This structure accounts for the presence of 11–12 % residual OH groups, which are incorporated in the Al-O layers. This structure is shown in Figure 2.7. MacKenzie assumed that homogeneous and inhomogeneous mechanisms of the dehydroxylation are possible. Water is lost from the first regions, which became micropores, and the structural continuity is preserved in the second regions, which became metakaolinite. From the model of MacKenzie, it could be except that the residual OH groups would be liberated at higher temperatures.

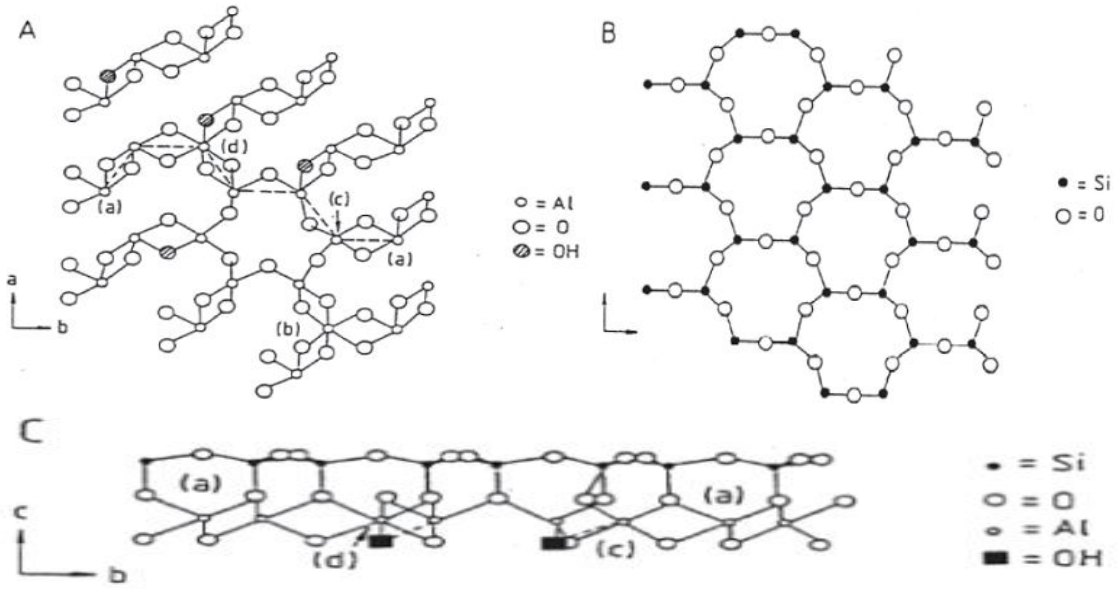


Figure 2.7: Structure of metakaolin by MacKenzie (1978)

2.4.1 Effect of acidification and alkalination on kaolin and metakaolin

The treatment of kaolin with acid and alkaline had been of great interest to clay researchers around the world for the past decades. However, improvement on the properties of kaolin by chemical methods is difficult because of the high passivity of this material. Thus, it is not significantly affected by acid or alkaline treatments, even under strong conditions (concentrated solutions and/or high temperatures). A pioneer in this area, Nutting (1943) while working with montmorrinolite, found that acid removed alkali metals, alkaline earths, iron and aluminum from clay. The first effect of acids is to remove the exchangeable cations, thereby producing H-clays. The alumina octahedral layer of a clay mineral is then attacked, and later the silica tetrahedral layer.

Alkalines first attack the tetrahedral layer and if the attack is prolonged and severe, the mineral structure is destroyed. The kaolinite structure on the other hand, resists prolonged treatment in concentrated sulfuric acid (Murray, 1951). Carroll and Starkey (1971) reported that kaolin is partly attacked by acid following montmorinollite and metabentonite on the reactivity series with acid, while sodium hydroxide attacks more strongly kaolin minerals in comparison with other clay families investigated. This method involves leaching of clay particles with inorganic acids, causing disaggregation of clay particles, elimination of mineral impurities, and dissolution of the external layers, thus altering the chemical composition and the structure of clays. This produces an increase in the surface area, the porosity, and the number of acid centers with respect to the parent clays, depending on the intensity of the treatment. The treated solids are composed of a mixture of non-attacked clay layers and a hydrous, amorphous, and partially protonated silica phase (Belver *et al*.,2002).

Additionally, the acid activation of metakaolins has been dealt with also in various articles (Caballero *et al*.,2007; Colina *et al*.,2002, Aderemi, 2000; Hanzliček *et al.*, 2002; Hulbert and Huff, 1970). These reports showed that metkaolin is more reactive and is easily attacked by both acids and alkalines, causing partial destruction of the metakaolinite structure. This is dependent on the concentration of the acid/alkaline and time of reaction.

The alkaline treatment of clays has been much less studied. *A priori*, the progressive leaching of aluminic and silicic layers may be predicted, both elements being soluble in alkaline conditions as aluminates and silicates. The alkaline treatment of fibrous or smectitic clays has received little attention, but the modifications of metakaolins have been widely studied. Most recently, it was observed that alkaline can be employed in leaching or reducing some unwanted phases in kaolinite clay.

2.5. Zeolite, Types, Classifications and Properties

2.5.1 Definition

Due to the enormous structural and chemical diversity of the zeolite family, it is difficult to find precise definitions of what a zeolite is. The classical definition of a zeolite is given as a micro porous crystalline aluminosilicate, composed of TO_4 tetrahedra (T = Si, Al) with O atoms connecting neighboring tetrahedra. For a completely siliceous structure, combination of TO_4 (T = Si) units in this fashion leads to silica (SiO_2), which is an uncharged solid. Upon incorporation of Al into the silica framework, the +3 charge on the Al makes the framework negatively charged, and requires the presence of extraframework cations (inorganic and organic cations can satisfy this requirement) within the structure to keep the overall framework neutral. The zeolite composition can be best described as having three components:

$$M^{m+}_{n/m} \cdot [Si_{1-n}Al_nO_2] \cdot nH_2O$$

extraframework cations framework sorbed phase

The extraframework cations are ion exchangeable and give rise to the rich ion-exchange chemistry of these materials.

2.5.2 Types of zeolitic materials

Typical types of zeolitic materials are represented in Figure 2.8. The novelty of zeolites stems from their microporosity and is a result of the topology of the framework. However, some relatively recent discoveries of materials virtually identical to the classical zeolite, but consisting of oxide structures with elements other than silicon and aluminum have stretched the definition. With the recent advances in zeolite world, the dynamics in terms of zeolite definition is quite enormous as more elements are being introduced into the structure, thereby expanding the classical definition, usage and types.

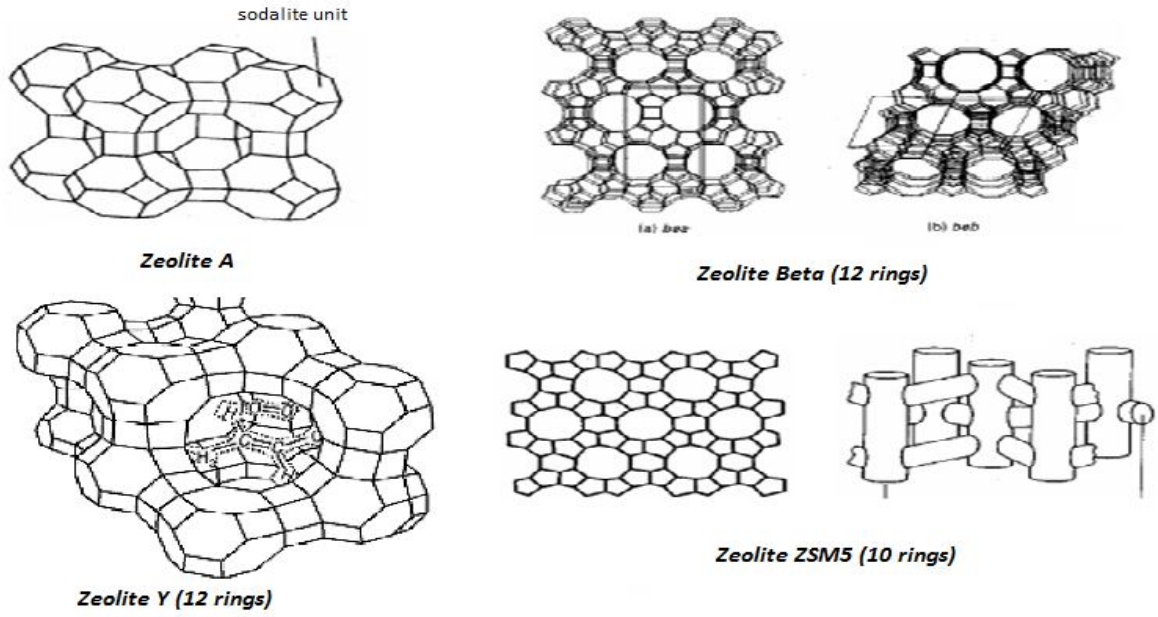


Figure 2.8: Representative of some zeolite materials

Most researchers now include virtually all types of porous oxide structures that have well-defined pore structures, due to a high degree of crystallinity, in their definition of a zeolite. Elements, such and B, Ge, Zn, P, and transition elements, can also be incorporated into the framework and are referred to as crystalline molecular sieves (Lok *et al*., 1984). Aluminophosphates (AlPOs) have strictly alternating AlO_2 and PO_2^+ units, and the framework is neutral, organophilic, and nonacidic. The alternation of Al or P leads to structures lacking in odd-numbered rings. Substitution of P by Si leads to silicoaluminophosphates (SAPOs), with cation-exchange abilities. Metal cations can also be introduced into the framework, including transition metal ions such as Co, Fe, Mn, and Zn.Accordingly, the discovery of these solids has led to the development of several new stuctures (Cheetham *et al.,*1999).

2.5.3 Features of zeolitic materials

The amount of Al within the framework can vary over a wide range, with Si/Al = 1 to the completely siliceous form being polymorphs of SiO_2. Lowenstein proposed that the lower limit of Si/Al = 1 of a zeolite framework arises because placement of adjacent AlO_4 tetrahedra is not favored because of electrostatic repulsions between the negative charges. The framework composition depends on the synthesis conditions. Post-synthesis modifications that insert Si or Al into the framework have also been developed. As the Si/Al ratio of the framework increases, the hydrothermal stability as well as the hydrophobicity increases. Typically, in as-synthesized zeolites, water present during synthesis occupies the internal voids of the zeolite. The sorbed phase and organic non-framework cations can be removed by thermal treatment/oxidation, making the intracrystalline space available.

The fact that zeolites retain their structural integrity upon loss of water makes them different from other porous hydrates. The crystalline nature of the framework ensures that the pore openings are uniform throughout the crystal and can readily discriminate against molecules with dimensional differences, giving rise to the name molecular sieves. Figure 2.9 gives a pictorial expression of the role of zeolite as molecular sieve.

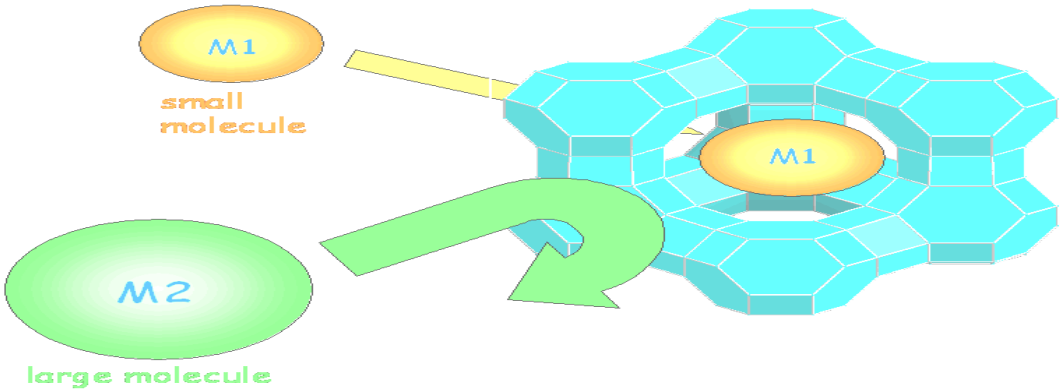


Figure 2.9: Molecular sieve property of type Y zeolite.

Thus, zeolite frameworks are typically anionic, and charge compensating cations populate the pores to maintain electrical neutrality. These cations can participate in ion-exchange processes (an important properties of zeolites) as illustrated in Figure 2.10 to give it an edge over other microporous materials.

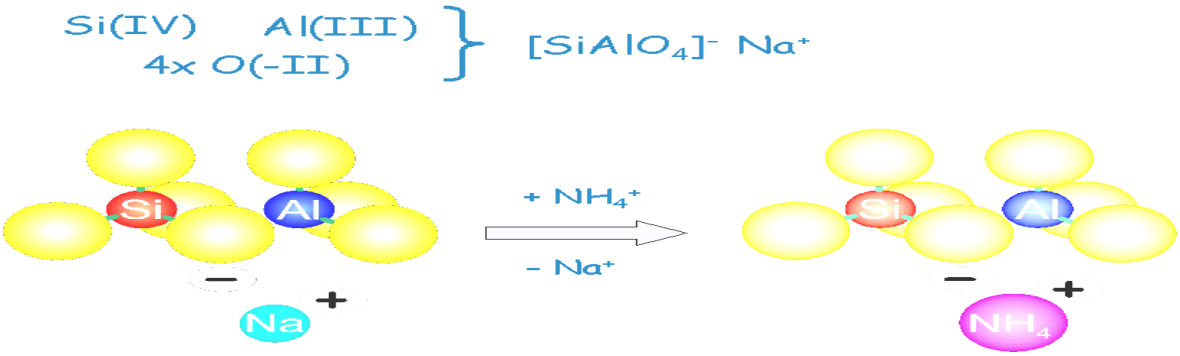


Figure 2.10: Ion exchange property of zeolitic material.

When charge compensating cations are "soft" cations such as sodium, zeolites are excellent water softeners because they can pick up the "hard" magnesium and calcium cations in water, leaving behind the soft cations. Figure 2.11 gives an illustration of this behaviour.

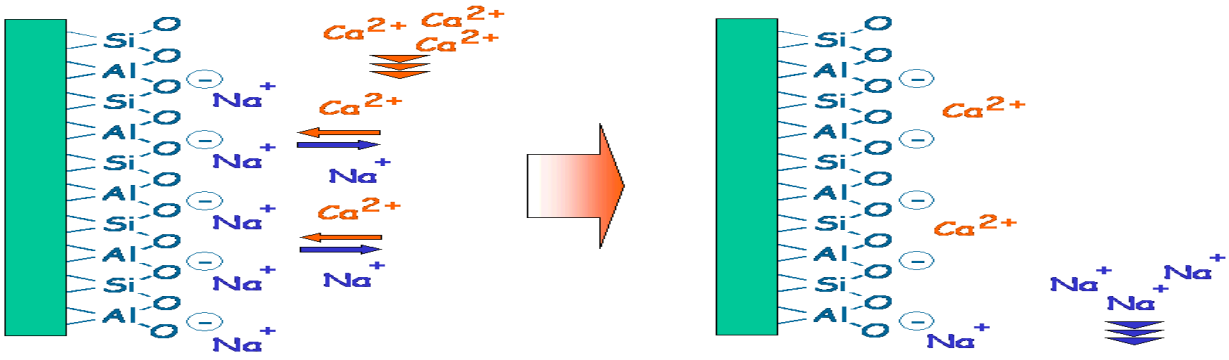


Figure 2.11: Principle of water softening using zeolites.

When the zeolitic cations are protons, the zeolite becomes a strong solid acid. Such solid acids form the foundations of zeolite catalysis applications, including the important fluidized bed cat-cracking refinery process. Other types of reactive metal cations can also populate the pores to form catalytic materials with unique properties. Thus, zeolites are also commonly used in catalytic operations and catalysis where zeolites are often termed "shape-selective catalysts". Figure 2.12 shows the framework projections and the ring sizes for commonly studied frameworks, as well as their pore size capacity.

CLO	
VFI	
AET	
AFI	
DON	
FAU	
MFI	
LTA	

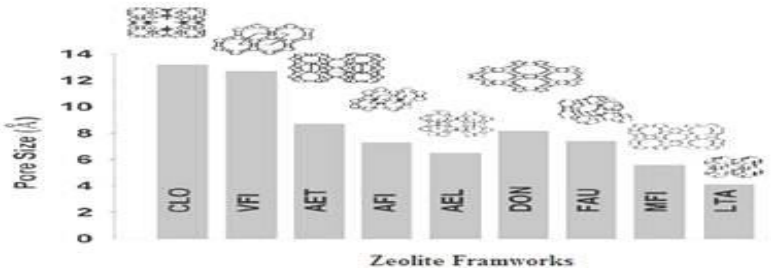


Figure 2.12: Comparison of pore size tolerance of different framework structures.

2.5.4 Catalytic properties of zeolites

The extraframework cations in zeolites are often sited in the cages in such a way that the charges and structure are balanced and suitable for their various designated application. These siting are pictorially described in Figure 2.13.

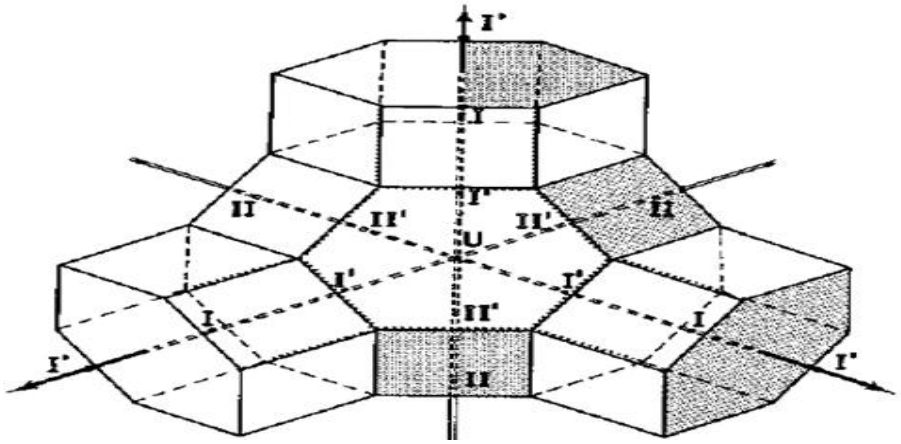


Figure 2.13: The cation sites in the faujasite framework.

Site I is in the hexagonal prism (D6R); is near the entrance to an hexagonal prism in the sodalite (h) cage. II is inside the sodalite cage near the single-6R entrances to the large (a) cage. II' is in the large cage adjacent to D6R and U is at the center of the sodalite cage. Other sites (IV, V) are in the large supercage cavities. (Abrioux *et al.*, 2008)

Zeolites have played an increasingly important role in industrial catalytic processes since the early 1950s. In zeolites, tetrahedral aluminum replaces silicon in certain lattice sites leading to negative charge. This -1 charge makes zeolite unstable, hence the presence of a cation in the general vicinity of this anion to preserve the electrical neutrality of the lattice. Three of the four types active sites found in zeolites are associated with and attributable to the substitution of aluminum for certain silicon sites in the framework. If the charge compensating cation associated

with tetrahedral aluminum is hydrogen, the zeolite surface obtains the capacity to act as a proton donor and, therefore, can serve as a Bronsted acid. If the zeolite is heated to 355^0C, scission of the Si-O-Al bond occurs resulting in the formation of a Lewis (electron pair accepting) acid site. According to the model of Ward, two bronsted acid sites are destroyed in the formation of a single Lewis acid site. If by conventional ion-exchange techniques, transition metal ions are introduced into the zeolite pore system, a third type of active site is generated. The fourth type of active site is the zero valent metal atoms produced in the zeolite pore system through the reduction of metal cations or the decomposition of metal complexes.

The intra-crystalline pore-cavity system in zeolites, called the zeolitic surface, is strongly influenced by the zeolite crystal field which surrounds it. Because Si-O-Si bonds are covalent, the ionic character of the zeolite crystal field is controlled by the alumina content, of the framework. Depending on the aluminum contents, zeolite range from weak to very strong electrolytes. Molecules adsorbed by zeolites, particularly polar or strongly polarizable ones, will be polarized by the zeolite and they will exert a similar effect on the zeolite crystal. The overall interaction between a zeolite and an adsorbate must tend to minimize the free energy of the zeolite adsorbate system. The simplest way to forecast thermodynamically favored reactions in zeolite is, therefore, to evaluate their effect on the stability of the zeolite crystal.

All industrially significant catalytic applications of zeolites rely on the shape selective effects generated by the pore dimensions of the intra-crystalline channels. Five types of shape selectivity have been reported in the literature i.e. reactant selectivity, product selectivity, cage or concentration effects, restricted transition state selectivity, and molar traffic control. ***Reactant selectivity*** occurs when only certain reactants have dimensions sufficiently small to enter the zeolite pore system, for exposure to the active sites. This type of selectivity is used in catalytic dewaxing where normal paraffin, are cracked and branched paraffins left, to remain intact.

Product selectivity occurs when only certain products have dimensions allowing them to exit the pore system. Product selectivity is used to produce paraxylene via the para selective alkalation of toluene. Cage and concentration effects are caused by the increased reactant density within the zeolite pore system, attributable to the electrostatic field interactions with the adsorbed molecule. The result of this form of selectivity is an increase in bimolecular reactions over unimolecular reactions. ***Restricted transition state selectivity***, as the name implies, results in the elimination of certain reaction pathways because the transition state leading to those pathways is larger than can be accommodated by the zeolite pore or cavity. These forms of selectivity were reviewed by Csicseri **(**1984**)**. The last form of shape selectivity known as ***molecular traffic control*** is thought to occur in zeolites such as ZSM-5 which have interconnecting pore systems in two directions, which are slightly different in pore diameter. Reactant molecules smaller than product molecules can enter the smaller pore system, get converted to product, and diffuse out the larger pore system. Counter diffusion is thereby minimized. These types of shape/size selectivity properties of zeolites are represented in Figure 2.14.

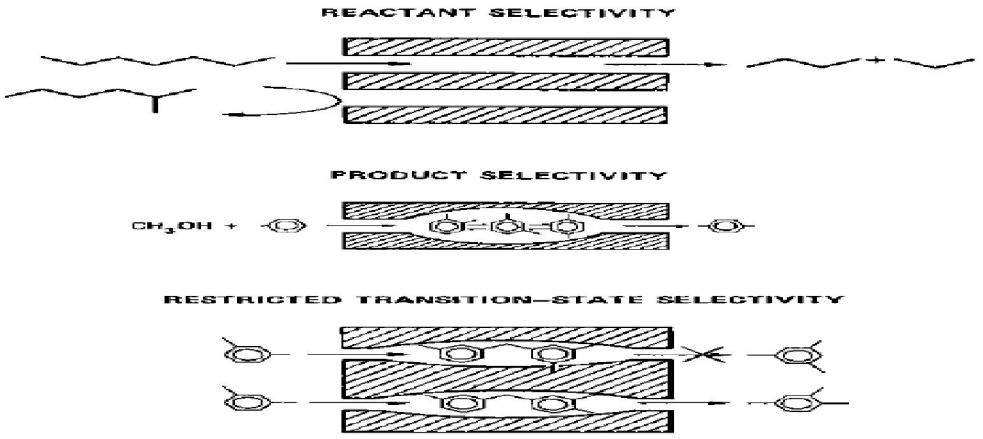


Figure 2.14: Different types of reaction selectivity imposed by the rigid pore structure of the zeolite. (adopted from Csicseri, 1984.)

2.5.5 Structure of zeolites

The fascinating and wonderfully exploitable properties of zeolite materials, such as their ion-exchange properties, their sorption capacity, their shape selectivity, their catalytic activity, or their role as hosts in advanced materials, are essentially determined by their structure. For example, sorption characteristics depend upon the size of the pore openings and the void volume; ion-exchange selectivity upon the number and nature of the cation sites and their accessibility; catalytic behaviour upon the pore openings, the dimensionality of the channel system, the cation sites, and the space available for reaction intermediates; and other host of applications on the size and spacing of the cages. Consequently, structural analysis is a fundamental aspect of zeolite science. Description of a zeolite structure almost always begins with a description of the framework type in terms of the size of the pore openings and the dimensionality of the channel system.

Information on the framework type alone can elucidate many of the observed properties of zeolites. The framework type, which describes the connectivity (topology) of chemical composition, defines the size and shape of the pore openings, the dimensionality of the channel system, the volume and cage arrangement and the types of cation sites available. Nonetheless, the chemical composition of the framework, the nature of the species within the channels, and the type of post-synthesis modification also play a very import role in determining the specific properties of a particular zeolite material. For example, an aluminosilicate framework has a negative charge whereas an aluminophosphate is neutral, a large cation can block or reduce the effective size of a pore opening, a small cation might distort a pore opening, or sorbed species can influence the catalytic, optical, magnetic, or electronic properties of a zeolite. Precise structural details, such as the nature of the distortion of a framework from ideal symmetry or the

exact location of non-framework species, are often needed to fully understand the properties of a specific zeolite.

Many of the interesting properties of zeolites are based on the fact that the framework is anionic and the balance cations are exchangeable. A pure silica (SiO_2) framework is neutral, but if some of tetravalent Si is replaced by trivalent Al to produce an aluminosilicate, the framework becomes negative and counterions such as Na^+ are needed to balance its charge. The neutral aluminophosphate or gallophosphate frameworks can be made anionic in a similar manner by inserting other elements into some of the T-sites. Even a small amount of a transition metal ion in the framework can make the material useful for catalysis or catalytic applications. Many elements have now been incorporated into zeolite framework structures. What was originally the realm of alumina and silica has expanded to include a significant number of elements of the periodic table. In some cases, only a few percent of the element is incorporated, while in others it is a major constituent.

The framework composition also affects the stability of a material. For example, a high-silica zeolite usually has a higher thermal stability than does the corresponding aluminosilicate and an aluminosilicate tends to be more stable than an aluminophosphate, and a gallophosphate.

Because zeolite scientists recognized very early that zeolite framework structures are fundamental to the understanding of the zeolite chemistry, classification of zeolitic materials by framework type, first proposed by Meier and Olson in 1970, has gained wide acceptance in the zeolite community. A framework type, as opposed to a framework structure, simply describes the conductivity of the tetrahedrally coordinated atoms (T-atoms) of the framework in the highest possibility symmetry. The framework composition in the observed symmetry and the actual unit-cell dimensions are not considered. In this way, many different materials can be

classified under one designation. For example, amicite, garronite, gismondine, gobbinsite, Na-P1, Na-P2, and SAPO-43 all have the GIS framework type. A three-letter code (e.g., GIS) is assigned to confirmed framework types by the Structure Commission of the International Zeolite Association according to rules set up by an IUPAC Commission on Zeolite Nomenclature. The codes are normally derived from the name of the zeolite or "type material," e.g., FAU) from the mineral faujasite, LTA from Linde Type A, and MFI from ZSM-5 (Zeolite Socony Mobil – five). Information pertinent to these framework types is published in the Atlas of Zeolite Framework Types and on the internet at htt://www.iza-structure.org/databases/. As of February 2007, 176 zeolite framework types had been confirmed by the Structure Commission.

The feature that is common to zeolite or zeolite-like materials is that they all have a 3-dimensional, 4-connected framework structure, constructed from corner-sharing TO_4 tetrahedral (basic building unit or BBU), where T is any tetrahedrally coordinated cation. This framework structure is relatively open and characterized by the presence of channels and cavities. Pore openings are characterized by the size of the ring that defines the pore, designated an n-ring, where n is the number of T-atoms (usually also the number of O-atoms in the ring. An 8-ring is considered to be a small pore opening, a 10-ring a medium one, and a 12-ring a large one, with free diameters or effective pore widths (calculated using an oxygen radius of 1.35Å) of ~ 4.1, 5.5, and 7.4 Å, respectively. Of course, rings can be distorted considerably, so these numbers should only be used as a rough guide.

Modern crystallographic techniques generally allow such information to be extracted from diffraction data, but there are some limitations that should be appreciated. The primary problem is the fact that extra-framework species do not generally follow the high symmetry of the framework, so they are called "disordered". For example, the Na^+ ion in an 8-ring of zeolite A is located off-center where it can approach three framework oxygen's, but because there is a 4-fold

axis running through the center of the 8-ring, there are four equivalent positions for the Na^+ ion. However, there is only room for one Na^+ ion per 8-ring. This Na^+ ion may hop between the four equivalent positions (dynamic disorder) or it may be stationary but occupy different positions in different 8-rings (static disorder).

2.5.6 Building zeolites

The overall structure – effect of zeolites – derive from the complex inter and intra-actions among the following factors: sizes of the framework and extra-framework component atoms, cations (T) and anions (O); sizes and charge densities of the Basic Building Units (BBU) and the Complex Building Units (CBU) and types of bonds (covalent and electrovalent), together with bond strength and angle of linkage.

The primary building block of all zeolites is a tetrahedron of four oxygen anions that surround a silicon or aluminum ion, as shown in Figure 2.15(a).

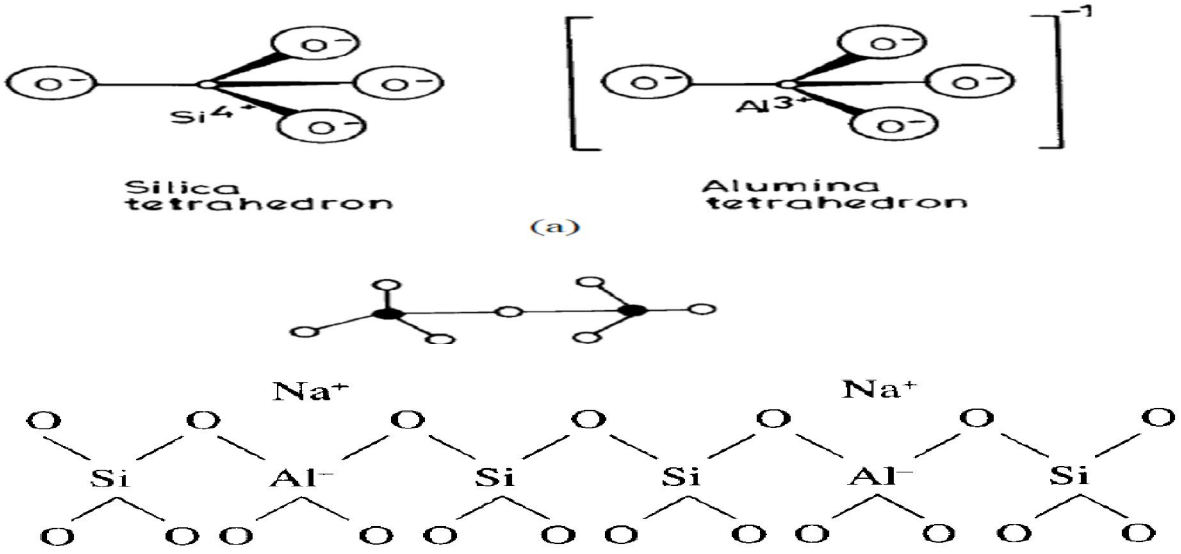


Figure 2.15**:** (a) Primary building blocks of zeolites, (b) Simplified surface structure of zeolite

These tetrahedra are arranged in such a way that each of the four oxygen anions is further shared by another silica or alumina tetrahedron. Altimately, the crystalline framework extends in three dimensions, where the –2 oxidation state of oxygen is accounted for. The +4 charge on each silicon ion is balanced by the four tetrahedral oxygen, making silica tetrahedral electrostatically neutral. On the other hand, the +3 charge on aluminum is not balanced by the surrounding four tetrahedral oxygens, leaving a residual charge of –1 on each alumina tetrahedron. Thus each alumina tetrahedron requires a +1 charge from a cation in the structure to be electrostatically neutral, as shown in Figure 2.15(b). The cations providing electric stability to alumina tetrahedron are generally sodium in the zeolite, where they occupy non-framework positions.

The tetrahedra are arranged in such a way that the zeolites have an open framework structure with a large specific surface area. The pore structure varies from zeolite to zeolite. The pore diameters in all zeolites are determined by the free aperture resulting from 4-, 6-, 8-, 10- or 12-membered rings of oxygen atoms, and their maximum values are calculated to be 2.6, 3.6, 4.2, 6.3, and 7.4^{o}A , respectively. As an example, Figure 2.16 shows the structure and pore size of Y zeolite. The silicon or aluminum ions are located at the corners and the oxygen ions near the edges. The aperture opening is 7.4^{0}A and unit cell size is about 25^{0}A. However, due to some elongation of the oxygen ring or the presence of cations near or within the pore apertures, the effective free aperture of the pore may be reduced, and the aperture may be elliptical. The zeolites with 8- and 12-membered oxygen ring or more are used in major catalytic applications rather than small aperture size as it places unacceptable size limitations on the molecules to be adsorbed. Many of the zeolites formed are not in the equilibrium state but only in the metastable state, which in time may convert to other more stable zeolitic phases or other mineral phases.

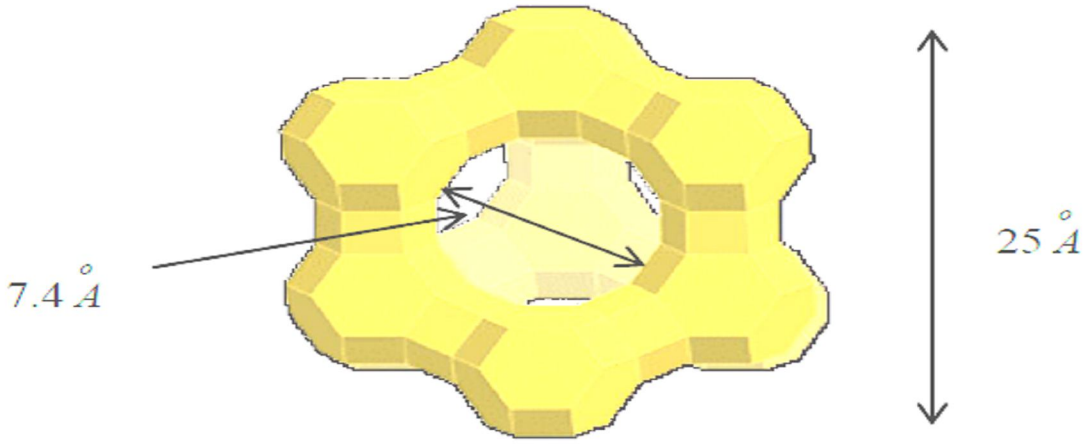


Figure 2.16**:** Perspective view of Y zeolite structure.

All zeolite frameworks can be built by linking in a periodic pattern, a basic building unit (BBU), the tetrahedron. In the center of the tetrahedra are atoms with relatively low electronegativities (Si^{IV}, Al^{III}, P^{V}, Zn^{II}, etc.) and in the corners are oxygen anions (O^{2-}). These combinations can be depicted as [SiO_4], [AlO_4], [PO_4], etc., and in what follows, the term TO_4 will be used to describe tetrahedra in general, where T stands for any tetrahedral species. The notation [$TO_{4/2}$] is often used to emphasize that each oxygen atom is coordinated to two T atoms. Figure 2.17 depicts several representations of the tetrahedron. Note that, each apical oxygen is shared with the adjacent tetrahedron and as a consequence the framework of zeolite materials always has a metal-to-oxygen ratio of 2. The tetrahedra in zeolite materials are somewhat rigid (Bartelmehs *et al.*, 1995; Dove *et al*., 1995; Dove *et al*., 1996; Hammonds *et al.*, 1998). In general, the O-T-O angle is close to the ‘‘ideal’’ value of 109^0 28’ for a geometrically perfect tetrahedron and deviations of more than a few degrees are not frequent. The T-O bond length depends on the particular metal cation. For SiO_4 tetrahedra the bond length is d(Si-O) ~1.59–1.64 A˚ (Deer *et al*., 1997).

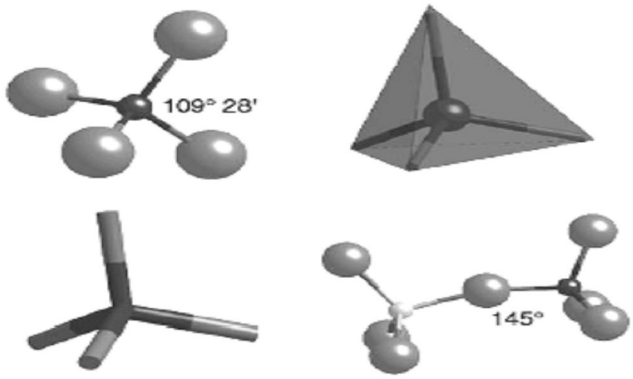


Figure 2.17: Several representations of the basic building unit of zeolites, the tetrahedron

For AlO_4 the bond length is usually d(Al-O) c 1.73 A˚ (Hill and Gibbs, 1979), while boron is the smallest cation that has been found in zeolite frameworks with a d(B-O)~ 1.44 A˚ and zinc is the largest with d(Zn-O)~ 1.95 A˚. To build zeolite frameworks the tetrahedra are linked via the apical oxygen (T-O-T). The T-O-T bond angle is quite flexible, in sharp contrast to the rigid O-T-O angle. For the case of silica tetrahedra the T-O-T angle is usually in the vicinity of 140–165^0, but values of 130–180^0 have been reported. The flexibility of the T-O-T angle is very important because it is the degree of freedom that allows the formation of the great variety of zeolite frameworks, without much thermodynamic penalty. The flexibility of the T-O-T angle allows the formation of rings and other more complex building units from which zeolite materials may be formed.

More complex composite building units (CBUs) can be formed, linking together groups of BBUs. The simplest examples of CBUs are rings. All zeolite structures can be viewed as if formed of rings of tetrahedra of different sizes. In general, a ring containing n tetrahedra is called an n ring. The most common rings contain 4, 5, 6, 8, 10, or 12 tetrahedra, but materials with rings formed of 14, 18, up to 20 tetrahedra have been prepared. Materials with 3-, 7- or 9-rings,

are rare. When a ring defines the face of a polyhedral unit, it is also called a **window**. In Figure 2.18 an illustration of the relative sizes of some n rings, frequently found in zeolites are shown.

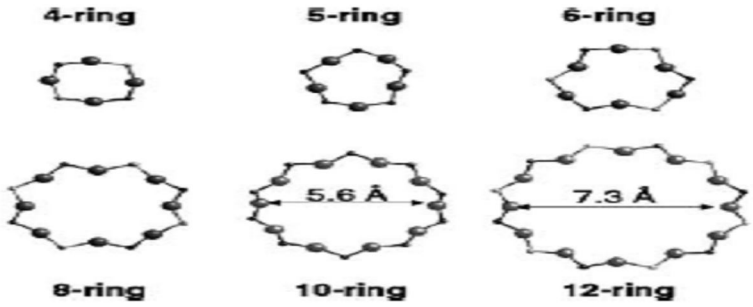


Figure 2.18: Relative sizes of n-rings frequently found in zeolites and related molecular sieves. The scale of the pore aperture is given for the 10-ring to give a sense of scale.

Although the rings are sometimes planar, more often they have more complicated shape and geometry. Elongated rings and rings that are puckered out of a plane are very common. The next level of complexity is obtained by constructing larger CBUs from n rings giving rise to a diverse and interesting set of structures. **Cages**, for example, are polyhedra whose largest rings are too narrow to allow the passage of molecules larger than water. It is usually considered that 6-rings are the upper limiting ring size to form a cage. As can be seen in Figure 2.19, cages of different shape and geometry can be built easily, connecting rings of different sizes.

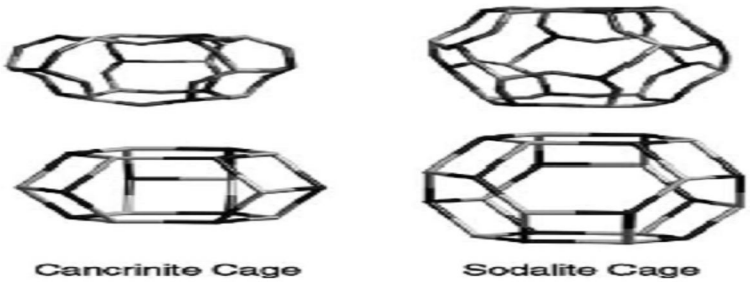


Figure 2.19: Two cages frequently found in zeolites. The oxygen and T atoms are depicted in the upper drawings. In the lower half, only the connections between T-atoms are indicated.

In this case, the cancrinite cage (or cage) and sodalite cage (or β cage) are formed connecting 4- and 6-rings in different arrangements. As one might guess, these two CBUs are building units of the zeolites cancrinite (CAN) and sodalite (SOD), but they are also found in several other zeolite structures.

In summary, it can be concluded that building of zeolites materials start from simple silica and alumina structure, in the presence of a mineralizer, which is metamorphosed into various cages from which the desired zeolite is eventually formed. These are depicted in Figures 2.20 and 2.21.

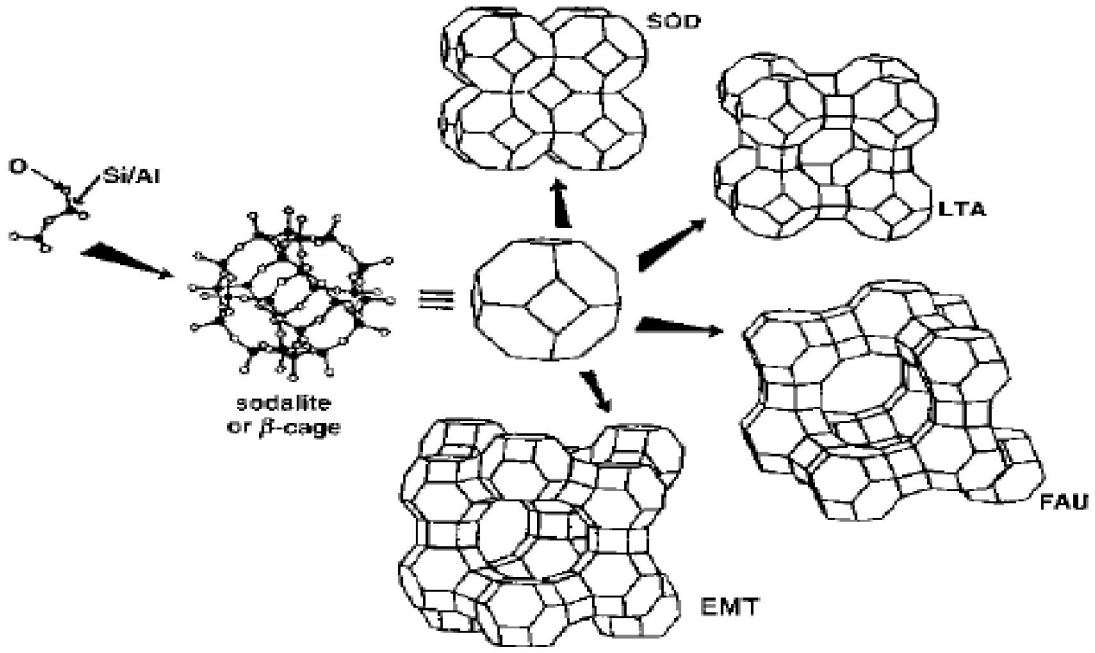


Figure 2.20: The construction of four different zeolite frameworks with sodalite or h cages.

A pair of TO_4 tetrahedra is linked to a single sodalite cage by T-O-T bonds. In a less cluttered representation, the oxygen atoms are omitted and straight lines are drawn connecting the tetrahedral (T) atoms. The sodalite cage unit is found in SOD, LTA, and FAU,-EMT frameworks. (Cheetam *et al.*, 1999)

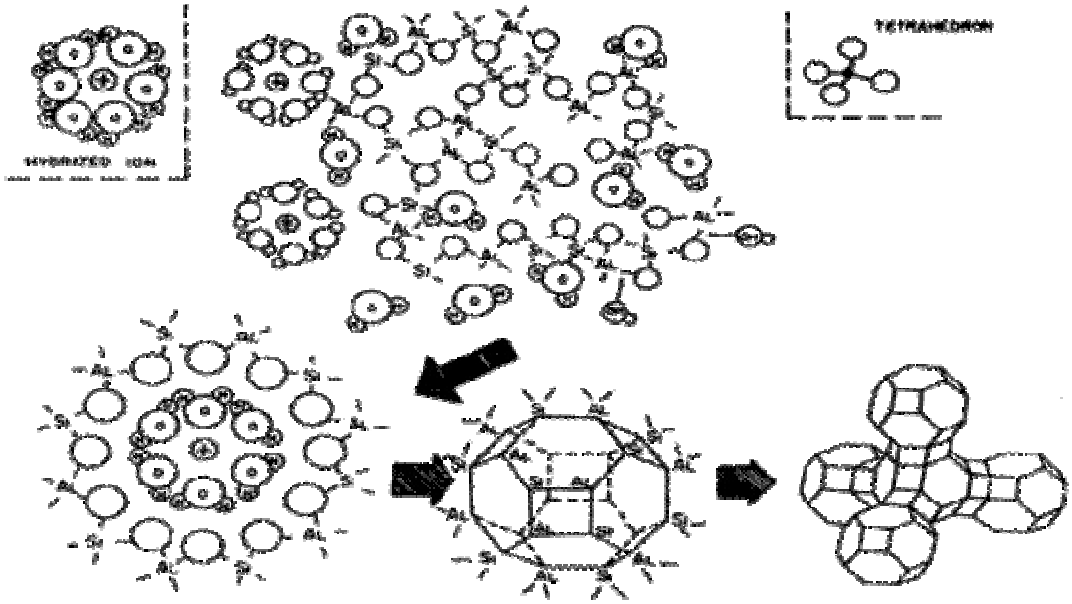


Figure 2.21: The first pictorial depiction of zeolite synthesis "Schematic representation of the formation of zeolite crystal nuclei in a hydrous gel". (Breck, 1974).

2.5.7 Faujasite type zeolite Y

Zeolite Y has an FAU-type structure and is widely used in petroleum refining (Xu *et al*., 2007). The basic structural units for Y zeolites are sodalite cages, which are arranged so as to form supercages that are cage-like voids interconnected to each other by 12-ring openings. It is made of secondary building units (SBUs) 4, 6, and 6-6. Figure 2.22 shows the supercage structure of zeolite Y (left) and the 12-ring pore opening (right) (http://www.iza-structure.org). The diameter of the supercages and the size of the 12-ring opening of Y zeolites are ~12 Å and ~7.4 Å, respectively. The combination of large void volume (ca. 50%), 12-ring pore openings and 3-dimensional channel system make zeolite Y ideal for many catalytic applications. The pore diameter is large at 7.4 Å since the aperture is defined by a 12 member oxygen ring and leads to a larger cavity of diameter 12 Å. The cavity is surrounded by ten sodalite cages (truncated octahedra) connected on their hexagonal faces. The unit cell is cubic (a = 24.7Å) with Fd-3m

symmetry. A typical zeolite Y type with Si/Al ratio of 2.43 has a void volume fraction of 0.48 and decomposes at 793^0C.

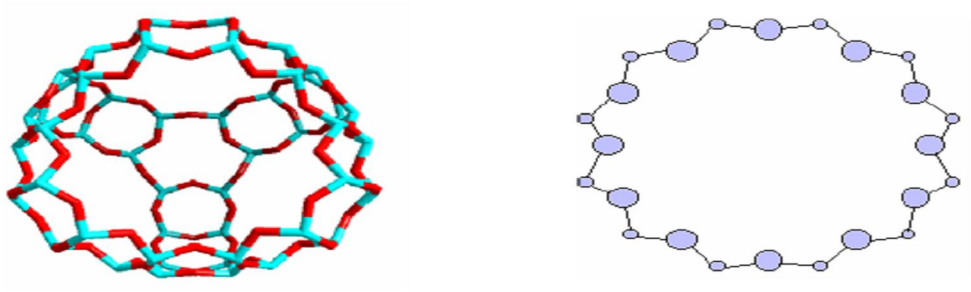


Figure 2.22: The faujasite framework structure of zeolite Y: the supercage structure (left) and the 12-ring viewed along (111) (right). In the right panel, the larger cycles represent T atoms (Si or Al) linked to each other by shared oxygen atoms (small cycles).

Typically, the zeolite frameworks contain aluminum atoms in place of some of the silicon atoms, and the structures are filled with non-framework anions and diffusing species such as water. Here, the focus is on all silicon–oxygen frameworks, also known as siliceous zeolites. All of the structures, which are built from SiO_4 tetrahedra, are shown in Figure 2.23. One length scale up from the SiO_4 tetrahedron, zeolites can be described by secondary building units (SBUs), which are named based on their geometry. For example, a 6R SBU is a ring structure made from six oxygen atoms and six silicon atoms. In SOD, the sodalite cages are directly joined on the 4R rings to form a cubic arrangement of cages. In FAU, the sodalite cages are joined by oxygen bridges on the 6R rings, resulting in a diamond arrangement of cages. LTA is a cubic arrangement of sodalite cages joined by oxygen bridges on the 4R rings. The atoms in each of the silica structures have a unique environment. The structures can be characterized by the distortion of individual tetrahedral and by considering the number of independent paths that lead away from a given atom.

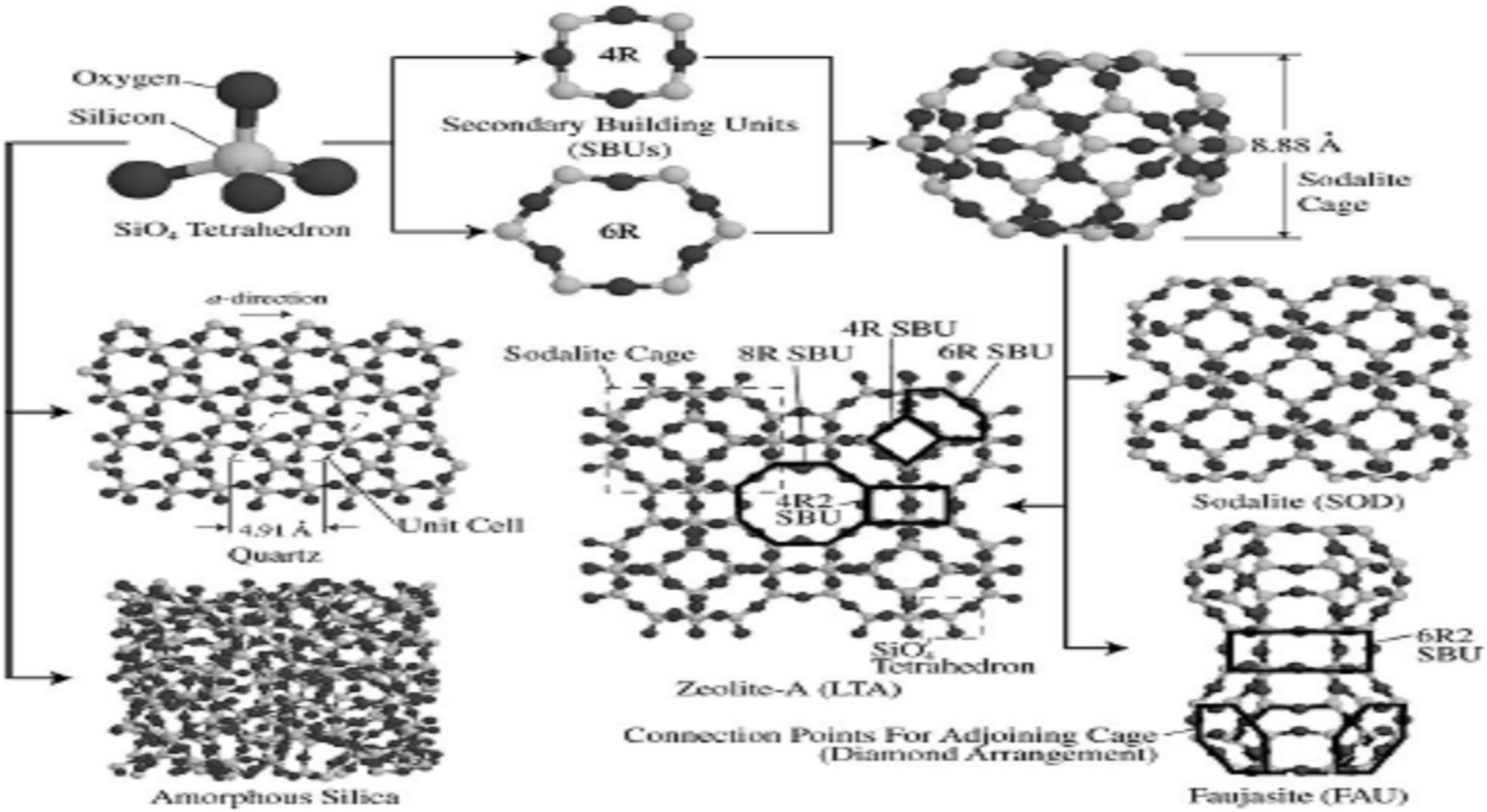


Figure 2.23: Silica structure building blocks and materials studied in the MD simulations.

2.6 Applications of zeolites

Some of the general practical applications of zeolites are:

- Ion-exchange beds in domestic and commercial water purification, softening, and separation of molecules (of certain range of sizes and shapes) for analyses.
- As catalysts in the petrochemical industry: for instance in fluid catalytic cracking and hydro-cracking. The hydrogen form of zeolites (prepared by ion-exchange) is powerful solid-state acids, and can facilitate a host of acid-catalyzed reactions, such as isomerisation, alkylation, and cracking.
- **Nuclear industry:** zeolites' alumino-silicate construction is extremely durable and resistant to radiation even in porous form. Once they are loaded with trapped fission products, the zeolite-waste combination can be hot pressed into an extremely durable ceramic form, closing the pores and trapping the waste in a solid stone block. This is a waste form factor that greatly reduces its hazard compared to conventional reprocessing systems (Dyer, 1988).
- **Heating and refrigeration: z**eolites can be used as solar thermal collectors and for adsorption refrigeration. In these applications, their high heat of adsorption and ability to hydrate and dehydrate while maintaining structural stability is exploited. This hygroscopic property coupled with an inherent exothermic (heat-producing) reaction when transitioning from a dehydrated to a hydrated form make natural zeolites useful in harvesting waste heat and solar heat energy. More importantly, the high pore volumes of zeolites are used to contain refrigerants with high volume part in unit mass, in the evaporated form.

- **Detergents:** the largest single use for zeolite is in the global laundry detergent market. This amounted to 1.44 million metric tons per year of anhydrous zeolite A in 1992.
- **Construction:** synthetic zeolite is also being used as an additive in the production process of warm mix asphalt concrete. It reduces weight per unit volume and helps moderate water content while allowing for slower drying which improves break strength (Dypayan, 2007)
- **Space hardware testing:** zeolites can be used as a molecular sieve in cryosorption pumps for rough pumping of vacuum chambers that can be used to simulate space-like conditions to test hardware bound
- **Medical:** zeolite-based oxygen concentrator systems are widely used to produce medical-grade oxygen. The zeolite is used as a molecular sieve to create purified oxygen from air using its ability to trap impurities, in a process involving the adsorption of nitrogen, leaving highly purified oxygen and less than 5% argon.
- **Agriculture:** clinoptilolite (a naturally occurring zeolite) is used as a soil treatment, by providing a source of potassium. If previously loaded with ammonium, the zeolite can serve a similar function in the slow release of nitrogen. Zeolites can also act as water moderators, in which they will adsorb up to 55% of their weight in water and slowly release it under plant demand. This property can prevent root rot and moderate drought cycles.
- **Animal husbandry:** both natural and synthetic zeolites have been used in animal nutrition mainly to improve performance traits and efficacy in the prevention of ammonia and heavy metal toxicities, poisonings as well as radioactive elements

uptake and metabolic skeletal defects (Degnan, 2000). It can be used in general odor elimination for all animal odors.

- **Aquarium keeping:** zeolites are marketed by pet stores for use as a filter additive in aquariums. In aquariums, zeolites can be used to adsorb ammonia and other nitrogenous compounds.
- **Cat litter:** non-clumping cat litter is often made of zeolite or diatomite.

2.7 Synthesis of Zeolites

The synthesis of zeolitic material can be categorized into two areas, i.e. natural synthesis and laboratory synthesis. The former is created from the power and uncontrolled natural forces, while the latter is under tamed and controlled conditions.

2.7.1 Synthesis of zeolitic material in nature

Naturally occurring zeolites are formed at temperatures below 200^0C from volcanic glass poorly crystallised clay, and feldspar or silica in wet situations, where there is a high ratio of Mg^{++} and H^+ to Na^+, K^+, and Ca^{++}. They are commonly found in a variety of sedimentary and igneous rocks and in soils. The main geological occurrences are in tuffs, tephra and volcaniclastic rocks in lakes or deep sea basins that have been subjected to relatively low temperature ($<200^0$C) hydrothermal alteration or burial diagenesis (Hay and Sheppard, 2001).

Original rock composition, temperature, pressure, pH, and the presence of some ions (Mg, H) and paucity of other ions (Na, K, Ca), control the type of zeolite produced. Less hydrous zeolites (laumontite, analcime and wairakite) are stable at higher temperatures than more hydrous

zeolites (clinoptilolite, chabazite and stilbite) (Sheppard and Hay,2001). Early formed zeolites are commonly replaced by other zeolites, such as the time sequence of clinoptilolite replaced by analcime, which in turn is replaced by laumontite (Hay, 1978). Also, the number of common species of zeolite decreases with increasing age (e.g. greater than 30 species in Cenozoic age rocks, 7 in Mesozoic, 4 in Late Paleozoic, 2 in Early Paleozoic and 1 common in Late Pre-Cambrian rocks) (Iijima, 1980). Experiments in the formation of natural zeolites have shown that the rate of formation is dependent on time, temperature, glass composition and the chemistry and flow rate of the pore water. Analcime, chabazite and phillipsite appear in five days from basalt glass maintained at 200^0C, and mordenite and analcime from rhyolite glass in 40-60 days at above 50^0C (Sheppard and Hay, 2001).

The pictorial description of events that lead to and favor the formation of zeolite in nature, is depicted in Figure 2.24.

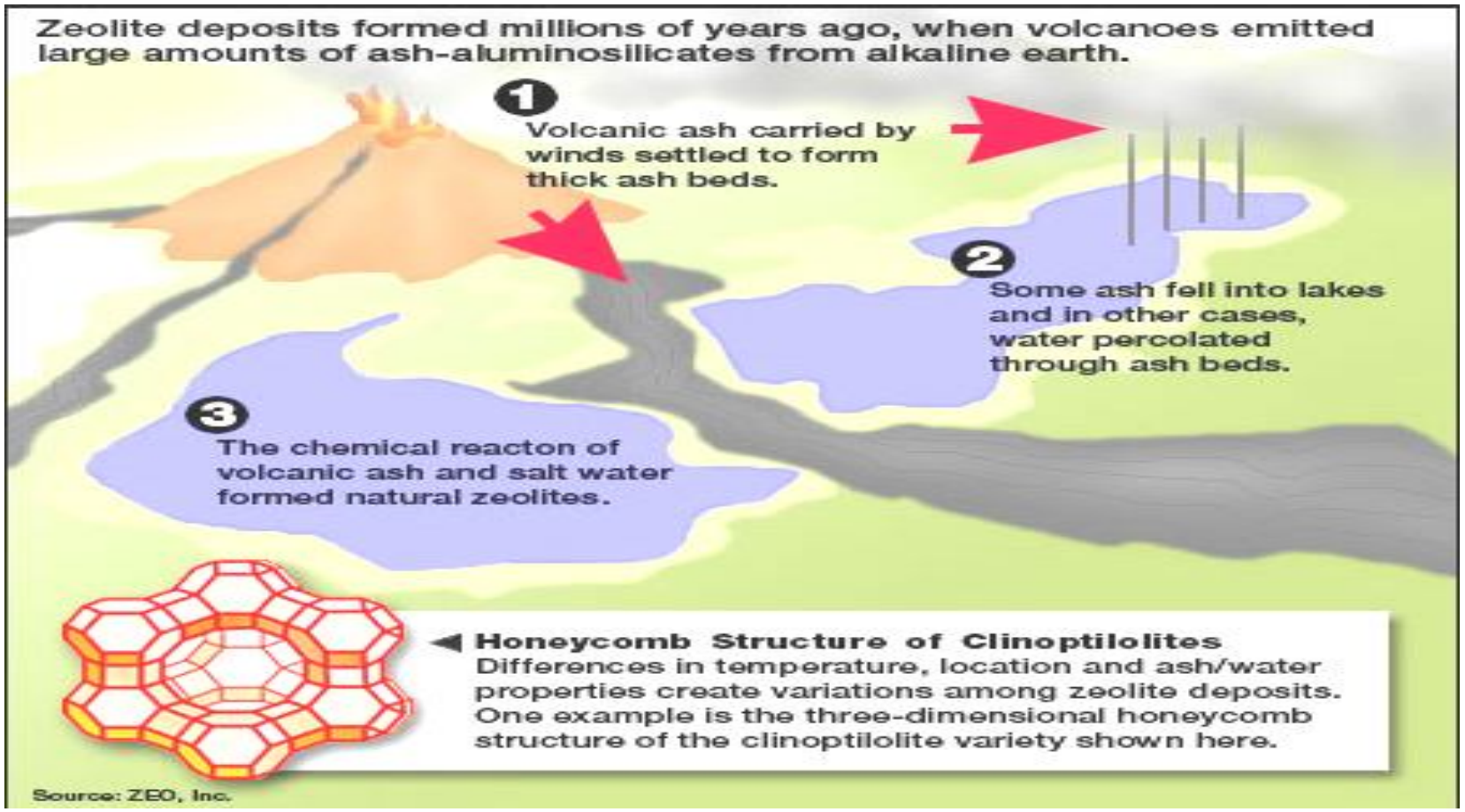


Figure 2.24: Formation of zeolite in nature

2.7.2 Laboratory synthesis of zeolites

The first claim to have made a named zeolite (levynite) in the laboratory was that of St. Claire Deville in 1862. Richard Barrer began his studies in the early 1940s, initially investigating the conversion of known mineral phases under the action of strong salt solutions at fairly high temperatures (ca. 170-270^{0}C). Using this approach in 1948, he synthesized the first zeolite unknown as a natural mineral-as two variants, species P and Q. (These materials were later found to have the KFI structure determined subsequently for zeolite ZK-5.

Robert Milton began his synthesis program in the laboratories of the Linde Corporation in 1949. The use of more reactive starting materials (freshly precipitated aluminosilicate gels) enabled reactions to be carried out under milder conditions. The rate of progress was astonishing. By the end of that year, zeolites A, B (now known as Na-P), and C (hydroxysodalite) had been prepared, together with a crystalline impurity designated X. In 1950, pure zeolite X (isostructural with the naturally occurring mineral faujasite) was isolated and also synthetic chabazite. The latter is notable as the original objective of both the Barrer and the Linde groups, since the scarce natural counterpart was the only material known at that time which was considered suitable for industrial separation applications, especially air separation and purification. By 1953, Milton and his colleagues (including, by that time, D. W. Breck) had synthesized 20 zeolites, including 14 unknown as natural minerals. The patents on zeolites A and X were filed in the same year, the publication date of 1959 reflecting the battles with the patent examiners over the novelty of these new types of materials (Milton, 1959).

2.7.3. Hydrothermal synthesis of zeolites

Since the pioneering work of Barrer and Milton on the synthesis of zeolites, the hydrothermal synthetic technique has become the basic route for zeolite synthesis. Hydrothermal synthesis usually refers to reactions occurring under conditions of high temperature-high pressure (>1000C,>1 bar) in aqueous solutions in a closed system. Nowadays, the concept of hydrothermal synthesis covers the entire region above room temperature and 1 bar. Hydrothermal synthetic techniques have been applied not only in the preparation of zeolites and related porous materials, but also in the preparation of most other important inorganic materials, such as superionic conductors, chemical sensors, electronically conducting solids, complex oxide ceramics and fluorides, magnetic materials, and luminescence phosphors.

2.7.3.1 features of hydrothermal reactions

The increasing interest in hydrothermal synthesis derives from its advantages in terms of high reactivity of reactants, easy control of solution or interface reactions, formation of metastable phases, and unique condensed phase, reduced air pollution, low energy consumption, etc.

On the basis of reaction temperature, the hydrothermal synthesis can be classified into subcritical and supercritical synthetic reactions. In **subcritical synthesis**, the temperature is in the range of 100-200^{0}C, while in **supercritical synthesis**, the temperature could reach 1000^{0}C and the pressure may increase up to 3000 bar. High temperature and pressure hydrothermal conditions accelerate the reaction rate among the complex ions, intensify the hydrolyzation reaction significantly, and change the redox potential of the reactants. Consequently, hydrothermal (high temperature and pressure) conditions can promote the reactivity of reactants with low solubility at ambient temperature.

Water can act as a mineralizer or a catalyst under elevated pressure-temperature conditions. The thermodynamic and transport properties of supercritical water are remarkably different from those of ambient water. The solubility of nonpolar species increases whereas that of ionic and polar compounds decreases. Under hydrothermal conditions, the physical and chemical properties of reactants also change significantly.

The dielectric constant of water will decrease with increase in temperature and increase with increase in pressure. However, it is more significantly affected by temperature than pressure. The high dielectric constant of water is confined to a small region of rather low temperatures. In contrast, in the supercritical region there is a large range where the dielectric constant is between 10 and 25-30. In general, electrolytes will be totally dissociated in water. However, the dissociated ions will tend to recombine as the temperature increases. For most of the substances, this transition occurs at 200-500^{0}C. The viscosity of water decreases with the increase in temperature. Consequently, the mobility of molecules or ions in water under hydrothermal conditions is enhanced significantly.

In general, under hydrothermal conditions (high temperature and pressure) water plays several roles which are as follows;

(i) acting as the solvent,

(ii) changing the chemical and physical properties of reactants and products,

(iii) accelerating the reaction,

(iv) participating in the reaction in some cases and

(v) Distribute the pressure.

Zeolites are crystallized in laboratory under mild temperature and pressure, by a hydrothermal synthesis process (Barrer, 1982). The nature of zeolite formed is determined by the specific synthesis conditions, i.e., reactant concentration, pH, reaction time, temperature, etc. The important factors affecting zeolite synthesis include: the nature of reactants, chemical composition and pretreatment, the method of reactant mixture preparation, the overall, homogeneity or heterogeneity of the mixture, pH of the mixture, and temperature of ageing of the gel, nucleation, seeding, presence of additives, temperature, pressure, and use of organic template. The resulting effects of these factors would be discussed later. The amorphous reactants containing silica and alumina are mixed together in presence of a cation source, usually with a high pH. The reactants for the source of alumina are generally sodium aluminate, aluminum nitrate, or aluminum phosphate. For the source of silica, generally sodium silicate, amorphous silica, or silica sol are used. Sodium hydroxide is normally used for the control of pH. The aqueous reaction mixture is heated to 100 ˚C or above in a sealed reactor. For some time after achieving the reaction temperature, the reactants remain amorphous. After this "induction period" the zeolite synthesis begins from the hydrous aluminosilicate amorphous gel. The carefully controlled conditions of the crystallization for the gel, gradually replaces all the amorphous phase into the desired zeolite phase. The sequence is shown as in Equation 2.7:

$$NaOH(aq) + NaAl(OH)_4(aq) + Na_2SiO_3 \xrightarrow{25^{\circ}C} \underset{gel\ phase}{Na_a(AlO_2)_b(SiO_2)_c \cdot NaOH \cdot H_2O}$$

$$\xrightarrow{25\text{–}175^{\circ}C} \underset{zeolite\ phase}{Na_j(AlO_2)_j(SiO_2)_y \cdot zH_2O} + solution \qquad 2.7$$

The resultant zeolite is then removed from the mother liquor, washed, and dried before any application (Bhatia, 1990; Szostak, 1998).The steps involved in zeolite synthesis are depicted in Figure 2.25. The key elements, i.e. Si and Al, which make up the microporous framework of

zeolite, are imported in an oxide form. These oxides and generally amorphous precursors contain Si-O and Al-O bonds. During the hydrothermal reaction in presence of a mineralizing agent, which is most likely an alkali metal hydroxide (e.g. NaOH), the crystalline zeolite product containing Si-O-Al linkages is created. Since the type of the bond of the product is very similar to that present in the precursor oxides, no considerable enthalpy change is anticipated. (Corma and Davis 2004; Cundy and Cox 2003; Navrotsky *et al.,* 1995; Piccione *et al*., 2002; Van Santen *et al*., 1989).

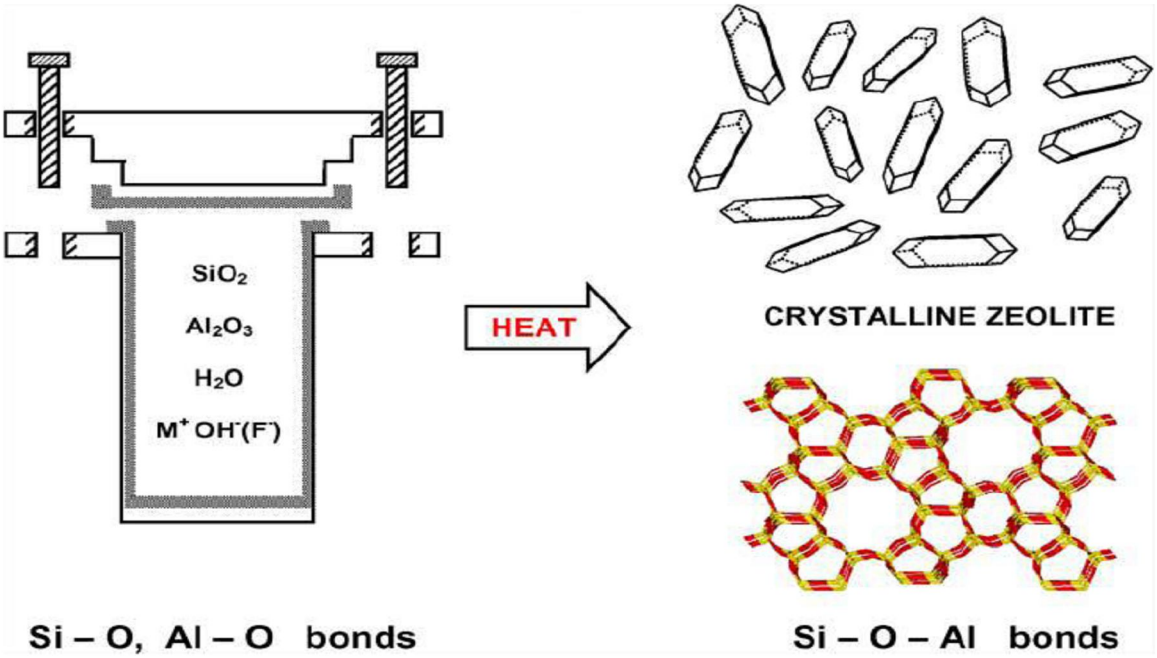


Figure 2.25: Hydrothermal zeolite synthesis.

The starting materials (Si-O and Al-O bonds) are transformed by an aqueous mineralizing medium, such as OH-and/or F-, into the crystalline product (Si-O-Al bonds). (Cundy and Cox, 2005)

Despite the fact that numerous studies have addressed the preparation of zeolites, it has been very difficult to model the complex mechanism by which they assemble from framework constituent precursor species. An improved understanding of the synthesis mechanism is pivotal for the design of new zeolites (only about 100 structures are known so far), and for the preparation of novel zeolitic assemblies such as zeolite thin films for membrane reactors, monoliths or functional nanostructures.

Although catalysis by zeolites has developed to a certain maturity, it is still a highly dynamic research area. Since the introduction of zeolite catalysts into petroleum refining in the early 1960s, the catalytic applications of zeolites have continuously conquered new fields. These include, in particular, the manufacture of synthetic fuels, fine and specialty chemicals, like pharmaceuticals, but also applications in environmental protection (Venuto, 1994). Substantial progress in the synthesis of (new) zeolites, increasingly sophisticated modification techniques, as well as improved computational and spectroscopic characterization tools have a major impact on the continuous improvement of zeolites as tailor-made materials for specific catalytic applications.

2.7.4 Mechanism of zeolite crystallization

Despite the advances made so far in zeolite synthesis, many ambiguities still exist concerning the mechanism of crystallization, including those concerning the autocatalytic kinetics of the crystallization process, the effect of alkalinity on the rate of crystallization, the specific nature of the induction period, the effect of seeding on reaction rate, and the effect of clathrating or templating cations. Relevant questions still exist concerning the role of solid and liquid phases in the heterogenous aluminosilicate systems responsible for the formation of zeolite crystalline phases. It is evident from series of review papers on mechanism of zeolite crystallization that it

represents one of the most complex chemical problems in crystallization phenomenon. The myriad of reactions involved in zeolite crystallization, including polymerization – depolymerization, solution – precipitation, nucleation – crystallization, declathration of certain zeolite precursors and the complex phenomenon governing aqueous colloidal dispersions, add to the overall complexity of these systems. As is pointed out by Barrer and Cole (1973), the result of this inherent complexity is that "The art of synthesizing molecular sieve zeolite has developed more quickly than the chemical science which would properly account for their formation in nature and in the laboratory from apparently simple aluminosilicate compositions."

The phenomenon of zeolite crystallization appears to be consistent with the simplicity principle proposed by Goldsmith (1953). In systems containing substances which can exist in the form of several polymorphs, those exhibiting most disorder or highest entropy will tend to crystallize first. The disordered form of an aluminosilicate gel is in a state of highest simplicity and entropy when compared to its ordered crystalline counterpart. During hydrothermal synthesis, in accordance with Goldsmith's simplicity principle, the formation and development of nuclei exhibiting maximum simplicity are preferred. Goldsmith states there is a gradual transition from simplicity to complexity and thereby, from maximum disorder to maximum order. Therefore, the nature of the phases present at a specific time during hydrothermal synthesis is governed by both thermodynamic and kinetic factors. A more complex structure which might be more stable under hydrothermal synthesis conditions is likely to require more time to evolve its complex ordering. Therefore, Goldsmith's principle states that the simple crystalline phase is kinetically favored and thermodynamically disfavored; whereas, the most complex crystalline phase is kinetically disfavored but thermodynamically favored. Fortunately, the nuclei of several metastable zeolite phases may develop before the nuclei of the most ordered structures. If not for this fact, synthesis of certain zeolites would not be possible. According to Breck, (1974), "It is

probable that many of the synthetic zeolites which do not have mineral relatives are non-equilibrium phases and do not exist when true equilibrium conditions prevail".

The schematic representation of the free energy relationships between the reaction mixture and various aluminosilicate phases is shown in Figure 2.26. The initial reaction mixture consists of components which first form the phase denoted A, which may subsequently be converted to B or C, given sufficient time. In the region of temperature where phases A or B both can form, the nucleation and growth rates are important because the metastable phase A, which preferentially forms, may transform to more stable phases B and C in succession, depending on various factors.

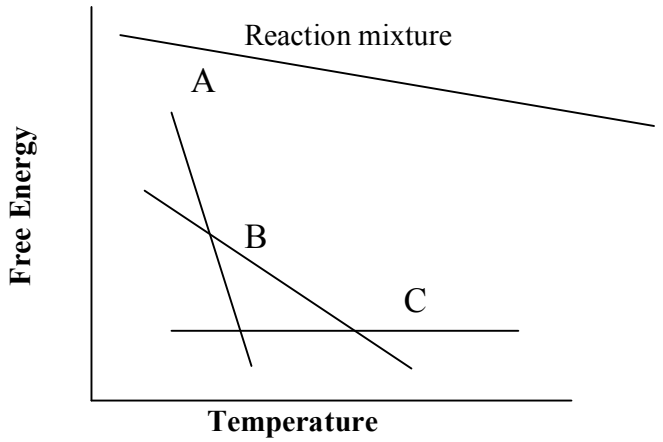


Figure 2.26: Schematic free energy relations between reaction mixtures and various zeolite phases, represented by A, B and C.

Inspite of the advances in zeolite synthesis, the mechanism of crystallization is not well understood. Zeolites can be synthesized using solid-containing gels and also from clear solutions. In this chapter, crystallization from solid-containing gels is covered in more depth for the reason that the commercial synthesis of zeolite uses an amorphous gel phase with high solid content as the starting material. The gel phase is formed by mixing silicate and aluminate solutions, at basic pH in which the source of silicon and aluminum is either polymeric or

monomeric. The synthesis generally takes place in the temperature range of 60-200ºC. Depending upon the operating conditions, the gel starts to dissolve in the solution and an intermediate in the form of an oligomeric aluminosilicate starts to grow. The intermediate crystallization phase is very complex process that cannot be described by a single crystallization mechanism. Finally, a crystalline phase starts to grow after an induction time (Serrano and Grieken, 2001). Conclusively, the most probable pathway to describe zeolite synthesis is a sequence of induction period, followed by nucleation and then crystal growth.

2.7.4.1 induction period

The induction period is a time interval (τ) between the start of the reaction and the time when the first crystalline product is observed. Generally this period is taken as the interval between the time at which the reactants reach the reaction temperature and the time when a method of analysis detects the first solid product. For precipitation reactions, the classical nucleation theory (Mullin, 2001) divides this period (τ) into three subunits:

$$\tau = t_r + t_n + t_g \qquad 2.8$$

where, t_r is considered as the relaxation time, which is the time required —for the system to achieve a quasi-steady-state distribution of molecular clusters. In case of zeolites, this may be considered as the equilibration reactions that take place upon mixing the reactants and allowing them to reach reaction temperature. During this period, a distribution of silicate and aluminate ions, and other species is established.

From equation 2.8, t_n and t_g are defined as the time required for the formation of a stable nuclei and the time required for the nucleus to grow to a detectable size, respectively. It is apparent from the above that the induction period covers all the important events in zeolite formation.

Before the induction period, there are only individual reactant molecules; and after the induction period, the reaction mixture contains a large number of small and stable zeolite crystals, which are on the path of further growth.

2.7.4.2 nature of amorphous phase

It was initially considered that the reactants, which were composed of an amorphous phase, remained essentially unchanged throughout the synthesis. Such an approach is normally adopted for reaction modeling purpose (Lowe, 1988; Thompson and Dyer, 1985a; Thompson, 1992a). On the other hand, the dynamic nature of the amorphous phase was first pointed out by several mechanistic studies. Flanigen and Breck (Flanigen and Breck 1960a) found that the transformation of amorphous phase takes place through polymerization and depolymerization catalyzed by excess hydroxyl ion. At the same time Zhdanov (1971a) and Kerr (1973) established that the initial amorphous phase comes to an equilibrium phase with the liquid phase and releases active soluble species into the solution. Such transformations in the amorphous phase are important in the early stages of synthesis reaction.

2.7.4.2.1 primary and secondary amorphous phase

When the synthesis reactants are mixed together, a visible gel is generally formed. This gel is considered as the primary amorphous phase. In some cases, e.g. synthesis from clear solution, this primary phase is colloidal and is invisible to naked eye. But its behavior and function are essentially the same. The primary amorphous phase is basically the initial and intermediate product from mixing the reactants. It is non-equilibrium and heterogeneous in nature and may contain precipitated amorphous aluminosilicates, coagulated silica and alumina that are precipitated from the starting material which is destabilized by change in pH and increase in salt content, and some unchanged reactants (Cundy and Cox,2005). Upon standing at room temperature for some time or heating the reactants to reaction temperature, the above amorphous

phase undergoes changes due to equilibration reactions and is converted into a pseudo-steady-state intermediate called the secondary amorphous phase. In the equilibration reaction, the relationship between solid and solution phases approaches equilibrium and a characteristic distribution of silicate and aluminosilicate anions is established. Figure 2.27 depicts this scenario.

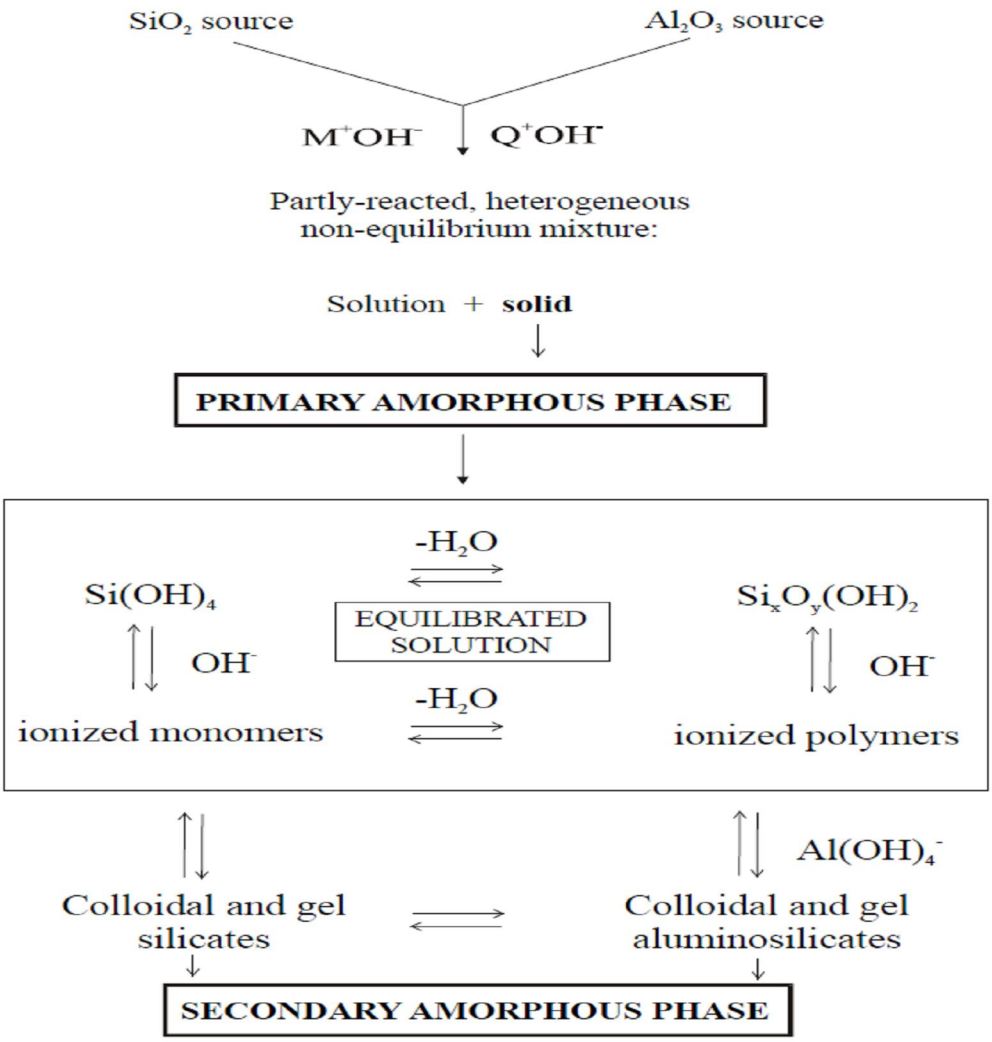


Figure 2.27: Equilibration of the starting mixture to establish a partly ordered secondary amorphous phase and a characteristic distribution of solution species. (Cundy and Cox, 2005)

In case of high silica zeolite synthesis the pH measurements start to change as the primary amorphous phase undergoes transformation into secondary amorphous phase, thus by monitoring pH changes one can monitor the course of this transformation. In the final stage of synthesis reaction at an elevated temperature for a prolonged period of time, the secondary amorphous phase is converted into crystalline zeolite product, as shown in Figure 2.28. Zhdanov (1971a) clearly represented the concept of equilibrated intermediate phase in synthesis process. He measured, for the first time, the effect of temperature in increasing the crystal growth rate, and observed that the crystal grew at a nearly constant rate over most of the synthesis period for zeolite A. Based on his measurement; Zhdanov was able to deduce the nucleation rate profile over the course of reaction. This reflects that the solid and liquid phases are connected through the solubility equilibrium, and the condensation reactions give rise to primary aluminosilicate blocks (4- and 6-membered rings) and crystal nuclei. The crystal growth takes place until the dissolution of amorphous phase is complete.

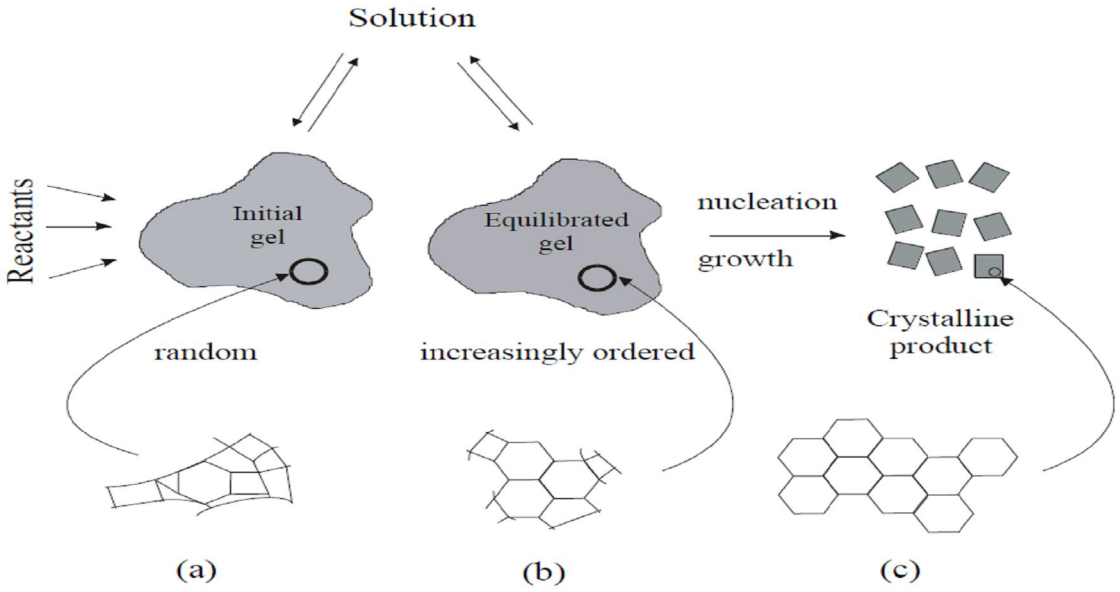


Figure 2.28: The emergence of order, from the primary amorphous phase (a) through the secondary amorphous phase (b) to the crystalline product (c). (Cundy and Cox 2005)

The conventional sigmoidal plot, as shown in Figure 2.29, indicated a typical crystallization mechanism of induction-nucleation period (about 3 days) followed by a crystal growth period (about 3-7 days), when examined with the XRD. On the other hand, the curve on the sigmoidal plot for IR crystallinity showed a completely different pattern. It showed that for a short span of synthesis time (i.e. 6hr), the IR spectrum detected larger than 60% crystallinity. The XRD, on the other hand, showed amorphous phase up to 6 hrs of operation and 97% of crystallinity after 3 days of reaction. To explain the marked difference between the two analyses, Scherrer formula was used which led to the establishment, that crystallite size below 8 nm was not detectable on the XRD machine, which led to the conclusion that the XRA zeolite must have crystals with less than 4 unit cells. The crystallinity under IR spectrometery for synthesis time less than 6 hr was not repeated. The XRA zeolite was loaded with Pt and tested for the hydro-conversion of n-decane, and compared with activities of HZSM-5, USY, and silica-alumina catalysts. It was established that XRA zeolite showed an activity very similar to that of HZSM-5 significantly higher activity when compared to silica-alumina catalyst (Jacobs *et al.*, 1981).

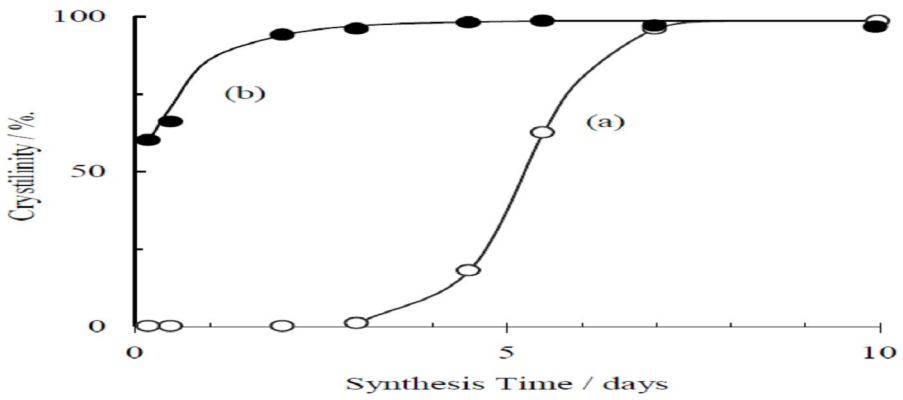


Figure 2.29: Change of the crystallinity of ZSM-5 materials with synthesis time: (a) X-ray crystallinity derived from peak summation between 2θ = 22 and 25°; (b) IR crystallinity using the 550 cm^{-1} skeleton vibration in a KBr pellet technique with the 2200 cm^{-1} vibration of KCN as internal standard. Redrawn with permission from Jacobs *et al.*, 1981.

The crystal growth mechanism has been described to occur in two different ways. The first mechanism was reported as crystallization by solid hydrogel transformation during the nucleation and growth process of various zeolites (Breck and Flanigen, 1967; McNicol *et al*., 1973). The second mechanism, in contrast to the first, demonstrated the role of liquid phase ion transportation in the growth of different zeolite nuclei.

Derouane *et al*., (1981) made a major contribution by proposing a theory to explain the mechanism of crystal growth through two distinct processes. Pentasil (ZSM) zeolites were synthesized in the presence of TPA, as structure-directing agent, by two different methods (Argauer and Landold, 1972; Chen *et al*.,1978). For ZSM-5 zeolite type A, Si/Al and Na/Si ratios were low and the source of silica was a solution of active silica (solid, polymeric), and the synthesis was found to take place by liquid phase ion transportation. For type B, Si/Al and Na/Si ratios were high and the source of silica was a solution of sodium silicate (liquid, mono- and poly-silicate anions), and the synthesis appeared to be solid hydrogel transformation. The sigmoidal plot, as shown in Figure 2.30, shows that 100% crystallinity was achieved in 300-330 hr for type A and in 45-50 hr for type B, thus establishing a distinct role of the type of silica.

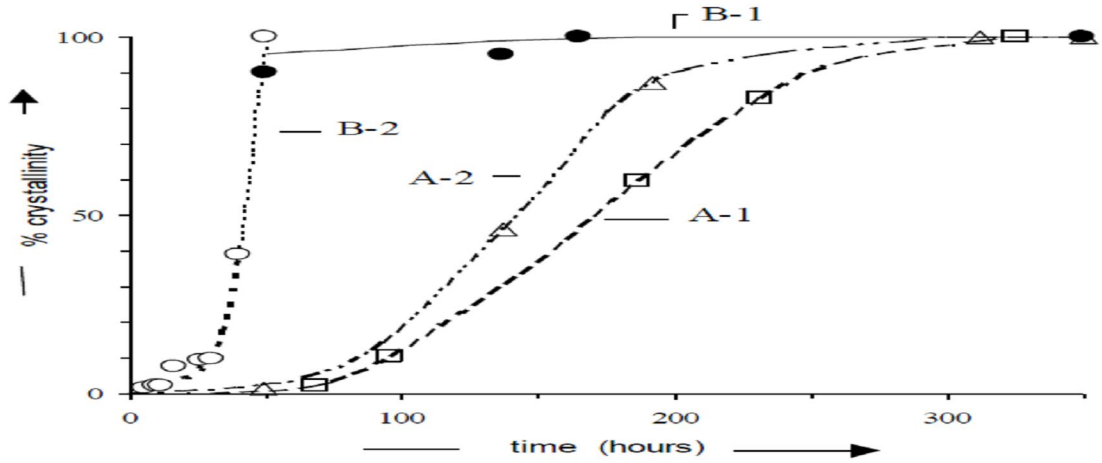


Figure 2.30: Crystallization curves for typical type A and type B syntheses. Redrawn with permission from Derouane *et al*. (1981).

Figure 2.31 depicts a schematic presentation of both mechanisms. In type A synthesis, solid (active) silica, initially present as colloidal silica particles dissolves in highly alkaline medium that leads to a depolymerization-hydration process that ultimately forms soluble monomeric silicate anions. As a result, a mixture of silica sol, dissolved silicate, and polysilicate ions is formed. The aluminum entities remain in solution in monomeric form.

The silica monomers are continuously produced on the surface of the colloidal silica particles and condensed with aluminate ions to form alumino-silicate complexes, which transforms the colloidal silica particles into a silica-alumina sol.

Changes occur on the surface of the silica-alumina sol and this restructuring moves inward as further depolymerization occurs. As the aluminum supply is progressively depleted, the inner core of the colloidal silica particles contains less aluminum than the surface, which leads to a non-homogeneous aluminum distribution. The inner core may be depolymerized at a lower rate than the outer shell, thus rendering the low depolymerization rate as the rate limiting step. As a result, gel composition remains low in the beginning and progressively increases with depolymerization. Thus, nucleation takes place at a limited rate from the available siliceous monomers and crystal growth takes place at a faster rate because its activation energy is less than nucleation (Erdem and Sand, 1979). The low depolymerization rates lead to small number of nuclei formation and hence large crystallites.

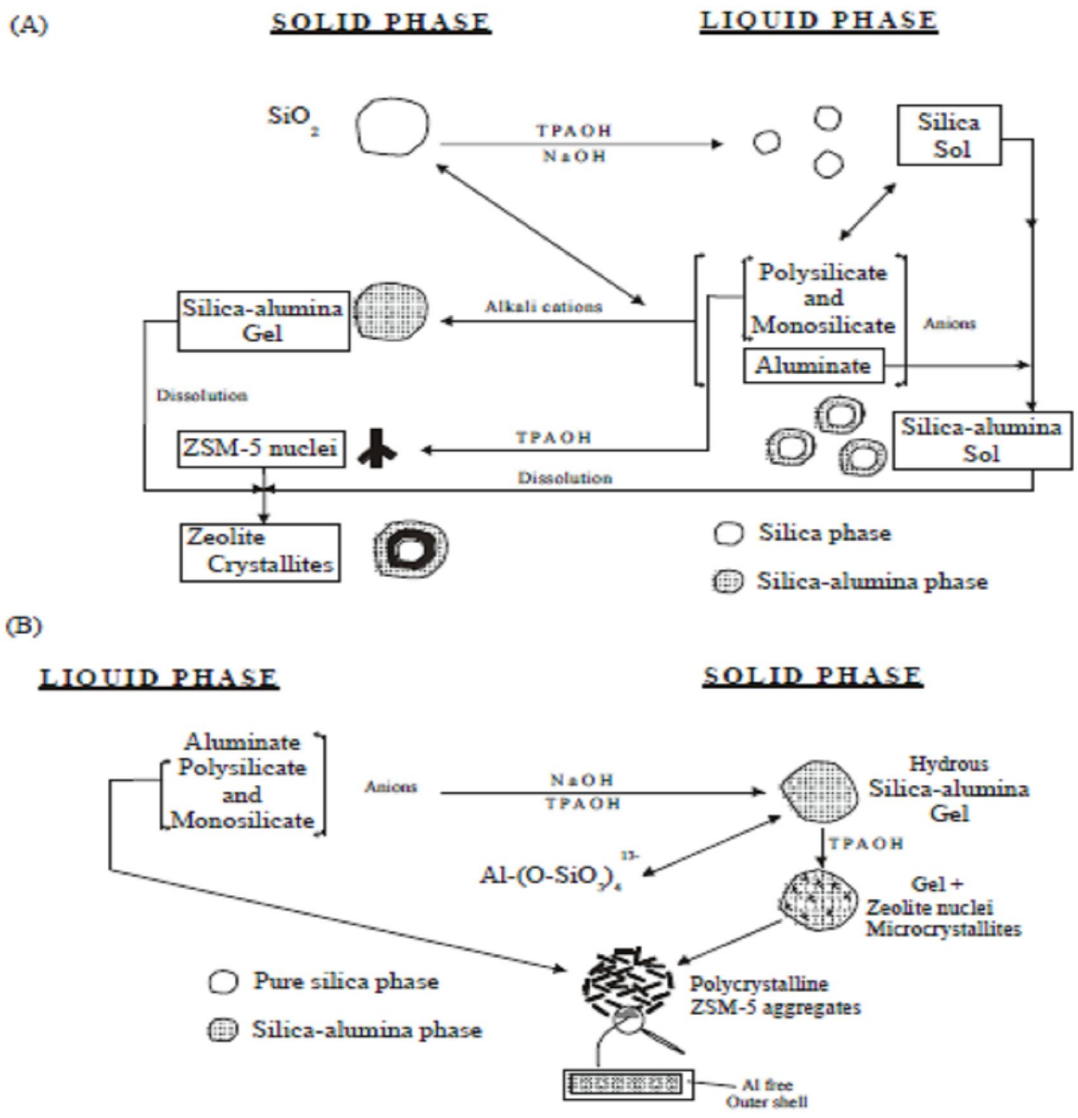


Figure 2.31: Zeolite crystallization mechanisms: (a) solution mediated process (type A); (b) hydrogel reconstruction (type B). Redrawn with permission from Derouane *et al*.,1981.

In type B synthesis, sodium silicate provides momomers in the presence of some small oligomer species and aluminate species in monomeric form (Moolenaar *et al*.,1970). A mixture of both species immediately yields a hydrous alumino-silicate gel within the solution with high Na content and some TPA cations. Since the supply of silicate anions is not limited by

depolymerization of Si reagent, the composition of the gel (Si/Al) throughout the synthesis process is therefore not much different from the reagent ratio. The high Si/Al and Na/SiO_2 molar ratio, and a uniform Al radial distribution throughout the gel favour a rapid nucleation rate with the help of TPA cations that are present throughout the gel. As a result, a rapid crystal growth yields a large number of small crystallites, which are not apparent in the SEM images until nearly 100% crystallinity is achieved. Under these conditions, a direct crystallization process is postulated involving a solid hydrogel transformation. The constant Si/Al molar ratio throughout the crystallization process shows that the growing crystallites and their gel precursors maintain the same composition, which further strengthens the direct hydrogel transformations through internal rearrangements. Studies of the syntheses of zeolite Y and mordenite further confirmed the mechanism of solid hydrogel transformations as low molecular weight species of Si were absent in the analysis of the solution by liquid 29SiNMR (Bodart *et al*., 1986).

It was also observed that solid hydrogel transformation process yielded polycrystalline aggregates instead of individual crystals. Furthermore, no evidence of crystal growth was observed for synthesis time less than 4 hours (Derouane *et al*., 1981). Many other groups have reported the existence of the secondary amorphous phase. Angell and Flank (1977) reported for zeolite A synthesis that the initially formed sodium aluminosilicate gel was converted to an amorphous aluminosilicate intermediate through solution transport. This material was further converted to crystal via basic medium dissolution. Fahlke *et al*., (1987) also observed for Y zeolite synthesis that there was an immediate precipitation of silica-rich primary amorphous gel, followed by its slow dissolution and then precipitation to a secondary amorphous gel having a similar Si/Al ratio to that of final zeolite product. In the late 1970s, Khatami and Flanigen (Breck, 1974) observed the crystallization of zeolite X in the absence of a liquid phase.

Interrupting the crystallization of zeolite X near the end of the induction period, the liquid phase of the gel was removed and the solid phase dried in ambient temperature to a free flowing powder of composition 1.1 $Na_2O.Al_2O_3.2.7Si_2O.4.6H_2O$. This dry powder which was initially X-ray amorphous showed 2% levels of crystalline zeolite X after 10 days at ambient temperature and 20% zeolite X after 47 days.

Among these groups, Montpellier group (Nicolle *et al.*,1993) performed a very informative study. Their study clearly indicates the multistage-nature of the zeolite synthesis reaction as shown in Figure 2.28. They prepared several samples of Na, TEAaluminosilicate gels with different compositions (TEA=tetraethylammonium), and heated to 150 ˚C for two sets of duration, i.e. for a short time and for a longer period of time.The solid products from each reaction time were removed and analyzed. The aim of using different heating times for a particular composition was to obtain an equilibrated gel and the final crystalline zeolite product. The four chosen compositions (A-D) were finally crystallized to (A) zeolite beta, (B) mordenite, (C) ZSM-12, and (D) ZSM-5.

The most interesting findings were obtained by analyzing the initial and equilibrated products. X-ray diffraction showed only the broad spectrum indicative of local ordering but no sharp peaks for crystalline structure. Analysis under ^{27}Al MAS NMR spectroscopy showed only tetrahedral coordination in aluminum and no zeolitic bands in their infrared spectra. Chemical analysis indicated that the hydrothermal treatment had largely changed the composition of the solid phase as compared to that before heating for the case when Na^+ cation was replaced by TEA^+. It was found that the TEA content was almost constant, i.e. one organic cation per 12-16 T-atoms, whatever the method of preparation or Si/Al ratio used. It was also established after the calcination of equilibrated samples A and B, the cation exchange capacities were in close

agreement with their aluminium content (i.e. ≈85 mmol NH_4^+/100 g). It was also established that the calcination of equilibrated samples A-C generated a micropore system having about 60% volume capacity as shown by zeolite beta crystallized from composition A.

The authors concluded that the equilibrated, amorphous samples were different from the gel that was initially precipitated at room temperature, and had been formed by dissolution or rearrangement within gel and reprecipitation. These secondary amorphous products were silicoaluminates and shared several properties with high-silica zeolites. For both durations of reaction time, the clusters of silica or alumina tetrahedral had gathered around the bulky TEA molecule, whose decomposition upon calcinations left a micropore system. The essential difference between the two classes of solids (equilibrated and zeolite) was defined by the dispersion of cluster geometry.

Zeolites show well-defined and repeatable site geometries, whereas the equilibrated amorphous products show irregular, aperiodical, and locally organized geometries. It has also been observed by other data that the above general observation is not only associated with the synthesis of zeolites templated by quaternary ammonium ion, but also similar phenomena is further observed in preparation of aluminous zeolites without using an organic template (Angell and Flank, 1977; Fahlke *et al.*,1987). In another study, Tsuruta *et al.*, (1986) investigated the initial product formation during the synthesis of zeolite A from concentrated solutions in the presence of an anionic surfactant. From the results of X-ray and electron diffraction, it was observed that the amorphous aluminosilicate, which was isolated from the solution under mild reaction conditions (i.e. 60 ºC, 15 min), contained a short-range order of Si and Al atoms similar to that in crystalline zeolite A. Subotic and coworkers (Subotic *et al.*,1994; Krznaric *et al.*, 1998) also investigated the

structural properties of X-ray amorphous sodium and potassium aluminosilicate gels, using electron diffraction, thermal analysis, and FTIR spectroscopy.

It was established that the X-ray amorphous material contained structurally ordered region or particles of a partially crystalline phase inside an amorphous matrix. A further hydrothermal treatment in 2M NaOH at 80 ºC formed the zeolite A and X. With the help of EXAFS and XANES spectroscopy, Walton and O'Hare (2001) examined the amorphous gallium silicates, which were separated in the early stages of hydrothermal synthesis of Ga-hydroxysodalite. It was established that Ga and Si K-edge EXAFS showed some degree of medium range order, indicative of an extended network of Ga(OSi)4 and Si(OGa)4 units, which resembled the structure of crystalline product. Yang *et al*., (2004) carried out a related study on the amorphous zeolite A precursors using multinuclear MAS NMR and neutron diffraction techniques. Noticeable change in the medium order before the crystallization was observed as the Al in the presence of Na^+ cations was incorporated into the Si network. At the same time, diffraction and spectroscopic techniques did not indicate the presence of well-defined structural units before the formation of zeolite crystals. Very similar results were obtained in an earlier study of various zeolite syntheses using 129Xe NMR technique (Ito *et al*.,1989). The gel structuring (large cavities) was found evident for Na,TPA-ZSM5, and NaY zeolites but not for Na,TEA-ZSM20. The NMR measurements for NaY only showed any appreciable microcrystalline formation in the absence of XRD crystallinity.

Another school of thought claimed that, zeolite synthesis starts and terminates within the solution phase. If during drying the sample was not dried properly, the little existing moisture which might seem insignificant could facilitate the progress of the reaction in an almost completely solid phase. Various authors are reporting this observation. Culfaz and Sand (1973)

proposed a mechanism wherein nucleation occured at the solid liquid interface. In this mechanism it was proposed that nucleation, mass transfer of species by surface diffusion, and zeolite crystallization occured in a boundary layer at the solid liquid interface. Support of this surface nucleation mechanism was given by Kerr and Ciric through the epitaxial growth which he observed in the co-crystallization of zeolite L, offretite and erionite. Most references concur with what was originally stated by Zhdanov in 1965 “The nuclei of zeolites begin to form in the liquid phase of gels or at the interface of gel phases”.

Morey and Ingerson (1937) proposed a mechanism for zeolite crystallization involving the formation of a solid amorphous precursor which is followed by a solution crystallization mechanism. Zhdanov, who reviewed the afore-mentioned mechanism, proposed that a quasi equilibrium between the solid and liquid phases in the gel occurs and further nuclei form and grow in the liquid phase (Zhdanov, 1971a).

Conclusively, it can be summarized that initially the reaction mixture for zeolite synthesis contains a non-equilibrium combination of components that is heterogeneous or may be partly reacted, and thus called primary amorphous phase. With time (t_r) and especially upon heating the reaction mixture, the silicate and aluminosilicate equilibration reactions start to take place that lead to a redistribution of species between the solid and the liquid phase as they approach equilibrium with each other.

Cations play a very important role of structure directing agent in the organization of the solid phase. The newly generated solid phase, created in the presence of cations, has a similar chemical composition that is attributed to the final zeolite product, but it lacks long-range periodical organization and hence remains X-ray amorphous, and thus called secondary

amorphous phase. Even though there remain some disagreement, the picture about the formation of zeolites from the initial amorphous gel to the final crystalline zeolites has become much clearer. Cundy and Cox have presented comprehensive reviews on the hydrothermal synthesis of zeolites in which the mechanistic aspects of zeolites synthesis are discussed in detail.

2.7.5 Conditions necessary for zeolite crystallization

In general the conditions used in zeolite synthesis are as follows:

- Reactive starting materials such as freshly co-precipitated gels, or amorphous solids.
- Reactively high pH introduced in the form of an alkaline metal hydroxide or other strong base.
- Low temperature hydrothermal conditions with concurrent low autogenous pressure at saturated water vapor pressure.
- A high degree of super saturation of the components of the gel leading to nucleation of a large number of crystals.

The term aluminosilicate gel is used to denote a hydrous metal aluminosilicate which is prepared from aqueous solutions, reactive solids, colloidal sols, or reactive aluminosilicate such as the dehydroxylated residue structure of metakaolin. A substantial increase in fluid viscosity generally occurs the instant a dissolved sodium aluminate species and sodium silicate species are mixed. This gel formation is thought to occur by the co-polymerization of individual silicate and aluminate species by a condensation polymerization mechanism.

The representative chemical reactions involved in the formation of gel and crystallization of zeolite in the Na_2O-Al_2O_3—SiO_2-H_2O system can be represented by Equations 2.7 (a and b).

$$NaOH\ (aq) + Na\ Al(OH)_4\ (aq) + Na_2\ SiO_3\ (aq)$$
$$\xrightarrow{T_1 = 25^0 C} (Na_a\ (AlO_2)_b\ (SiO_2)_c . NaOH\ .\ H_2O)\ gel \quad \text{.....2.7}(a)$$

$$(Na_a\ (AlO_2)_b\ (SiO_2)_c . NaOH\ .\ H_2O)\ gel$$
$$\xrightarrow{T_2 = 25\ to\ 175^0 C} Na_x\ \left((AlO_2)x\ (SiO_2)y\right) . mH_2O + solution \quad \text{.....2.7}(b)$$

As shown in the Equations 2.7(a) and 2.7(b), there are three major components which lead to the formation of an aluminosilicate gel. The first component, typically sodium hydroxide, serves to contribute charge compensating cations and also adds hydroxyl ion to increase the pH of the system. Note that the rate of depolymerization of silica and alumina depends on the level of alkalinity of the reacting medium. The second and third major components are the aluminum source and the silicon source. Accordingly, it becomes imperative for researchers in this area to be acquinted with the chemistry of both silica and alumina, as these are the two basic ingredient needed for zeolite synthesis.

2.7.5.1 Chemistry and depolymerization of alumina

At moderated Na_2O concentration less than 25 wt% (alkaline solution) the anionic form of aluminum is known to exist as $Al(OH)_4^-$. But if Na_2O concentrations exceed 25 wt%, the $Al(OH)_4^-$ anion dehydrates to yield AlO_2^-. Two possible dehydration steps are shown in Equations 2.8 (a and b).

$$Al(OH)_4^- \rightarrow AlO(OH)_2^- + H_2O \quad \text{.....2.8(a)}$$

$$2Al(OH)_4^- \rightarrow ((OH)_3Al\text{-}O\text{-}Al(OH)_3)^- + H_2O \quad \text{.....2.8(b)}$$

Although existing evidence is not conclusive, the Equation 2.8b dehydration process is considered more probable. Dehydration of the $Al(OH)_4^-$ anion to AlO_2^- is likely to prevent the

dehydration polymerization process from which zeolites are formed. Increasing alkalinity at constant temperature ($Na_2O + H_2O \rightarrow 2NaOH$) influences the crystallization kinetics in the same direction as increasing temperature at constant alkalinity.

The effects of increasing alkalinity at constant temperature; i.e. shortening the induction time and increasing the crystallization rate, occurs only within a certain stability field for a given zeolite. If the alkalinity is increased outside the stability field of Na_2O-SiO_2-Al_2O_3 ternary phase zone, zeolite formation is slowed and prevented.

It is likely that the dimmer Al-O-Al bond formation in Equations 2.7 (a and b), occurring by the second dehydration mechanism, can only serve to reduce the rate of zeolite crystallization. It has been stated before that according to Lowenstein's rule, Al-O-Al bonds cannot occur within the zeolite framework. The possible formation of this aluminum hydroxide dimmer therefore, would reduce the diffusion rate of the aluminum to the growing zeolite surface as it is a more bulky anion. Further, if one end of this dimmer underwent dehydration polymerization with a surface silicic acid, a zeolite could not be subsequently formed unless the Al-O-Al bond was cleaved. Aluminate solutions are, therefore, relatively simple, as the $Al(OH)_4^-$ ion are the dominant anionic species. With silicate solutions, this is not the case and silicate chemistry is more complex in general because of the multitude of polymeric species which are known to occur.

2.7.5.2 Chemistry and depolymerization of silica

Silica is used as an abbreviation for silicon dioxide in all of its forms; i.e. crystalline, amorphous, hydrated, or hydroxylated. The structure and chemistry of silica are very similar to that of water. Silica and water consist mainly of oxygen atoms with smaller hydrogen or silicon atoms

interstices. In neutral or acidic solution silica exists as the hydrated monomer $(SiOH)_4$, while in basic solution it exists as silicate ions . "Some properties of water and silica are so similar, that the transition between hydrated silicic acids and the aqueous matrix is a gradual one". The dissolution of silica involves simultaneous hydration and depolymerization. The dissolution depolymerization reaction resulting in silicic acid is represented by Equations 2.9a to 2.9d

$$(SiO_2)n + 2nH_2O \rightarrow nSi(OH)_4 \quad \text{.....2.9}a$$

$$Si(OH)_4 + H_2O + OH^- \rightarrow (H_2O)Si(OH)^-_5 \quad \text{.....2.9}b$$

$$\frac{(H_2O)\,Si\,(OH)_5}{(OH)^-(Si(OH))_4^-} = 2.85\,x\,10^4 \quad \text{.....2.9}c$$

$$(SiO_2)_X + 2H_2O \underset{DEHYDRATION}{\overset{HYDRATION}{\longleftrightarrow}} (SiO_2)_{x-1} + Si(OH)_4 \quad \text{.....2.9}d$$

Silica is relatively water insoluble compared to other minerals, which upon dissolution results in weak silicic acid as shown in Equation 2.9a. If the assumption is made that the concentration of the monomer $Si(OH)_4$ does not change with pH, the increased solubility of silica with increasing pH can be explained on the basis of the equilibrium constant shown in Equation 2.9(c) (Breck,1974). The overall reaction showing the dissolution and deposition of silica in water is shown in Equation 2.9(d).

The solubility of silica in water is defined as the concentration of $Si(OH)_4$ reached at steady state in the depolymerization – polymerization equilibrium. Certain materials have the capacity to catalyze the rate of dissolution of silica. The catalysts is here referred to as a materials that can be chemi-adsorbed and increases the coordination number of a silicon atom on the surface to more than 4, thus weakening the oxygen bonds to the under-lying silicon atoms.

On the silica's surface there are spaces between the oxygen ions sufficiently large to accommodate hydroxyl ions. The surface hydroxyl groups which are called silanol groups are exposed to the aqueous phase. Loss of hydrogen from a silanol group causes the surface to be ionically charged; therefore the mobile silicon atom which can be ruptured from the silica's surface have the tendency to enter the solution as a silicate ion. **If the pH of the solution is above 11, the silicate ion is relatively stable, but if the pH is below 11, the silicate ion hydrolyzes to soluble silica $Si(OH)_4$ and OH^- ions.**

2.7.5.2.1 Stability and activation energy of silica structure

It has been established that silica is a very stable polymeric material that tends to recombine via siloxane viz-a-viz silanol bridges. The activation energy required for formation of zeolite (E_A') from siliceous material is seen to be higher compared to that required for the recombination of silica (E_A") as shown in Figure 2.32. Perhaps, this is the reason why it appears that virtually all the surface of the earth is mainly siliceous. This observation also points to the fact that silica is the most stable phase of all the minerals existing in the world. And perhaps, the similarity of the structure and chemistry of silica and water, may be suggestive the abundance of water, also on earth.

In addition, one can conclude from Figure 2.32, that synthesis of zeolite should be done with instant product removal, to avoid the following; (i) recombination of unconverted silica to more stable phase –quartz- and (ii) termination of the hydrogel synthesis.

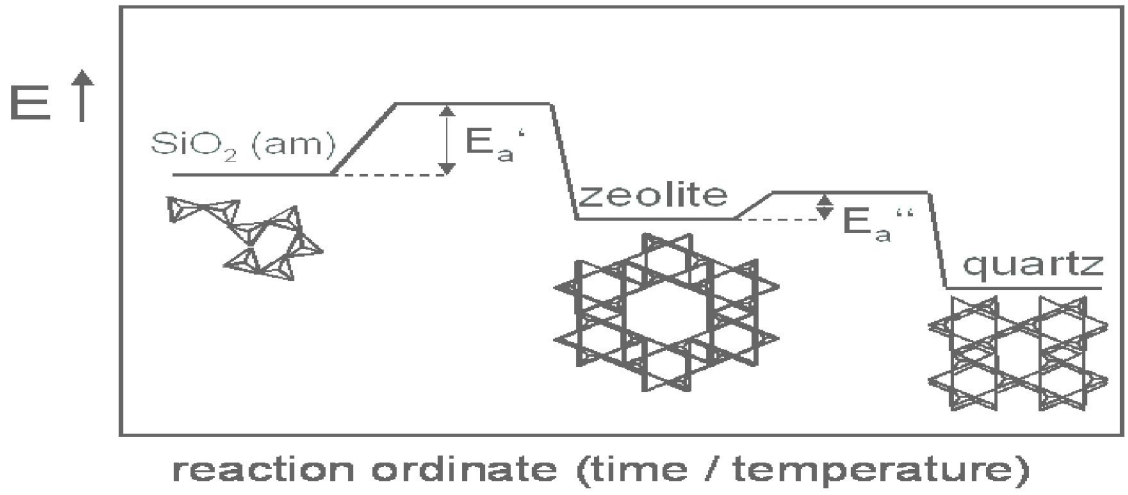


Figure 2.32: Activation energy requirement for silica stabilization

Zeolite formation is both thermodynamically and kinetically controlled process, as suggested in Figure 2.32. Zeolites are reaction intermediates during the formation of dense phases from silica precursors. Provided the reaction time is long enough (up to some million years in nature) or the reaction rate is enhanced, e.g. due to high temperature, dense silica or silicon oxide phases are the thermodynamically stable products. In zeolite synthesis, the reaction is quenched when the thermodynamically meta-stable zeolite phase is formed. Prolonged aging and/or extended reaction time at high temperature and/or high pressure usually results in dense phases.

2.7.6 Factors influencing type of zeolites synthesized.

Many factors influence the polymerization sequence in which zeolites are synthesized. The thermodynamic variables include temperature, pressure, and the overall starting batch composition of the reactor mixture. Kinetic variables also influence the products obtained during hydrothermal synthesis, because the reaction mixtures are generally heterogeneous and

metastable. Nucleation appears to be kinetically determined as does Ostwalds rule of successive transformations (Barrer, 1982).

During hydrothermal synthesis, a competition usually exists between co-existing phases which are concurrently or successively polymerized. In accordance with Ostwalds rule, when competing phases appear, there is a tendency for the least stable phase to crystallize first and then be replaced by a more stable form again and again until the most stable product eventually results. **The kinetics involved in the crystallization of a zeolite phase are often determined by its prerequisite phase and the rate of dissolution or depolymerization of the monomers.** The nutrients involved in the polymerization of the zeolite often are made available only by the dissolution of a pre-existing less stable phase.

In addition to the thermodynamic and kinetic parameters outlined, other factors also influence the nature and type of zeolite synthesized. These factors include the treatment of reactants prior to crystallization, the chemical and physical nature of the reactants, the influence of seeding, aging and blanking (using organic based nitrogen dye), the influence of mineralizer and the templating effect of certain cations and additives, aside the operating conditions effect.

While the synthesis procedure of zeolites seems simple, the synthetic chemistry of zeolites is rather complex. Most zeolites are formed as metastable phases under hydrothermal conditions. Zeolites crystallization represents one of the most complex chemical problems in crystal nucleation and growth which involves complex reactions, such as solution-precipitation, polymerization-depolymerization and nucleation-crystallization (Zhdanov,1968; Senderov and Khitarov, 1971). The manner in which zeolite syntheses are carried out has a bearing upon the

products yielded and their quality. It is therefore critical to examine the factors which influence the outcome of zeolite synthesis reactions.

i. reagents (silica and alumina source)

The reagents are the most obvious and significant factor in any synthesis (Dyer, 1988; Kűhl, 2001). Purity of reagents is key to forming the appropriate product, free from impurities. The chemical as well as physical natures of the reactant have important effects on the crystallization of zeolites. Aluminosilicates zeolite requires a source of silicon, aluminium and oxygen. Charge balancing cations are also necessary, and are usually supplied in the form of an hydroxide. The silicon sources commonly used in the synthesis of zeolites are sodium water-glass, colloidal silica sol, fumed silica, tetramethylorthosilicate (TMOS), sodium metasilicate and tetraethylorthosilicate (TEOS), as reported by Xu *et al*., (2007).

The choice of the silicon source has a significant effect on the crystallization of zeolites, as reflected in Breck's work. Different silicon sources differ in reactivity and solubility. The nature of the polysilicate species and their distributions are different from one silicon source to another, which play important roles in the nucleation and crystallization of zeolites. It was established that different surface areas of the silicon source could affect the crystallization rate, the crystal size and the particle size distribution as in the synthesis of zeolite A (LTA).

Silica with high specific surface area dissolves more easily in basic medium than that with low surface area. The former leads to a higher supersaturation and a faster nucleation in basic solution, which is favourable for the formation of small crystals, while the silicon source with low surface area and low solubility favour the formation of large crystals.

Since the silica sources influence the size and morphology of zeolite crystals much work has been performed with the aim of controlling zeolite crystals size by proper choice of the silicon source used in the synthesis. Studies showed that less-reactive silicon source might provide less nucleation sites and favour the formation of large crystals. A novel method called "bulk material dissolution" (BMD) technique which is based on the use of a bulk source of silica instead of the conventional powder or solution form of silicon source to reduce dramatically the surface area and, thus, slow down the rate of dissolution, to produce less nucleation sites, was recently innovated. By using this method, very large zeolite crystals could be prepared.

Alumina sources also have an influence on the crystallization of zeolites. The alumina sources commonly used in zeolite synthesis are sodium aluminate, pseudo-bochmite, aluminum hydroxide, aluminum isopropoxide nitrate, aluminum sulfate, and aluminum metal (alumina powder or foil), as reported by Xu *et al*., (2007). Sano and co-workers investigated the effect of the aluminum source on the hydrothermal synthesis of high-silica mordenite in the presence of tetraethylammonium and fluoride ions at 170^0C. It was found that pure MOR-type zeolite could be obtained when $AlCl_3$, and $Al(NO_3)_3$ were used as an Al source, whereas zeolite beta (BEA) was prepared as the main product or a byproduct with $Al_2(SO_4)_3$.

Gladly, clay can be used as combined source of both silica and alumina for zeolite synthesis, with or without pre-treatment, depending on its impurity level. The challenge associated with use of clay is the presence of other competing materials inherently found in it. Zeolites formed from non-soluble salts, i.e. from mineral ores are associated with low crystallinity and yield, presence of other phases and undepolymerized stubborn quartz mineral.

ii. batch composition

As is well recognized, the batch composition of the reaction of mixture plays a crucial role in determining the crystallinity and type of zeolite products. The phase diagrams in Figure 2.33, taken from work of Breck, clearly demonstrate the influence of batch composition on the resulting phase (Breck, 1974). The synthesis displayed in Figure 2.33(a) was conducted in the Na_2O-Al_2O_3 SiO_2-H_2O system at 100^0C using sodium silicate as the silica source and 90-98% water content. Zeolite A (LTA), X (FAU), Y (FAU), B (ANA), and HS (SOD) were obtained in different regions, while two phases may co-exist within one batch composition in the boundary region.

Decreasing the water content to 60-85% in the gel, while keeping other conditions identical as in Figure 2.33(a), the only crystalline phase obtained was zeolite HS (SOD) depicted in Figure 2.33(b). As shown in Figure 2.33(c) using colloidal silica as silica source instead of sodium silicate in Figure 2.33(a) resulted in a modified phase region for zeolites A, X, and Y, and in the formation of zeolites R (CHA) and S (GME). The synthesis displayed in Figure 2.33(d) was conducted in the K_2O-Al_2O_3 SiO_2-H_2O system at 100^0C with water content of 90-98%. In this system, only two zeolite phases W and H, were formed.

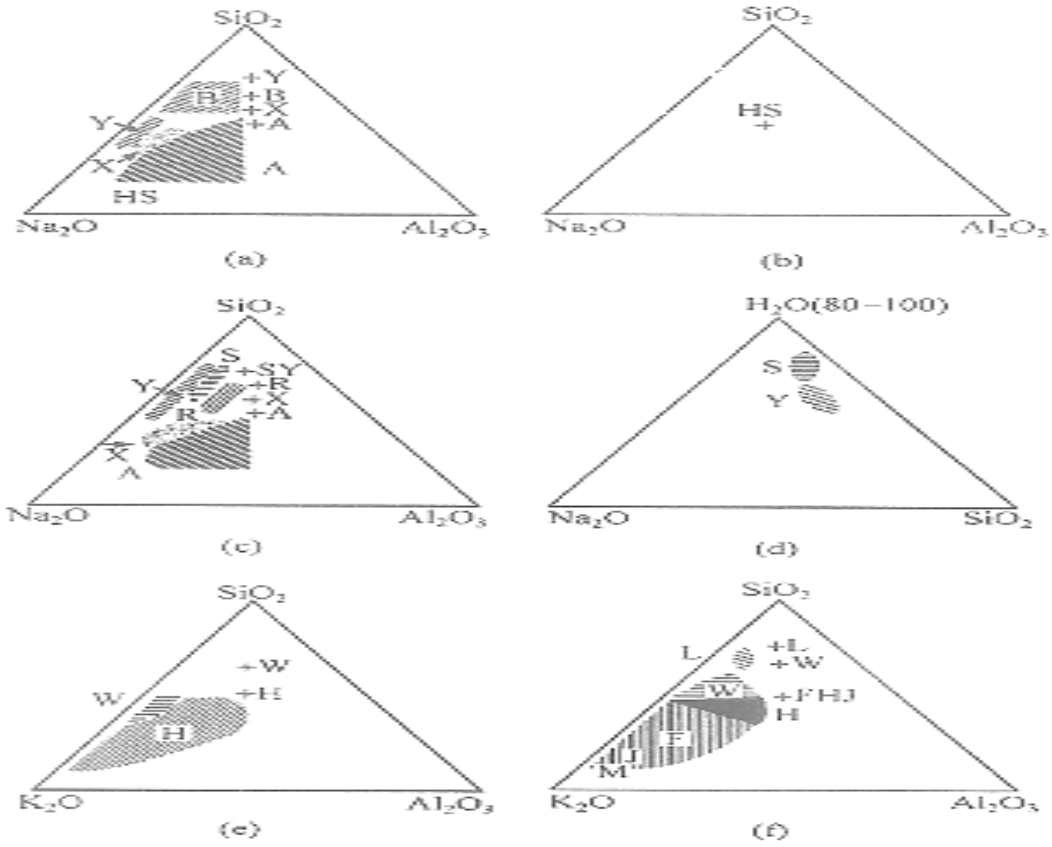


Figure 2.33: Reaction composition diagrams.

Areas identified by letters refer to compositions which yield the designated zeolite. The points marked with (+) show the typical composition of the zeolite phase (modG). (a) Na_2O-Al_2O_3 SiO_2-H_2O system at 100^0C H_2O content of gels is 90-98 molG; silica source, colloidal silica; and (d) $K_2O.Al_2O_3$ SiO_2-H_2O system at 100^0C, H_2O content of gels is 95-98 molG. $K_2O.Al_2O_3$ SiO_2-H_2O system at 100^0C with a water content of 95-98%. In this system only two zeolite phases W and H were formed.

iii. alkalinity

Most zeolites are crystallized from basic Na_2O-Al_2O_3-SiO_2-H_2O systems. For this specific system, the alkalinity is defined as OH^-/Si ratio and the H_2O/Na_2O ratio. A higher alkalinity increases the solubility of the Si and Al sources, decreases the polymerization degree of the

silicate anions, and accelerates the polymerization of the polysilicate and aluminate anions and their distribution. Consequently, the increase of alkalinity will shorten the induction and nucleation periods and speed up the crystallization of zeolites. Vicinic *et al*., (2003) reported that, the types of zeolite formed from coal fly ash depend significantly on the ratio of Na_2O/SiO_2 present in the reaction medium. Other authors reported tremendous increase in crystallinity and type of zeolite formed, with increase in amount of sodium hydroxide used, resulting from accelerated crystal growth and shortened the induction period (time before viable nuclei form) Barrer (1981) and Rees and Chandrasekhar (1993).

The change of alkalinity also has an effect on the particle size of zeolites. Figure 2.34 (a & b), shows the effect of different alkalinity on the crystallization rate (including induction period and growth rate) and particle size distribution of the product, zeolite A. Apparently, with an increase of alkalinity the crystallization process is enhanced, the particle size is decreased, and the distribution of the particle size is narrowed due to an increased nucleation rate and an increased polymerization rate between polysilicate and aluminate anions.

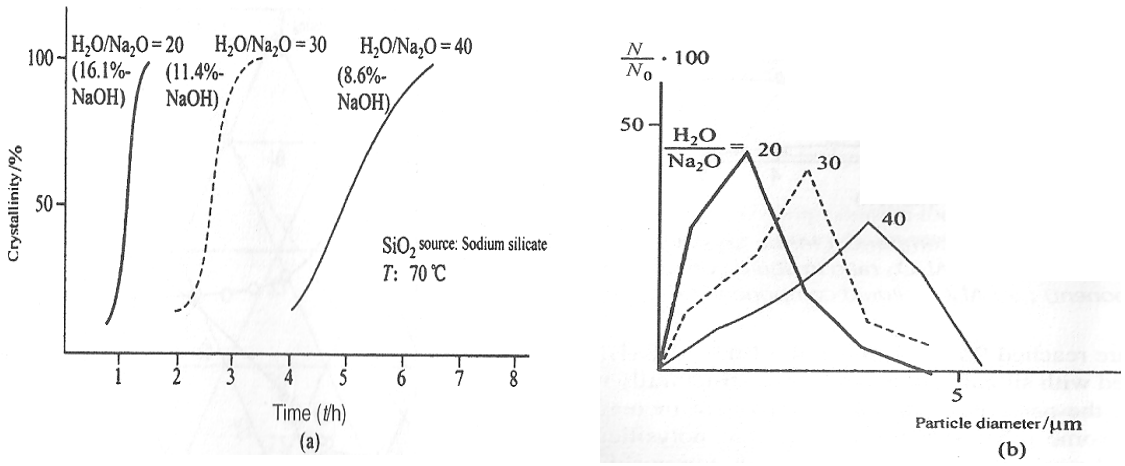


Figure 2.34: (a)-Effect of alkalinity on the crystallization of zeolite A. (b)- Effect of alkalinity on the particle-size distribution of zeolite A (adopted from Meise and Swochow, 1973)

Another effect of alkalinity on the crystallization of zeolites is that increasing the alkalinity of the system favors the formation of aluminum-rich zeolites. The most remarkable example is faujasite zeolite. High-silica Y zeolite can only be synthesized from the precursor gel with a low alkalinity.

Alkalinity can also affect the morphology of zeolites. For example, higher aspect ratio (length/width) was observed for MFI crystallized at lower alkalinity, suggesting that the aspect ratio of MFI increased at lower supersaturation. OH ion modifies the nucleation time by influencing transport of silicates from the solid phase to solution. It enhances the crystal growth and controls the phase purity. In a study conducted by Terres (1996) on MCM-41, it was found that the OH/Si ratio influences the pore size i.e. the higher the ratio, the wider were the pores.

Li *et al.,* (2002) shed some light on the role of addition of NaOH on the synthesis of zeolite Y. Using a molar composition of 2.46 $(TMA)_2$*xNa_2O*1.0Al_2O_3*3.4SiO_2*370 H_2O*13.6 EtOH from clear solution, with the concentration of NaOH ranging between ($0.03 < x < 0.43$). It was established that a larger Na_2O/Al_2O_3 ratio (0.43) favored the formation of zeolite A with a high yield and a shorter crystallization time. On the other hand, using a lower Na_2O/Al_2O_3 ratio (0.03), the synthesis favored the formation of zeolite Y with a lower yield and a longer crystallization time. It was established that the sodium was the growth-limiting factor in the synthesis of zeolite Y.

Li *et al.,* (2002) also tested a mid-synthesis addition of sodium to observe changes, if any, in zeolite yield with zeolites A and Y as final product. It was established that the addition of sodium before the completion of nucleation did not produce a single-crystalline phase even when

the amount and rate of mid-synthesis addition of sodium was kept low. Addition of 1M NaOH after a nucleation time of 6.5 days significantly influenced the zeolite phase. A one-time addition of NaOH still produced a mixture of zeolites Y and A, which was indicative of excessive sodium concentration forcing nucleation of zeolite A. To control sodium concentration, its addition was divided in several equal portions and added into the synthesis mixture at different time intervals. They found that the sodium addition with small number of equal portions and shorter time intervals produced a mixture of zeolites A and Y with higher concentration of zeolite Y.

On the other hand, a large number of equal portions and longer time intervals indicated that the crystalline phase in the final product was strongly dependent on the addition frequency. A pure zeolite Y with a slightly increased size and an increase in yield of more than 6-fold, was synthesized by the addition of NaOH in eight equal portions with addition time interval of 8 hr. ***It was concluded that the synthesis of pure zeolite Y, the mid-synthesis addition of sodium, with controlled amount and rate of addition was pivotal.***

iv. aging

Ageing of the amorphous gel at low temperature followed by elevated temperature of crystallization was simulated by population balance methods (Cook and Thompson, 1988). The ageing step resulted in the formation of viable nuclei that effectively lay dormant until the temperature was raised. For gel-based synthesis, population balance models suggest that the ageing step involves formation of nuclei, whose number rather than size is the critical parameter in determining crystallization dynamics.

Aging refers to the period from homogeneous mixing of the reagents to the onset of heating to the crystallization temperature. Extensive studies revealed that aging has an important effect on

the gel chemistry, thus affecting the nucleation and crystal growth kinetics of zeolites. It is believed that the germ nuclei, are formed during aging period, which effectively lie dormant until the reaction temperature is elevated, during moderate aging periods. Even though the processes occurring during the aging period are not yet well understood, it appears that aging has the following influences on the nucleation and crystallization of zeolites: (i) increasing the nucleation rate; (ii) reducing the induction period and duration of crystallization; (iii) reducing the crystal size; and (iv) increasing the crystal population.

Increase in ageing time increased the growth rate and number of growing nuclei in the system, which is the consequence of more germ nuclei present on increased aging that are active in further growth. (Koroglu *et al.,*2002).

Once the gel is made, it can either be heated straight away, or left to age at room temperature prior to use. The ageing process is said to provide a period for nuclei, which are the building blocks of the final crystals – to be formed. Traditionally, nucleation takes place in the initial heat up period of the gel to reaction temperature. However, if microwave heating is employed, the slow heat up phase is effectively eliminated, and the ageing step is beneficial. If the precursor nuclei are present already then the crystallization stage can occur sooner and reduce the necessary heating time.

According to ‘‘acid’’ hydrolysis the Si–O–Al bonds of the framework are split as schematically described by reaction in equation 2.10.

$$H^+ + OH^- + H^+(\equiv Al - O - Si \equiv) \leftrightarrow H_2O + (\equiv Al) + (HO - Si \equiv) \qquad 2.10$$

This process runs over the whole framework but especially attacks Al-rich frameworks. The ‘‘alkaline’’ attack follows according to the reaction in equation 2.11.

$$H^+ + OH^- + (\equiv Si - O - Si \equiv) \leftrightarrow (\equiv Si - OH) + (HO - Si \equiv) \qquad 2.11$$

The reaction starts immediately on Si-rich frameworks forming a high number of silanol groups. With increasing temperature the rate of decomposition rises in both cases due to the increasing dissociation of water. The molar Si/Al ratio in the filtrate amounts to ca. 1000, evidencing the high selectivity of NaOH towards silicon leaching.

The finding shows that two stages occurred during gel formation from kaolinite, namely: dissolution and gelation stages. The dissolution stage, begins immediately after the alkali solution comes into contact with the dealuminated metakaolin. In this stage, the high OH^- concentration of the alkaline medium favours the break of covalent Si-O-Si, Si-O-Al and Al-O-Al bonds present in metakaolin. This led to the release of silicon and aluminium ions into the solution, where they form species with a higher number of Si-OH and Al-OH. During the gelation stage, ionic species present in the solution (monosilicates and monoaluminates units) condense to form Si-O-Al and Si-O-Si bonds, giving rise to a three-dimensional aluminosilicate gel with alkaline cations compensating the deficit charges associated with Al and Si substitution. Notably, the rate of formation of dissolved monomers is greater than the rate of precipitation of the gel.

Chandrasekhar and Pramada (2004) reported on synthesis of zeolite Y from Thiruvananthapuram kaolinite clay sourced in India, that the crystallinity and phase purity of zeolite Y increased with increase in aging period. Okubo and co-workers (2003) also studied the effect of aging on the formation of aluminosilicate species in the hydrogel prior to crystallization of zeolite FAU by

using ^{21}Si solid state NMR technique. The reaction solution was aged at room temperature while stirring for 0 or 1 hr, 2 and 7 days followed by crystallization at 90^0C. Their studies showed that less aging resulted in the formation of other phases including sodalite, chabazite and analcime. The formation of pure-FAU required at least 1 day of aging and sufficiently long aging resulted in a shorter crystallization time and narrow size range distribution.

It was found that the composition and structure of aluminosilicate gels were metastable and changed over time, and the primary and secondary gel could be formed and aged in this period as well. Nucleation occuring at this stage was significantly affected by the composition and structure of the gel. Thus, ***the purpose of aging may be said to adjust synthetic conditions such as temperature and time to assist the transformation of gel to the zeolite structure and to speed up nucleation.***

Other reports exist in the literature pertaining to positive effect of aging on nucleation, crystallization, quantity and quality of the desired phase products formed. It is expected that during this period, the silica content is subjected to chemical destruction or depolymerization.
For the synthesis of Y zeolite, the use of colloidal silica sol was a preferred source of silica. When colloidal silica was used, ageing of the synthesis gel was carried out before heating for synthesis of NaY zeolite (Breck 1974). Ginter *et al*., (1992a, 1992b) studied the ageing of the starting gel as another feature, which is related to the nucleation step in the synthesis of zeolites (Ginter *et al.,*1992a; Ginter *et al.,*1992b).

These workers performed two different studies; to quantify the physical and chemical transformations occurring during the ageing of aluminosilcate gel produced from colloidal silica, and to investigate the effects of ageing on the synthesis of NaY zeolite. For the two studies,

colloidal silica and sodium aluminate solutions were used as starting materials. In the first study, it was established that upon mixing of colloidal silica sol and sodium aluminate solutions, a gel was immediately formed due to the flocculation of silica particles in the sol. By mixing, the gel was homogenized into small granules in the order of 1 mm in diameter. However, no chemical transformation was observed upon mixing, but during ageing, the silica particles were slowly dissolved and released silicate anions into the surrounding solution.

These species reacted with aluminate anions and formed aluminum silicate species, which precipitated due to their low solubility. The solid amorphous aluminosilicate thus formed was rich in Al and hydrated Na^+ cations. The precipitation of aluminosilicate consumed the dissolved Al and prevented the accumulation of Si in solution. When the entire dissolved Al was consumed in aluminosilicate formation, the remaining colloidal silica started to dissolve in the solution, which decreased the basic pH and started to release silicate anions in the solution. The aluminosilicate slowly reacted with the silicate anions in solution, which resulted in an increase in Si/Al ratio and a decrease in Na/Al ratio. In their second study, as shown in Figure 2.35, it was established that room-temperature ageing of colloidal silica gel strongly affected the kinetics of NaY crystallization at 100ºC. With ageing, the crystallization was accelerated and the final crystal size was decreased, especially ageing up to 12 hours. Their results are consistent with the generally accepted hypothesis that ageing enables the formation of nuclei from which crystals subsequently grow (Barrer, 1982).

Ginter *et al.,* (1992a and b) established that high pH and Al content in the solution during the first 12 hours lead to the formation of amorphous aluminosilicate gel with Si/Al = 1 and Na/Al = 2, from which it was proposed that this amorphous phase coexists with un-dissolved silica, and

upon heating of aged gel, the remaining colloidal silica dissolved quickly and released silicate anions into solution. The silicate anions react with amorphous aluminosilicate gel and form NaY nuclei under high concentration of hydrated Na^+ cations in amorphous aluminosilicate gel.

It was suggested that the high concentration of Na^+ cations in the amorphous aluminosilcate seemed to stabilize the faujasite structure. It was further confirmed that by crystallization of the gel, fewer NaY nuclei were formed and a denser structure, such as NaS and NaR, was produced. Ageing beyond 12 hours incorporated more Si into the aluminosilcate, which led to a decrease in the size of Al-rich zones in the gel. Upon heating the gel, aged for more than 24 hours, smaller and single crystals were formed.

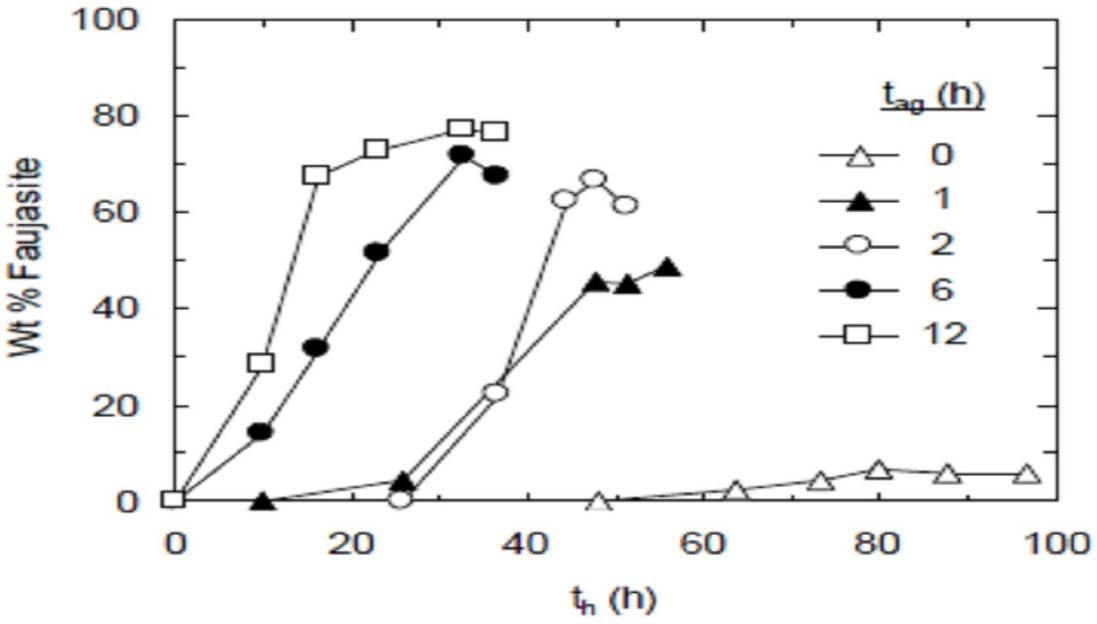


Figure 2.35: Effect of ageing of starting gel on the synthesis of zeolite NaY; wt% of NaY in the solid phase isolated from synthesis gels as a function of heating time for ageing time up to 12 h as determined by powder X-ray diffraction. Adopted from Ginter *et al.,* 1992a

Additionally, ageing under elevated temperature using microwave technique was also studied and reported by Slangen and co-workers (1997b).

v. pH

Gel pH also plays an important role in determining the composition and structure of the zeolite formed (Lechert, 2001). Zeolites are crystallised from gels with a high pH. This pH influences the quantity of species in solution made available for reaction, and this impact on the rate of product formation. Established pH-values have been discussed in only a few publications in connection with the parameters of the crystallization and Figure 2.36 presents the findings.

Generally, the different zeolite types crystallize within rather narrow ranges of pH. For faujasites, values between 12.3 and about 13.8 are observed. Robson has discussed procedures of a synthesis of NaY with Si/Al = 5 at pH = 11 (Robson, 1998). Between 11.3 and 12.7 mordenite usually crystallizes; at lower values ZSM-5 is obtained (Barrer, 1981 and Robson, 1989). Donahoe and Liou (1985) have found a linear dependence of the Si/Al ratio of phillipsite and merlinoite on the pH range 13.3-13.7 in crystallization experiments from clear solutions of systems with extremely high silica content. In a series of publications, single values of the pH or pH changes before and after crystallization are reported. These differences are usually 1-2 units on the pH-scale.

The pH of the reaction mixture does not relate directly to the total OH content of the system, but pH does appear as an important parameter in the synthesis of the zeolites in terms of the presence of free OH in the system (Szostak,1989). A marked change in pH is noted to accompany crystal formation which can be observed with crystallization. This increase in pH is the indication that the SiOH in colloidal state incorporates in the framework in the form of SiO_2. This is due to

SiOH being acidic in nature. The pH of the system is also very important to stabilize the sol. It also controls the particle size.

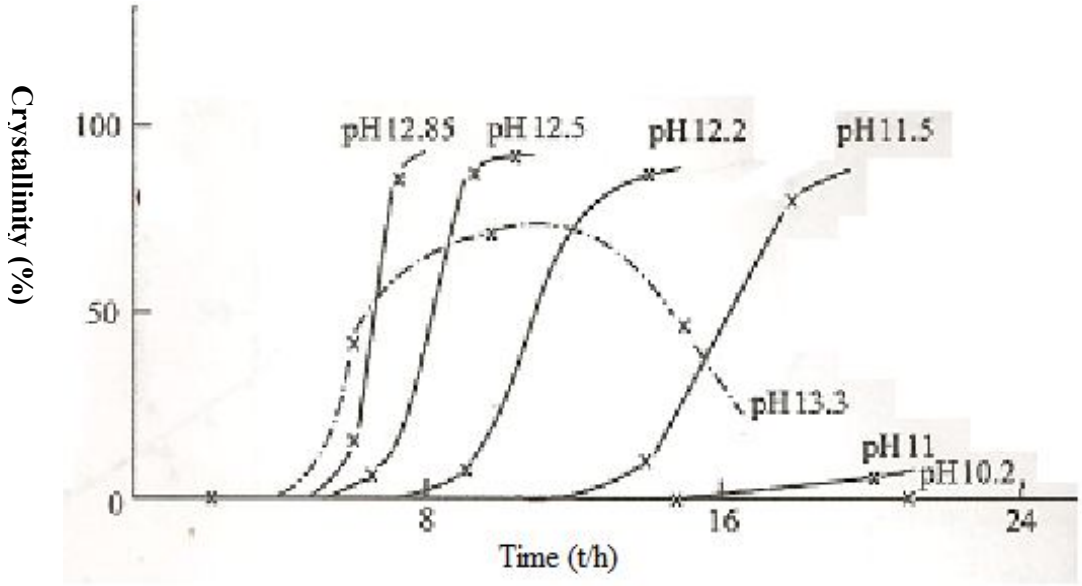


Figure 2.36: Effect of pH on the crystallization rate for the synthesis of mordeniete at 300^0C (adopted from Barrer, 1982)

vi. silica-alumina ratio

The Si/Al ratio in the parent mixture plays an important role in determining the structure and composition of the final crystallized product. However, there is no quantitative correlation between the Si/Al ratio in the product and that in the batch composition. Roughly, zeolites with low Si/Al ratio such as zeolite A (LTA), hydroxysodalite (SOD), KH, and KJ can be crystallized from a parent mixture (precursor gel) with low Si/Al ratio and strong alkalinity, whereas high-silica zeolites (high Si/Al) such as mordenite (MOR, Si/Al=5-9) and beta (BEA, Si/Al>8) can be crystallized from a gel with high Si/Al ratio and weak alkalinity. Usually, the Si/Al ratio in the precursor gel is always higher than that in crystallized product.

The excess of silicon is left in the mother liquor in form of silicate ion. For some zeolite structures, the Si/Al ratio in the crystallized product changed without the loss of structure. For instance, some, but not all zeolites can have both high- and low-silica forms. Furthermore, some zeolites such as low-silica FAU (X, Si/Al = 1-1.5), high-silica FAU (Y, Si/Al = 1.5- 3), GME (Si/Al = 2.3-2.95), zeolite Pt (Si/Al= 1.6-2.65), ANA (Si/Al = 1.4-4.1), and MOR (Si/Al = 4.5-9.75) can only be crystallized within a narrow Si/Al ratio. Those zeolites with a Si/Al >3, high-aluminum ZSM-5, ZSM-11, and BEA, and other high-silica natrolites, are very difficult to synthesize. They cannot be synthesized by simply varying the Si/Al ratio of the parent mixture. Special synthetic conditions, such as a special SDA or secondary synthesis approach, are needed for their preparation.

For example, X is a low-silica faujasite zeolite with a typical Si/Al of 1-1.5 and Y with a typical Si/Al of 1.5-3, can easily be synthesized from the Na_2O-SiO_2-Al_2O_3-H_2O system by varying the batch composition. However, little success has been reported for the synthesis of Y zeolites with Si/Al >3 from this synthetic system. Kacirek & Lechert (1975, 1976) have carefully studied this case and concluded that the crystallization process of high-silica Y zeolite was controlled by reaction dynamics. These authors further pointed out that the activation energy of the polymerization of poly silicate and aluminate anions in the solution is very high, resulting in a low reaction rate constant, k. Thus, the structure of high-silica Y zeolite is very difficult to crystallize under normal conditions. Figure 2.37 shows the Si/Al ratio of high silica Y zeolite as a function of its reaction rate constant k.

The correlation between Si/Al ratio in the parent gel and in the crystallized product is very complicated. Beside, the dynamic factor just discussed, thermodynamics and crystal structures of the resulting zeolites can also affect the Si/Al ratio in the final product.

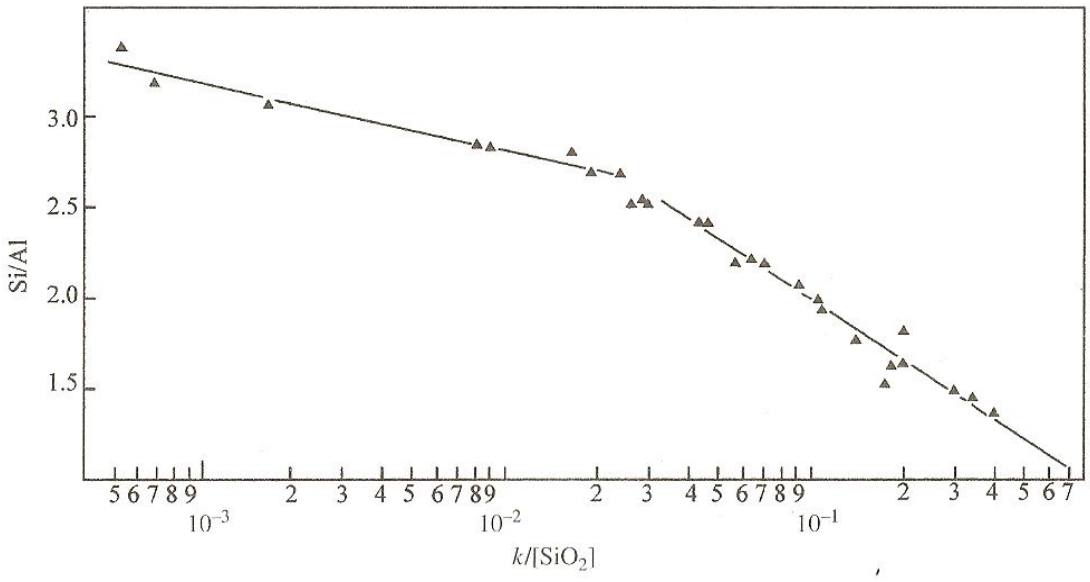


Figure 2.37: Correlation between the Si/Al ratio in faujasite-type zeolite and the reaction rate constant k (crystallization temperature of 88^0C).

Increasing the silica / alumina ratio affects the following physical properties of the zeolite:

a. Increases acid resistance.
b. Increases thermal stability.
c. Increases hydrophobicity.
d. Decreases affinity for polar adsorbents.
e. Decreases cation content.

Decreasing the silica / alumina ratio affects following physical properties of the zeolite:

a. Increases hydrophilicity.
b. Increases cation exchange properties.
c. Decreases the pore size for same numbered ring, as Al has lower atomic radius than Si.

Also depending on the phase diagram, this ratio can vary the nature of the final zeolite.

vii. solvent

Zeolites synthesis is typically conducted in aqueous medium, mainly water. The discussion presented in the first part of Section 2.7.3.1, was from this perspective. Bibby and Dale (1985) showed that it was possible to grow zeolites also in non-water media such as alcohols. The properties of solvents are important for the crystallization of zeolites. The effect of solvents on the synthesis can be discussed on the basis of their interactions with the reaction species, in particular the SDAs. Morris and Weigel (1997) classified the (organic) solvents into four categories based on their tendency to form hydrogen bonds: high, high-medium, low-medium, and non-hydrogen bonding. First of all, a successful SDA needs to be intermediate in its ability to interact with the solvent.

Strong interaction with the solvent will prevent the framework species from forming interactions with the template. Therefore, high hydrogen-bonding solvent may not be good choice because these will shield the framework species and the SDAs from interaction with each other, thus preventing the nucleation. In the case of high-medium and low-medium hydrogen-boding solvents, favourable interactions between solvent, SDA, and the framework species can be achieved. The balance of interactions between solvent, SDA, and the framework species is crucial to the success of an attempted synthesis. The solvent-template balance can be tipped against the templating reaction if either no templating will occur or it will be the hydrated template which acts to direct the structure of the resulting framework.

The solvents may also affect the size and morphology of the crystallized zeolites, via their viscosity. Solvents with higher viscosity than water may reduce convection currents, especially in gel system. In this case, mass transfer only occurs by diffusion, thus reducing secondary nucleation and preventing crystallization by sedimentation. On the other hand, increasing viscosity of a solvent will also reduce the rate of diffusion of reaction species. It is believed that

solvents of both intermediate viscosity and intermediate hydrogen-bonding ability should be favourable media for zeolite synthesis, in particular for that of large-size crystals.

viii. reaction vessels

As a consequence of the high pH normally used, standard borosilicate glass is an inappropriate reaction vessel. Leaching of silicon from the glass may occur, and lead to altering the quantity and quality of silicon in the gel and hence affecting, not only the Si/Al ratio, but perhaps the product formed. Durable inert polypropylene plastic containers are more commonly used. It is necessary to thoroughly clean the containers between uses, or at least use them for one zeolite type only, as any crystals remaining from previous reactions may act as seed crystals. Earlier reseachers claimed that use of glass material in zeolite synthesis tends to introduce impurities that subsequently hamper the successful synthesis of the desired zeolite phase (Aderemi, 2000).

ix. stirring

Stirring during the ageing process or reaction can cause an increase in collisions between species in solution, and prevent a local depletion of reagents around the forming crystals. In some instances, this may be beneficial and lead to a reduction in reaction time, through increased rates of nucleation. However, stirring may also break down existing species and stimulate production of undesired structures. For example, in the synthesis of zeolite Na-X (FAU), Freund (1976) performed the same reaction with differing stirring speeds ranging from 0 to 350 rpm. Whilst the time taken to yield crystalline products decreases with increasing stirring speed and the purity is compromised by the co-crystallisation of zeolite Na-P (GIS).

In the laboratory, zeolites are typically synthesized under static conditions. Several studies have shown that stirring can effectively modify crystallization kinetics, in particular the crystal size. Smaller crystals are obtained by stirring, since supersaturation can be rapidly achieved due to the

accelerated mass transfer. In addition, it is observed that stirring modifies the selectivity for the formation of different zeolite phase. For example, zeolite A (LTA) was preferred to zeolite X (FAU) in stirred system, and MH was favoured instead of TON from an unstirred synthetic system.

Anderson and co-workers (2000) showed that stirring has an effect on the intergrowth of zeolite Y polymorph. Crown ether 18-crown-6 and 15-crown-5 selectively give the hexagonal polymorph (EMT) and the cubic polymorphs (FAU), respectively, and mixtures (of two crown ethers) lead to the intergrowths of the two polymorphs. Using different concentrations of 18-crown-6 and 15 crown-5, a significant difference in the crystallized product was observed when the synthetic mixtures were stirred as compared to unstirred conditions during the crystallization process. Stirring favoured the formation of the hexagonal polymorph of Y (EMT) which was dominant even when the concentration of 18-crown-6 was as low as 33%.

Without stirring, the intergrown structures were preferred up to a high "apparent" concentration of 18-crown-6. This is due to fluctuations of the local concentration at the growing surface, owing to diffusion-limited transport and consequently often to a low "apparent" concentration. This work also showed that stirring in the synthetic mixture affected crystals size producing small crystals.

Marrot *et al.,* (2001) also claimed that shearing mobiles modify the faujasite nucleation process and growth; even if the initial composition of gel is the same, these modifications are harmful on the purity of the latter. The period of ripening corresponds to a structural reorganization and is a factor determining the crystallinity of faujasite. Shearing during this period of reorganization tends to form the most stable zeolites. Noreen *et al.,*(2000) also gave a good report of stirring effect on the synthesis of intergrowths of zeolite Y polumorphs.

x. seeding

In the seeding method, a small amount of zeolite is introduced in the synthetic system, usually just before the hydrothermal treatment, in order to direct crystallization toward a given zeolite and control the size of final crystals. Adding a seed crystal to a crystallization system has typically resulted in increased "crystallization rates. The enhanced rate might be due to simply increasing the rate at which solute is integrated into the solid phase from solution, due to the increased available surface area, but also might be the result of enhanced nucleation of new crystals. In slightly supersaturated systems, primary nucleation does not take place and seeds provide the whole growth surface. In this case, seeding enables a faster crystallization and small final crystals, as shown in the case of zeolite Y (FAU).

On the other hand, in more supersaturated systems, the surface of seeds can compete for supersaturation with primary nuclei, and thus primary nucleation can be suppressed and seeding results in the formation of larger crystals. Seeding is an important factor in determining types of zeolite formed, since the crystallization reaction of zeolitic materials tends to follow the autocatalytic reaction, requiring the presence of product in the reaction medium. As an alternative to ageing, seed crystals, or even 10% by weight of aged gel, can be added to the zeolite gel (Slangen *et al.,*1997b). After adding the aged gel or seed crystals, the rate of crystallization was found to be enhanced compared to un-aged zeolite gels. Adding seed crystals to a crystallization system has typically resulted in increased crystallization rates. Understanding the precise role of seed crystals is an area of ongoing investigation. Zhao *et al.,* (1997), among other authors, reported that increase in the amount of seeds added to the reaction mixture $15Na_2O*1Al_2O_3*15SiO_2*300H_2O$ targeted for zeolite Y, with aluminosilica sourced from fly ash, led to continuous increase in the yield and crystallininty of the zeolite Y synthesized.

xi. water content

Water has been established to act as a solvent in the hydrothermal synthesis of zeolites. Typically, the amount of water is varied within a certain range for the synthesis of a particular zeolite. However, the concentration of reactants will be altered with the variation of the amount of water, thus affecting the crystallization of zeolites. In general, an overall dilution of the synthetic mixture causes lower supersaturation, crystal growth is favoured at the expense of nucleation, and consequently, large crystals can be obtained. The alteration of water content can also change the crystallization region of zeolite phases, as reflected in the early work of Breck shown in Figures 2.34 (a and b).

The illustration in Figure 2.38 serves to buttress the significant role of water in zeolite synthesis. Thus, the water content of the synthetic mixture modifies, to some extent, the structure-directing ability of SDA and as a result different pore architectures can be made by the same SDA. For example, using the TMA^+ cation as an SDA, all-silica CHA was formed for H_2O/SiO_2 ratio of 3.0, while at ratios of 7.5-10, SSZ-23 (STT) formed in gels with the molar composition SiO_2:0.5HF:05TMAOH:wH_2O at 150^0C.

The effect of water content on the phase selectivity may be related to the nucleation step and, hence, is probably a kinetic effect.

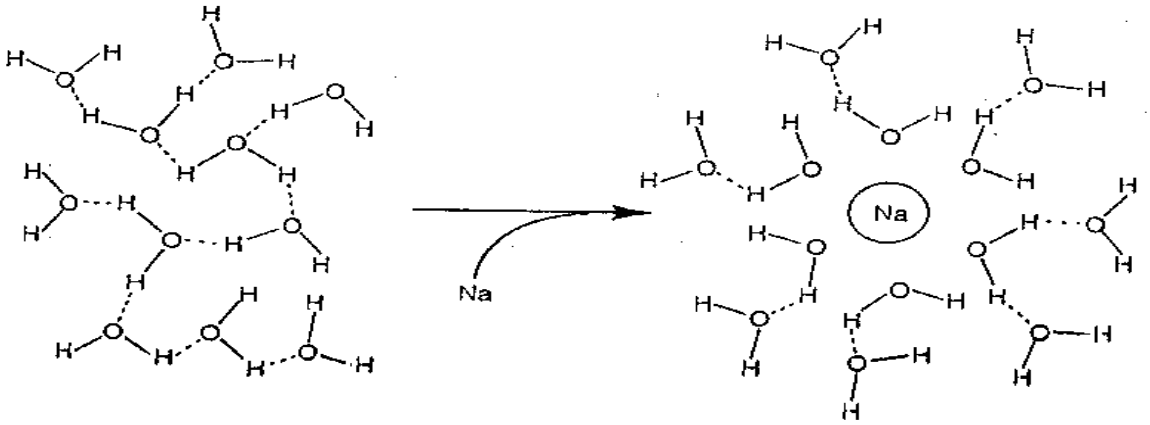


Figure 2.38: Schematic diagram of the structure-making interaction of a sodium cation with water molecules (dotted lines indicate hydrogen bonds)

xii. salting

Addition of salts to the synthetic system decreases supersaturation, and large crystals are obtained, as shown by Cocks and Pope (1995) who described how the rate of crystallization and zeolite yield was enhanced by the addition of Cl^-, Br^-, and I^- salts.

The presence of certain salts increase the rate of dissolution of silica and the presence of others retard it. The rate of dissolution of quartz in aqueous sodium chloride solutions of concentration $10^{-3,}$ 10^{-2} and 10^{-1}N was found to be 4, 14, and 67 times that of pure water (VanLier, 1979). Sasaki (1952) found that both zinc and aluminum greatly inhibited the rate of dissolution of fused silica. He found that concentration of 3.4×10^{-3}N aluminum and 5×10^{-3}N zinc completely inhibited the dissolution of silica in 0.1N sodium hydroxide.

Certain organic compounds strongly increase the solubility of silica. Myer and Yen (1974) found that quinoline plus potassium hydroxide dissolved crushed quartz at a rate substantially faster than saturated aqueous potassium hydroxide. Strong quaternary ammonium bases like tetramethyl ammonium hydroxide dissolves silica rapidly, forming the silicate salt (Iler, 1979). But the major challenge in adoption of these approaches are negative effect of organic materials

on the environment and the fact that potassium compound would inhibit the successful synthesis of zeolite Y, hence the necessity to search for an alternative approach to silica solubilization and depolymerization.

xiii. particle size

The knowledge of physical and chemical kinetics, i.e. transport phenomena and reaction engineering indicates that resistances in mass transfer and subsequently, occurrence of reaction can be countercited by reducing the particle size of the reactants.

This hypothesis is a very common practice in other fields of material and catalysts development. Yagi and Kunni (1955, 1961) visualized several steps occurring in succession during chemical reaction involving solid particle and fluid. Among the five stages listed by them, only one is chemical reaction dependent, while others are either external or internal diffusion driven. According to the empirical models for the various resistance stages, the time required for complete reaction depends greatly on the radius of the solid particle as shown in equations 2.12, 2.13, 2.14, where these equations represent diffusion through gas film, ash layer and chemical reaction control.

$$\tau = \frac{\rho_B R}{3bk_g C_{Ag}} \quad \text{.....2.12}$$

$$\tau = \frac{\rho_B R^2}{6bD_e C_{Ag}} \quad \text{.....2.13}$$

$$\tau = \frac{\rho_B R}{bk'' C_{Ag}} \quad \text{.....2.14}$$

Additionally, conversion and rate of reaction is a direct function of particle size, i.e. radius. Analogically, this model can be extended to zeolite synthesis.

xiv. order of mixing of the reactant

This is another factor that is recently being considered in zeolite synthesis. It is assumed and believed that the order in which the ingredients are mixed can determine the phase, type and crystallinity of the product formed. Another school of thought claims that order of mixing can alter the rate of nucleation and hence enhance crystal growth. (Markus and Cormier, 1999).

xv. inorganic cations

Inorganic cations are defined as species, whose introduction, induce the crystallization of a specific zeolite structure that could not otherwise be favoured. These cations perform the following functions:

a) Balance the framework charge.

b) Act as structure directing agents.

c) Determine the morphology of the zeolite.

d) Influence the crystal purity

e) Affect the product yield.

These agents determine which of the competing frameworks is actually formed (Rollman & Valvoycsik, 1999).

Al-rich zeolites are commonly prepared under basic conditions by using alkali-metal hydroxides as the alkali source. The nature of the inorganic cation is important for the crystallization of zeolites. In some cases, both sodium and potassium ions were used for the preparation of zeolites, such as zeolites BEA, low-silica-type X (FAU), NAT, OFF, PAU, and PHI. Cations existing in the synthetic system have important effects on the formation of the framework structures of zeolites.

From these properties, Flanigen (2001) suggested two roles of alkali-metal cations in the synthesis of zeolites: (i) as the source of hydroxide ions needed to solubilize silicate and aluminate species; and (ii) a limited structure-directing role. In general, the cation is added as a base in the form of MOH, resulting in the mutual control of OH^- and cation. The hydroxide ion affects dissolution and polymerization-depolymerization reactions of silicates and aluminosilicates. In view of the structure-directing role of cations, they are believed to influence the ordering of water molecules in aqueous solution.

The structure-directing role of the hydrated alkali-metal cations is proposed to involve the ordering of water molecules around the cations with subsequent displacement by silicate and aluminate species to form regions of micro-organization that lead to nucleation centers. Figure 2.38 shows the interaction of the sodium cation with water molecules. These organized water molecules surrounding the cations can be partially replaced by silicon and aluminum tetrahedral and thereby lead to the formation of cage-like structures- required for linkages leading to zeolite formation.

xvi. organic template/ SDA

Barrer and Denny, (1961) initiated the introduction of an organic cation, tetramethylammonium, in zeolite synthesis, which allowed higher Si/Al ratio zeolites to be produced. The presence of TMA^+ cations appeared to have a structure-directing role in the formation of specific building units. Since then, many other quaternary ammonium cations have been used, resulting in the extension of the compositions to high Si/Al ratios ($SiO_2/Al_2O_3 \geq 20$) and the formation of new siliceous zeolites. In 1982, Wilson et al, reported a family of aluminophosphate molecular sieves using organic amines and quaternary ammonium ions as the templates or SDAs.

Lok *et al.,*(1984) reviewed the role of organic molecules in the early zeolite synthesis. Templating was defined as the phenomenon occurring during either the gelation or the nucleation process whereby the organic species organize oxide tetrahedral into a particular geometric topology around them and thus provide initial building blocks for a particular structure. Suggestions were advaned that both gel chemistry and template species play important roles in the formation of a specific structure and that templating becomes operative only in the environment of the right "gel chemistry".

Davis and Lobo (1992) clarified the definition of templating as a structure-directing rather than a strict templating action for the organic guest molecules. The roles of organic guest molecules are summarized as follows based on the specificity of the inorganic host and organic guest: (i) space-filling species; (ii) SDAs; and (iii) templates. Structure-directing role means that a specific structure is synthesized via a single organic species. For example, crown ether 18-crown-6, in the synthesis of hexagonal faujasite (EMT), in fact, plays such a structure-directing role. A true "templating" occurs only when a zeolite structure adopts the geometric and electronic configurations that are unique to the templating molecule and upon removal of the organic species retains the shape of the guest molecules. This is demonstrated in the synthesis of ZSM-18 (MEI) using a specific triquaternary amine (tri-quat) $C_{16}H_{36}N_{33}^{+}$.

The SDAs or templates in a broader context, significantly affect the formation of zeolites by (i) influencing the gelation and/or nucleation process; the TO_4 units are organized into a particular geometry around themselves and as a result provide precursor species for further nucleation or crystal growth: and (ii) lowering the chemical potential of the lattice formed upon inclusion of the templates during zeolite synthesis. This template inclusion contributes to the stability by new

interactions (H-bonds electrostatic, and London dispersion interactions) and further controls the formation of a particular structure through its geometry (form and size). It is evident that changes in cation density brought about by geometrical or physical properties of the template will be reflected in the chemical composition (Si/Al) of a given topology.

The effect of structure-directing agents (tetraalkylammonium ions, TAA+) on the structural and physiochemical properties of aluminosilicate gels was investigated in depth by Bodart *et al*., (1986) and Nagy *et al*., (1995), using various NMR. The gel was obtained by mixing $Al(OH)_3$ solution with fumed silica, which is typically used in the synthesis as starting material. The role of the structure-directing agents (TAA^+) was determined by varying the aluminosilicate gel composition in their preparation under different operating conditions. When the TAA-Br was added at neutral pH in the absence of Na+ cation (gel I), it was found that the tetrahedral Al atoms were not well dispersed throughout the gel.

Due to the presence of TAA-Br crystallites, some large (40-60 ºA) and medium (21ºA) cavities were detected. On the other hand, when TAA-OH was used in absence of Na^+ cation (gel II), it was found that tetrahedral Al atoms were very well dispersed throughout the gel and TAA^+ cations took the place of counter cations of the negatively charged gel. When TAA-Br was added to the gel containing NaOH (gel IV), it was observed that Al atoms were better dispersed but the counter cation for the gel remained essentially the sodium ions, this caused less dispersion of TAA^+ cation within the gel. The textural characterization of the gels using ^{129}Xe NMR showed a monomeric high dispersion of structure-directing agent when TAA-OH was use in gel formation. Hence, this suggested a direct role of TAA cations in zeolite synthesis.

xvii. crystallization temperature and time

All the zeolite synthetic works pay a particular attention to the crystallization temperature due to its strong effect on the formation of zeolites. The desired zeolite phase typically can only be obtained within a specific temperature range. Most aluminosilicate zeolites probably could be obtained at temperatures below 100°C in alkaline solutions. This is generally the case for zeolites with a low Si/Al ratio. However, in order to reduce the reaction time (especially for zeolites with a high Si/Al ratio) and to control crystallite sizes, morphologies, and compositions, some syntheses are performed at temperatures above 100°C, under autogeneous pressure in autoclaves (Schmidt, 2005).

The nucleation and crystal growth are strongly affected by the crystallization temperature. The increase in temperature will increase both the nucleation rate and the crystal growth rate, in particular the crystal growth rate over the nucleation rate. The higher growth rates and larger crystals have been obtained at higher temperatures. As illustrated in Figure 2.39, the growth rate of zeolite NaX (FAU), as measured by the $0.5\Delta l/\Delta t$, where Δl is the increase in crystal dimension in time Δt, is significantly accelerated with increase of crystallization temperature.

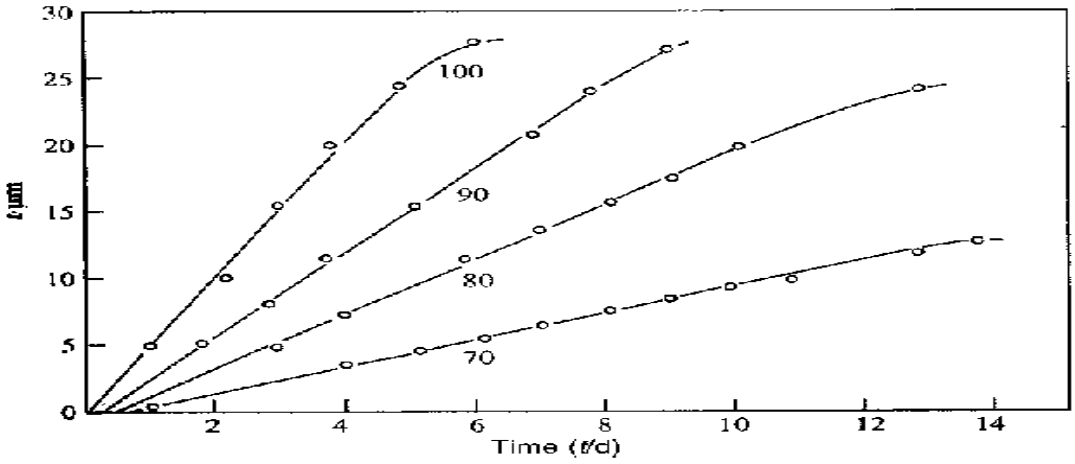


Figure 2.39: Growth rate curves of zeolite NaX at various crystallization temperatures.

The rate of crystallization is directly proportional to temperature while the rate of nucleation is inversely proportional to temperature. As both processes progress simultaneously for large period of time, the operating temperature need to be optimized for maximum zeolite yield. The reaction mixture, being in disordered state, is at higher entropy than the crystalline, ordered state (Iler, 1979). Usually, zeolites are synthesized below 350^0C, with some exceptions (Szostak, 1989). Higher temperatures, generally, yield more condensed phase species. Temperature influences several factors in zeolite synthesis; it can alter the zeolite phase obtained as well as change the induction period before the start of crystallization.

This induction period decreases with increasing temperature. Temperature does not only affect the crystal size but also the morphology of crystals. Moreover, the variation of crystallization temperature can affect many other factors during the synthesis, such as the polymerization reaction between the polysilicate and aluminate anions contained in the liquid phase of the gel; the polymeric state of the silicates; the formation, dissolution, and transformation of the gel; the nucleation and crystal growth; and the phase transition of metastable phase resulting in the formation of zeolites with different pore structures from a single synthetic system.

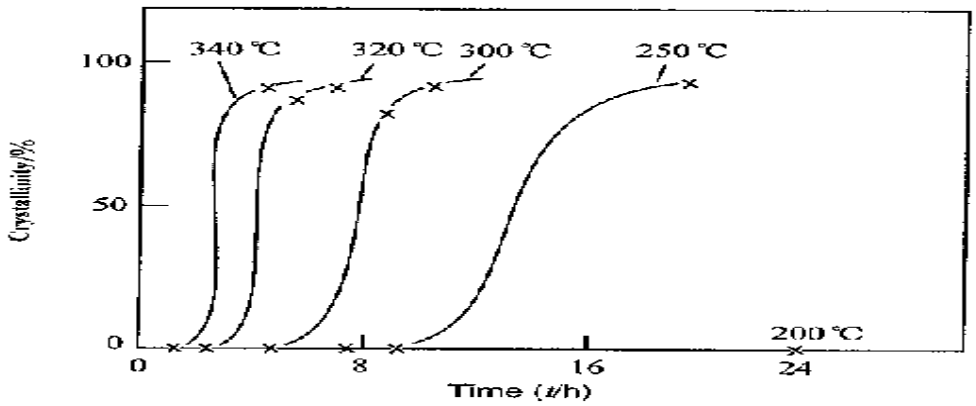


Figure 2.40: Effect of temperature on the crystallization of MOR.

It is evident from these crystallization curves shown in Figure 2.40 that the crystal growth was significantly speeded up and the aging induction period was obviously shortened with an increase of crystallization temperature. This phenomenon was also observed in the crystallization of MOR, LTA, FAU, etc.

Crystallization time is also a synthetic parameter to be considered for zeolites. In general, the crystallinity increases with crystallization time. However, it should be noted that zeolites are thermodynamically metastable phases. In general, Ostwald's law of successive reactions is followed in zeolite synthesis, i.e metastable phase appears first and then successively more stable phases replace it and this continues until the appearance of unchangeable phase. For example, with prolonged crystallization time, zeolite A (LTA) and zeolite X (FAU) dissolve to form zeolites sodalite (SOD) and P (GI), respectively when synthesized in alkaline aluminosilicate gel. However, it should be borne in mind that the formation of zeolites cannot be rationalized on a thermodynamic basis alone and kinetics must be considered as well.

xviii. presence of impurities

Breck was the first to report on the negative effect of some inherent impurities in the raw material (Breck, 1974). He reported that the presence of potassium cation in the synthetic system Na_2O-Al_2O_3-SiO_2-H_2O significantly changed the type and structure of the zeolites crystallized from the parent mixture, which might be caused by the different templating ability of the cations on the SBUs of the zeolites. The presence of this impurity will also lead to three main changes in their crystallization field:

a. The crystallization field or the chemical composition of the zeolites could be significantly changed. When the ratio of K_2O/R_2O (R=K+ Na) is low, the zeolites crystallized from the original sodium aluminosilicate system can still be crystallized but have an altered

chemical composition, such as Si/Al ratio. For instance, NaX zeolite with modified chemical composition can be crystallized from a parent mixture with SiO_2/Al_2O_3=3-4, H_2O/R_2O=30-45, and K_2O/R_2O<0.15 as depicted in Table 2.1. Any change in the composition leads to formation of other zeolite phases as shown in Figure 2.29.

Table 2.1: Chemical compositions of zeolite X crystallized from K-Na gels

K_2O/R_2O (in parent gel)	K_2O/R_2O (in zeolite)	SiO_2/Al_2O_3 (in zeolite)
0.02	0.04	2.65
0.05	0.09	2.58
0.10	0.14	2.44
0.15	0.17	2.39

The change of the chemical composition of the resulting zeolite may be caused by the change of the framework charge since the K^+ ion cannot enter the β cage. When the ratio of K_2O/R_2O is greater than 0.15, zeolite NaP is formed instead of NaX, as shown in Figure2.41.

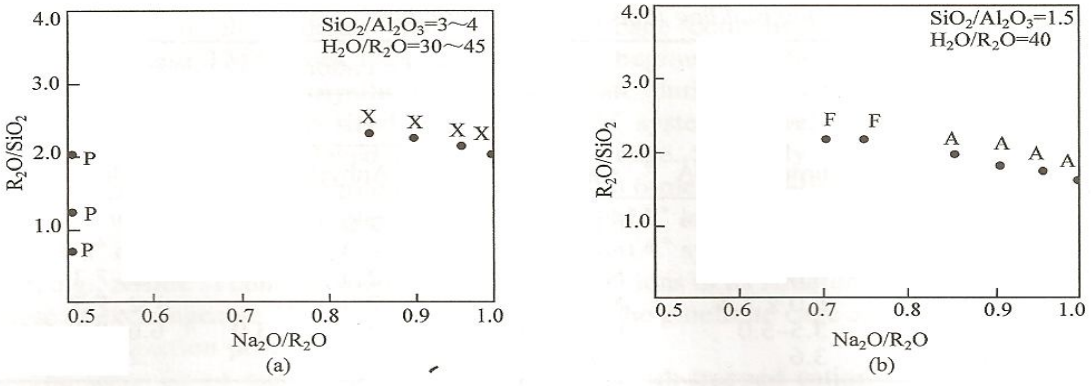


Figure 2.41: Effect of K^+ on the crystallization-field change of zeolite NaX (a) and zeolite NaA (b) at 100^0C.

The presence of small amounts of potassium cations in the parent gel which originally produces zeolite NaY will lead to the crystallization of zeolites NaP and W as shown in Figure 2.42. This is one of the reasons why the impurity of zeolite NaP always existed when kaolin or pumice was used as source material to prepare NaX or NaY zeolites (Xu *et al.*,2007).

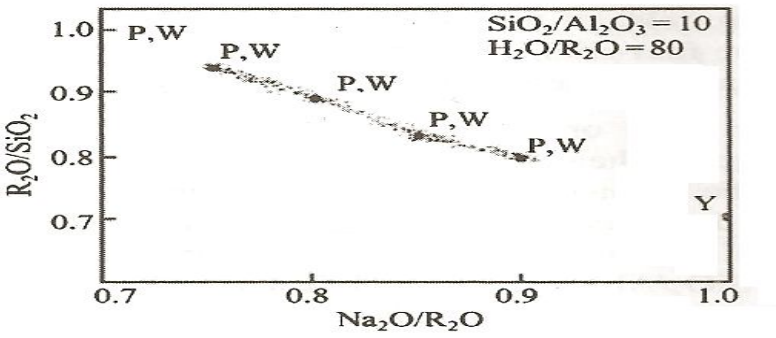


Figure 2.42: Effect of K^+ on the crystallization-field change of zeolite NaY.

b. New zeolite structure containing mixed cations could be formed. As shown in Figure 2.43, decreasing the ratio of Na_2O/R_2O or increasing the ratio of K_2O/R_2O results in the formation of zeolites NaY, D and L from the parent mixture with a SiO_2/Al_2O_3=20-28 and H_2O/R_2O=25-30.

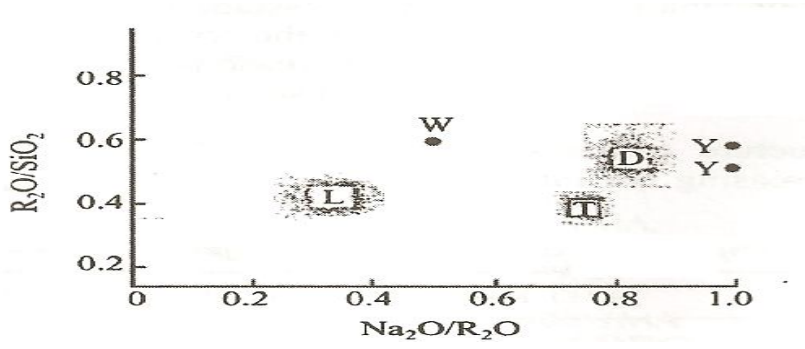


Figure 2.43: Effect of K^+ on the crystallization-field change of zeolite NaY(100^0C), where SiO_2/Al_2O_3=20-28; H_2O/R_2O=25-40

In Figure 2.41(b), zeolites NaA and F have the same Si/Al ratio and structure. However, when the ratio of Na_2O/R_2O is decreased, zeolite KF is obtained instead of zeolite E. Zeolite KF has the same Si/Al ratio as that of zeolite E but a different structure.

c. Owing to the presence of K^+, the crystallization field of potassium-type zeolite is less affected by the variation of Na_2O/R_2O ratio. For instance, as shown in Figure 2.42, zeolite KW will be crystallized instead NaY from the parent mixture with SiO_2/Al_2O_3 ratio of 10, H_2O/R_2O ratio of 80 and R_2O/ SiO_2 ratio of 0.8-1.0 when the ratio of Na_2O/R_2O is decreased from 1.0 to 0.9-0.7 (zeolite NaP impurity exists).

Another incredible fact responsible for presence of impure zeolitic phases along with NaY when kaolin is used is the molecular size of potassium ion in comparison with sodium ions, resulting in "molecular eclipse" and higher rate of crystal formation around potassium. This is diagrammatically represented in Figure 2.44.

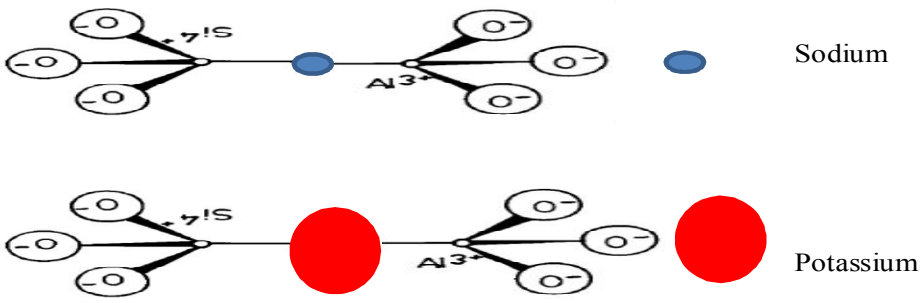


Figure 2.44: Comparative molecular sizes of potassium and sodium.

The higher rate of crystal growth around potassium can be attributed to the fact that potassium is ahead of sodium in the reactivity series, hence more reactive and with higher force of attraction. The observations from Figures 2.42 and 2.43 further buttressed the already discussed effects of

silica –alumina ratio and water content on type and phase of zeolite formed. Another common impurity in kaolinite clay is ferric ions, which is presently being debated whether its presence affect the rate of nucleation of zeolite Y synthesis or not.

The role and effect of alkali metal cations on the properties of aluminosilcate gels, as the starting material, during zeolite synthesis, has been investigated by different spectroscopic techniques. Ivanova *et al.,* (1994) investigated the aluminosilicate gel obtained by mixing the alkali-silicate and aluminate clear solutions using multinuclear NMR. They found that the tetrahedrally coordinated Al was homogeneously dispersed throughout the gel, irrespective of the type of alkali metal cation. However, when the textural properties of the gel were investigated using ^{129}Xe NMR, they found a dependence on the type of the alkali metal cation present in the material.

Subotic *et al.,* (1994) used two types of dry amorphous aluminosilicate gel containing Na^+ and K^+ cations. A part of the gel was heated to 500ºC for 1 hr and finally stirred in 2M NaOH solution at 80ºC to reach complete crystallization. The samples were investigated before heating, after heating, and after complete crystallization using XRD, FTIR, and differential thermogravimetry (DTG). It was found that the sample containing the "structure-forming" Na^+ cation showed a similar endotherm which was observed for the sample after complete crystallization and without being exposed to high temperature. This led to a postulation that the presence of Na^+ induced the formation of structural subunits or complex structures in the range of 5-20 nm, which were also present in the complete crystalline product and were beyond the detection limits of XRD.

On the other hand, the sample containing "structure-breaking" K^+ cation did not show any endotherm at a similar location, which led to an assumption that structural subunits were either not formed or formed in a considerably lower quantity in the presence of K^+ inside the X-ray amorphous solid aluminosilicate gel. This was further confirmed by the electron diffraction pattern (EDP). The effect of heating the sample before crystallization was investigated through FTIR for both types of samples and it was found that the formation of structural subunits was further deteriorated, which affected the rate of hydrothermal transformations of X-ray amorphous solid aluminosilicate gel into the crystalline product. An interesting observation was made when the samples were crystallized at high temperature. The sample containing Na^+ cation showed deterioration in the formation of structural subunits as expected, but K^+ containing sample formed pure zeolite, small crystal size, large number of crystals and the shortest time of synthesis which remained a question beyond explanation.

The production of side products such as zeolite A and zeolite P may also occur along with zeolite Y, as the main product. It has been established that the production of side products is dependent on different factors such as; alkali concentration, Si/Al ratio, ageing time, and hydrothermal treatment (Den Ouden and Thompson, 1991; Lechert and Kacirek, 1991).

2.8 Mechanism of Nucleation and Crystal Growth

Two extreme alternatives - homogeneous and heterogeneous mechanisms - have been suggested to explain nucleation and crystal growth during zeolite synthesis. In the homogeneous mechanism, the nucleation is visualised to occur directly from the liquid phase. Once the embryos reach a critical size, they grow into crystals by progressive incorporation of soluble species. If any amorphous solid phase is present in the solution, it may serve as a reservoir of nutrients for the growing crystals. In the heterogeneous mechanism, it is assumed that zeolite

crystallization proceeds by reorganization of the amorphous phase hydrogel which is present in the solution from the beginning of synthesis. Therefore, the nucleation takes place within the hydrogel and the crystals are formed by solid-solid transformation (Szostak, 1998).

Nucleation is basically the next step after the formation of the gel and ageing in a conventional crystallization process before crystal growth. The crystallization of zeolites from aluminosilicate gels and their transformation from metastable phase to a more stable phase is a solution-mediated process. In this process, the metastable phase is the precursor of the aluminosilicate species that is required for the formation and growth of a stable phase. As submitted earlier, the induction period (τ) composed of three components i.e.t_r, t_n, t_g (see Section 2.7.4.1). Among these t_n is the time required to form a stable nucleus. Figure 2.45 depicts the classical concept of critical nuclear radius, which is explained by change in free energy (ΔG) during nucleation process.

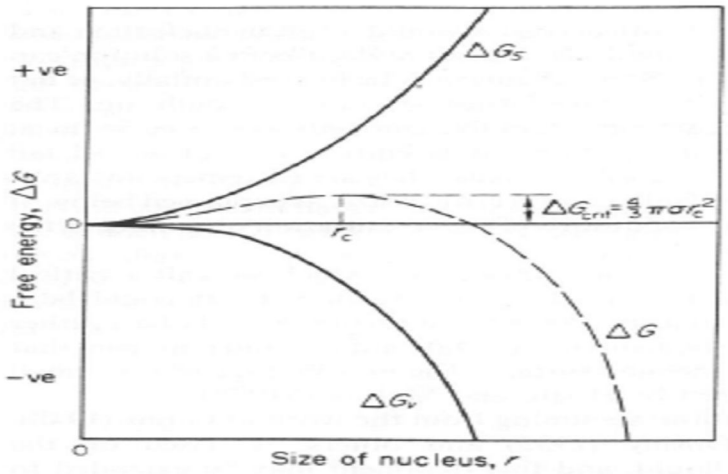


Figure 2.45: The energetics of nucleation, illustrating the concept of a critical nucleus of radius rc; beyond this size, the net energy gain from the resultant (ΔG) of cohesive (ΔGv) and surface (ΔGs) terms is favourable to growth (Mullin, 1993).

The overall change in the free energy (ΔG) between a small solid particle of solute and the solute in the solution is equal to the sum of change in surface free energy (ΔG_s) and the change in the volume free energy (ΔG_v). Whereas, the surface free energy (ΔG_s) is the change in the free energy between the surface of the particle and the bulk of the particle, on the other hand, the volume free energy (ΔG_v) is the change in the free energy between a very large particle ($r=\infty$) and the solute in solution (Mullin, 2001).

Figure 2.45 shows that when the nuclear radius reaches the critical size (i.e. $r = r_c$), a sufficient amount of matter comes together in an ordered way that the cohesive energy (ΔG_v) of the matter becomes stronger than the energy (ΔG_s) which is expended in creating a surface dividing the nucleus from continuum. This makes a stable unit to be formed as stable nucleus capable of further growth. In zeolites, the critical size is estimated around 1-8 unit cells by Thompson and Dyer (1985a). At the same time, the chemical and physical processes which govern the formation of critical size are subjected to the experimental conditions. If these conditions are changed, then rc will also vary. This phenomenon can generally be expressed as in equation 2.15.

$$r = \frac{2\sigma\nu}{kT \ln S} \qquad 2.15$$

where σ is the interfacial tension (surface energy per unit area), ν is the molecular volume and S is the super-saturation ratio *i.e.* $S = c/c^*$ (Mullin, 2001).

In general, the nucleation rate (J) can be defined as the rate of production of unit cells having radius $r \geq r_c$. It has generally been assumed that $J \alpha \frac{1}{\tau}$ (Cundy and Cox, 2003; Culfaz and Sand, 1973), subject to when t_n is greater than t_r and t_g (Subotic *et al.*, 1999; Warzywoda *et al.*,1989). It can safely be assumed that though the formation of nuclei for zeolite crystal formation is more

complex due to its complex assembly as compared to simpler substances whose unit cells are smaller and contain fewer molecules, but there may be no difference in the basic principle of nucleation (Cundy and Cox, 2005). The direct experimental data on nucleation is very difficult to obtain since an extremely small fraction of the total mass is involved. Also, it is very difficult to distinguish the nuclei from the surrounding reactants of similar nature and composition.

Furthermore, more reliable information is available for the early stages of crystal growth behavior rather than nucleation. So far only cryo-TEM (Regev *et al.,* 1994) and HRTEM studies (Mintova *et al.,* 1999a; Mintova *et al.,*1999b; Mintova *et al.,*2002) have provided direct evidence of nucleation phenomena. Other studies estimated the nucleation rate based on crystal growth rate (Culfaz and Sand, 1973). Zhdanov and Samulevich (1980) further improved the approach and were able to determine the isothermal nucleation rate profiles from the crystal growth rate and its size distribution. This method was first used in the analyses of NaA (Zhdanov, 1971b) and NaX (Zhdanov and Samulevich, 1980) crystallization, and subsequently used for other zeolite systems including silicalite (Golemme *et al.,*1991; Cundy *et al.,*1990).

In this method, it was assumed that all the crystals in a batch possess the same growth rate behavior, thus making it possible to calculate the total growth time for each crystal. Based on these findings the nucleation point for each crystal can be obtained by linearly extrapolating the time to zero. Thus the nucleation profile for the whole batch can be determined.

Adding seed crystals to zeolite reaction mixtures provide an effective way of reducing synthesis time and a direction towards a desired product with consequent reduction in impurities (Cundy *et al.,* 1995; Cundy *et al.,* 2003; Kacirek and Lechert, 1975; Verduijn, 1993). Basically, the seed crystals provide a surface area upon which the product can grow. This step eliminates the need of

the surface which is required to be generated through primary nucleation (t_n), thus reduces the induction time (τ). The seed crystals added to synthesis mixture may behave in different ways. They may remain inert, or dissolved, or act as pure seeds upon which the mass is deposited and start to grow. They can also lead to secondary nucleation and hence another crop of crystals. Therefore, it is generally required that a sufficient area is available to have an effect. It is rare for a very small quantity of large crystals to cause any significant change in the synthesis reaction rate. They remain inert or may show some signs of attack, which are due to dissolution in solution. If they show the signs of dissolution then their contribution will mainly be in changing the stoichiometry of the reactants.

The balance between seed growth and the secondary nucleation depends upon the quantity of the seed crystals added and the degree of agitation. If the surface of the added seeds is sufficient to absorb most of the flux of the growth species and prevents the supersaturation of the solution from reaching high levels, then most of the crystal growth will take place on the seed crystals. In this way, the crystal size and the growth rate can be controlled (Cundy *et al.,*1995; Kacirek and Lechert 1975; Kacirek and Lechert 1976; Thompson and Dyer1985a; Thompson and Dyer 1985b; Thompson 1992b). On the other hand, if the quantity of the added seed crystals is reduced (i.e. reducing the available surface area), then supersaturation and self-nucleation will not be suppressed anymore, thus allowing a variety of crystal sizes to grow, and a better control on crystal size and growth rate may be difficult to achieve.

A further aspect of using seed crystals was viewed by Bronic and co-workers. The syntheses of zeolites Y and P (Dutta and Bronic, 1994) and zeolite A (Bronic *et al.,*1999) were investigated using a 2-compartment reactor in which the seed crystals and reactant gel were separated by a submicron membrane. The crystal growth took place in both compartments, but zeolite Y was

formed on seed crystal side of the membrane and zeolite P were observed on the gel side of the membrane. This difference was indicative of the fact that seed crystals were the major participants in modifying the crystallization process when they were in physical contact with the gel. It can be deduced that the growth species travel freely through the membrane, and the nucleation is better controlled locally.

So far in this section, the nucleation is considered from an experimental point of view. A nucleation mechanism will be discussed, now, in the light of the foregone information. In a typical reaction sol, it may contain amorphous material, a solution phase, and one or more crystalline phases. It is relatively easy to identify crystalline phase. Whereas, the distinction between amorphous material and solution phase is less clear and is a subject of misunderstanding. Considering a simple case of traditional synthesis of zeolite X or Y in which amorphous material is visibly solid in nature, at the low Si/Al ratio and high pH of the precipitation nearly all the Si, Al-derived nutrients are present in solid gel phase, and the balance of the nutrients exist as monomers or oligomers in highly alkaline ($Na^{+}OH^{-}$) solution phase (Barrer, 1982).

The separation of the two phases through filtration or centrifugation makes it possible to acquire a division of the reaction mixture into a liquid phase containing mainly true solution species, and a solid phase from which a proportion of crystalline to amorphous material can be determined through XRD analysis. The situation becomes complicated when a higher Si/Al ratio with lower pH is used for high molecular weight silicate and aluminosilicate components. It becomes difficult to distinguish between colloidal material and solution related polymers (Andersson *et al.,* 1982; Iler, 1982; Iler, 1979). At the same time the polymeric species e.g. $Si_1, Si_2, \ldots Si_n$ cannot be considered as a continuum because the larger components may behave like particulate

and can be phaseseparated, thus resembling an invisible precipitate. The end result is that a part of the silicate and aluminosilicate reactants in the liquid phase behaves like a true solution species, and at the same time the colloidal part of the reactant species resembles a separate amorphous phase. The colloidal phase is equal, in term of energetics, to solid phase that is amorphous and visible, but it is invisible to optical detection and is inseparable from the liquid phase by filtration and centrifugation. Therefore, in the systhesis of zeolites using "clear solution", all the amorphous feedstock is stored in the solution in this manner and provides the driving force for the crystallization of zeolite product (Andersson *et al.,*1982; Cundy *et al.,*1990; Iler, 1982; Schoeman *et al.,*1994; Watson *et al.,*1997; Thompson and Dyer, 1985c; Iler, 1979; Ueda *et al.,*1980). Thus it may be emphasized that during the nucleation and crystal growth in hydrothermal synthesis of zeolite, the role of amorphous components at all levels should be accounted for.

In the light of foregone explanations it becomes easier to explain how the equilibration reactions lead to the formation of semi-ordered secondary amorphous phase, and how the related processes further form the zeolite nuclei. As shown in Figure 2.29, that the primary amorphous phase does not show any order in elements. Thus, a driving force for zeolite formation may depend upon the ratio of the solubility constants (K_s) of the precursor and the final product. Since this is directly related to the solution supersaturation, the driving force for the zeolite crystallization reaction (i.e.,change in free energy, ΔG) may be expressed by equation 2.16

$$\Delta G = -RT \ln\left(\frac{K_{s,gel}}{K_{s,zeolite}}\right) \qquad 2.16$$

Equation 2.16 and Figure 2.27 elaborate that the negative sign in the equation signifies a trend for the primary amorphous phase to become more and more ordered as the phase transforms

toward secondary phase and so on. Flanigen and Breck (1960a and b), and also Chang and Bell (1991) focused on the chemical route by which the progressive transformation from amorphous phase to ordered phase took place. The breaking and re-making of Si, Si—O—Al, Al (T—O—T) bonds under the catalytic action of hydroxyl ion (-OH-) with a related condensation reaction are expressed as follows:

$$T-OH+^{-}O-T \Leftrightarrow T-O-T+OH^{-} \qquad 2.17$$

$$T-OH+HO-T \Leftrightarrow T-O-T+H_2O \qquad 2.18$$

It should be noted that anions are not the only ones to take part in breaking and remaking of bonds but they are accompanied by cations (e.g. Na^{+}) that play a crucial role in the ordering of process. The cations will gather around themselves energetically favourable coordination spheres of oxy-species and will generate certain preferred geometries. In doing so the cation dependent elements, which will finally form the zeolite product, are gradually assembled. This idea originally came from Breck (1964), and was further refined by Brunner (1992). The structuring of silicate and aluminosilicate units by electrostatic force (in case of organic templates) and van der Waals force (in case of inorganic material e.g. NaOH) has also been proposed by Flanigen (Flanigen *et al.*,1978; Flanigen 1980), Chang and Bell (1991), and Burkett and Davis (1995b; 1995a). Based upon these ideas and proposals, Cundy and Cox (2005) developed an argument to suggest a specific mechanism for the zeolite lattice construction.

According to the proposed scheme, as shown in Figure 2.46, first of all a cation (e.g. Na^{+}) migrates to a temporary site in a developing structure for nuclei where the coordination geometry may be suitable but not ideal. The cation initially maintains a hydrated shell (i.e. surrounded by water molecules).

Once settled on this site, it starts to mediate the acquisition of T-units from the solution, which is formed through condensation reactions as presented before. The cation guides the new acquired T-units into more favorable coordination geometry, thus generates a periodic regular local structure. In due time, either most of the cation hydration shell is gradually replaced by lattice oxygen donors making it a fixture at the newly created site, or the cation may move to any other more suitable location to do the similar function.

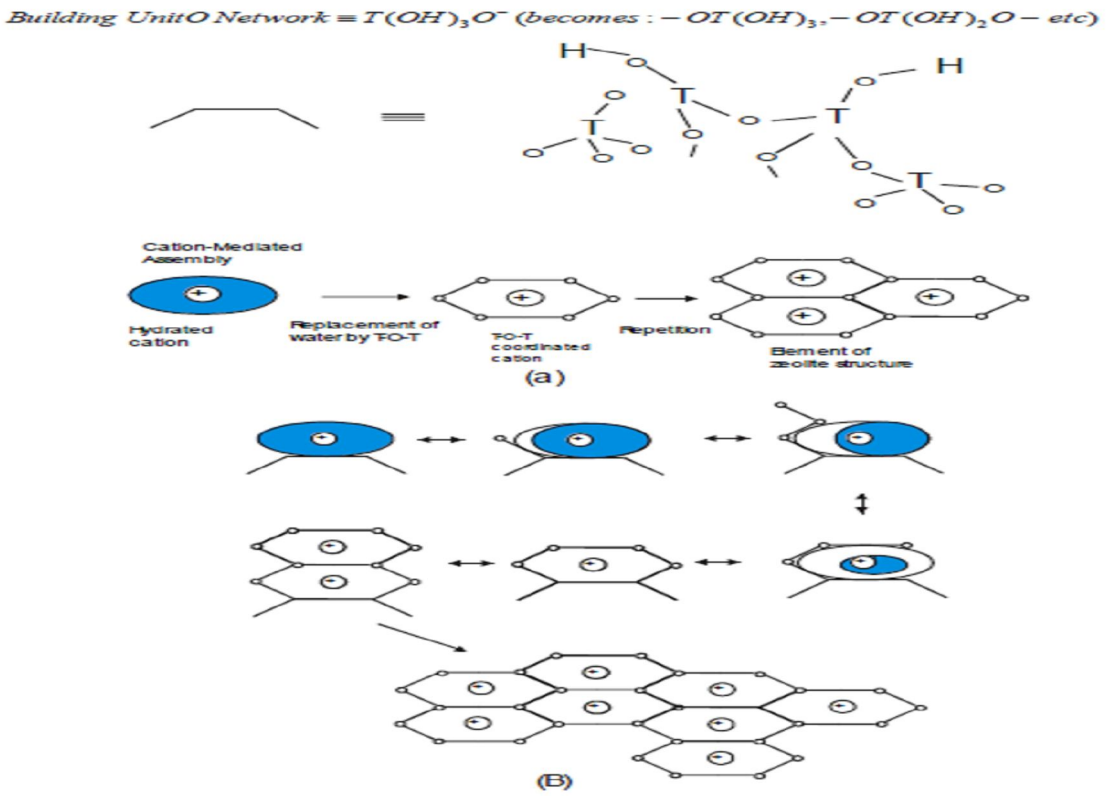


Figure 2.46: The basic mechanism for the cation-mediated assembly of ordered regions: (A) nomenclature and symbolism; (B) details of in-situ construction process by addition of solution units to a surface site. The same mechanism can be applied to zeolite crystal growth. (Cundy and Cox 2005)

For this reason, some areas of the overall structure are more ordered as compared to others. Therefore, in due time, particular "islands of order" are established randomly throughout the newly developed semi-ordered network, as shown in Figure 2.28. These islands of order are dynamic, and at any time such islands are being created, up-graded, or even destroyed by dissolution. However, the overall effect will be a trend that moves towards a more ordered system. Ultimately, some areas of the newly ordered system will be able to make a periodic lattice that can propagate further, i.e. the nucleation has started to occur. Such transformation can be taken as a first order phase transition, and corresponds to the formation of critical radius (r_c) as mentioned earlier.

From this point, the kinetics of the growth in increasing order become dominant as compared to the kinetics of the dissolution resulting in a net growth. As a result, the reversible equilibration reactions which correspond to the t_r component of induction period (τ) are superceded by the initial net growth (t_g). At the same time, the underlying chemistry remains the same and the reactions still maintain a significant reverse component of dissolution (Cundy and Cox, 2005). The nucleation in zeolite may be considered as a discreet event which could be defined as "a phase transition whereby a critical volume of a semi-ordered gel network is transformed into a structure which is sufficiently well ordered to form a viable growth centre from which the crystal lattice can propagate".

Cundy further added comments to this definition. The critical volume in this definition corresponds to the requirement that the initial structure needs to be of a certain minimum size which refers to the critical radius (r_c) as explained earlier. Following this requirement, it is further assumed that the potential nucleus may not need to be perfect in its structure; rather it may be "good enough" to function as a nucleus in prevailing circumstances. This indicates the

condition that r_c is not a fixed quantity but may vary, depending upon the other operating conditions such as temperature and supersaturation.

Thus under such variable environment a rather defective potential nucleus may remain dormant or even dissolve under quasi-equilibrium conditions but may start to grow into a crystal under a high supersaturation driving force. The logic of gradual evolution of such a nucleus can further be explained by cutting a new key for a tumbler lock. Initially, there are no chances that the key will function to open the lock. As the machining of the key progresses, the key will become more and more perfect and a point will reach when it will open the lock. If the new key is compared with the original master key, it will show errors and imperfections in new key but within a certain tolerance it will perform the required function in the prevailing circumstances. It is good enough to do the function of opening the lock, but if the circumstances are changed (e.g. lock becomes hot and expands) then it is possible that the imperfect key may not function any further to open the lock (Cundy and Cox, 2005).

Experimental results of zeolite crystallization and transformation can be mathematically described by a simple kinetic relation shown in equation 2.19 (Subotic et al. 1980; Zhdanov 1971b)

$$f_z = Kt^q{}_c \qquad 2.19$$

Where f_z is the fraction of zeolite formed at time t_c , and K and q are constants. Generally q is a function of nucleation and crystal growth mechanism. For example, in a solidcrystal transforming system with constant supersaturation, q = 3 and nucleation is most likely heterogeneous. If q = 4, nucleation is homogeneous in the case of linear and size independent growth. However, in a real solid-crystal transforming system, the value of q is less than 4. On the

other hand, in the case of crystallization of zeolites from gel (i.e. gel-crystal transformations), the value q could be greater than 4, which shows that the nucleation rate increases during the crystallization process. Zhdanov (1971b) explained such an increase in the nucleation rate as autocatalytic nucleation by postulating "that not only the aluminosilicate blocks formed in the liquid phase, but also the blocks with an ordered structure occurring in the gel skeleton can be nuclei of crystals".

Based on Zhdanov's work, Subotic and Graovac, and Golemme and co-workers developed a theory to support the presence of non-solution mediated nucleation processes (Golemme *et al*.,1991; Subotic and Graovac, 1985). The development was kinetic model for zeolite growth, homogeneous nucleation, heterogeneous nucleation, and autocatalytic nucleation. Experimental results were compared with numerical solution of their model and the particles of zeolites were found to be formed by heterogeneous and autocatalytic nucleation. The role of homogeneous nucleation was insignificant. Furthermore, it was established that the gel crystal transformation followed an exponential dependence on synthesis time with an increase in nucleation rate during the crystallization process.

Postulatation was not limited to the formation of heterogeneous nuclei in the liquid phase (i.e. on the surface of gel and liquid interface), but also the formation of similar entities inside the amorphous gel with ordered structures and called quasi crystalline zeolite. According to them, the growth of the quasi crystalline phase is not possible inside the gel phase but may take place when the gel is dissolved during the progress of crystallization and releasing it into the liquid phase. It was also established that the ageing of the gel increased quasi crystalline phase (ordered structural entities) at room temperature. Subotic and Graovac, and Golemme et al's works led to

the conclusion that the crystallization of zeolites could be explained by their kinetic model where the nucleation takes place at the external surface of the gel i.e. heterogeneous nucleation, or in the inside the pockets of the gel i.e. autocatalytic nucleation. What was missing was the contribution of homogeneous nucleation under the conditions of synthesis. Further conclusion from the experimental evidence was that the increase in the rate of nuclei formation during synthesis, production of a large portion of fine particles towards the end of synthesis, and the influence of gel ageing on the crystallization process could not be explained by the surface heterogeneous nucleation. These led to the suggestion that a significant contribution from autocatalytic nucleation exists during zeolite crystallization.

Thompson (1992b) and Gonthier *et al*., (1993) showed that the autocatalytic nucleation model did not fit all the experimental data. Literature (Golemme *et al*.,1991; Subotic and Graovac, 1985) suggested that the number of crystals formed by autocatalytic nucleation would be approximately 20 times greater than the number formed by the heterogeneous nucleation. Thompson (1992b) and Gonthier *et al*., (1993) found that the nucleation began very early in the synthesis process and the fraction of crystals formed by the heterogeneous nucleation mechanism was low. It was also established that the nucleation of all crystals was essentially complete before the crystallinity of ZSM-5 reached 10%. This behaviour was not expected as more than 95% nuclei were still contained in the amorphous gel and was yet to be released by the dissolution of 90% of the remaining amorphous gel.

Thompson (1992b) and Gonthier *et al*.,(1993) modified the original autocatalytic hypothesis model based on the hypothesis that the nuclei formed by autocatalytic nucleation mechanism were located preferentially near the outer surface of the amorphous gel particles rather than being

uniformly distributed throughout the gel phase. The results of their model agreed well with the experimental data. However, the agreement did not necessarily prove the conceptual validity of the model but suggested the possible existence of a nuclei source other than from the solution (homogeneous nucleation) and solid surface (heterogeneous nucleation).

Homogeneous nucleation is frequently assumed as a possible process for the formation of primary zeolite particles in the liquid phase. It has been shown during the crystallization of different types of zeolites from clear solutions that nucleation may take place in the liquid without the presence of a solid amorphous gel. Using the classical theory of homogeneous nucleation, Bronic and Subotic tested the kinetics of homogeneous nucleation of zeolite A and Y. They found that the time required for the first nuclei to appear through the process of homogeneous nucleation was infinite.

This was because supersaturation, which is typical for most of the zeolites, was considerably lower than the critical supersaturation required for homogeneous nucleation. So, it is realistic to expect that heterogeneous and autocatalytic nucleation mechanisms are dominant for the crystallization from gels (Bronic and Subotic 1995). Mintova and others (Mintova *et al*.,1999a; Mintova *et al*.,1999b) have reported, for the first time, the direct imageing of nucleation mechanism of zeolite Y and A using high resolution transmission electron microscopy (HR-TEM) at 100 ˚C and room temperature, respectively. They studied the synthesis mechanism of nano-sized zeolites from a clear solution. It was established by HR-TEM images, that the freshly prepared solution at room temperature contained the aggregates of amorphous gel particles in the size of 25-35 nm having sharp edges, whereas x-ray diffraction indicated that these colloidal particles were amorphous. After heating the solution for different times at 100 ˚C, the colloidal

gel particles of aluminosilicate remained amorphous for 24 hrs and then the first sign of crystal formation appeared after 28 hr of heating. The images were captured and it was discovered that the crystals nucleated at the periphery of the amorphous gel aggregates which supported the nucleation mechanism discussed by Gonthier *et al.*, (1993). Each aggregate of amorphous gel was seen to form only a single crystal and the particles were rather uniform. Mintova and others visualization was confirmed by a further analysis under dynamic light scattering (DLS) technique. As the synthesis time increased to 48 hrs, it was observed that the size of the zeolite-gel particles remained the same suggesting that the nutrients for the crystal growth were primarily provided by the gel particles. This was further confirmed by the mass balance under several conditions of operation. Upon further heating to 100 hrs, the crystal size was further increased, suggesting that the extended growth of crystals was due to colloidal zeolites themselves as no gel particles remained in the solution after 48 hrs. These colloidal zeolites were able to grow to bigger crystals through the dominant mechanism of mass transfer in solution over macroscopic distances. Figure 2.47 shows all the stages of zeolite nucleation and crystal growth which were captured as a direct evidence using HR-TEM (Mintova 1999a).

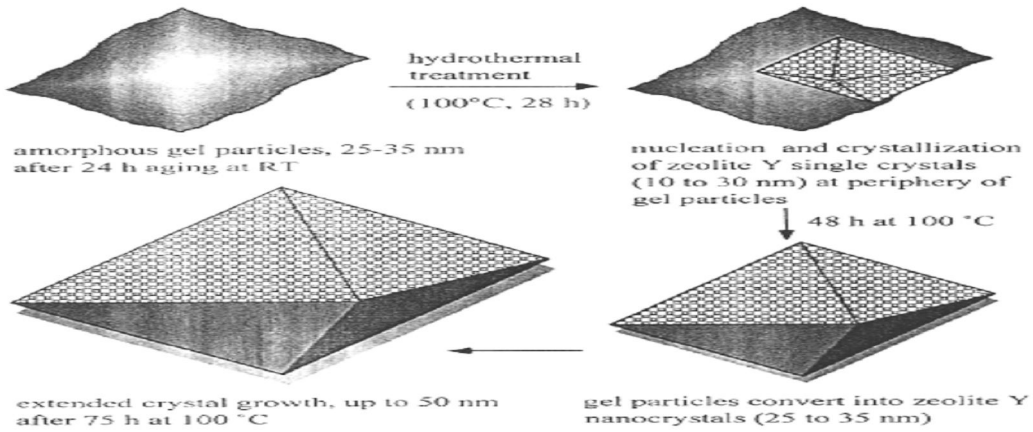


Figure 2.47: Proposed reaction scheme for the zeolite growth mechanism in colloidal solution. Adopted from Mintova *et al.*, 1999a

Li *et al*., (2002) used two different synthesis temperatures, and a two stage varying-temperature technique to further elucidate the mechanism of the nucleation kinetics of zeolite Y. These authors prepared two solutions containing source of alumina and source of silica separately and mixed them together before the hydrothermal treatment. In the one-stage synthesis at 100 ºC, 30-40 nm particles were observed before and during the first three days of hydrothermal treatment. The particles were characterized using dynamic light scattering (DLS). Both solutions were separately analyzed and it was found that only the silica-based solution contained particles of 5nm, which was consistent with previous studies (Li *et al*., 1999). Thus, the 30-40 nm particles were amorphous aluminosilicate, which were formed after mixing the two solutions. Similar findings were also reported by Mintova *et al*., (1999b).

The amorphous particles were observed for the first 4 days of hydrothermal treatment and then slowly decreased to the size of 20nm before a second larger population of zeolite Y was detected after 4 days. This population increased and grew linearly to a size of 75nm after 7 days. A similar pattern was observed at a temperature of 130 ºC, with the exception that the crystal size increased to 137 nm, reaction time reduced to 3 days, the crystal concentration was reduced to one-quarter as compared to the operation at 100 ºC, and the yield was slightly increased. In order to determine the nucleation time for zeolite Y at 100 ºC, a two-stage varying-temperature process was applied. The crystallization was started at 100 ºC and the temperature was changed to 130 ºC to stop further nucleation. In the initial first two days of synthesis the crystal size was unaffected by the temperature.

However, for a longer reaction time the effect of change in temperature was prominent. Therefore, the number of crystals nucleated in the final product (crystal concentration), influenced by the temperature variation, were used to determine the time when nucleation was

completed. Figure 2.48 shows that the process of nucleation continued until the crystal concentration reached a constant value.

Figure 2.48 also shows that for the first-stage of temperature at 100 ºC, the crystal concentration gradually increased to a constant value in 6.5 days and switching to the second-stage at 130 ºC did not reduce the crystal concentration, it only hindered further nucleation. They concluded that the nucleation period was extended over the entire period of crystal growth.

Throughout the crystallization neither SiO_2 nor Al_2O_3 were dissolved in a mother liquid mixture of ethylenediamine and triethylamine. There was a constant molar SiO_2 / Al_2O_3 ratio in the solid phase, which strongly supports the solid-solid mass-transformation mechanism. It was found that the effect of Na_2O was very similar to the effect in aqueous synthesis.

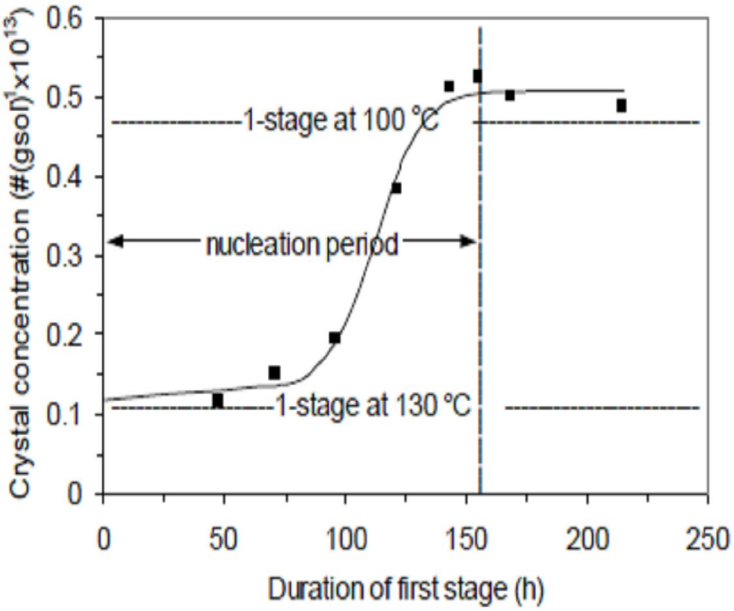


Figure 2.48: Crystal concentration of zeolite Y after two-stage syntheses. (Li *et al.*, 2002).

No effect of Na_2O was observed on the selectivity of ZSM-5 or ZSM-35. However, the initial molar ratio of SiO_2 / Al_2O_3 was crucial in determining the type of zeolite as the ratio did not change during the crystallization. A lower molar ratio (SiO_2 / Al_2O_3 = 18) led to the formation of ZSM-35. Likewise, lower molar ratios of $C_2H_8N_2/Na_2O$ favored ZSM-35 synthesis. The most significant effect was the molar percent of triethlyamine and SiO_2 that determined the formation of ZSM-35 or ZSM-5.

It was found that the presence of different alkali metal chlorides greatly slowed down the crystallization rate with the exception of NaCl. It is well known that Na^+ is the most effective structure-directing agent of all the alkali metal cations. The stronger the capability of the structure-directing cation is, the shorter is the induction time, and higher is the crystallization rate. Actually Na^+ forms a double five-member ring, essential for ZSM-48. Other alkali metal cations showed structure-breaking effects due to their lower polarizability.

It was also observed that the presence of Cl^- anion affected the crystallization rate in the non-aqueous system. The morphology and the size of ZSM-48 were greatly influenced by the use of different metal alkali chlorides. However, the bulk composition of SiO_2 / Al_2O_3 did not vary, owing to the mechanism of heterogeneous crystallization. On the other hand, XPS analysis showed significant changes in the surface composition. This was due to the non-homogeneous distribution of Al from the surface to the crystal core. This was attributed to the structure-directing or breaking abilities of alkali metal cations.

2.9 Synthesis of Zeolites from Soluble Salts, Clay and other sources.

2.9.1 Synthesis of zeolites from soluble salts

The synthesis of zeolites can be traced back to the nineteenth century, when Jean-Baptiste Guimet was able to produce an artificial version of the highly valued and expensive natural pigment ultramarine, an aluminosilicate sodalite containing polysulfides in its cavities. For this discovery he was awarded a French national prize in 1828. In 1862, synthesized levyne (levynite) Ca_9 $[Al_{18}Si_{36}O_{108}]$.$50H_2O$ by heating potassium silicate and sodium aluminate in a glass ampoule. A large increase in synthesis of zeolites was seen after 1940 when X-ray diffraction became a common tool for analysis. Zeolites are traditionally synthesized from soluble salts of aluminates and silicates in a highly basic medium, heated under hydrothermal conditions at temperatures ranging from 100-250^{0}C, in the presence of template or structure directing agent. The template or SDA is not a compulsory condition for successful synthesis of zeolitic material. The silica can be sourced from cabosil, sodium silicate or $Si(OEt)_4$, while the alumina is high surface area aluminum oxyhydroxide, $Al(OEt)_4$, sodium aluminate, etc. It has also been established that low silica content requires low synthesis temperature, i.e. 70-100°C, while more siliceous – hydrothermal condition, required relatively higher temperatures. Various works exist in the open literature and patent on successful synthesis of zeolite Y from chemical salts, some of which are: Yoshida (1995); US Patent 5785944, US Patent 3939246; US Patent 3515511; US Patent 4178352, etc.

2.9.2 Synthesis of zeolites from clay and waste materials

Clay minerals have been used for the synthesis of zeolites as early as 1961(Barrer and Denny,1961). The first reported synthesis of zeolite A from kaolin was by Howell (1961).

Beneficiation and processing improves the quality of clay to some extent, but traces of impurity minerals still remain, which affect the synthesis conditions and properties of the products. Subjecting this pretreated clay to high temperature gives an X-ray amorphous and highly reactive metakaolin, which on hydrothermal treatment with alkali leads to formation of zeolite A. Additional silica or removal of alumina is required in the reaction mixture to get zeolites X and Y. Howell *et al*.,(1965) reported preparation of zeolites X and Y from kaolin and found that the firing temperature of the kaolin precursor influenced the yield of zeolite X (Howell and Acara, 1964; Howell *et al*., 1965). These authors prepared zeolite Y with Si/Al ratio 1.75 in the presence of NaCl, which enhanced the crystallization of the zeolite. Acid-leached metakaolin was used in the starting material for synthesizing zeolite Y of higher Si/Al ratio (2.05), and longer reaction time was needed for crystallization (Barrer, 1978). Work done by Aderemi (2000) indicated successful production of zeolites A, D, F, W and HS from Nigerian kaolin clay, despite the original intent for the synthesis of faujasite type zeolite.

Other researchers have reported the successful synthesis of zeolite Y from foreign kaolinite clay and other sources like fly ash, rice husk ash, etc. Selected publications on the subject matter are: Mason (1969); Chandrasekhar and Pramada (2004); Zhao *et al*.,(1997); Liu *et al*., (2003); Chang and Shih (1998); Shih (1996); Chandrasekhar and Pramada (1999); Akolekar *et al*., (1997), Yang and Yang (1989), Penilla *et al*., (2003), Stamboliev *et al*., (1985) etc.

2.9.3 Application of dyes in zeolite synthesis

Synthesis of zeolites always encounter problems like impure phases, low level of crystallinity, prolonged aging either at room or elevated temperature, and “stubbornness” of silica toward the mineralizer. In the manufacture of faujasite-type zeolites, the prior art routes require, especially for commercial scale manufacture, that the mixed reactants should be highly reactive, of pure

grade and aged quiescently at ambient temperature, and then heated rapidly to a crystallization temperature of, say 100^0C, for conventional heating. This temperature is maintained for 48 to 120 hrs, and the reactant must undergo no significant thermal gradients across the reaction mixture. Such conditions are, of course, extremely difficult to maintain.

It has been, surprisingly, discovered that certain basic nitrogen containing dyes (salts and esters thereof) absorb very strongly on specific zeolites, or only on zeolite having related framework structures. If such basic dyes are employed, this property can be used to suppress the formation of unwanted impurities or side-zeolites products during the manufacture of more desirable products (Whittam, 1977). It is believed that the basic dyes adsorb on nuclei of unwanted species and inhibit nucleation and subsequent crystal growth. The net result of the discovery is that it is now possible to manufacture desired zeolite products under more advantageous operating conditions which would not be employed in the absence of said basic dyes. Furthermore, it was found that it is possible to inhibit the formation of known zeolitic products in favour of the formation of other novel zeolites.

This understanding now provides a platform for the manufacture of synthetic zeolites, wherein the normal reaction of the reactant mixture is altered by the addition of selected additive comprising of a basic dye or mixture of dyes containing nitrogen (or salts or esters of such dyes), where the additive: Al_2O_3 molar ratio being less than 0.1: 1 molar ratio. Such a basic dye containing nitrogen is one which suppresses the formation of unwanted zeolite products. A suitable additive is a dye (or mixture of dyes) which absorbs strongly on unwanted zeolite products, as depicted in Table 2.2 (Whittam, 1977).

It has been found that the presence of potassium ions acts as an inhibiting agent in the formation of zeolite Y, therefore, a basic dye containing nitrogen will be absorbed on potassium ions and

the nuclei of unwanted zeolite species, thereby blanking the potassium ions as well as ameliorating the synthetic conditions.

This additive, containing nitrogen is introduced in the gel preparation stage of the synthesis of the zeolite just before sodium hydroxide solution is added and then ageing stage is bypassed as such allowing it to only crystallize. The amount of added dye is a function of the gels' composition i.e. Si/Al ratio, R_2O/SiO_2 ratio, H_2O/ R_2O ratio and the level of acid radical in the system, as reported by Whittam (1977).

The advantages resulting from use of dye in zeolite synthesis are:

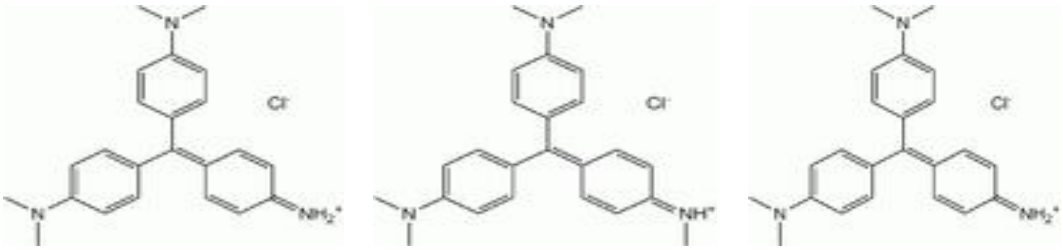
- Suppression of undesired zeolite phases
- Use of any type of silica sources, irrespective of its activity
- Reduction in reaction conditions, i.e. aging, temperature, pressure etc

Table 2.2: Absorption of Dyes on Zeolites

	Adsorption on Zeolites	
Zeolite	***Strong Adsorption***	***Medium strong adsorption***
B (near gismondite)	Crystal Violet, Nuclear Fast Red	Methyl Violet, Methylene Blue
R (near chabasite sodium)	Toluidene Blue, Methylene Blue	
D(near chabazite-Potassium-Sodium)	Toluidene Blue, Methylene Blue	
KM (Potassium near Phillipsite)	Malachite Green, Nuclear Fast Red	Magenta, Crystal Violet
F	Methylene Blue, Malachite Green	
A	Acriflavine	
X, Y, Y□		Acriflavine

2.9.3.1 Crystal violet as dye in zeolite Y synthesis

It is interesting to note that strong theoretical basis is available for the role of dyes in zeolites. Crystal violet is also known under the name of gentian violet. It is a protein dye which stains the fatty portions of sebaceous sweat a deep purple color. Being a protein dye, crystal violet dye can also be used as an enhancer for bloody fingerprints. Crystal violet dye is also used on most types of adhesive tapes, because conventional powders adhere to the entire sticky side of the tape and are not selective to the latent prints. Its molecular formula is given as $C_{24}H_{28}N_3Cl$, with molar mass of 393.958 g/mol and melting point- 137 °C (http://en.wikipedia.org/wiki/Methyl_violet). Depending on the amount of attached methyl groups, the color of the dye can be altered. The type employed in this work was the methyl violet 10B type, as shown in Figure 2.49.



Methyl Violet 2B Methyl Violet 6B Methyl Violet 10B

Figure 2.49: Different types of crystal violet

The color that crystal violet exhibits is due to the extensive system of alternating single and double bonds, which extends over all three benzene rings and the central carbon atom. This alternation of double and single bonding is termed conjugation, and molecules which have extensive conjugation are usually highly colored. The color is due to continuous movement of electrons between single and double bonds. When crystal violet reacts with a base ($-OH$), the conjugation is disrupted and the color is lost. It is necessary to note that in the reaction product, the three rings are no longer in conjugation with one another, and hence the material is colorless. This reaction has kinetics slow enough that the change in color can be observed over time as the

molecules are being changed. As the reaction progresses, less and less of the ionic form of the crystal violet is present, so the solution's color becomes less and less intense (www.cnx.org, 2009).

The role of dyes in enhancing formation of the desired product can only be traced to the chemistry of interaction between it and the major impurity in the gel or starting material.

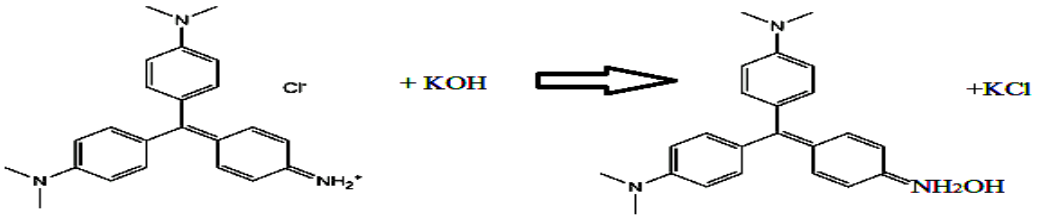


Figure 2.50: Mechanism of reaction between potassium salt(s) and crystal violet.

The reaction mechanism shown in Figure 2.50 emanates from the author, resulting from the known properties of potassium hydroxide and crystal violet. It is speculated that this reaction takes place at room temperature with the formed product serving as a blanket for other sources of impurities. The KCl formed is more soluble in water with less level of dissociation in compared with the initial potassium salt (www.wikipedia.org, 2009). As expected NaOH also would tend to react with the dye, but more of KOH succeeded in attaching itself to the dye, while the free Cl^- was engaged by the K^+. Additionally, it was speculated that, the potassium salt so formed is intercalated within the dye structure, taking the place of Cl^- ion, but in more stable form. It is also speculated, that crystal violet can further dissociate to give more OH- needed to quickly digest the silica, hence the instant depolymerization without aging.

2.9.4 Characterization of zeolite

Zeolitic materials are often characterized or identified through various methods namely, elemental analysis using Energy Dispersive X-ray Flourescence (EDXRF), mineral structure identification using X-ray Difractograph (XRD), surface bond type type identification using Fourier Transform Infrared Spectroscopy (FTIR), shape structure, particle size and morphology using Scanning Electron Micrograph (SEM) and Braunner-Emmett-Teller Surface Area Measurement (BET).

i. Energy Dispersive X-ray Fluorescence

XRF spectroscopy is an analytical technique that exposes a solid sample to an x-ray source. The x-rays from the source have the appropriate excitation energy that causes elements in the sample to emit characteristic x-rays. A qualitative elemental analysis is possible from the characteristic energy, or wavelength, of the fluorescent x-rays emitted. A quantitative elemental analysis is possible by counting the number (intensity) of x-rays at a given wavelength.

Three electron shells are generally involved in emissions of x-rays during XRF analysis of samples: the K, L, and M shells. Multiple-intensity peaks are generated from the K, L, or M shell electrons in a typical emission pattern, also called an emission spectrum, for a given element. The focus of XRF analysis is directed on the x-ray emissions from the K and L shells because they are the most energetic lines. K lines are typically used for elements with atomic numbers from 11 to 46 (sodium to palladium), and L lines are used for elements above atomic number 47 (silver). M-shell emissions are measurable only for metals with an atomic number greater than 57 (lanthanum).

As illustrated in Figure 2.50, characteristic radiation arises when the energy from the x-ray source exceeds the absorption edge energy of inner-shell electrons, ejecting one or more electrons. The vacancies are filled by electrons that cascade in from the outer shells. The energy states of the electrons in the outer shells are higher than those of the inner-shell electrons, and the outer-shell electrons emit energy in the form of x-rays as they cascade down. The energy of this x-ray radiation is unique for each element.

An XRF analyzer consists of three major components: (1) a source that generates x-rays (a radioisotope or x-ray tube); (2) a detector that converts x-rays emitted from the sample into measurable electronic signals; and (3) a data processing unit that records the emission or fluorescence energy signals and calculates the elemental concentrations in the sample.

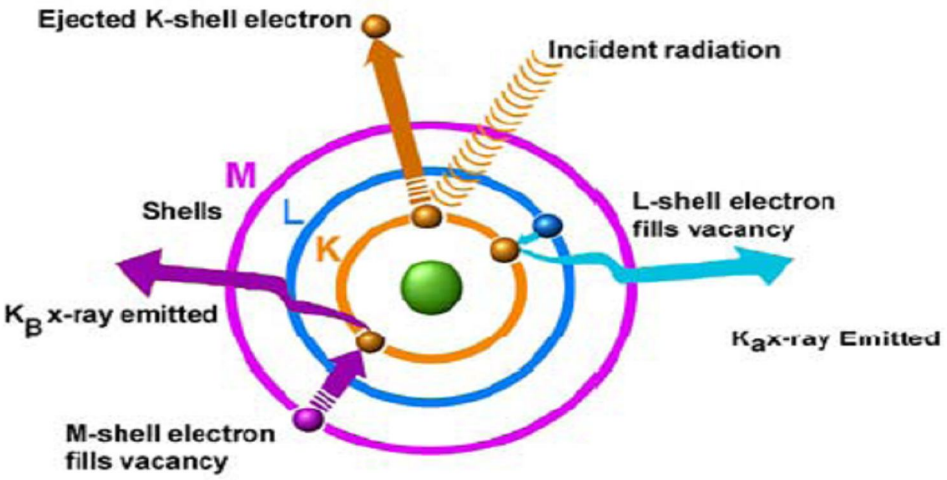


Figure 2.51: The XRF Process

ii. X-ray Powder Diffraction

X-ray powder diffraction (XRD) is a rapid analytical technique primarily used for phase identification of a crystalline material and can provide information on unit cell dimensions. The analyzed material is finely ground, homogenized, and average bulk composition is determined.

Max von Laue, in 1912, discovered that crystalline substances act as three-dimensional diffraction gratings for X-ray wavelengths similar to the spacing of planes in a crystal lattice. X-ray diffraction is now a common technique for the study of crystal structures and atomic spacing.

X-ray diffraction is based on constructive interference of monochromatic X-rays and a crystalline sample. These X-rays are generated by a cathode ray tube, filtered to produce monochromatic radiation, collimated to concentrate, and directed toward the sample. The interaction of the incident rays with the sample produces constructive interference (and a diffracted ray) when conditions satisfy Bragg's Law ($n\lambda=2d \sin \theta$). This law relates the wavelength of electromagnetic radiation to the diffraction angle and the lattice spacing in a crystalline sample. These diffracted X-rays are then detected, processed and counted. By scanning the sample through a range of 2θangles, all possible diffraction directions of the lattice should be attained due to the random orientation of the powdered material. Conversion of the diffraction peaks to d-spacings allows identification of the mineral because each mineral has a set of unique d-spacings. Typically, this is achieved by comparison of d-spacings with standard reference patterns.

All diffraction methods are based on generation of X-rays in an X-ray tube. These X-rays are directed at the sample, and the diffracted rays are collected. A key component of all diffraction is the angle between the incident and diffracted rays. Powder and single crystal diffraction vary in instrumentation beyond this.

X-ray diffractometers consist of three basic elements: an X-ray tube, a sample holder, and an X-ray detector. X-rays are generated in a cathode ray tube by heating a filament to produce electrons, accelerating the electrons toward a target by applying a voltage, and bombarding the

target material with electrons. When electrons have sufficient energy to dislodge inner shell electrons of the target material, characteristic X-ray spectra are produced. These spectra consist of several components, the most common being K_α and K_β. K_α consists, in part, of $K_{\alpha1}$ and $K_{\alpha2}$. $K_{\alpha1}$ has a slightly shorter wavelength and twice the intensity as $K_{\alpha2}$. The specific wavelengths are characteristic of the target material (Cu, Fe, Mo, Cr). Filtering, by foils or crystal monochrometers, is required to produce monochromatic X-rays needed for diffraction. $K_{\alpha1}$and $K_{\alpha2}$ are sufficiently close in wavelength such that a weighted average of the two is used. Copper is the most common target material for single-crystal diffraction, with CuK_α radiation = 1.5418Å. These X-rays are collimated and directed onto the sample. As the sample and detector are rotated, the intensity of the reflected X-rays is recorded. When the geometry of the incident X-rays impinging the sample satisfies the Bragg Equation, constructive interference occurs and a peak in intensity occurs. A detector records and processes this X-ray signal and converts the signal to a count rate which is then output to a device such as a printer or computer monitor.

The geometry of an X-ray diffractometer is such that the sample rotates in the path of the collimated X-ray beam at an angle θ while the X-ray detector is mounted on an arm to collect the diffracted X-rays and rotates at an angle of 2θ. The instrument used to maintain the angle and rotate the sample is termed a *goniometer*. For typical powder patterns, data is collected at 2θ from ~5° to 70°, angles that are preset in the X-ray scan.

iii. Fourier Transform Infrared Spectroscopy

FTIR is most useful for identifying chemicals that are either organic or inorganic. It can be utilized to quantitate some components of an unknown mixture. It can be applied to the analysis of solids, liquids, and gasses. The term Fourier Transform Infrared Spectroscopy (FTIR) refers to

a fairly recent development in the manner in which the data is collected and converted from an interference pattern to a spectrum. Today's FTIR instruments are computerized which makes them faster and more sensitive than the older dispersive instruments. FTIR is perhaps the most powerful tool for identifying types of chemical bonds (functional groups). The wavelength of light absorbed is characteristic of the chemical bond as can be seen in this annotated spectrum. By interpreting the infrared absorption spectrum, the chemical bonds in a molecule can be determined. FTIR spectra of pure compounds are generally so unique that they are like a molecular "fingerprint". Because the strength of the absorption is proportional to the concentration, FTIR can be used for some quantitative analyses.

iv. Braunner-Emmett-Teller Surface Area Measurement

The gas adsorption method is used for measuring the amount of gas adsorbed on the surface of a powder sample as a function of the pressure of the adsorbate gas, and is used to determine the specific surface area of a powder sample.

When the gas is physically adsorbed by the powder sample, Equation 2.20 holds when P/P_0 is in the range of 0.05 to 0.30 for pressure P of the adsorbate gas in equilibrium for the volume of gas adsorbed, V_a.

$$\frac{1}{V_a\left(\frac{P_0}{P}-1\right)} = \frac{(C-1)}{V_m C} * \frac{P}{P_0} + \frac{1}{V_m C} \qquad 2.20$$

where, P=Partial vapor pressure of adsorbate gas in equilibrium, (kPa)

P_0= Saturated pressure of adsorbate gas

V_a=Volume of gas adsorbed at equilibrium, ml

V_m= Volume of gas adsorbed in a monolayer, ml

C= Dimensionless constant related to the enthalpy of adsorption and condensation of the adsorbate gas.

The specific surface area, S, is determined from V_m , the volume of gas adsorbed in a monolayer on the sample.

$$S = \frac{V_m * N * a}{m * 22400} \qquad 2.21$$

where, S=Specific surface area, m^2/g

N=Avogadro constant

a=Effective cross-sectional area of one adsorbate molecule, m^2

m=mass of the test powder, g

v. Scanning Electron Microscope

The scanning electron microscope (SEM) is a type of electron microscope that images the sample surface by scanning it with a high-energy beam of electrons in a raster scan pattern. The electrons interact with the atoms that make up the sample producing signals that contain information about the sample's surface topography, composition and other properties such as electrical conductivity.

The types of signals produced by a SEM include secondary electrons, back-scattered electrons (BSE), characteristic X-rays, light (cathodoluminescence), specimen current and transmitted electrons. Secondary electron detectors are common in all SEMs, but it is rare that a single machine would have detectors for all possible signals. The signals result from interactions of the electron beam with atoms at or near the surface of the sample. In the most common or standard detection mode, secondary electron imaging or SEI, the SEM can produce very high-resolution

images of a sample surface, revealing details about less than 1 to 5 nm in size. Due to the very narrow electron beam, SEM micrographs have a large depth of field yielding a characteristic three-dimensional appearance, useful for understanding the surface structure of a sample.

In a typical SEM, an electron beam is thermionically emitted from an electron gun fitted with a tungsten filament cathode. Tungsten is normally used in thermionic electron guns because it has the highest melting point and lowest vapour pressure of all metals, thereby allowing it to be heated for electron emission, and because of its low cost. Other types of electron emitters include lanthanum hexaboride (LaB_6) cathodes, which can be used in a standard tungsten filament SEM if the vacuum system is upgraded and field emission guns (FEG), which may be of the cold-cathode type using tungsten single crystal emitters or the thermally-assisted Schottky type, using emitters of zirconium oxide.

The electron beam, which typically has an energy ranging from a few hundred eV to 40 keV, is focused by one or two condenser lenses to a spot about 0.4 nm to 5 nm in diameter. The beam passes through pairs of scanning coils or pairs of deflector plates in the electron column, typically in the final lens, which deflect the beam in the *x* and *y* axes so that it scans in a raster fashion over a rectangular area of the sample surface.

When the primary electron beam interacts with the sample, the electrons lose energy by repeated random scattering and absorption within a teardrop-shaped volume of the specimen known as the interaction volume, which extends from less than 100 nm to around 5 µm into the surface. The size of the interaction volume depends on the electron's landing energy, the atomic number of the specimen and the specimen's density. The energy exchange between the electron beam and the sample results in the reflection of high-energy electrons by elastic scattering, emission of

secondary electrons by inelastic scattering and the emission of electromagnetic radiation, each of which can be detected by specialized detectors. Electronic amplifiers of various types are used to amplify the signals which are displayed as variations in brightness on a cathode ray tube. The raster scanning of the CRT display is synchronised with that of the beam on the specimen in the microscope, and the resulting image is therefore a distribution map of the intensity of the signal being emitted from the scanned area of the specimen. The image is captured and displayed on a computer monitor and saved to a computer's hard disc. Magnification in a SEM can be controlled over a range of up to 6 orders of magnitude from about 10 to 500,000 times.

CHAPTER THREE

3.0 INSTRUMENTATION, EQUIPMENT AND METHODOLOGY

3.1 Instrumentation and Equipment

In carrying out this experiment, the underlisted instruments and equipment were used.

3.1.1 Clay beneficiation

- 10 litres plastic drum and buckets
- Raw tapwater and distilled/deionized water
- Sieving material with mesh size of 250μm
- Raw Kankara (from different site) and Elefun kaolinite clay samples
- Domestic pulverising machine, for size reduction of the dried kaolin

3.1.2 Calcination

- Locally fabricated ceramic crucible of sizes 2L, 1L and 250mL.
- Electric furnace (Model No: LH 120/14, Max Temp-1400^{o}C)
- Dessicator with silica gel

3.1.3 Dealumination

- 1L conical flask, 250mL beaker, measuring cylinder (1L and 250mL)
- Heating mantle with voltage regulator (500mL capacity)

- Electronic weighing machine (PW 184, M: 180g Accuracy 10^{-4}g)
- 1L three-neck-round bottom flasks with thermometer and reflux condenser
- Metakaolin- calcined Kankara and Elefun kaolin
- 96% w/w sulfuric acid (H_2SO_4) from a range of sources
- Vacuum pump (Edward High Vacuum Pump, Model No: ES00)
- pH meter

3.1.4 Gel formation

- Sodium hydroxide (NaOH) supplied by Aldrich, England
- Calcined dealuminated metakaolin
- Distilled/deionized water
- 1L rubber container, for aging purpose
- Electrically driven magnetic stirrer and domestic blender

3.1.5 Zeolite synthesis

- Laboratory oven (Model No: MD6C-64, Michem Instrument)
- Teflon/polyethylene jacketed batch reactor
- Commercial zeolite Y (obtained from Zeolyst)
- Crystal violet, methylene blue, fuscin, magenta
- pH meter

- ❖ 5 kW electricity generator, for continuous power supply

3.1.6 Characterization

- ❖ BET, using water adsorption method, Ahmadu Bello University (ABU), Zaria, Penn State University, USA and University of Witwaterstrand, South Africa.
- ❖ X-ray fluorescence (XRF) at National Metallurgical Development Council, Jos and National Geoscience Research Laboratory (NAGRL), Kaduna
- ❖ FTIR spectrometer at Nuhu Bamalli Poly, Zaria and National Research Institute for Chemical Technology (NARICT), Zaria
- ❖ X-ray diffraction (XRD) at Engineering Material Development Institute, Akure, Penn State University, USA and University of Witwaterstrand, South Africa, NAGRL, Kaduna and Sheda Science and Technology Complex (SHESTCO),Garki, Abuja. Nigeria
- ❖ Inductive couple Plasma-mass spectrometer (ICP-MS) at Penn State University (PSU), USA.
- ❖ Scanning electron micrograph (SEM) at University of Witwaterstrand, South Africa, Penn State University (PSU), USA and SHESTCO,Garki, Abuja.

3.2 Methodology

This section gives a detail description of the process which the raw material – kaolin – was subjected to, its transformation into zeolitic material. The procedure described here, documents the five different phases or stages in the attempts to synthesis zeolite Y, from kaolinite clay. The stages are hereby termed Categories I, II, III IV and V (descrided in Table 3.1), which give a historical development and findings made during the course of this work. It also illustrates synthesis of zeolite Y from soluble salts, which served as control.

Table 3.1: Decription of the stages involved in zeolite synthesis

Category	Description
I	Sample (Kankara white) dealuminated via heating method ➢ Aged for 4, 6 and 8 days ➢ Dyed with methylene blue, toluidine, blue crystal violet and malachite green ➢ Effect of crystallization time and temperature ➢ Calcination temperature effect on zeolite type formed
II	Sample (Kankara white and red) dealuminated via both heating and non-heating method ➢ Aged for 3,5,7,9,11 and 13 days ➢ Seeding effect with low concentration of seeded material aged for 1-3 days ➢ Alkaline effect using Na_2O/SiO_2=0.4-0.7 ➢ Effect of pH on zeolitization
III	Sample (Kankara red) dealuminated via heating method ➢ Aged for 9 days, with pH of 12.8 and a further improvement on categories I and II
IV	Sample (Kankara white and Elefun) dealuminated via heating method ➢ Aged for 3,5,7,9,11 and 13 days ➢ Dyed with crystal violet ➢ Seeded with higher concentration without ageing ➢ Alkaline effect
V	Improvement studies on best points from category IV (sulphate removal attempts)

3.2.1 Transformation stages of kaolinite clay into Zeolite Y

3.2.1.1 Beneficiation

About 2 kg of raw kaolin sourced from Kankara (Red and white, in colour) and Elefun were soaked in water for a period of five days with periodic mastication and agitation in a 10L plastic drum filled up to three quarter (3/4) height. Once after twelve hours (12hrs) when the kaolin was completely settled, the supernatant was decanted, together with accompanying floating dirts. The process of thorough mastication of kaolin resulted in the removal of stony particles achieved via handpicking or slurry decantation. Thereafter, fresh water was spouted (gushed), into the muddy kaolin, to effect frothy thorough mixing, follow by layered settling in accordance with Stoke's law. The process of mastication, sorting, agitation and decanting was done repeatedly until less noticeable solid layers at the bottom of the container. The topmost layer of the resulting slurry was exfoliated and separated into different container, washed with water and sieved using a 250micron mesh. The sieved material was dewatered, air dried and further dried at 120^0C in an electric oven (Model No: MD6C-64, Michem Instrument) for 6hrs. The resulting dried cake was crushed using a jaw crusher and ball milled to very fine particle size, which was subsequently packaged for analyses.

3.2.1.2 Calcination

The optimal temperature used in this work was arrived at after investigating the effect of calcination temperature and time on amorphousity and rate of solubility and digestion in acid/alkali, for all the kaolinite components, on one hand. On the other, a preliminary investigation was conducted to understudy the best metakaolinization temperature required to convert both alunmina and silica into more reactive, highly digestible form for zeolitization. The

result of the aforementioned preliminary investigations, informed the choice of calcining the beneficiated kaolin (from Kankara and Elefun) at 850^0C and 950^0C, respectively. For this process, the clay was heated in a programmable electric furnace (Model No: LH 120/14), from room temperature (T) to the calcination temperature (T_{cal}) at heating rate of $10^0 Cmin^{-1}$. The sample was held at T_{cal} for 6hrs. Calcination was achieved by evenly placing about 1kg of beneficiated kaolin into a large rectangular locally fabricated crucible on a very flat depth, to allow for a relative good heat distribution, since the specific heat capacity and latent heat of kaolin is poor. The metakaolin obtained was transferred into a big desiccator for cooling in a controlled environment, prior to characterization and use.

3.2.1.3 Dealumination

The silica-alumina ratio for the resulting metakaolin was determined from the compositional analysis, using either XRF or ICP. The inherent Si/Al ratio for metakaolin was not good enough for the synthesis of faujasite type zeolite.

Accordingly, to meet the compositional requirement for the synthesis, removal of alumina (dealumination) and other impurities from metakaolin was carried out. This was achieved by making the calcined kaolin to react with sulfuric acid. Sulfuric acid dealumination reaction was done using both ***heating and non- heating method*** for Category II, and only ***heating approach*** for Categories I, III and IV. The extent of dealumination was determined by varying the reaction times, which differs for the mode of dealumination.

(a). heating method of dealumination

This method often requires the input of external source of thermal energy to facilitate the needed kinetic energy for effective collision and successful reaction between the metakaolin and sulfuric

acid. In all cases, dealumination was done by using three fold of the stoichiometric amount of 60wt% sulfuric acid required. This was done to enhance mass transfer and to reduce cake formation tendencies (Aderemi, 2000).

About 50 g of the metakaolin (from samples in Categories I to IV) was mixed with appropriate quantity of deionized water and acid, followed by vigorous stirring to obtain mixed slurry. The slurry was poured into a three-necked round bottom flask and fitted on the central neck with a reflux condenser, which was placed on the heating mantle. A thermometer was placed on the second neck while the third neck was closed using a rubber cock. The reaction time was varied between 3 and 27 minutes, in intervals of 3 minutes in order to establish the reaction time required to give the targeted silica-alumina ratio of 10. For further investigation on the relationship between reaction time and silica-alumina ratio, a reaction time interval ranging from between 5 and 60 minutes. At the end of the reaction period, the samples were quenched with water.

The dealuminated samples were washed thoroughly, with hot deionized water to ensure almost complete removal of excess unreacted acid and other soluble salts resulting from the leaching process. These were subsequently dewatered, using suction pump and dried in an oven at 110^0C for 3hrs. The dried dealuminated samples were packaged for various analyses. The effect of the quality/source of acid employed, on the rate of dealumination reaction was also investigated.
The calculation for dealumination reaction for Categories I, IIa, III and IV (note that Category IIa denoted samples in Category II subjected to heating method of dealumination) are contained in Appendix A.

(b). Non-heating method of dealumination

This method of dealumination reaction does not require an external source of thermal energy to facilitate the dealumination of the metakaolin, but instead it employed the heat released when sulphuric acid is mixed with water.

The approach presented in Section 3.2.1.3(a) was repeated but without the addition of external source of thermal energy, as reaction time was varied only between 3 and 27mins for samples categorized under Category IIb. The dealuminated samples were washed thoroughly with hot deionized water to remove excess unreacted acid and other soluble salts resulting from the leaching process. These were subsequently dewatered using suction pump and dried in an oven at 110^0C for 3hrs. The dried dealuminated samples were packaged for various analyses.

3.2.1.4 Gel formation and Synthesis

a) Synthesis of zeolite Y from soluble salts

For the laboratory synthesis of zeolite Y from soluble salts, the procedure described by Ginter and partner (1992b) was employed. In this process, about 2 g of sodium hydroxide, 4 g of sodium aluminate and 20g of water was stirred vigourously until the solid was completely dissolved to form solution A. To solution A, 23 g of sodium silicate was added, stirred moderately for at least 10 minutes and later allowed to age at ambient temperature for 1 day under quiescent condition, which is refered to as seed B.

In separate beaker, about 0.15 g of sodium hydroxide, 14 g of sodium aluminate and 131g of deionized water was stirred vigourously until the solid was completely dissolved to form solution C. 142 g of sodium silicate was added to solution C, stirred vigourously until the gel appears

somewhat smooth, this is refered to as feedstock D. The prepared colloidal seed B was slowly added to feedstock D with vigourous stirring until the the later finishes.

The resulting gel was transferred into an autoclavable polypropylene batch reactor and aged for 24hr at ambient temperature. After aging, the reactor was placed in a calibrated electric oven, with the crystallization time and temperature set for 24hr and 105^0C, respectively. The completion of crystallization was established when the gel separated into a solid and a clear supernant liquid. The product was properly washed with deionized water until the pH of filtrate was below 9, and dried at 110^0C. The dried samples were properly packaged and subsequently subjected to various analyses.

The aforementioned was done to serve not only as control but also to see the useability of chemicals procured locally for the purpose of synthesizing zeolite Y.

b) Synthesis of zeolite Y from pretreated kaolin

i. aging effect

The desired molar composition for zeolite Y is given as shown in Equation 3.1

$$\frac{SiO_2}{Al_2O_3} = x; \quad \frac{Na_2O}{SiO_2} = 0.6; \quad \frac{H_2O}{Na_2O} = 25 \qquad 3.1$$

The SiO_2/Al_2O_3 ratio used in Equation 3.1 was obtained from the compositional analysis of the dealuminated samples, while the other ratios were kept constant. The value of "x" in Equation 3.1 was already made to be 10 for thermal approach and 6 for non-thermal approach during the dealumination procedure. Accordingly, the mass of NaOH $(Na_2O + H_2O \rightarrow NaOH)$ and volume of water required for gellating 20gm of dealuminated metakaolin was calculated, as shown in Appendix B, for Categories I, IIa, IIb, III and IV, respectively. The dealuminated sample was

mixed with NaOH (to form Na_2O/SiO_2 ratio of 0.6) and aged for: 4, 6 and 8 days for Category I; 3 to 13 days, in interval of 2 days for Categories IIa and b; only 9 days for Category III and 3 to 11 days for Category IV. The reaction was conducted in a jacketed polypropylene reactor placed in an autoclave or electric oven set at 110^0C for 72hrs. At the end of the reaction, the sample was washed free of excess NaOH using deionized water, dried at room temperature and kept under vacuum before packaging for analyses. The completely dried samples were properly packaged and sent for various analyses, namely XRD, SEM, and BET.

ii. addition of blanking agents effect

Gel with the same composition as prepared in Section 3.2.1.4b (i) was treated with different type of nitrogen based dyes, such as malachite green, methylene blue, fuscin, toluidene and crystal violet, but without ageing. The compositions of the added dyes were varied while the other components of the reacting species were kept constant, as shown in Table 3.2. Appendix C shows the calculation done to obtain the required quantity of dye used.

Table 3.2: Composition of dyes added to the gel

	Moles of dye/moles Al_2O_3				
Name of dye	Category I	Category II	Category III	Category IV	Category V
Malachite green	0.001	n.a	n.a	n.a	n.a
	0.002	n.a	n.a	n.a	n.a
	0.005	n.a	n.a	n.a	n.a
	0.01	n.a	n.a	n.a	n.a
	0.015	n.a	n.a	n.a	n.a
Toluidine blue	0.001	n.a	n.a	n.a	n.a
	0.002	n.a	n.a	n.a	n.a
	0.005	n.a	n.a	n.a	n.a
	0.01	n.a	n.a	n.a	n.a
	0.015	n.a	n.a	n.a	n.a
Methylene blue	0.001	n.a	n.a	n.a	n.a
	0.002	n.a	n.a	n.a	n.a
	0.005	n.a	n.a	n.a	n.a
	0.01	n.a	n.a	n.a	n.a
	0.015	n.a	n.a	n.a	n.a
Crystal violet	0.001	n.a	n.a	0.0001	n.a
	0.002	n.a	n.a	0.0005	n.a
	0.005	n.a	n.a	0.005	0.005
	0.01	n.a	n.a	0.001	0.001
	0.015	n.a	n.a	0.01	n.a
Magenta	0.001	n.a	n.a	n.a	n.a
	0.002	n.a	n.a	n.a	n.a
	0.005	n.a	n.a	n.a	n.a
	0.01	n.a	n.a	n.a	n.a
	0.015	n.a	n.a	n.a	n.a

n.a=not applicable

The resulting gels were subjected to heating in an electric oven for 24hrs at temperature of 95^0C. After the speculated time, the products were washed thoroughly with deionize water to remove excess dye and sodium hydroxide, dried at room temperature and kept under vacuum before packaging for analyses.

iii. alkali concentration effect

The gel having the same composition as in Section 3.2.1.4b (i) was used, expect that the Na_2O/SiO_2 ratios for Categories I, II, III and IV ranged from 0.5 to 1.0, 0.6 to 0.9, only 0.6; and

0.5 to 0.9, respectively. The resulting gels were subjected to heating in an electric oven for 72 hrs at temperature of 105^0C. After the specified time, the products were washed thoroughly with deionize water to remove sodium hydroxide, dried at room temperature and kept under vacuum before packaging for analyses.

iv. pH effect

The procedure presented in Section 3.2.1.4b (i) was repeated only that to the gel, five different quantities of NaOH were added, maintain a pH between 9.5 and 13.5, and aged for 11days. The resulting gels were placed in a teflon reactor and subjected to heating in an electric oven for 72 hrs at temperature of about 105^0C. At the end of the heating period, the product was washed thoroughly with deionize water to remove sodium hydroxide, dried at room temperature and kept under vacuum before packaging for analyses. This step was done only for samples categorized under Category II.

v. seeding effect

The procedure mentioned in Section 3.2.1.4b (i) was repeated only that the gel was seeded with commercial zeolite Y (in proportions of 2, 4, 6 and 8 wt% to the used metakaolin) and also aged for 1 and 3 days, for Category II, while the proportion was changed to 0.1, 0.15, 0.2, 0.25 and 0.3wt% with respect to metakaolin before ageing for a day, for Category IV. The resulting gels were placed in a jacketed polypropylene reactor and subjected to heating in an electric oven for 72 hrs at temperature of 105^0C. After the specified time, the products were washed thoroughly with deionize water to remove excess sodium hydroxide, later dried at room temperature under vacuum before packaging for analyses.

3.2.1.5 Improvement study

The procedures described in Section 3.2.1.4b (i, ii, iii and iv) were choosen and repeated for some resulting products based on the observed promising XRD peaks attributable to faujasite zeolite. This procedure was undertaken to check the result of the improvement study and reproducibility of the procedure. In addition, some modification to the procedure was made to correct/address observed shortcomings.

In order to address issues observed, post-dealumination calcinations was done for 3hrs at 450^0C, after thorough washing with deionized water, from the previous experimentation. An additional calculated amount of NaOH was introduced as not only depolymerizing agent but also needed to neutralize unwanted sulfates. Apart from this, the resulting gel were mixed thorough and for a longer time compared to the previous mixing pattern and time.

3.2.2 Characterization technique

(i) X-Ray diffraction (XRD) analysis

The kaolinite, zeolite and other related samples' mineralogy was evaluated by conducting XRD spectrometry using Philips Analytical graphite monochromator at Penn State University, Pa, USA, National Geoscience Research Laboratory (NAGRL), Kaduna, University of Witwaterstrand, South Africa, and Sheda Science, Technology Complex (SHESTCO),Garki, Abuja and from a different company at Engineering Material Development Council (EMDI), Akure.

Powder X-ray diffraction (PXRD) was carried out using Cu Kα1 radiation on a Panalytical MPD PRO X-ray powder diffractometer equipped with a PW3050/60 goniometer (Theta/2Theta) and a

curved germanium (1 1 1) primary monochromator. The samples were scanned in the 2 theta range of 4–50^0, with step size of 0.0131 and counting time of 100 s. The data files presented by X'Pert Graphics and identify data collection software were used to identify the minerals present in the samples. PXRD indexation of the as-synthesized samples was carried by the TREOR program in SHESTCO, Abuja and NAGRLS, Kaduna.

A similar analyses but with less precinction were conducted at Engineering Material Development Institute (EMDI), Akure with 2 theta range of 10-50^0 known not to be suitable for proper identification of most zeolitic materials.

(ii) Scanning Electron Microscopy

Scanning electron microscopy (SEM) analysis: A Hitachi X-650 Scanning Electron Microanalyzer was used to take the micrographs of the samples, at an accelerating voltage of 10.0 kV and a working distance of 10.0 mm. The samples were first calcined and later mounted on aluminium stubs using conductive glue and were then coated with a thin layer of carbon paste tape on copper pegs and coated with a film of evaporated gold, prior to the observation.

(iii) X-Ray fluorescence (XRF)

X-ray fluorescence (XRF) experiments were performed by a BRUKER-AXS S4 Explorer apparatus. Before the analysis, the well washed and dried samples were fused with $Li_2B_4O_7$ at 1573 K. The samples were properly homogenized and pressed into a pellet, after which it was placed on the sample holder of the machine for scanning and recording.

(iv) Fourier transform infrared (FTIR) spectrometry

Approximately 15 mg of the kaolin and zeolite samples, plus 1 g of KBr was weighed out, milled and ground in an agar mortar and pestle for 5 min, until a fine smooth powder of even particle size was obtained. A quarter (~0.25 g) of the zeolite and KBr mixture was then pressed with a steel die at 10 ton cm^{-2} into a pellet (or wafer). IR spectra of the samples were recorded on a Perkin Elmer Paragon 1000 PC, FT-IR Spectrometer, in the range between 4000–400 cm^{-2}.

(v) *Water-Adsorption-BET surface area determination*

The specific surface area of the zeolite samples were determined by using a water adsorption method developed and detailed by Adefila et al (2003).

CHAPTER FOUR

4.0 RESULTS AND DISCUSSION

4.1 As Mined (Raw) Clay

4.1.1 XRF Analysis

The elemental analysis conducted on raw and beneficiated kaolin (both red and white Kankara and Elefun) indicated presence of impurities in all the raw clay. Table 4.1 gives a descriptive illustration of the effect of beneficiation on all the treated raw kaolin, for various stages.

With reference to impurities, the compositional analysis of the raw kaolin depicted in Table 4.1 indicated its richness in oxides of potassium, iron, titanium and magnesium. It was observed that some of the kaolin samples were low in iron but rich in potassium. This was attributed to sources, location and mode of formation i.e. either potash or ferric kaolin. The effect of these inherent impurities could be noticed in the silica/alumina ratio of the starting kaolin. Theoretically, the silica/alumina ratio for pure kaolin is expected to be 2 or slightly less than 2 but not greater than 2. The closest Si/Al ratio to theoretical value was that of kaolin sourced from Elefun, despite its high iron content. It is also worth mentioning; that the word 'Elefun' literarily means whitish in Yoruba language and this kaolin was observed to be white in colour, despite its iron rich nature. The ability for this clay to maintain its whitish colour was traced to the high titanium oxide content, clearly shown in Table 4.1.

Table 4. 1: Compositional analysis for raw and beneficiated Kankara and Elefun kaolinite samples

	Category I			Category II			Category III			Category IV			
Sample ID	**A**	**B**		**C**	**D**		**E**	**F**		**G**	**H**	**I**	**J**
SiO_2	47.300	45.100		51.100	50.860		48.300	46.500		50.300	50.600	49.040	49.100
Al_2O_3	36.800	35.200		36.060	37.800		32.200	35.200		40.010	40.500	40.100	42.000
CaO	0.080	0.140		0.200	0.550		0.150	0.140		0.320	0.370	0.210	0.060
Fe_2O_3	0.710	0.818		0.720	1.080		3.160	2.280		1.080	0.990	2.950	1.580
K_2O	***1.010***	***0.680***		***6.400***	***4.060***		***1.260***	***0.680***		***2.020***	***1.600***	***0.250***	***0.230***
MgO	0.160	0.640		0.940	0.960		1.040	0.640		0.760	1.020	0.910	0.900
MnO	0.040	0.000		0.140	0.070		0.090	0.040		0.090	0.020	0.020	0.006
Na_2O	0.050	0.070		0.080	0.070		0.120	0.070		0.050	0.020	0.080	Nd
TiO_2	0.160	0.540		0.040	0.050		0.840	0.340		0.100	0.170	3.970	2.890
SO_3	0.065	0.090		0.065	0.045		0.090	0.089		Nd	Nd	Nd	0.060
LOI	13.450	12.330		13.540	11.780		12.567	11.479		12.236	10.985	11.659	10.361
Si/Al (mol %)	2.185	2.178		2.409	2.287		2.550	2.246		2.137	2.124	2.079	1.987
SSA (m^2/g)	18.2	15.1		21.4	19.2		29.7	25.9		19.6	16.1	24.3	20.5

A	Raw Kankara white
B	Beneficiated Kankara white
C	Raw Kankara white-same deposit but different pit
D	Beneficiated Kankara white- same deposit but different pit
E	Raw Kankara red
F	Beneficiated Kankara red
G	Raw Kankara white- same deposit but different pit
H	Beneficiated Kankara white- same deposit but different pit
I	Raw Elefun
J	Beneficiated Elefun

Nd- Not detected

LOI-Loss on ignition

SSA-Specific surface area

4.1.2 FTIR Analysis

The FTIR spectrum of the beneficiated kaolin, depicted in Figure 4.1, showed peaks at 3688, 3632, 1101, 920 and 777cm^{-1}, which agree with the characteristics peaks of kaolinite (Saikia *et al.*, 2003; Ekosse, 2010). The bands at 3688 and 3632 cm^{-1} were attributed to OH^- vibration and the bands of the stretching OH groups coordinated to the octahedral cations. Well-crystallined kaolin exhibits two peaks at 3669 and 3652, which were not noticeable in both kaolins, used in this work. This would indicate that our samples might have low purity (Russell and Fraser, 1994).

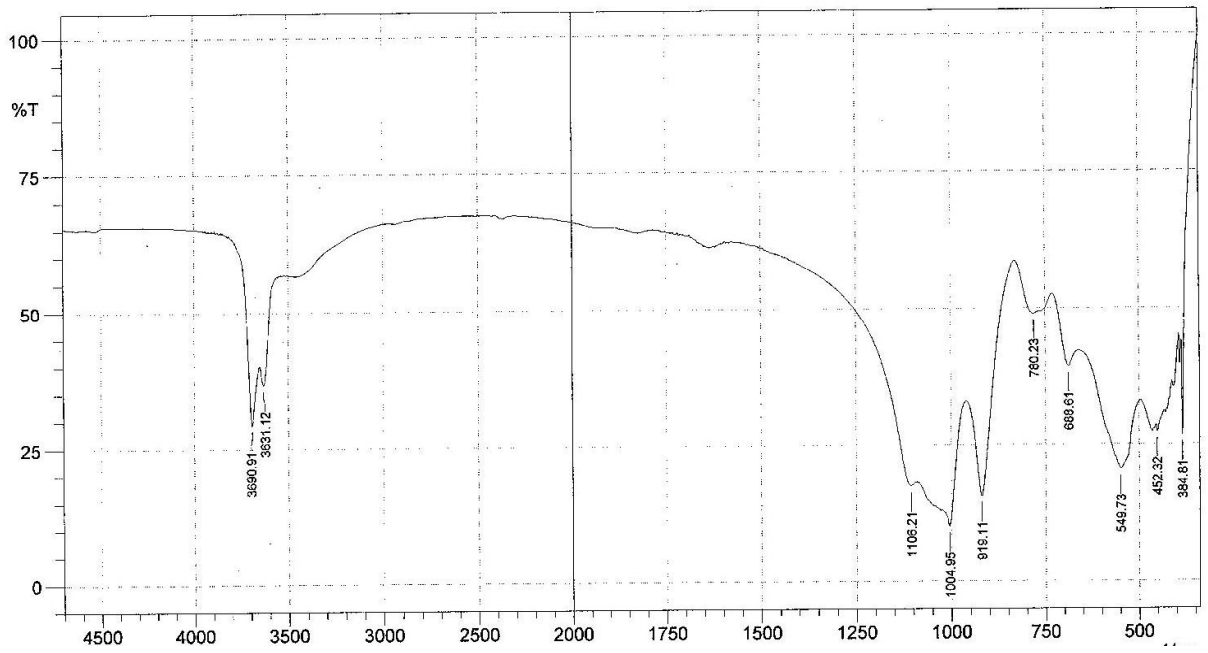


Figure 4.1: FTIR spectra for the beneficiated Kankara kaolin

The Si-O stretching bands were observed at 1028 and 1008cm^{-1}, while bands at 777cm^{-1} was assigned to both Si-O-Si and free silica or quartz material. On the other hand, the bands 543 and 688cm^{-1} were attributed to both Si-O-Al bending or Al octahedral and Si-O out-of-plane bending

respectively. Those bands noticeable at 430 and 464cm^{-1}, were respectively assigned to Si-O stretching and Si-O-Si in plane bending (Belver *et al.*, 2002).

4.1.3 XRD Analysis

The XRD pattern of the selected raw kaolin gave all the characteristic kaolinite peaks, with some peaks that can be attributed to quartz, illite, smectite, halloysite and muscovite (see Figures 4.2(a-c)). These peaks were found to conform satisfactorily to those in the open literature (Pinheiro *et al.*, 2005; Lenarda *et al.*, 2007; Panda *et al.*, 2010). The parent clay showed well defined reflections at 2Θ values of 12^0 and 30^0 (corresponding to the d values of 7.154Å; a reflection from [001]) giving typical characteristic peaks of kaolinite. The red Kankara kaolin was found to contain, aside anatase, phases like potassium iron oxide and forsterite, resulting from the presence of potassium and ferric oxide in the raw kaolin.

The XRD peaks were found to correlate with the XRF and FTIR result pointing to the presence of other inherent associated phases in the kaolin. It was also observed that the kaolin contains other phases namely halloysite, illite, smectite, mica and muscovite, as depicted in Figure 4.2 (Panda *et al.*, 2010, Sei *et al.*, 2006, Pinheiro *et al.*, 2005).

4.1.4 SEM and BET

The SEM study (Figure 4.3) shows the flaky-like card or platy morphology of kaolinite material and presence of rod or tubular material attributed to halloysite, clinochlore (Haq *et al.*, 2009) mica and muscovites, which supports the FTIR and XRD findings. The kaolin EDX spectrum (not shown) was characterized by nearly equal peak height of Al and Si, which is further confirmation of the predominance of kaolinite in the raw samples (Siddiqui and Ahmed,2005).

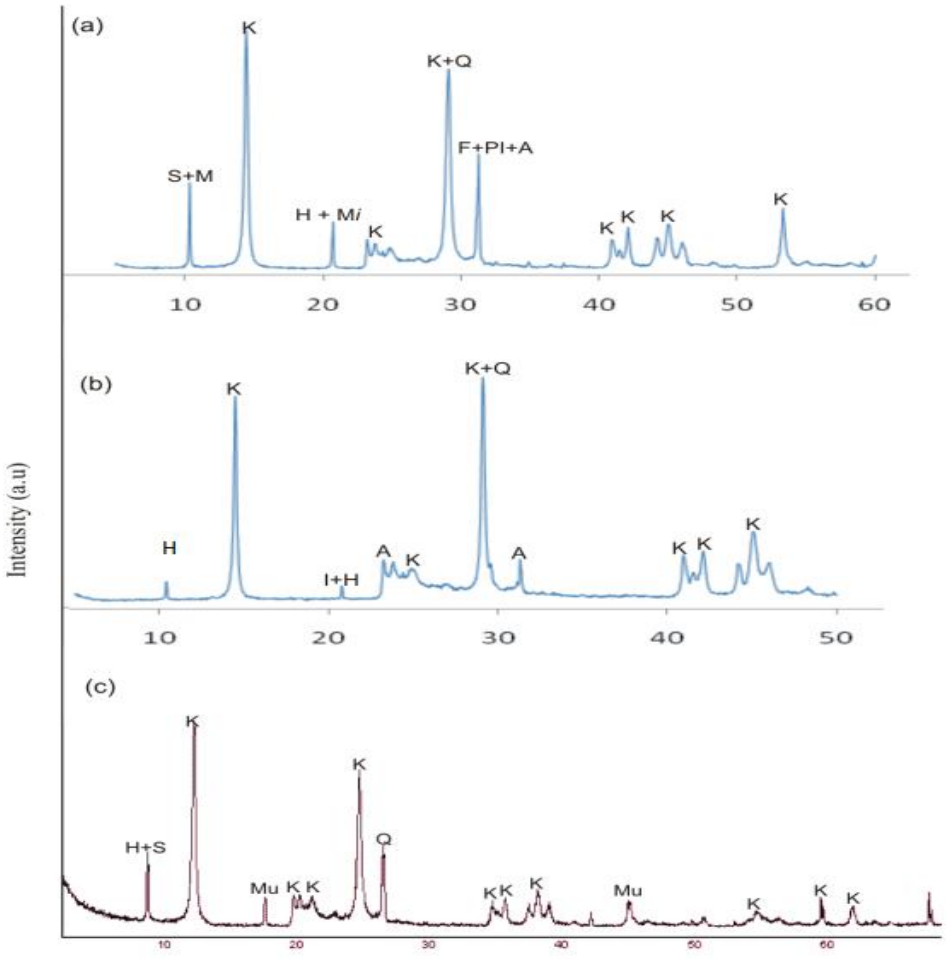


Figure 4.2: XRD patterns for raw kaolin, (a) Red Kankara (b) Elefun and (c) White Kankara

The closely packed flaky particles are stacked together in agglomerates and seem to be predominant in the sample analysed, as depicted in Figure 4.3. Noticeable small aggregate particles found in between the silica-alumina plates, under higher magnification, are indicative of inherent impurities, as shown in enlarged forms in Figure 4.3.

The specific surface area (s.s.a) for raw kaolin samples are shown in Table 4.1. These values were observed to increase with iron content and to some extent with potassium content, which is

in agreement with the work reported by Sei *et al.*, (2006). All the s.s.a values obtained for the samples are within the range generally reported for kaolinite, i.e. 5-70m^2/g. Selected BET isotherms for the surface area determination are shown in Appendix D.

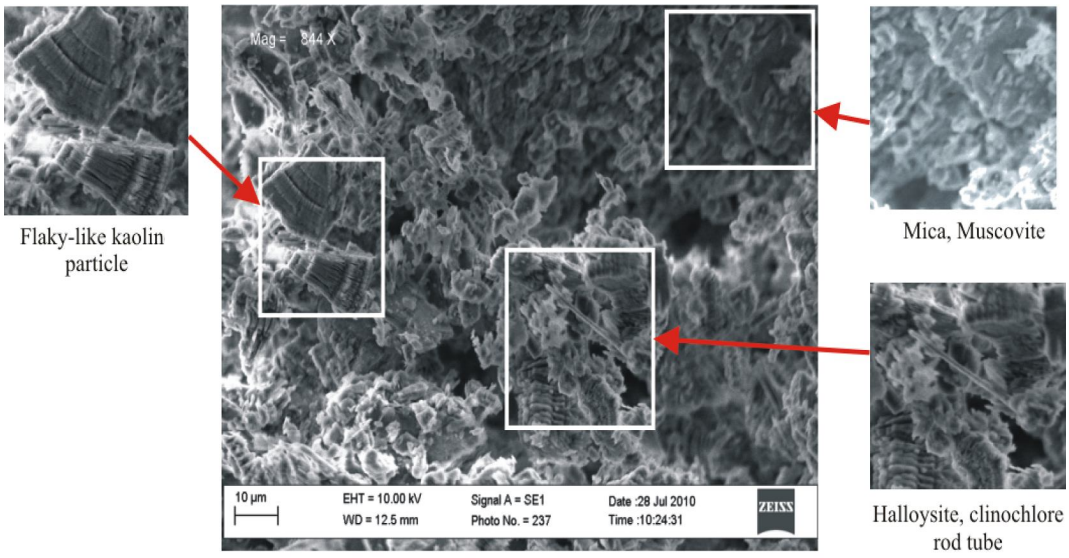


Figure 4.3: A typical SEM showing kaolin morphology for raw sample

4.2 Clay Beneficiation

4.2.1 XRFAnalysis

Beneficiation process is expected to shift silica/alumina ratio to 2, by reducing the free silica, iron, potassium and other impurities, which can be removed through dissolution or floatation. The silica content was observed to reduce with beneficiation treatment except for Category IV, where it was noticed to increase slightly, as shown in Table 4.1. The alumina content was noticed to increase in all samples at all stages in proportion to removal of impurities. The potassium and iron contents were observed to reduce for all categories but at Category II, where an increase in both oxides was recorded. The reason for this was attributed to proportional

reduction in silica content. This same reason was speculated for increase in iron content, since during the beneficiation process only plastic materials were used both for soaking and drying, hence no contact with metallic materials or external source of impurities was expected.

4.2.2 XRD Analysis

The effect of beneficiation, even though marginal with respect to compositional analysis was able to partially reduce some inherent impurities below the XRD detection limit as shown in Figure 4.4. The crystallinity of the beneficiated samples were observed to reduce with beneficiation. It was speculated that the amorphousity of kaolin tended to manifest with the introduction of water. Additionally, the intensities of some peaks noticed in the raw samples were seen to reduce or disappear, which was attributed to removal of the free or water soluble minerals found in the starting phases. The peak for quartz was found to increase for Elefun and Kankara white, pointing to removal of other phases and enrichment of less water soluble phase.

Ironically, the beneficiated white Kankara kaolin was observed to be richer in muscovite mineral and a weak zeolite phase- Gmenilite K- was noticed along with chlinochlore.

4.2.3 SEM and BET

The SEM image in Figure 4.5, shows retention of kaolinite structure but with noticeable small aggregate particles in between the silica-alumina plate (under higher magnification), an indication of left over impurities in the beneficiated kaolin. The halloysite phase noticed in the raw kaolin was no longer observed in the SEM for the benficiated one. The SEM image agreed with both the XRD and XRF results. The dark and bright patches observed in the image were attributed to presence of imbedded chemical water and almost completely dried portion of the sample, respectively.

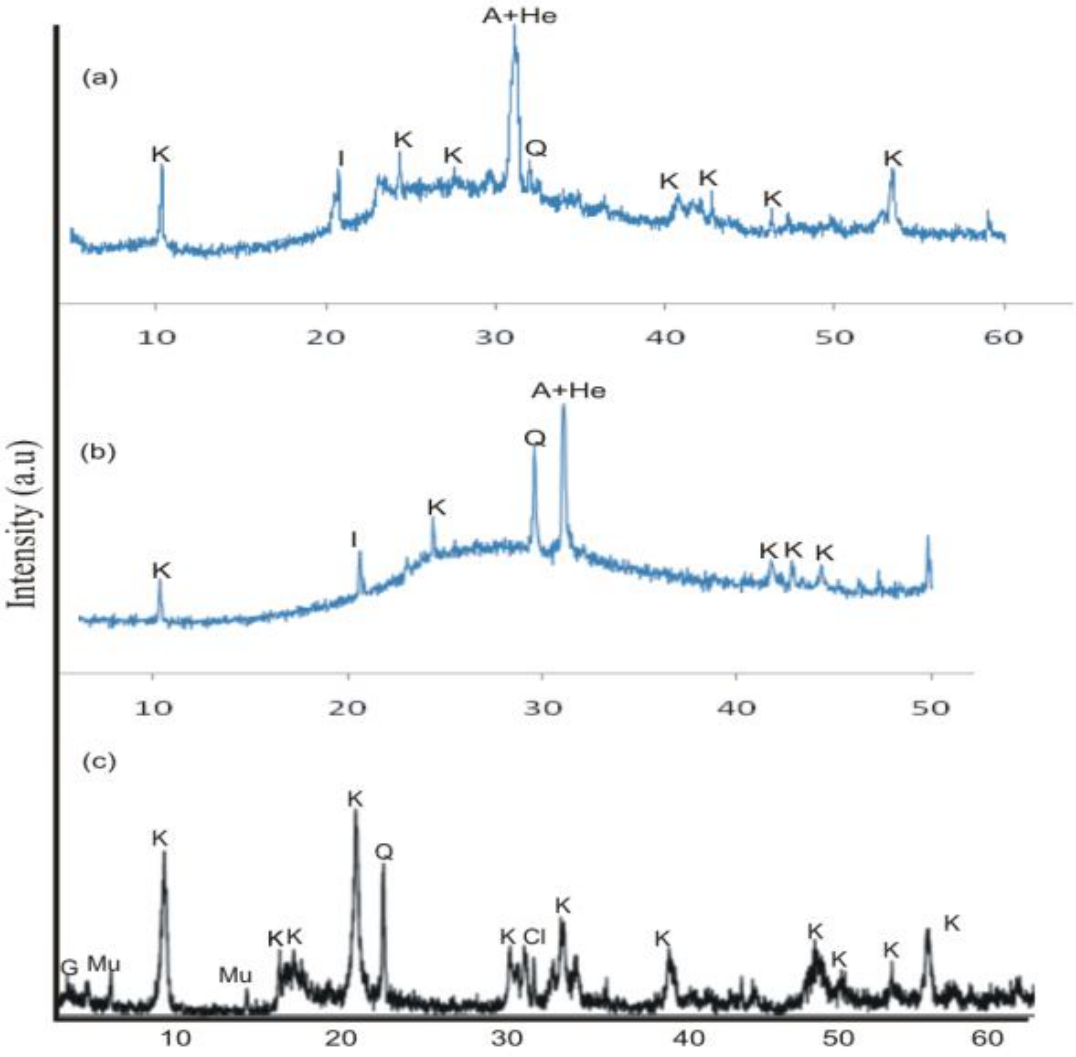


Figure 4.4: XRD patterns for beneficiated kaolins (a) Red Kankara (b) Elefun (c) White Kankara

The presence of fibrous patches and dispersed particle between the silica and alumina plate observed in Figure 4.5 is indicative of the shortcomings of the wet beneficiation method to produce pure kaolinite. These impurities were identified to be hematite and muscovite, which is in agreement with the XRD and FTIR findings. It was observed that the SEM for beneficiated kaolin was lean in the earlier identified fibrous materials.

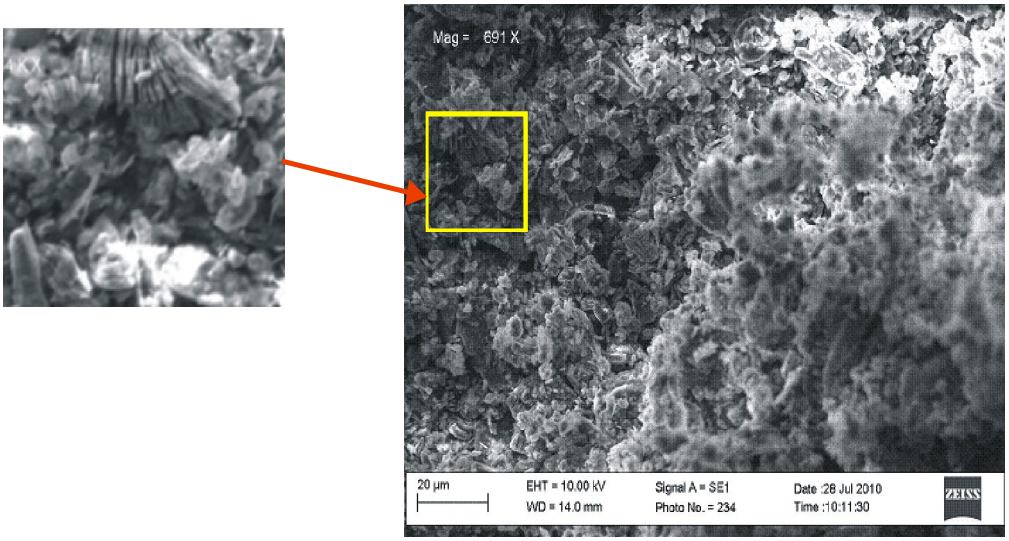


Figure 4.5: Selected SEM image for beneficiated kaolin

The specific surface area (s.s.a) for the beneficiated kaolinite samples are shown in Table 4.1. These values were lower than that of the starting material. The reduction in s.s.a could be attributed to either presence of intercalated water from the beneficiation process and/or removal of impurities in the starting mineral. This result shows that associated inherent oxides in kaolin have an important influence on its surface properties. Selected BET adsorption isotherms used for surface area determination are shown in Appendix D.

4.3 Calcination of Kaolin

Metakaolin is essentially a highly reactive disordered structure of anhydrous alumina-silicate obtained from the calcination of kaolinite clay. In order to determine the optimum calcination temperature for the synthesis of zeolites, the clays were subjected to thermal treatment at the following temperatures of 600, 700, 800 and 900^{0}C, in the furnace, for residence time of 6hrs.

4.3.1 XRD Analysis

The XRD patterns of the calcined products presented in Figures 4.6 are amorphous. The peaks for kaolinite disappeared but it was observed that some phases were relatively passive to the thermal treatment. These observations were similar to those reported for metakaolins by other researchers (Akolekar *et al.*, 1997, Belver *et al.*, 2002, Elimbi *et al.*, 2011). The intensity of some inherent impure phases like microcline, illite, dickite and brookite were also observed to reduce drastically with thermal treatment.

Judging by the intensity of quartz and other material left in the calcined sample, it was observed that the highest level of amorphousity was attained when calcined at 900 degree. Ironically the quartz intensity was seen to increase at 700^0C compared to that calcined at 600^0C.This was attributed to loss of chemical water and vapours embedded in the kaolinite structure. Further drop in the quartz level tended to agree with the mechanism of calcinations, where silica sublimes as temperature increases.

Our results suggest that during the calcination process of the clay fractions, the state of disorder within the metakaolinite structure increased with temperature. While the temperature of 900^0C gave the highest disorder, subsequent calcination was carried out at 850^0C for reasons that are given in Section 4.5.

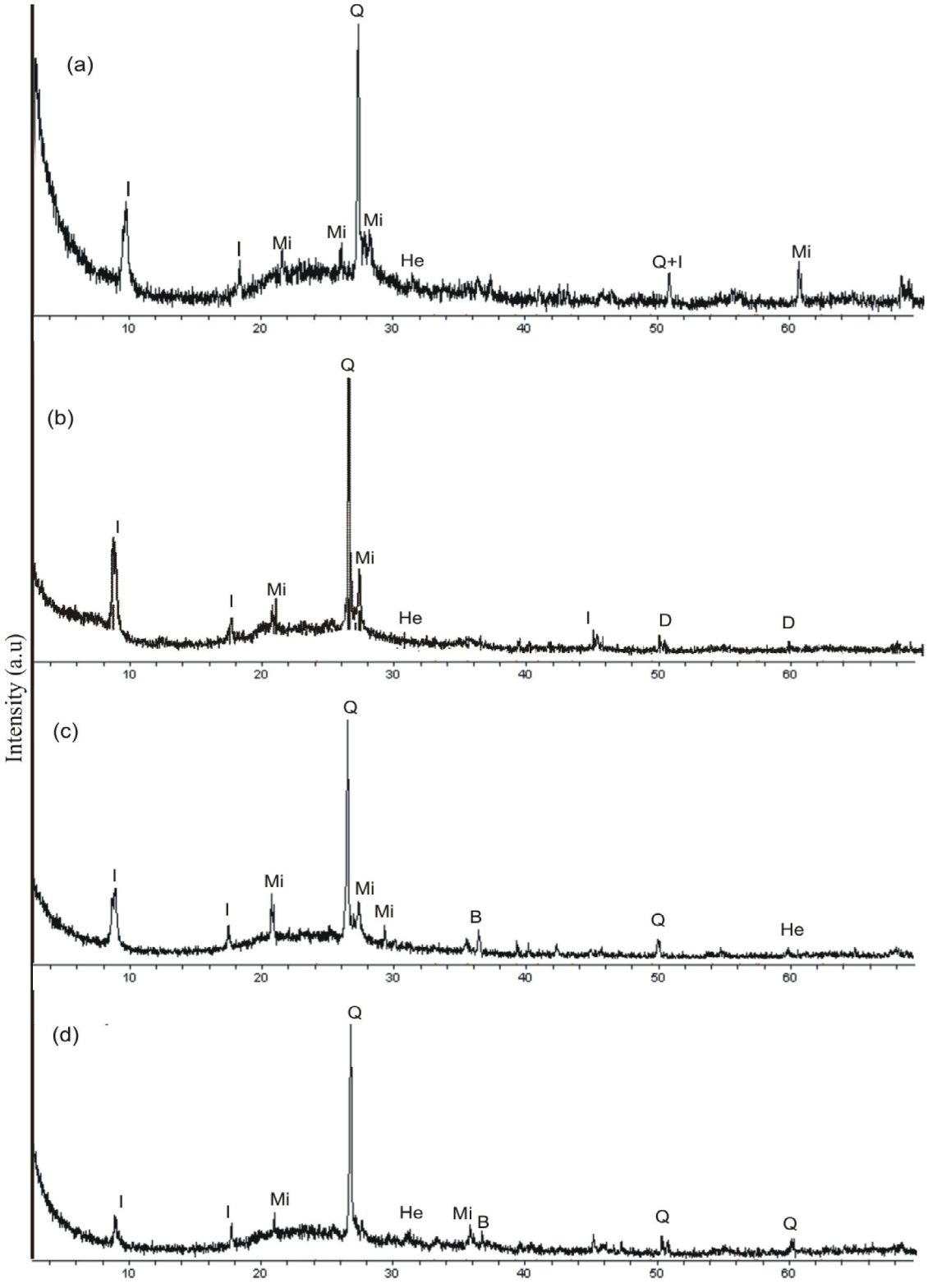


Figure 4.6: XRD patterns for metakaolin samples (a) 600^0C (b) 700^0C (c) 800^0C (d) 900^0C

The XRD patterns for Kankara red kaolin subjected to thermal treatment at 850^0C and Elefun kaolin at 850^0C are shown in Figures 4.7(a and b), respectively. Figure 4.7a revealed a typical semi-amorphous phase of metakaolin for Category IV, having little or no impurities. The impurities then noticed in Figures 4.6(a-d) were therefore attributed to the source material. It is imperative to mention here, that the Kankara kaolin used in Category IV was compositionally different from that of Categories I, II and III, even though it was mined from the same deposit.

Figure 4.7b showed the XRD pattern for metakaolin obtained from Elefun kaolinite clay, with retained peaks at 2theta around 30 and 32, attributed to the presence of quartz and hematite (Fe_2O_3), respectively. Those two minerals were observed to be passive to thermal treatment despite the elevated temperature of calcination, which is in agreement with the works reported by Chandrasekhar and Pramada (1999) and Lenarda *et al.*, (2007). In general, it could be concluded that Elefun kaolinite clay responded better to thermal treatment compared with Kankara, judging from the XRD patterns obtained, in term of the level of disorderliness.

4.3.2 XRF Analysis

The compositional analysis of the treated samples shown in Table 4.2, revealed a slight difference in the composition with a reduced loss on ignition (LOI), resulting from the expurgence of inherent water in all forms. The values of LOI were seen to decrease with increasing calcination temperature. The silica-alumina ratio was not observed to be altered considerably with thermal treatment, neither was the compositional make up.

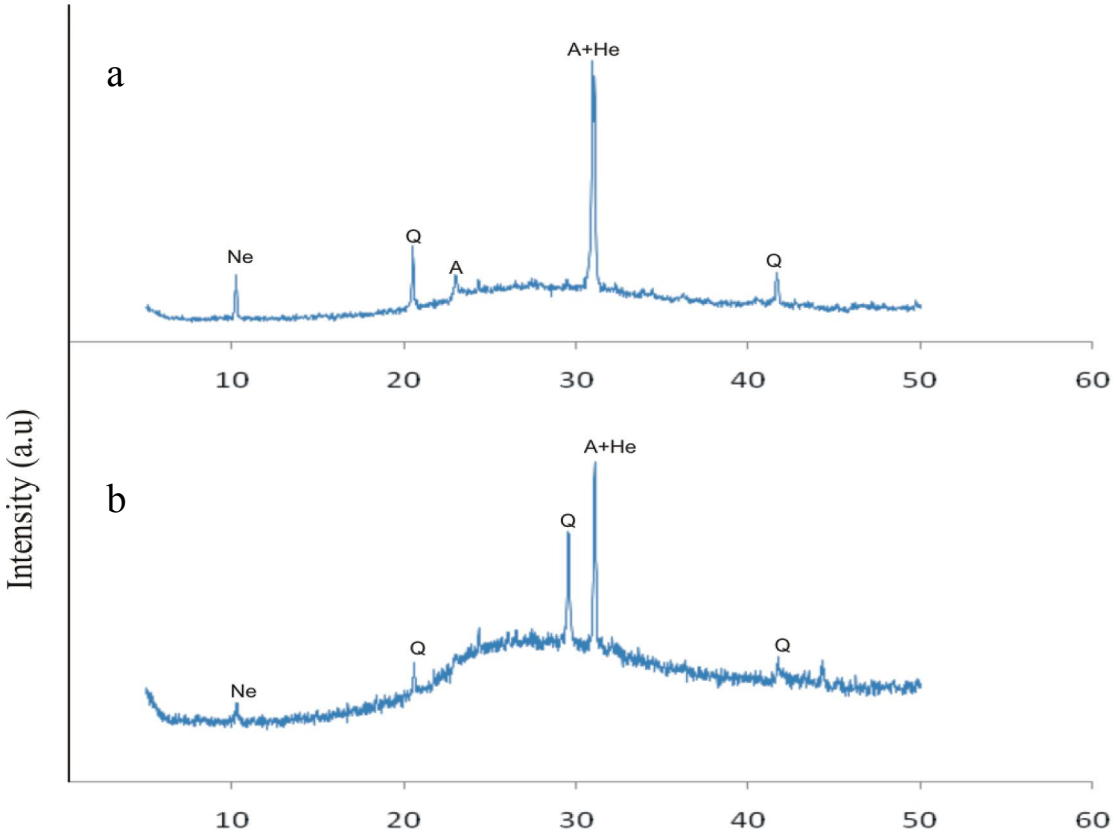


Figure 4.7: XRD patterns for metakaolin samples treated at 850^0C (a) Kankara (b) Elefun

4.3.3 BET and SEM

The calcined kaolin (irrespective of its source and treatment) had a specific surface area ranging from 8.5 and 10.6m^2/g which was observed to be lower than that of both beneficiated and raw kaolin. This reduction in the surface area is likely the result of aggregation of particles when structural water molecules were removed.

Figure 4.8 (a-d) showed the SEM images for kaolinite clay calcined at 600, 700 800 and 900^0C, respectively.

Table 4.2: Compositional analysis for calcinated samples in weight percent

Sample ID	MK 6	MK 7	MK 8	MK 9	MKR	MKW	EKC
SiO_2	54.6	53.9	53.8	53.6	49.79	52.08	47.6
Al_2O_3	35.8	35.9	35.9	35.6	36.65	41.01	44.1
CaO	0.15	0.15	0.15	0.15	0.49	0.32	0.03
Fe_2O_3	3.46	3.37	3.41	3.41	2.10	0.90	1.77
K_2O	1.31	1.32	1.32	1.37	0.40	1.57	0.13
MgO	1.09	1.11	1.07	1.08	1.02	0.98	0.76
MnO	0.07	0.07	0.05	0.06	0.07	0.01	0.01
Na_2O	0.09	0.10	0.09	0.10	0.11	0.07	Nd
TiO_2	0.90	1.01	0.85	0.94	0.07	0.16	2.55
SO_3	0.09	0.08	0.07	0.06	0.03	Nd	0.04
LOI	8.80	7.90	7.50	7.10	7.21	8.11	9.78

Legend

Sample ID	Description
MK6	White Kankara kaolin calcined at 600^0C for 6hrs
MK7	White Kankara kaolin calcined at 700^0C for 6hrs
MK8	White Kankara kaolin calcined at 800^0C for 6hrs
MK9	White Kankara kaolin calcined at 900^0C for 6hrs
MKR	Red Kankara kaolin calcined at 900^0C for 6hrs
MKW	White Kankara kaolin calcined at 850^0C for 6hrs
EKC	Elefun Kaolin calcined at 850^0C for 6hrs

The SEM images, observed under same magnification, pointed to progressive destruction of the silica-alumina plates with increasing temperature. The overlaying plate observable in Figure 4.3

disappeared, with the appearance of small aggregates, shown in Figure 4.8. These small aggregates were indication of destruction of kaolinite structure, which was observed to depend directly on the temperature of calcinations. Figures 4.8 (a&b) showed clear formation of the micelles with increased population with metakaolinization temperature, indicating enhanced rupture and breakdown of the kaolinite clay, though with some retained kaolinite structure, especially for metakaolin obtained at lower temperature, i.e. 600^0C (see Figure 4.8 (a & b)).

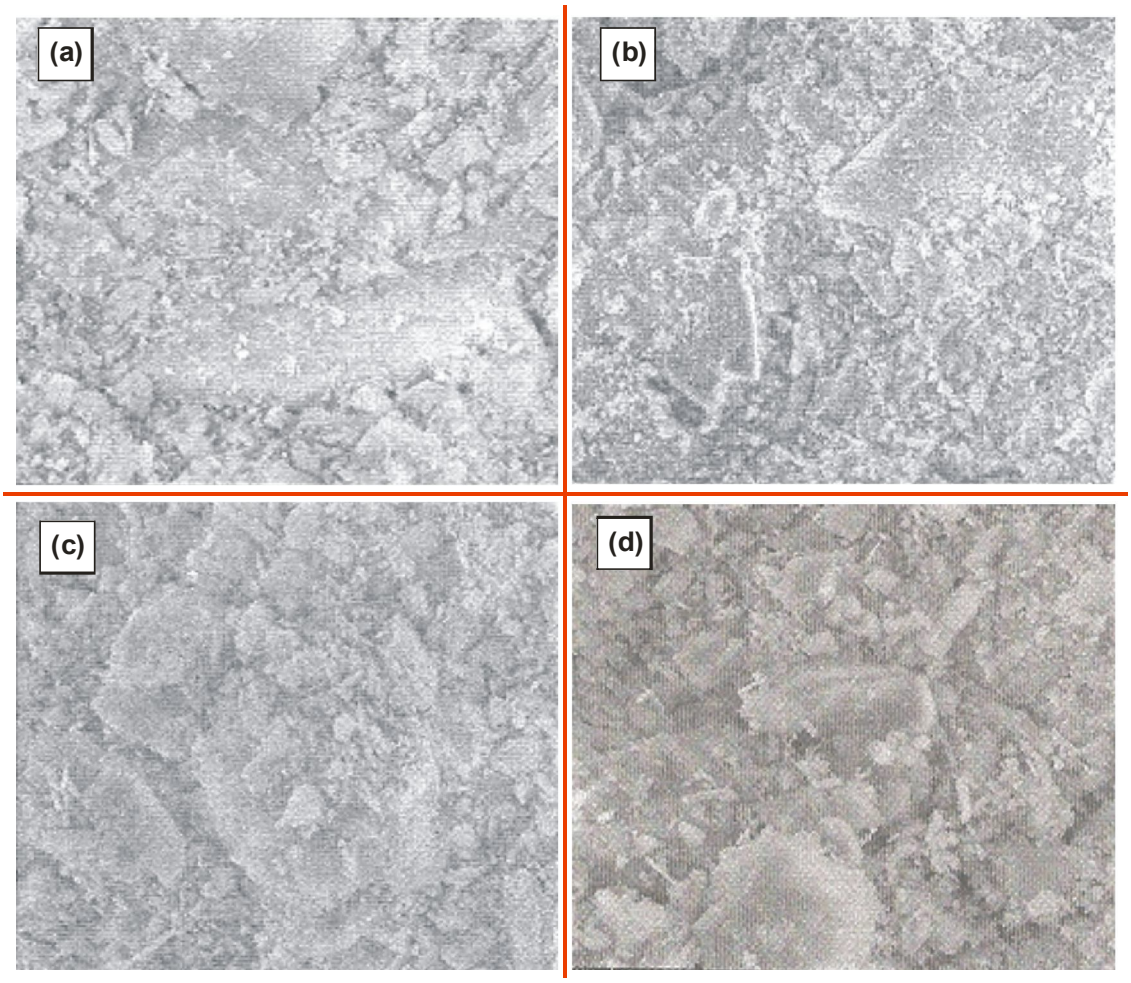


Figure 4.8: SEM images for metakaolin calcined at (a) 600^0C (b) 700^0C (c) 800^0C (d) 900^0C

Figures 4.9 (a and b) showed the SEM images for Kankara (white) and Elefun metakaolin, respectively, obtained at calcination temperature 850^0C. The SEM images for the samples were seen to be similar, despite the source of the starting kaolin. The images gave an evidence of partial destruction of the initial kaolinite structure and formation of the semi-amorphous metakaolin. The SEM images in Figure 4.9 seem to give a better and more uniform destruction of kaolininte structure compared to those in Figure 4.8.

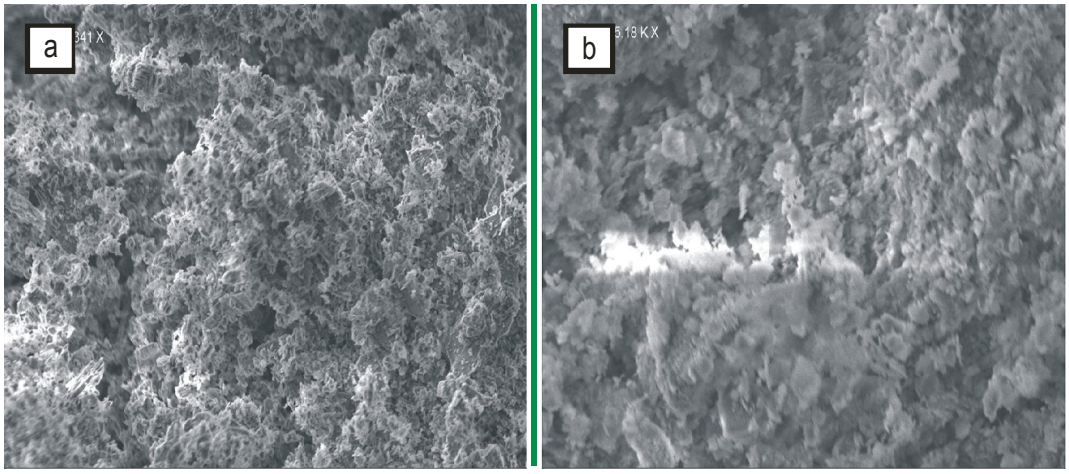


Figure 4.9: SEM images for metakaolin at 850^0C (a) White Kankara and (b) Elefun

4.4 Dealumination of Metakaolin

4.4.1 XRD Analysis

Figures 4.10 (a-c) are typical diffractographs for dealuminated Kankara and Elefun metakaolin, respectively. Irrespective of the source of kaolin and mode of dealumination employed (either heating or non-heating), it was observed that peaks attributed to metakaolin were found to decrease/disappear progressively with appearance of other phases, possibly ensuing from the acid treatment, which affected the crystalline character of the clay (Delhez *et al.*, 1982).

The inherent impurities were noticed to be resistant to the acid attack, as evidenced by the corresponding persistent peaks which remained unmodified despite the acid treatment. Additionally, it could be deduced that the decreased crystallinity favoured transformation of alumina into the tetrahedral coordination (Sánchez *et al.*, 1999) which probably increased the rate of alumina extraction. This conversion is needed since both silica and alumina are expected to change their oxidation states. The oxidation states of both silica and alumina were observed to change in the new phases, like microcline, kalsite, andalusite, silhydrite etc, identified by XRD, shown in Figure 4.10. Apparently, the kaolin sourced from Elefun gave more digestable alumina and silica phases, for the purpose of gellation.

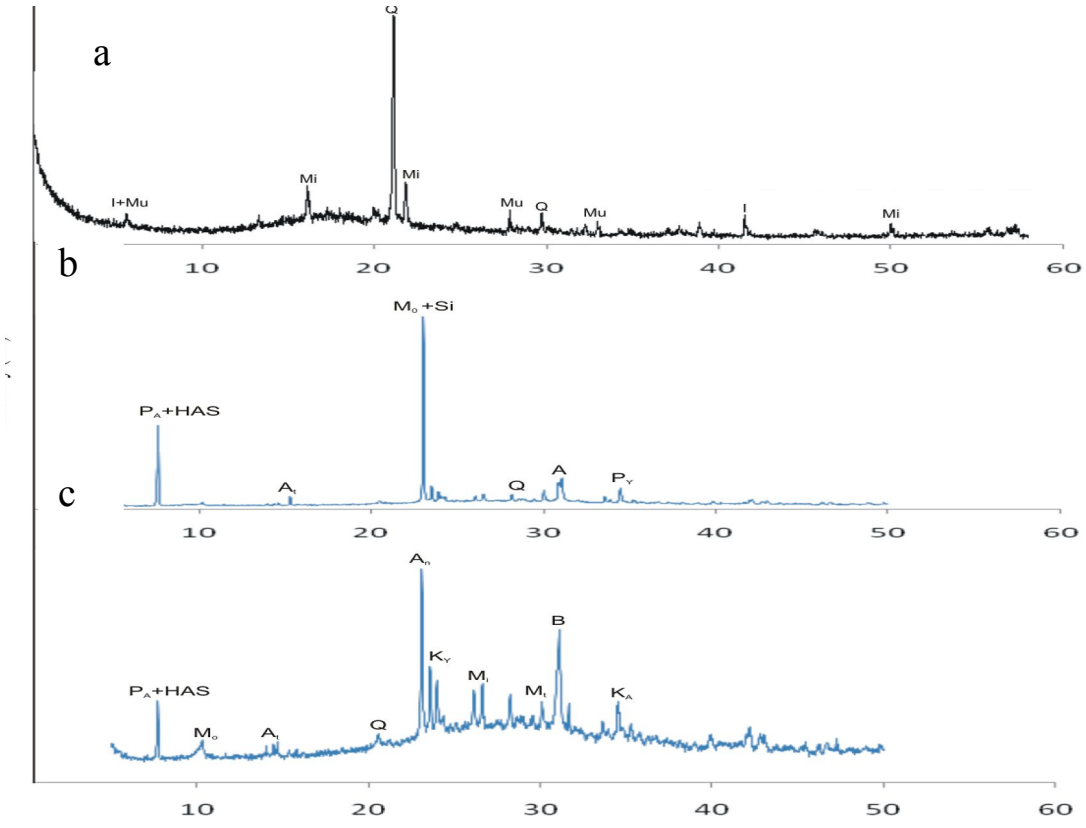


Figure 4.10: XRD patterns for dealuminated metakaolinite samples (a) Kankara calcined @ 850^0C (b) Kankara calcined @ 900^0C and (c) Elefun calcined @ 850^0C.

4.4.2 XRF Analysis

The results of compositional analysis carried out for the dealuminated samples are given in Table 4.3(a-c), for Kankara metakaolin (heating and non-heating dealuminated) and Elefun.

During the acid treatment, it was observed that the composition of the parent clay changed considerably. As the reaction time progressed, the contents or components were observed to reduce except for K_2O that did not follow an orderly pattern (Belver *et al.*, 2002). The silica-alumina ratio was observed to increase with reaction time. This resulted from decrease in the alumina content which was ascribed to leaching of Al^{3+}ions from the octahedral layer, due to hydrolysis under acidic conditions. It is suggestive that leaching occurred in sequential manner due to attack at the octahedral layer as the acid strength and reaction time increased. The acid strength was believed to be dependent on the quality and purity of the acid; hence a study of this effect on dealumination was carried out.

Table 4.3a: Chemical composition (in wt%) of the thermally dealuminated samples

ID	SiO_2	Al_2O_3	Fe_2O_3	MgO	CaO	Na_2O	K_2O	MnO	CuO	SO_3	s.s.a	Si/Al (mol)
DMK5	63.86	11.01	0.81	0.96	0.53	0.06	5.89	0.03	0.05	11.4	126.34	9.86
DMK10	80.5	6.4	0.55	1.13	0.45	0.01	3.37	0.03	0.05	6.89	149.33	21.383
DMK15	77.1	4.08	0.47	1.73	0.4	0.03	3.54	0.03	0.06	7.56	137.25	32.125
DMK20	83.8	3.8	0.55	1.13	0.51	0.13	3.89	0.02	0.06	8.6	141.23	37.489
DMK25	84.41	3.47	0.46	1.16	0.46	0.04	3.89	0.03	0.05	4.89	143.56	41.353
DMK30	89.83	2.63	0.48	1.12	0.31	0.08	6.05	0.03	0.03	4.92	138.79	58.065

Legend

ID	Description
DMK5,10,15,20,25,30	Metakaolin dealuminated thermally for 5,10,15, 20,25,30minutes

ID	SiO_2	Al_2O_3	Fe_2O_3	MgO	CaO	Na_2O	K_2O	MnO	TiO_2	CuO	SO_3	s.s.a	Si/Al (mol)
DAK3	66.56	18.98	0.8	0.91	0.22	0.51	7.35	0.02	0.07	0.06	1.93	130.37	5.962
DAK5	66.85	18.03	0.8	1.29	0.22	1.01	6.8	0.02	0.06	0.03	3.12	131.48	6.303
DAK7	67.95	14.67	0.7	1.19	0.23	1.04	6.69	0.02	0.13	0.06	5.51	134.97	7.874
DAK9	63.13	13.47	0.69	1.22	0.21	0.85	6.28	0.02	0.07	0.09	10.04	124.34	7.967
DAK12	59.89	12.01	0.75	1.03	0.21	0.93	7.55	0.02	0.1	0.04	14.1	116.22	8.477
DAK15	68.74	13.89	0.59	1.04	0.22	0.85	6.98	0.02	0.1	0.03	6.01	135.79	8.413
DAK18	68.2	7.6	0.52	1.01	0.74	0.41	3.57	0.03	0.06	0.03	7.05	141.22	15.255
DAK21	80.02	5.11	0.46	0.86	0.21	0.9	3.92	0.03	0.05	0.02	6.03	147.34	26.621
DAK24	71.54	6.48	0.49	0.85	0.21	1.23	4.16	0.02	0.06	0.04	8.61	143.57	18.769
DAK27	78.3	5.59	0.41	0.82	0.21	0.9	3.99	0.04	0.04	0.03	8.32	146.76	23.812

Table 4.3b: Chemical composition, in weight percentageof the non-thermally dealuminated samples

ID	Description
DAK3,5,7,9,12,15,18,21,24,27	Metakaolindealuminated non-thermally for 3,5,7,9,12,15,18,21,24,27minutes

Table 4.3c: Chemical composition (wt %) of the thermally dealuminated samples-use of analytical grade acid

ID	SiO_2	Al_2O_3	Fe_2O_3	CaO	K_2O	TiO_2	CuO	SO_3	s.s.a	Si/Al (mol)
KD1	62.84	16	0.61	0.2	1.29	0.18	0.06	15.6	127.94	6.678
KD3	64.7	12.08	0.82	0.28	1.64	0.28	0.05	13.7	132.76	9.105
KD5	76.2	5.5	0.24	0.33	1.53	0.33	0.09	10.3	131.35	23.553
KD7	92.8	3	0.14	0.24	1.3	0.24	0.07	1.3	134.51	52.587
KD9	90.1	3.08	0.2	0.2	0.11	0.2	0.05	5.49	133.98	49.731
ED1	66.4	19	0.46	0.19	0.13	0.19	0.05	7.35	140.87	5.941
ED3	75.68	13	0.49	0.22	0.29	0.19	0.07	2.4	149.33	9.879
ED5	77.6	7.4	0.26	0.31	0.22	0.19	0.05	8.01	137.25	17.827
ED7	92.8	1.75	0.17	0.2	0.08	0.29	0.06	1.6	141.23	90.149
ED9	86.9	1.38	0.22	0.3	0.18	0.26	0.07	9.27	143.56	104.051

Legend

ID	Description
KD1,3,5,7,9	Kankara metakaolin dealuminated thermally for 1,3,5,7,9 minutes
ED1,3,5,7,9	Elefun metakaolin dealuminated thermally for 1,3,5,7,9 minutes

The samples tagged DAK3 (Table 4.3b), DMK5 (Table 4.3a), DMK82 (see Table 4.4), KD3 and ED3 (Table 4.3c) were therefore choosen to serve as the monomer for the gel formation and subsequently for zeolite synthesis. This decision was made based on their silica-alumina ratio, which happens to fall within the values suitable for zeolite Y synthesis.

4.4.3 BET and SEM

The surface area of the dealuminated sample was found to directly depend on calcination temperature and time, as well as on concentration of acid and residence time used for dealumination (Mendioroz *et al.,* 1987). Accordingly, the specific surface area of some selected samples were determined and tabulated as shown in Table 4.3 (a&b), testifying to the role of amorphous silica on s.s.a as reported by other authors (Belver *et al.,* 2002). It was observed in this work that the surface area increases with the silica content in the dealuminated sample. The results show that the increase in s.s.a with silica content was not dependent on the mode of dealumination. The relatively high surface area observed for the dealuminated sample served as an enhancement factor for gel formation, by providing the surface area required for the gellation and subsequent crystallization.

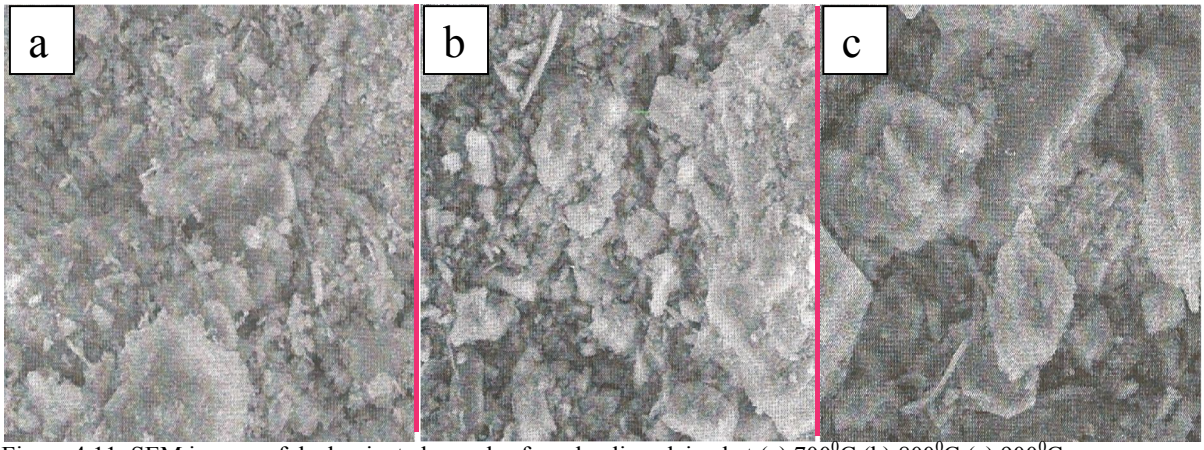


Figure 4.11: SEM images of dealuminated samples from kaolin calcined at (a) 700^0C (b) 800^0C (c) 900^0C

Apparently, the degree of structural degradation and characteristics of the acid- leached products, were observed to depend on the temperature used for the transformation of crystalline kaolin as shown in Figures 4.11(a-c) and Table 4.2.

The typical SEM images of the dealuminated Kankara and Elefun shown in Figure 4.12 (a & b) indicate the disaggregation of metakaolin structure on acid treatment, surface roughness and clustering of newly formed structure. The large white particles appear to be formed by several flaky particles stacked together to form well bonded agglomerates. These observations were found to favourably agree with the works reported by Lenarda *et al.,* (2007) and Panda *et al.,* (2010). Additionally, it was observed that some materials remained unaffected by the acid treatment.

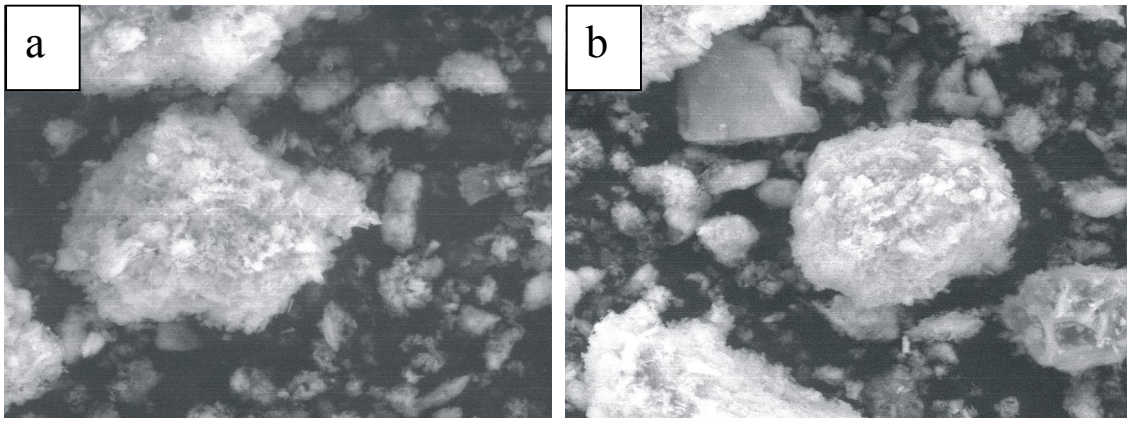


Figure 4.12: SEM images of dealuminated samples from (a) Kankara and (b) Elefun

4.4 (a) Novel approach to metakaolin dealumination

The motivation for this investigation was to reduce the dependency of dealumination process on electrical power supply. The idea is to use the heat of sulphonation resulting from mixing acid and water, which leads to phenomenological increase in the boiling water volume and buoyancy. This buoyancy assisted in agitation, increased level of collision and subsequently the overall ability of acid-water mixture to do work, required for realisation of chemical reaction. The silica-alumina ratios shown in Figure 4.13, increase with acid concentration.

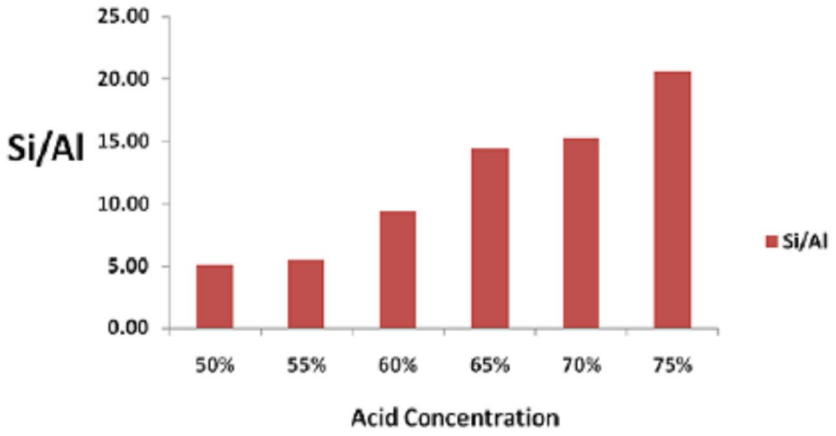


Figure 4.13: Silica-alumina ratio as a function of sulphuric acid concentrations.

For the purpose of the production of faujasites, a decision was taken to use 60wt % of sulphuric acid concentration in this investigation. The result in Figure 4.13, suggests use of higher acid concentration for the synthesis of highly siliceous zeolites.Figure 4.14 presents the comparative silica-alumina ratio obtained from the three different methods of dealumination used in this investigation.

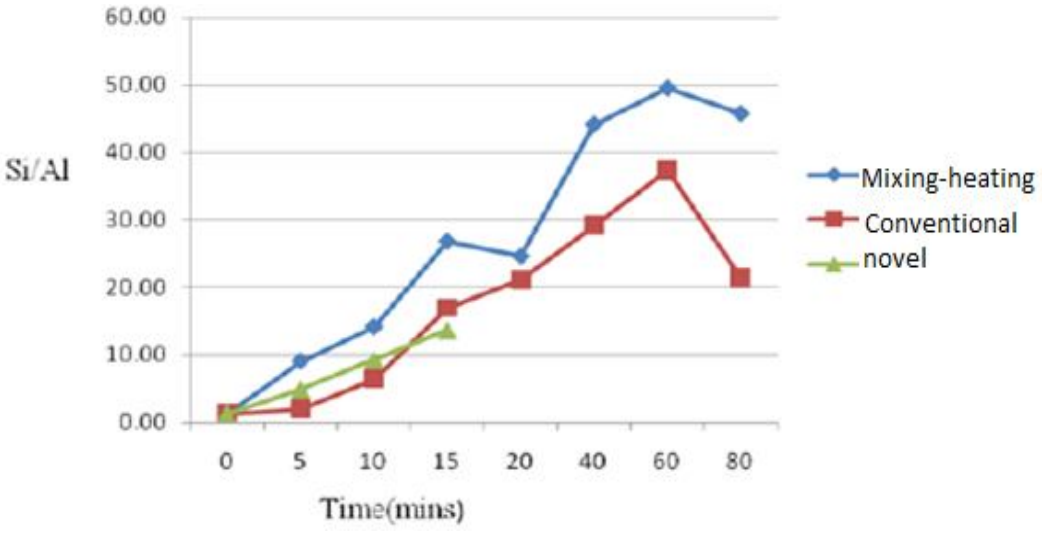


Figure 4.14: Comparative silica-alumina ratio for various method of dealumination

The silica-alumina ratio is an indication of the rate of removal of alumina from the kaolinite framework during dealumination. As observed from Figure 4.14, the rate of alumina removal was higher in mixing-heating approach, which is a combination of the novel and conventional methods. During mixing-heating method, the heats of mixing and external source of heating were combined, hence continuous increase in silica-alumina ratio. In the mixing-heating method, the amount of heat released by the acid water mixture was used in conjuction with the heat supplied by the heating mantle. This subsequently favoured higher rate of dealumination as reported by Ajayi *et al.,* (2010).

4.4 (b) Effect of acid quality on rate of metakaolin dealumination

Various factors affect the rate of Al^{3+} leaching from kaolin residue, namely calcinations temperature, leaching time, temperature of the reacting species and acid concentration. The acid concentration and its leaching power are found to depend on the purity *viz-a-viz* quality of the acid. Aderemi *et al.,* (2001) established an optimal concnentration of acid required to leach Al^{3+} and to overcome mass transfer resistances. Reproducibility of their study was rendered difficult, due to the diverse quality of acid procured in the open market.

The extent of alumina leaching from metakaolin was established by monitoring the silica-alumina ratio and quantity of alumina extracted from the starting material. Figures 4.15 and 4.16 show the silica-alumina ratio and Al^{3+} extracted for thermally dealuminated samples (using normal and analytical grade acid) as well as non-thermally dealuminated metakaolin, respectively.

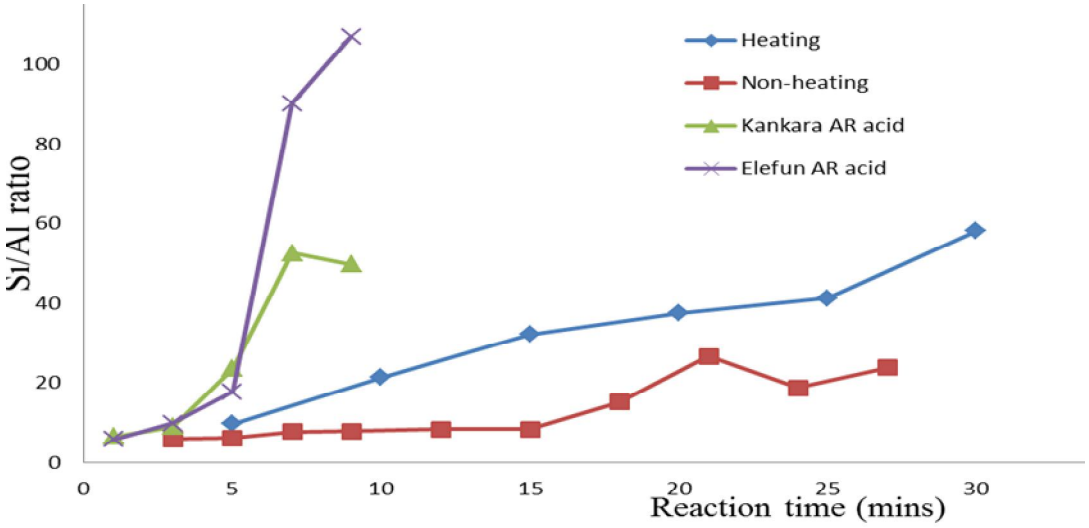


Figure 4.15: Silica-alumina ratio for different methods of dealumination

It was observed from Figure 4.15 that the amount of alumina extracted was higher at shorter time for Kankara and Elefun dealuminated using analytical grade acid, compared to the others leached using ordinary acid. This observation suggested that the strength of analytical grade acid used was good enough to achieve higher rate of leaching and hence higher Si/Al ratio, as depicted in Figure 4.16.

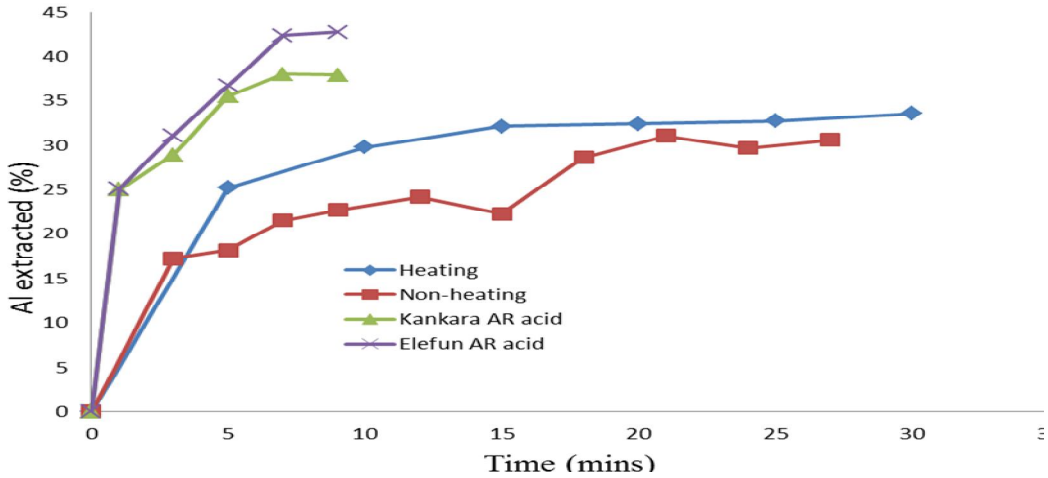


Figure 4.16: Quantity of alumina extracted for methods of dealumination and type of acid

4.4 (c) Effect of calcination temperature on rate of metakaolin dealumination

It had been reported that the temperature required for metakaolin formation depended on the type and impurities present in the starting kaolin (Sonuparlak *et al.,*1987). It was also established from chemistry that most materials could and would disintegrate when treated at elevated temperatures. It was observed that about 75% of Al was removed for metakaolin calcined at 800^0C, while the others varied between 57 and 59%, as shown in Table 4.4.

Table 4.4: Compositional analysis for dealuminated samples calcined at various temperatures

Sample ID	Compositions										Ratio
	Al_2O_3	BaO	CaO	Fe_2O_3	K_2O	MgO	MnO	Na_2O	SiO_2	SO_3	Si/Al
DMK 72	8.9	0.05	0.07	0.86	1.77	0.32	0.01	0.14	83.7	0.31	15.99
DMK 82	14.5	0.05	0.13	1.65	1.55	0.66	0.01	0.11	76.5	0.18	8.97
DMK 92	14.8	0.05	0.11	1.69	1.32	0.66	0.01	0.10	77.6	0.16	8.91

Legend

DMK 72, 82 and 92	Dealuminated metakaolin of clay calcined at 700^0C, 800^0C and 900^0C

This may be related to the beginning of sintering of kaolinite particle at 900^0C and/or perhaps the beginning of the transformation from kaolinite to mullite, though, reported at 980^0C in the literature. At lower temperature, i.e. 600 and 700^0C, it was speculated that probably there are still more crystalline phases in comparison with the amorphous phases in the metakaolin samples, as represented in Figure 4.17.

A follow up of this work, carried out at calcinations temperatures of 750, 850 and 950^{0}C, was done and the cumulative effect of these metakaolinization temperatures on zeolitization was also understudied.

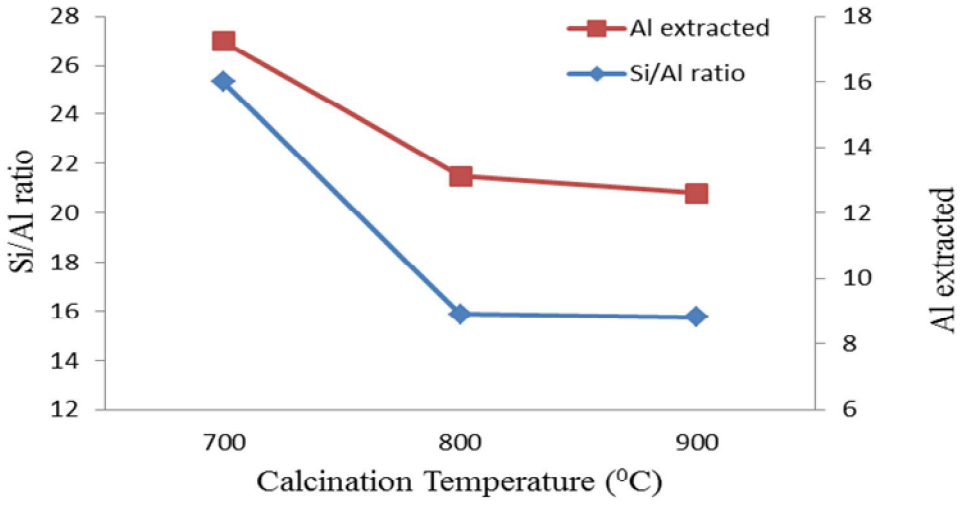


Figure 4.17: Silica-alumina ratio and alumina extracted against calcinations temperature

The results obtained suggested that metakaolin resulting from calcinations at 950^{0}C gave relatively high crystalline zeolite from Elefun clay and from Kankara at 850^{0}C. Accordingly, these temperature ranges were adopted as the desired calcinations temperature for the clays used.

The relationship shown in Figure 4.18 gave an illustration of how dependent intensity of as-synthesized zeolite is on metakaolinization temperature. This Figure was developed by choosing a common peak for zeolite Y and the intensity was determined and plotted. This sheds more light on the conclusion reached from Figure 4.17.

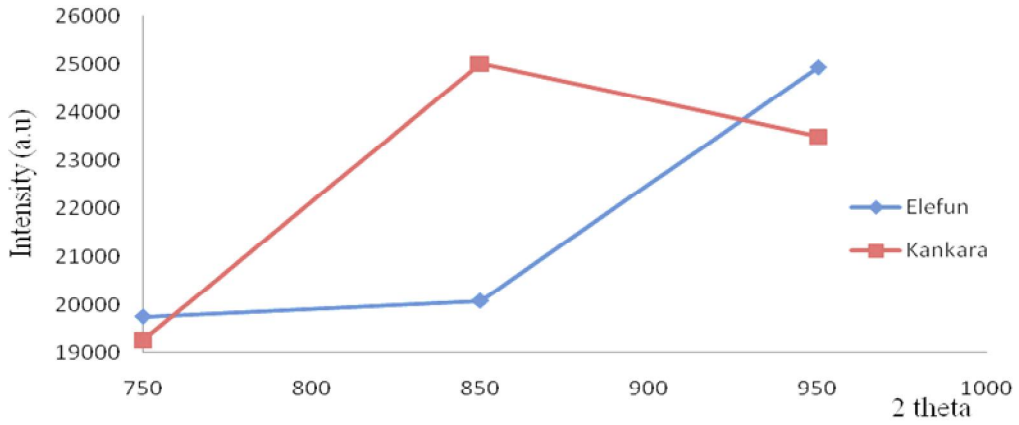


Figure 4.18: Intensity of zeolite Y against calcination temperature

It is also pertinent to check the mineralogical composition condition for successful synthesis of zeolite Y when the monomer is subjected to different calcination temperature. The ratio of Na_2O and Na_2O+K_2O is expected to tend toward unity, i.e. very low K_2O for zeolite Y to be synthesized. From Figure 4.19, it can be concluded that Kankara treated at 850^0C and Elefun at 950^0C had this ratio very close to one, confirming the finding in Figure 4.18.

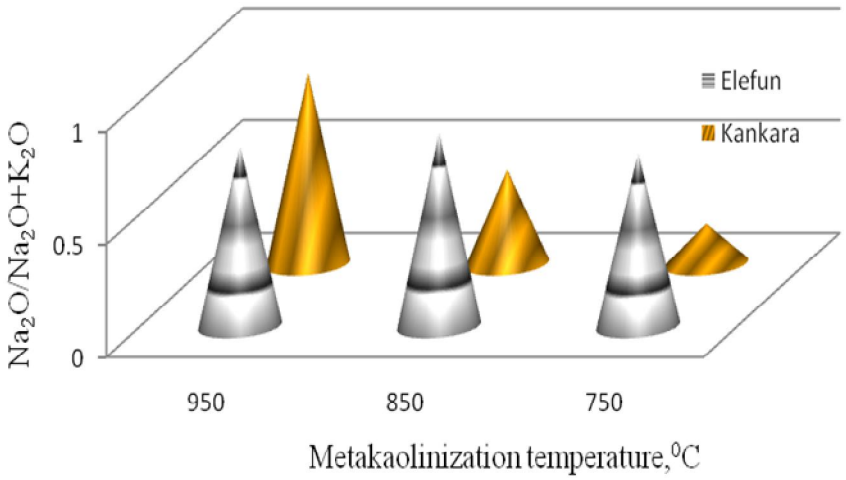


Figure 4.19: Metakaolinization temperature and mineral composition effect

4.4(d) Effect of sulphate salts level on extent of dealumination

It is expected that the silica-alumina ratio should increase with contact time, whose value is subjected to the extent of washing i.e. sulphate salts removal. The charts in Figures 4.20 and 4.21 show the relationship between the sulphate level, silica-alumina ratio and reaction time, for thermally and non-thermally dealuminated metakaolin.

From Figures 4.20 and 4.21, it can be concluded that the Si/Al ratio improves with reduction in sulphate salts level detected in the various samples. The Si/Al ratio was noted to vary without necessarily following a specified pattern, which was attributed to incomplete washing of the sulphate salts formed during dealumination.

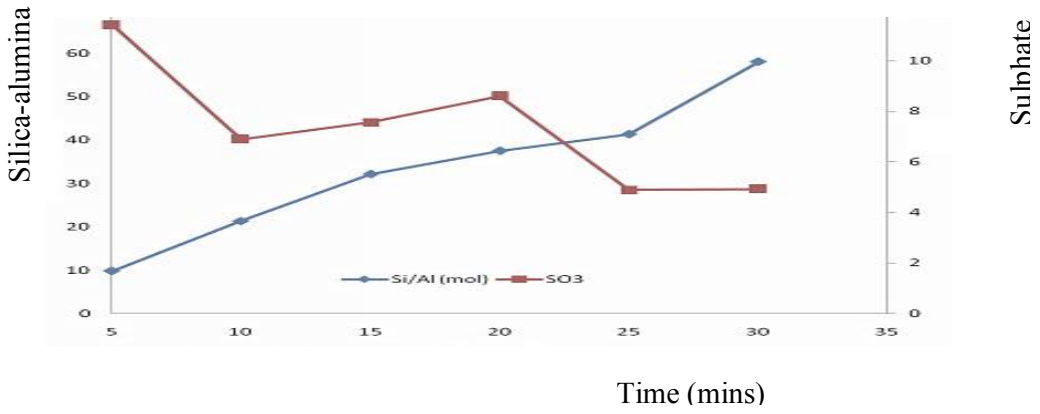


Figure 4.20: Sulphate salt effect on Si/Al ratio for thermal method (Kankara white)

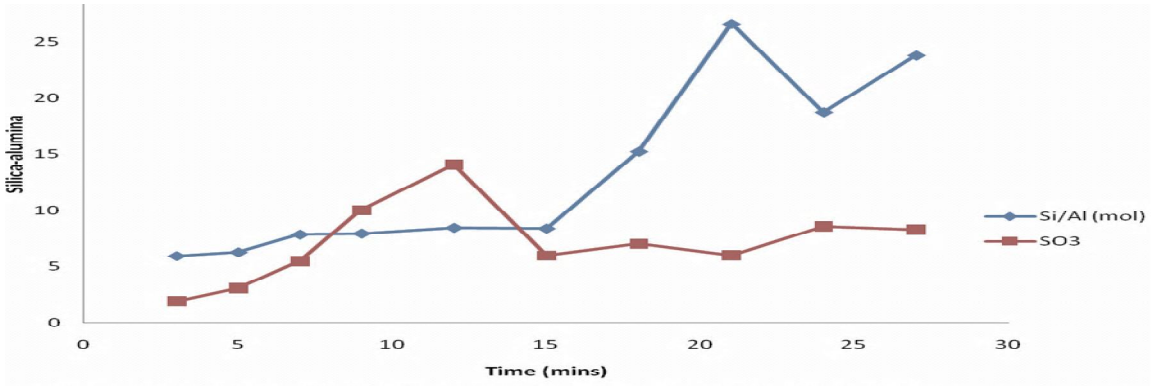


Figure 4.21: Sulphate salt effect on Si/Al ratio for non-thermal method (Kankara white)

Figure 4.21 shows that the Si/Al ratio was lower for non-thermal approach, which is associated with lower sulphate level. This observation is almost opposing to what was seen in Figure 4.20, which is speculated to have resulted from the strength of acid used and mode of dealumination.

Irrespective of the mode of dealumination, it was observed that the Si/Al ratio increased with decreasing sulphate levels. The flunctuations noticed in the sulphates level, resulting from either improper washing and/or passivity of some products from dealumination was observed to be more in the sample dealumintaed non-thermally and it had the highest value of sulphate salt left in the residue.

4.5 Gel formation

4.5.1 XRD Analysis

The gels formed were observed to have closely related minerals as shown in Figure 4.22 (a & b), not withstanding the source of kaolinite clay used, temperature of calcination and mode of dealumination. The new phases formed namely-CIT-1, TNU-9, Go, RUB's noticed in the gels from Kankara and Elefun, testify to the action of NaOH introduced. The quartz peak was still noticeable in Elefun kaolinite clay. It worth mentioning, that the gel was analysed without subjection to aging, hence the reason for quartz peak in Elefun.

Conclusively, it can be seen from the coordinated state of phases seen in the XRD spectra, in Figure 4.22 that the gels contain Si which retains it IV coordinated state, while Al's coordinated state changed from VI to IV, an essential requirement for zeolite synthesis (Rees and Chandrasekhar, 1993). The disordered form of aluminosilicate in the gel is in a state of higher simplexity and higher entropy, which is required for crystallization.

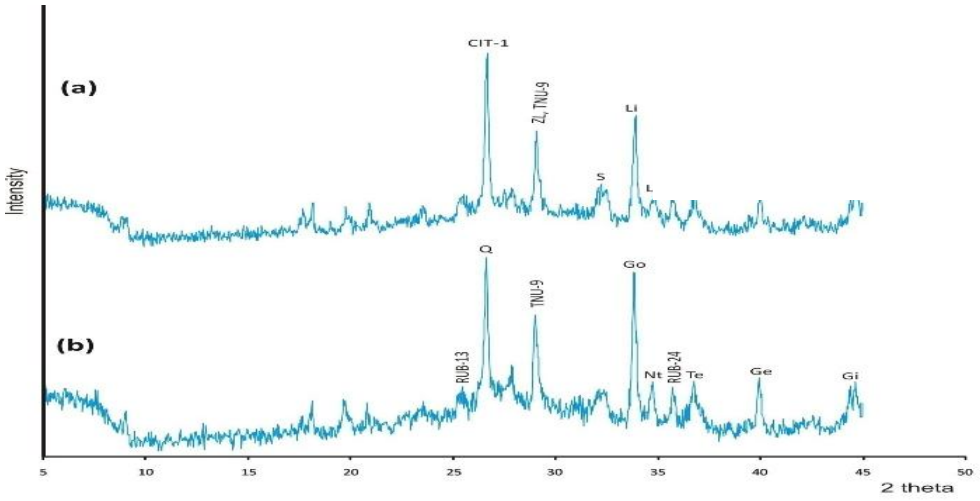


Figure 4.22: XRD patterns for gels from (a) Kankara and (b) Elefun

4.5.2 XRF Analysis

Table 4.5 shows the compositional analysis of the gel fromed. There is an increase in the sodium content, slight increase in Al_2O_3 and TiO_2 with considerable reduction in the SiO_2 content. The reduction in the silica content might be suggestive of the partial depolymerisation of silica content in the gel formed. The Na_2O content was observed to increase considerably, from about 0.27-0.45 to 10.9-11.4 resulting from the introduction of NaOH into the medium. It was also observed that the SO_3 content reduces from 13.7 to 3.50 and 2.4 to 0.36, respectively, for Kankara and Elefun.

Table 4.5: Compositional analysis for gel from Kankara and Elefun

ID	SiO_2	Al_2O_3	CaO	Fe_2O_3	K_2O	MgO	Na_2O	TiO_2	SO_3
KG	60.3	22.0	0.03	0.63	0.17	0.03	11.4	6.51	3.50
EG	53.2	15.5	0.10	0.64	0.20	0.04	10.9	4.53	0.36

Legend

Sample ID	Designation
KG	Gel obtained fromKankara kaolin
EG	Gel obtained from Elefun kaolin

4.5.3 BET and SEM

The BET result for specific surface area gave values of 234 and 248m^2/g respectively for gels resulting from Elefun and Kankara kaolin. This high value of surface area is required in order to: (i) reduce the level of segregation between the reacting species and (ii) enhance the reaction rate via availability of large surface area. Also, Belver *et al*., (2002), reported that the crystalline nature of the gel formed in their work had large particle size, responsible for the lower surface area.

The SEM image actually correlates the aforementioned speculation as shown in Figures 4.23 (a & b), where the bulky though flaky particle observed in Figures 4.12 (a & b) were noticed to have broken down into smaller closely packed particles. The gel obtained from Kankara was observed to retain a relatively large portion of the flaky but bulky particle, embedded in amorphous aggregates, suggesting its compositional resistance to alkaline treatment.

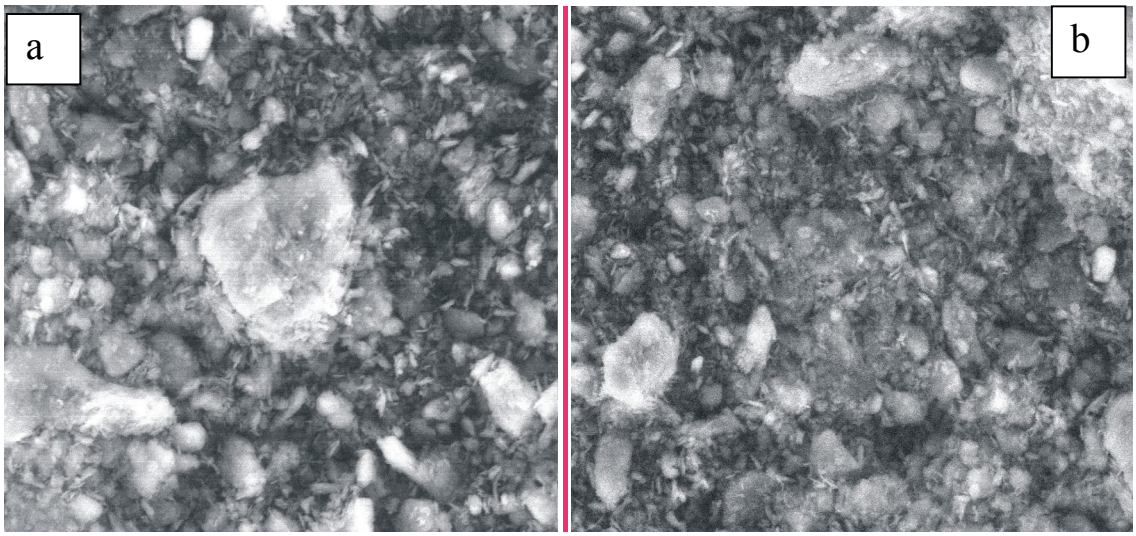


Figure 4.23: SEM images for gels from (a) Kankara and (b) Elefun

4.6. Commercial zeolite

4.6.1 XRD Analysis

The XRD peaks for the commercial zeolite (ZEOLYST, Holland) gave the prominent NaY zeolite peak at 2 theta value of about 6.2. The other phases identified alongside the zeolite Y were Ferrerite, Neutralinte and ITQ32. This XRD pattern shows that the commercial zeolite was not of pure grade, but blended with other inert mineral phases, in order to reduce its high activity and to avoid over-cracking during its usage.

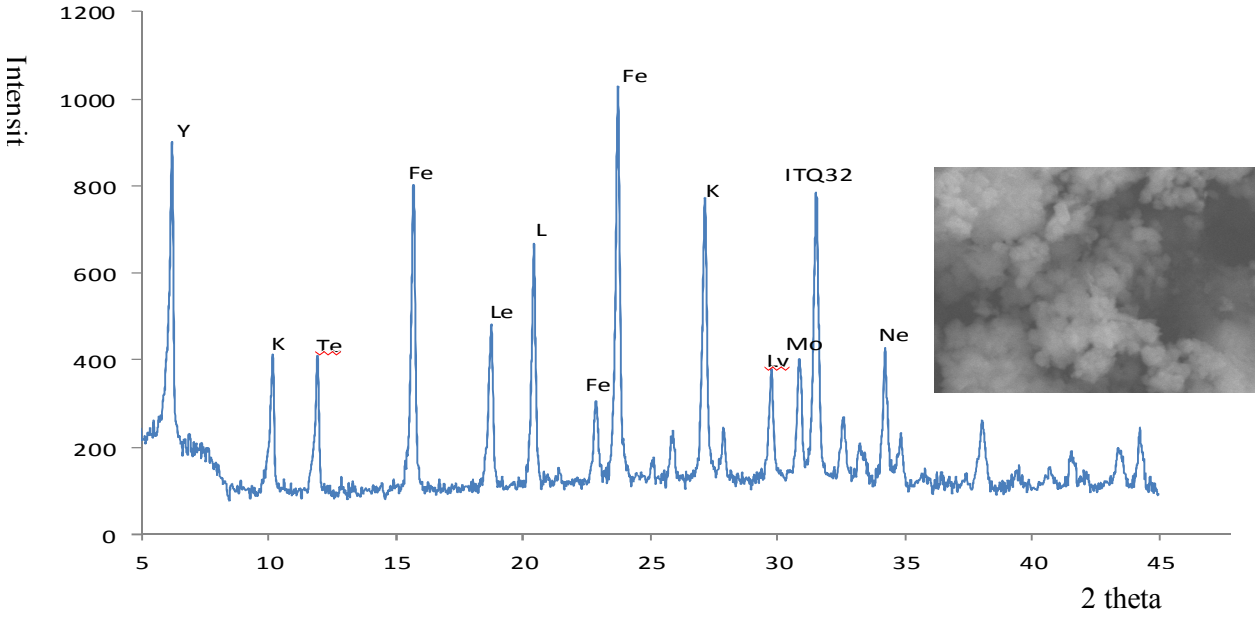


Figure 4.24: XRD patterns and SEM for commercial zeolite Y

The XRD patterns for the as-synthesized sample clearly indicated the successful synthesis of zeolite Y as depicted in Figure 4.25, with peaks at 2theta values of 6.21, 20.47 and 21.96 characteristic for zeolite Y. These peaks were X-ray finger printed using commercial zeolite Y,

scanned with the same XRD, procured from ZEOLYST Holland (Figure 4.24), as basis for comparison.

4.6.2 SEM and BET

The SEM for commercial zeolite shows clouded crystalline materials; reason for this is not readily available, as shown in Figure 4.24. The BET was determined to give 730m^2/g, which conveniently conforms to the assay given by the producer.

Zeolite Synthesis-Crystallization Reaction

4.7.1 Synthesis of zeolite Y from soluble salts

This section describes the findings for synthesis of faujasite zeolites from chemical reagents, which is to serve as control in this work.

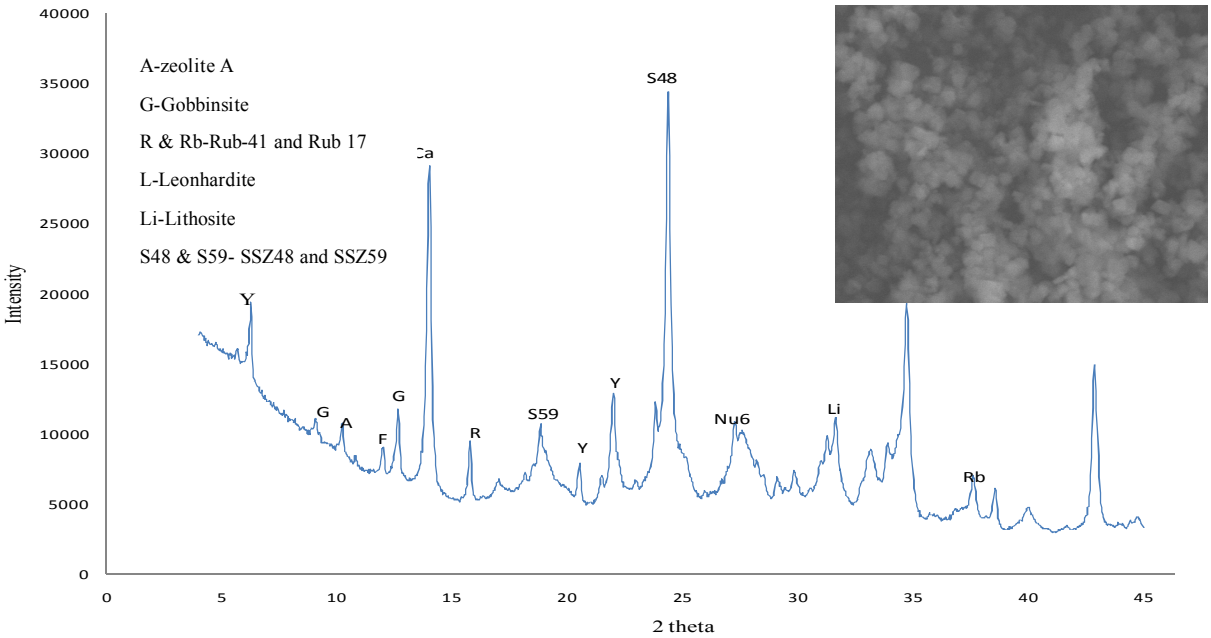


Figure 4.25: XRD pattern and SEM for zeolite synthesized from soluble salts.

The product obtained contains other phases, but the most prominent were cancrinite and SSZ48, highly siliceous materials. Their formation alongside zeolite Y was attributed to the inability of the used NaOH to completely depolymerise the aluminosilicate used. It was speculated that, probably, the depolymerised but unspent silica recombined to form a relatively stable phase- SSZ48 and SSZ56, as well as other minor phases in line with Figure 2.32. It was also suggested that less incorporation of Al atoms in the faujasite framework occurred, because the Al–O bond length in tetrahedral groups is larger than the Si–O bond length.

Recombination of highly siliceous material observed further buttressed the claims made under Section 2.7.5.2.1 (Figure 2.32) that, in the presence of any little undigested or digested but unspent silica in the zeolite liquor, formation of more thermodynamically stable/ favoured silica polymer is achieved. If the contact time is prolonged further, even the already formed zeolite might break down with its silica content being consumed. All the aforementioned led to the conclusion that, probably there is an existence of the structurally ordered phase in the gel matrix. This would be consistent with the observation of Subotic *et al*.,(1994) who confirmed the existence of these phases using FTIR, which is able to detect the presence of small fractions of crystalline phase even in trace, in the gel matrix.

4.7.2 SEM and BET

The surface area for the as-syntheszied zeolite Y in the matrix formed was determined to be 535m^2/g, which is consistent with literature values. The relatively high value of the surface area obtained could be related to the number of silica rich phases formed along with zeolite Y.

4.8. Synthesis of zeolite Y from pretreated kaolin

aging effect

4.8.1.1 XRD

Figure 4.26 shows the XRD spectra of the Kankara gel aged for 9 days at room temperature, i.e. the product resulting from Category III. The XRD pattern for the fresh product analysed confirmed synthesis of mixed crystalline phases quantitatively determined as: zeolite X (39.37%), zeolite Y (13.01%), quartz (13.13%), anatase (8.22%) and unnamed zeolite (6.56%).

The as-synthesized product was later subjected to post-synthesis aging to ascertain; firstly, the metastability of the product formed and secondly to confirm the unidentified zeolite phase. It was observed that ageing at room temperature for 95 days was not even good enough to depolymerize the quartz and neither did it reduce the anatase content. Figure 4.26 shows the XRD spectra obtained after 95days aging at room temperature.

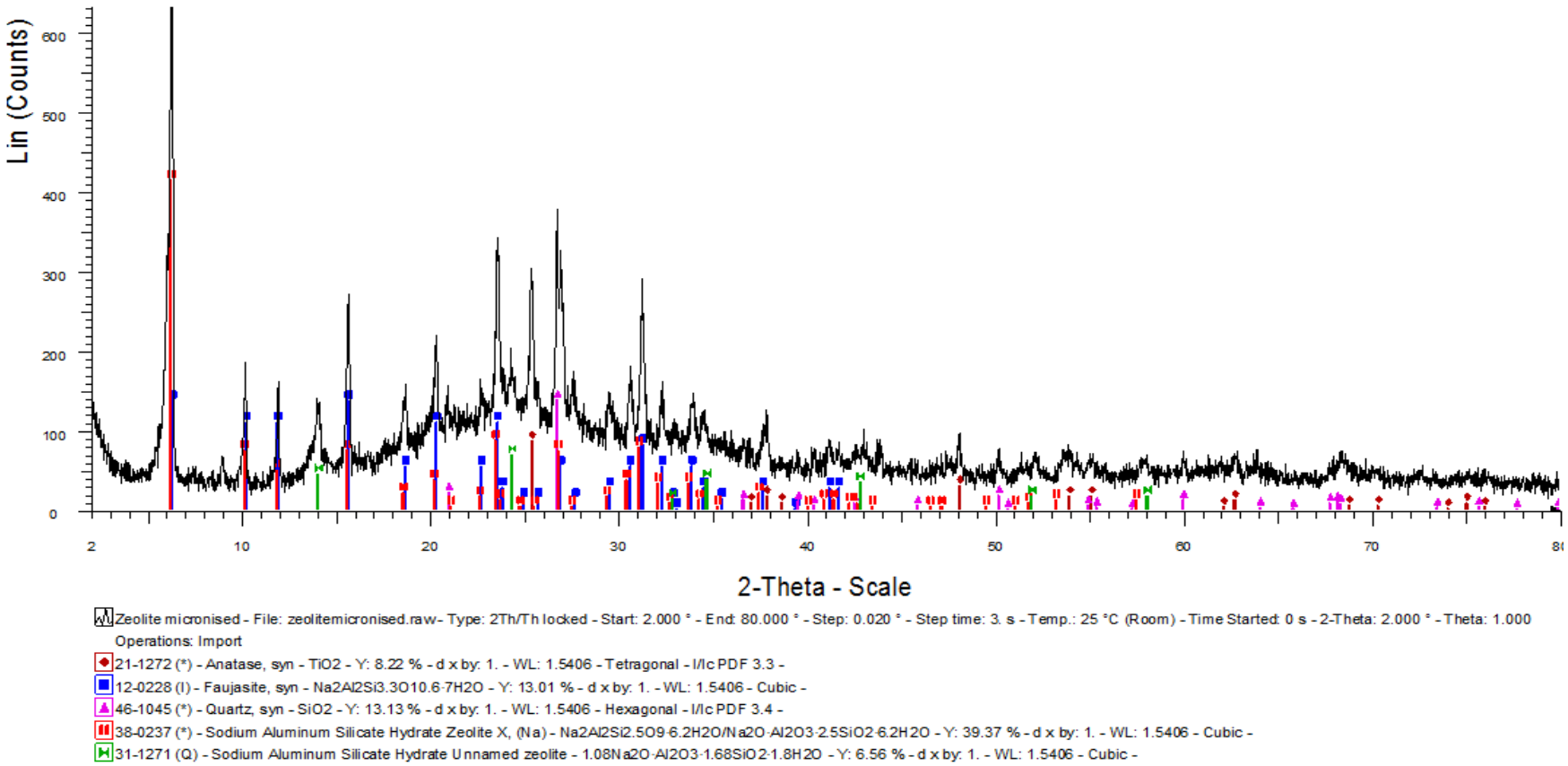


Figure 4.26: XRD pattern for matrix/composite zeolitic material

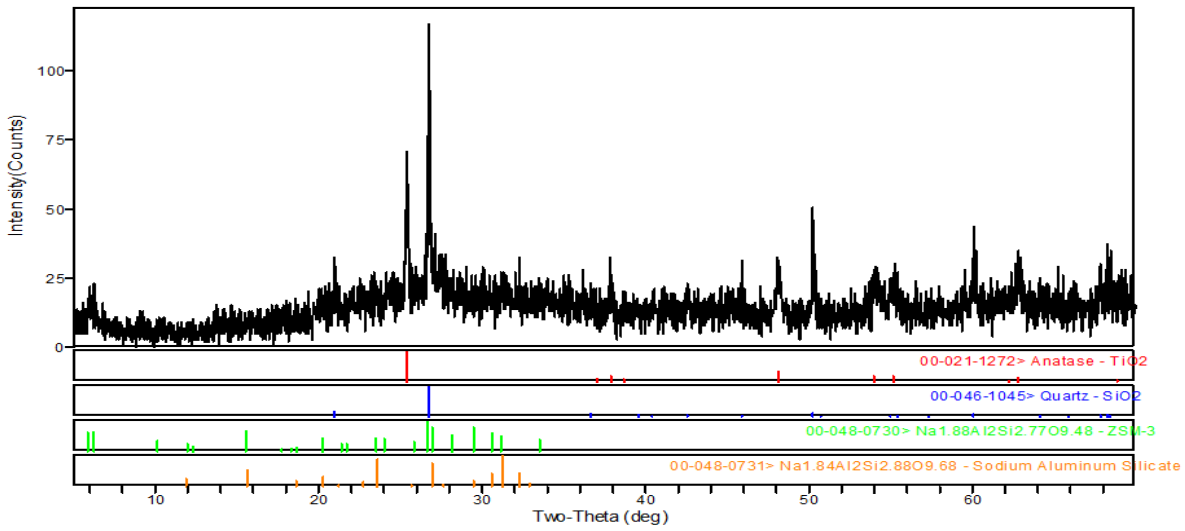


Figure 4.27: XRD Pattern for Zeolite ZSM3

The pattern in Figure 4.27 shows disappearance of peaks responsible for faujasite zeolite and increase in the intensity of peaks attributed to ZSM3 zeolite. The anatase and quartz still persisted and remained in the system, aside the remaining unconverted sodium alumino-silicate that could serve as ingredient for further transition.

It was suggested that the mechanism of this transformation could have been a combination of both solid gel phase" or "solution phase", with the solution phase serving as the initiation stage leading to crystallization. The dried sample left to age for 95 days was not calcined, enabling some intercalated water molecules present in the sample, which apparently were enough to further the progress of the reaction. This observation is in agreement with reports of other researchers in this field who claimed that zeolitic materials are metastable and continuously metamorphoses from one state to another, provided favourable conditions for further reaction to

exist in the medium. For example, Dwyer and Chu (1974) observed the transformation of faujasite to ZSM4 although their work was carried out in the presence of a templating agent.

It can be deduced that aging even for 95 days was not good enough to depolymerise the inherent quartz phase in the gel. This observation further confirms the fact that the activation energy for silica formation is less compared to that for zeolite formation. Also as-synthesized zeolites have the tendency of changing into quartz, as the chart Figure 2.32 clearly suggests.

For Kankara based gel, the siliceous materials remained intact not until after seven days of ageing as shown in Figure 4.28. The intensity of quartz related materials picked by the XRD in the gel were not observed in the products obtained. The products resulting from gels aged for 3, 5 and 7 days had peaks attributable to highly siliceous families of zeolites, namely SSZ's, ITQ's, TNU9, RUB's and chabazite-K. This observation suggests that more time was required for NaOH to epolymerize the ingredients in Kankara. Gladly, 9 days of ageing gave the prominent peak for zeolite NaY, whose intensity was observed to decrease slightly on the 11^{th} day, resulting from the appearance of silica rich mineral phases, like RUB17, RUB41, SSZ53 and SSZ48.

The results, sugests that the formation of small zeolitic crystals depends on the amount of aluminosilicate nuclei present in the precursor gel. The product-promoting effect of aging was attributed to the action of polycondensation reactions in the formation of groups facilitating crystallization. Longer aging time of the seed solution results in higher concentration of primary particle aggregates, and thus more mass gain through the higher surface area of these aggregates, which leads to faster crystallization rates.

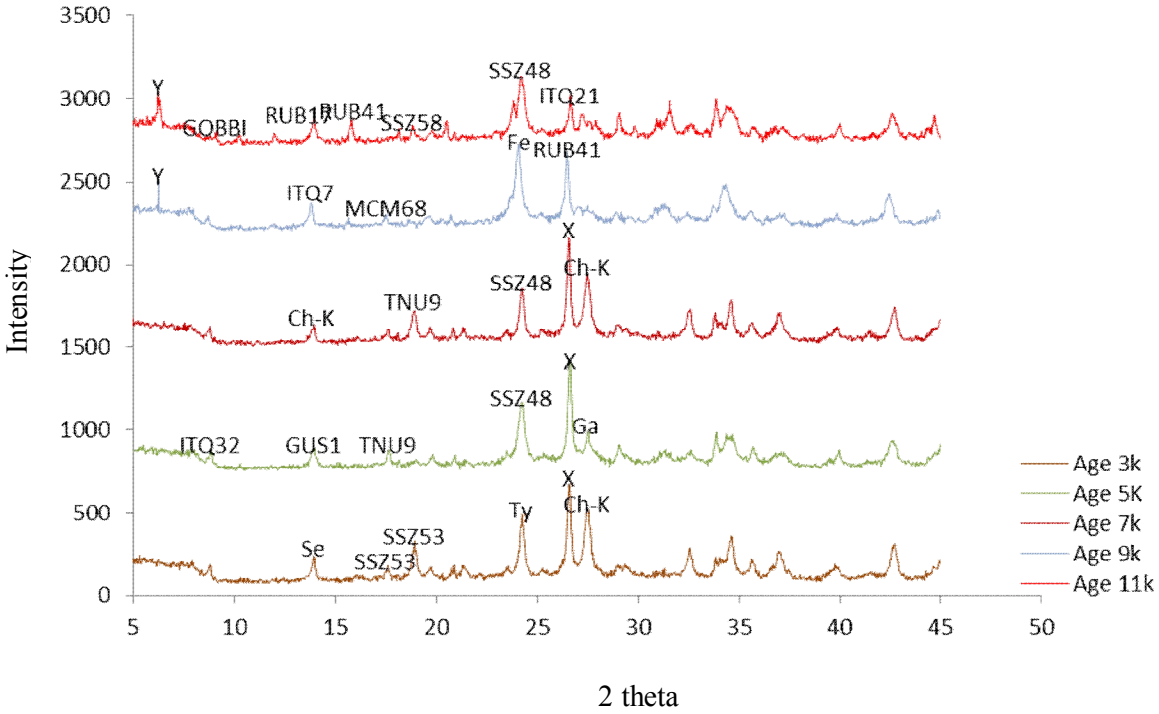


Figure 4.28: XRD patterns for as-synthesized zeolite from Kankara gel aged for 3-11days

This is consistent with our observation that a high degree of crystallinity was obtained with increasing aging time. However, when the aging time increases more than 9days, the relative crystallinity changed considerably. The reason proposed here by the author was that zeolite nucleation occurs at the gel-solution interface forming loose crystallites which grow by drawing nutrients from the gel and later from the clear solution. As the crystallites grow in size, they contact and bond with the surface via condensation of silanol groups on the zeolite with those on the silicon (silanols on silicon were formed by oxidation in the strongly alkaline solution). This suggestion is consistent with the model of Jansen *et al.,* (1992) and Koegler *et al.,*(1994) which identifies the gel layer, i.e., layer of loosely connected amorphous particles, as the site of crystallization. Crystal growth continues until the synthesis solution is depleted to a certain extent.

The XRD spectra in Figure 4.29 depicts the crystalline phases developed from Elefun gel under different aging conditions, namely between 3 and 11days at room temperature (Category IV). During the aging period, the silicate (in any mineral form) species were gradually broken down, in order to form siloxane network (Si-O-Si), which is expected to be depolymerised easily with the introduction of NaOH and later the incorporation of alumina into the framework. The quartz peaks and other minerals noticed in the gel (Figure 4.22) disappear or reduce.

The product obtained from 3 and 5 days of ageing was a matrix, comprising of different forms of undepolymerized silica. This was also observed for gel aged for 7 days, but it also contained other phases identified as ERS7, zeolite ITQ's, TNU-21 with traces of zeolites IM,NaX, offretite and quartz in tridymite form.

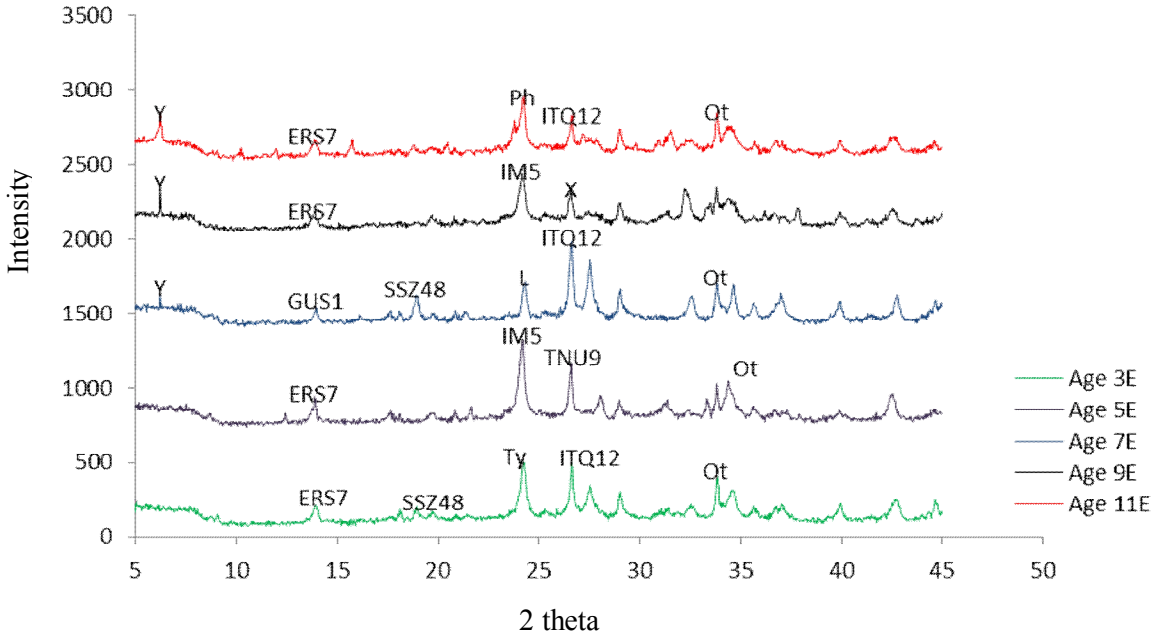


Figure 4.29: XRD patterns for as-synthesized zeolite from Elefun gel aged for 3-11days

Some of these minerals were also observed for gels aged for 9 and 11 days; though with lower intensity. Products obtained after 7 days ageing tends to have the peak attributed to NaY. The intensity, howver, was noticed to increase with ageing period. Accordingly, Elefun clay would only be useful in the synthesis of NaY zeolite after 7 days ageing. The formation of multiphase phases of zeolitic material from the kaolinite clay is an indication of active inherent impure mineral phases, which corroborates the work reported by Querol *et al.,* (1995). Selected results obtained for aging in Categories I and II are shown in Appendix E. It suffices to mention here, that the result though not discussed here but were useful in assisting the author during critical decision making process.

4.8.1.2 BET and SEM

The BET specific surface areas were determined to be 462 and 493m^2/g, respectively, for as-synthesized zeolites from Kankara and Elefun. The values of the specific surface area were found to be close to that of commercial grade despite its low level of NaY crystallinity. The reason for these values was attributed to contribution of the highly siliceous zeolitic phases formed on the bulk surface area.

The morphologies for as-synthesized zeolite matrix and ZSM3 from Category III (whose XRD patterns are depicted in Figures 4.26 and 4.27) are shown in Figure 4.30 (a and b) while that from Kankara and Elefun with optimal crystallinity (choosen from Figures 4.28 and 4.29) are shown in Figure 4.31(a and b).

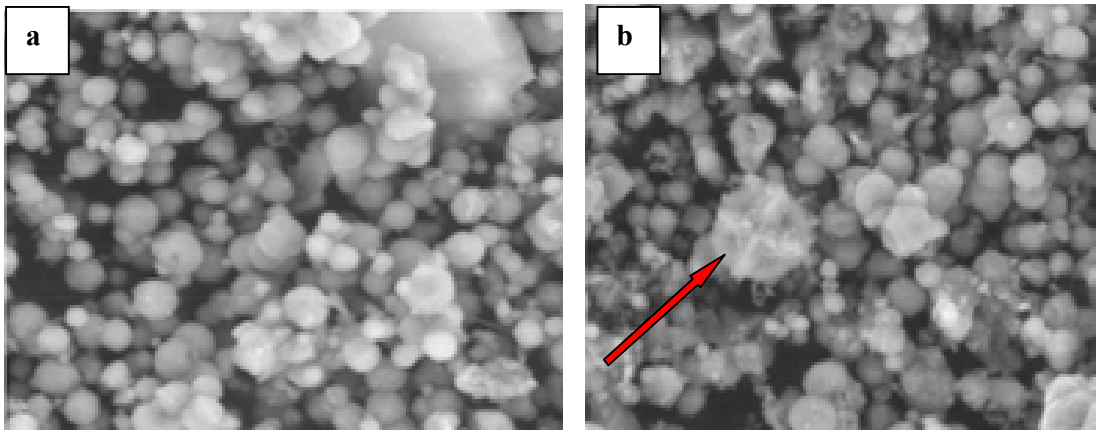


Figure 4.30: Scanning Electron Micrographs for (a) zeolite Y and (b) ZSM3

The SEM pictures (Figure 4.30(a)) in agreement with the XRD analysis points to formation of not only zeolite Y, but testify to presence of other phases. The tetragonal crystallite was attributed to presence of anatase, cubic to faujasite and the ZSM3 zeolite, while the hexagonal, for quartz, as depicted in Figure 4.30(b).

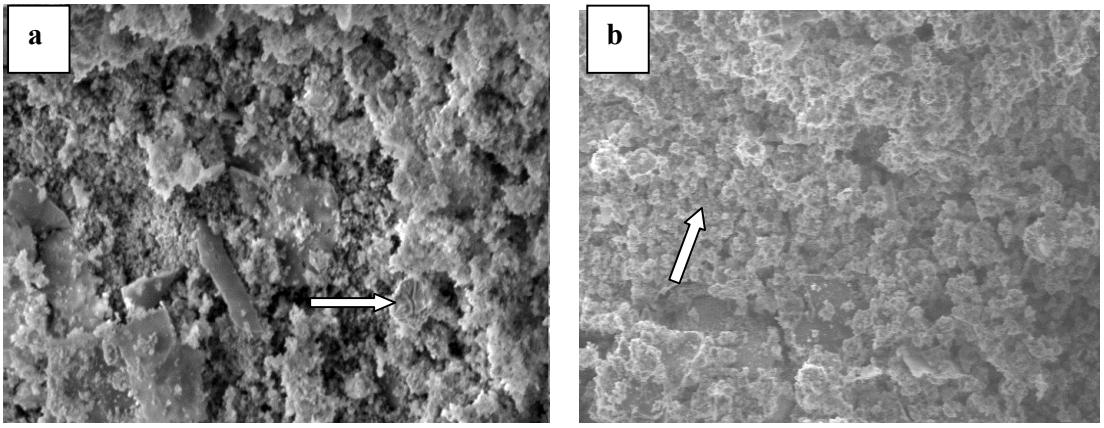


Figure 4.31: Scanning Electron Micrographs for zeolite Y from (a) Kankara and (b) Elefun

The SEM in Figure 4.31(a &b) shows the presence of zeolite Y with arrow surrounded by quartz materials as indicated by the XRD. Products resulting from Elefun gel, gave a relatively better

quality and high number of crystalline materials, from SEM image (as depicted in Figure 4.31b) compared to Kankara, which had the as-synthesized zeolite masked with quartz and other zeolitic materials (Figure 4.31a).

4.8.2 blanking agent (dyeing) effect

4.8.2.1 XRD Analysis

Some selected dyes have the ability to suppress the production of unwanted zeolite phases, as well as catalyse the rate of silica depolymerization. The introduction of crystal violet in the gels formed from both Kankara and Elefun, gave highly amorphous material, even after crystallization as shown in Figures 4.32 and 4.33, respectively. The quartz and siliceous phases which were present in the gel (Figure 4.23) decreased in intensity, thus suggesting that the dyes were effective in breaking down the rigid materials, which should increase the concentration of reactant for crystallization reaction. This is expected to result in formation of crystalline desired materials, but unfortunately this was not the case and it appears that the introduced dyes acted as inhibitors, not only to the inherent impurity, but also to the reconstitution of the already broken down silica and alumina. This observation was noticed for both gels from Kankara and Elefun.

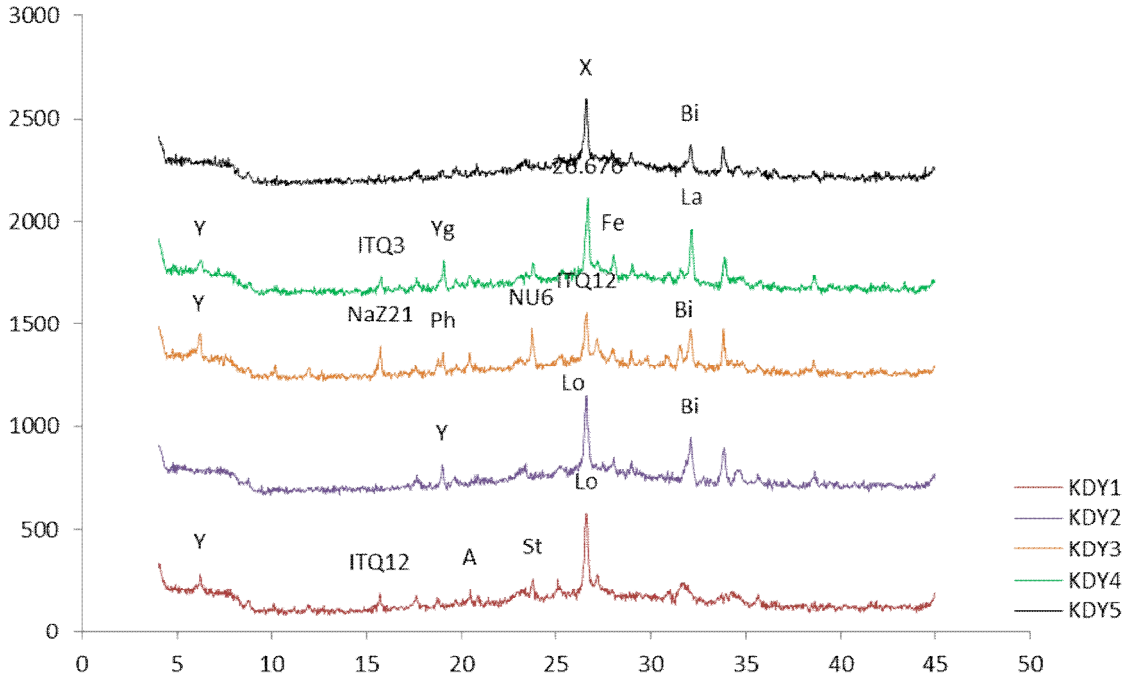


Figure 4.32: XRD patterns for zeolites from Kankara gel with varied dye concentration

KDY1, KDY2, KDY3, KDY4, KDY5: Kankara base gel dyed with 0.0001, 0.0005, 0.001, 0.005 and 0.01, respectively, with crystal violet

The mineral phases identified by the XRD patterns for Kankara (Figure 4.32) were observed to be mainly of sodium base, while very little have potassium or other inherent impurities, an indication that the dye was effective in suppressing the nucleation of impure based minerals. The sample tagged KDY3 had the most intense peaks attributed to NaY, with impure phases like NaZ-21, Ph, Nu (6) and ITQ12. The product KDY4 had traces of zeolitic phases and highly amorphous, which later disappeared completely (as seen in KDY5) and transformed into an amorphous material and high silica zeolite. This sugests, that the silica reconstitution process and high level of amorphousity, increases with dye concentration.

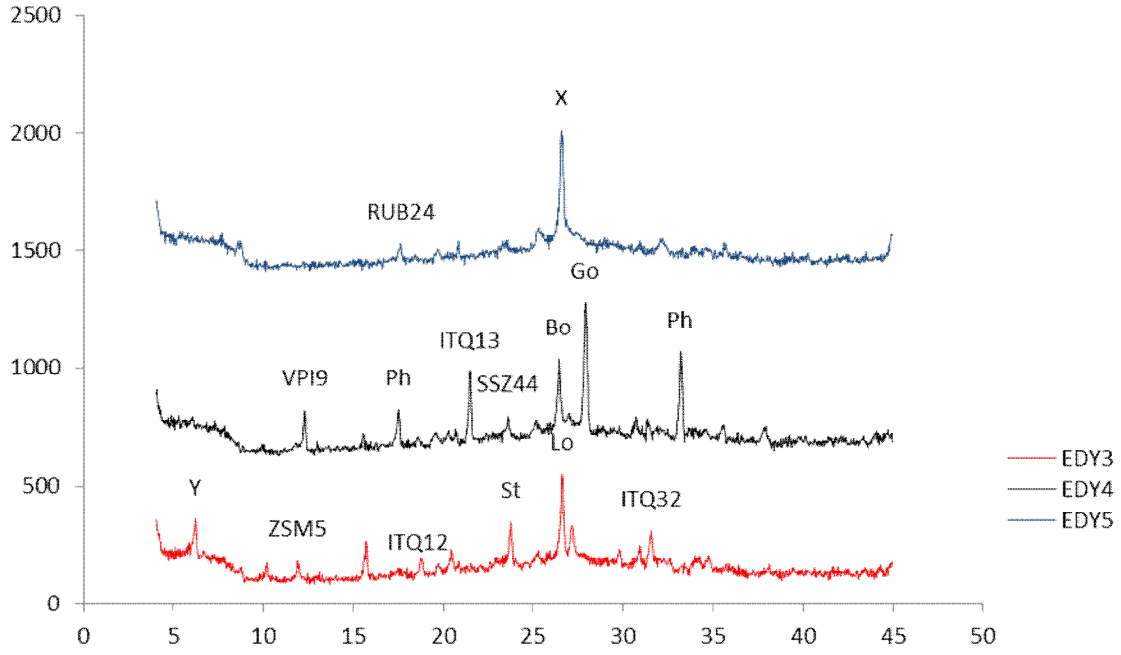


Figure 4.33:XRD patterns for zeolites from Elefun gel with varied dye concentration

EDY1, EDY2, EDY3, EDY4, EDY5: Elefun base gel dyed with 0.0001, 0.0005, 0.001, 0.005 and 0.01, respectively, with crystal violet (Note: samples EDY1, EDY2 were not returned from the centered where analyses were conducted)

The XRD pattern shown in Figure 4.33 for Elefun sample treated at various gel-dye ratio, gave matrix material for EDY3, comprising of NaY, ITQ12, ITQ32 with traces of ZSM5, Stilbite and Losod. At higher dye ratio, i.e. EDY4 more complex phase mixtures were obtained containing phillipsite, VPI9, SSZ44 and other high silica zeolites. This can only imply that the silicalization process starts at this dye ratio, meaning that the added dye concentration exceeded the depolymeization limit, now entering a new facet-polymerization. Normally, in situ polymerization starts with dissolution, depolymerisation and reconstitution. Accordingly, it is suggested that higher dye concentration favours formation of more amorphous phases. The

sample tagged EDY5 almost gave a confirmation of this speculation, as the level of amorphous increased compared to the preceding one (EDY4).

For Elefun, dye addition did not have any meaningful effect on the crystallization reaction. Since dyes are supposed to suppress incorporated impurities in the nucleation process, the observed trends were expected as Elefun had little inherent impurities.

The XRD spectra for the other dyes used in this work are presented in Appendix F.

4.8.2.2 SEM and BET

The SEM of product KDY3 shown in Figure 4.34 (a) gave small amount of identifiable zeolite Y shape which is masked by presence of other phases and some unconverted materials. It was suggested that probably the sticky-like material noticed in Figure 4.34(a) could have resulted from excess NaOH and/or unconverted gel material. The SEM for Elefun in Figure 4.34(b) had more crystalline materials and few shapes attributable to NaY. The conversion was observed to be better than that of Kankara. The product which had a fairly good closeness to zeolite NaY from Elefun was selected for SEM analysis, in this case, EDY3.

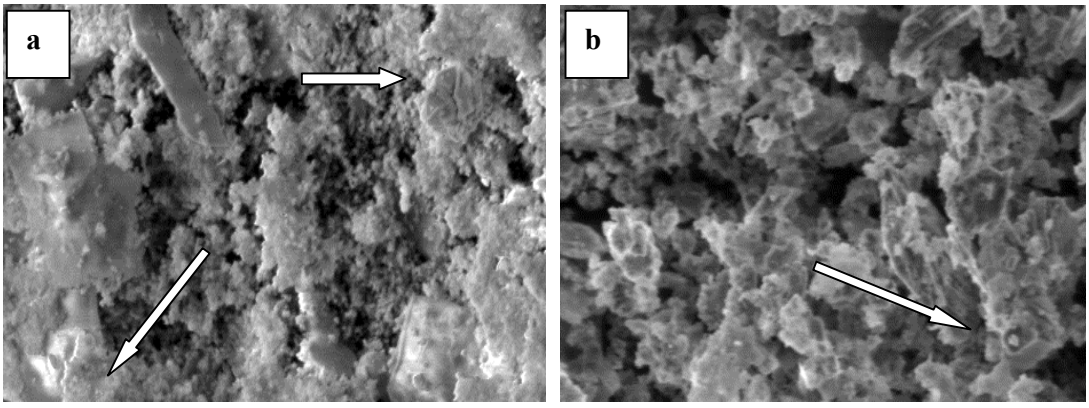


Figure 4.34: Scanning Electron Micrograph for zeolite Y (a) Kankara and (b) Elefun

4.8.3 alkali concentration effect

Addition of NaOH increases the degree of supersaturation of the system and concurrently the rate of nucleation, resulting from salting out effect (enrichment of the aluminosilicate sol with silicon). It is also found that, this promotes structure formation (Na^+, Li^+)/disruption (K^+, Cs^+) of the initially formed crystals, which facilitate an acceleration of crystallization and control the crystal morphology and size.

4.8.3.1 XRDAnalysis

The Kankara based gel was observed to loose all its inherent phases with alkaline treatment as shown in Figure 4.35. The figure reveals that the crystallinity of zeolite-like materials increased with NaOH concentration, while the degree of dissolution for quartz was also greatly enhanced. This observation was noticed not only for Kankara but also in Elefun, with better crystallinity at higher NaOH concnentration.The controversial debate on whether zeolite material begins to crystallize before all the metakaolinite has been converted to a gel or not and whether, was not addressed, due to lack of tools. Also, with a higher NaOH concentration, the time span during which the concentration of soluble Al species drops to zero is shorter. These findings indicate that zeolite production is promoted with a higher NaOH concentration. The zeolite generation reaction from kaolin is considered to consist of a dissolution process for soluble Si species and soluble Al species, and a zeolite generation process with both species (Alkan et al, 2005).

The products resulting from Kankara gel (Figure 4.35) increased with Na_2O/SiO_2, while the converse was true for Si_2O/Al_2O_3 ration which is in agreement with the data of Occelli and Robson (1989). In general, lowering the alkalinity of the synthesis solution could prolong the dissolution time of silica-alumina sources, reduce the overall reactivity, increase the

polymerization degree of silicon species and thus result in higher silicon incorporation into the zeolite Y framework. However, when the alkalinity is excessively high, the crystalline structure of zeolite Y, in the metastable state, is liable to dissolve and the crystallinity will decrease.

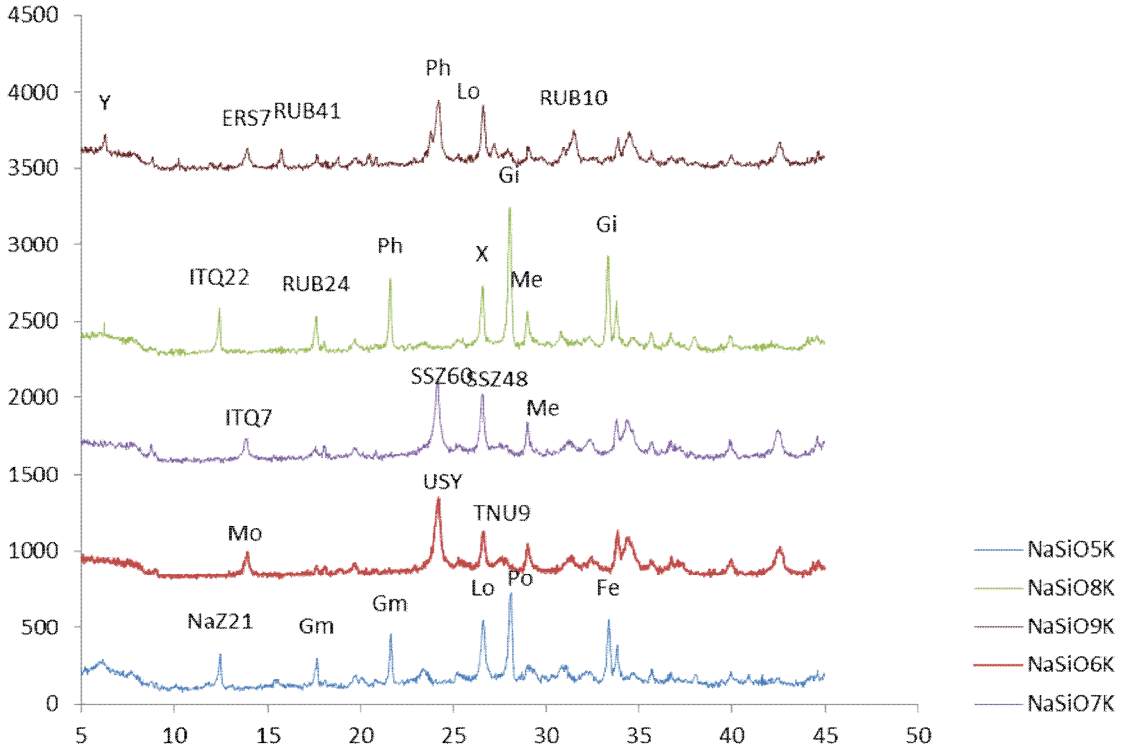


Figure 4.35: XRD patterns for zeolite from Kankara with different concentrations of NaOH.

NaSi05K, NaSi06K, NaSi07K, NaSi08K, NaSi09K -Kankara gel with Na/Si of 0.5, 0.6, 0.7, 0.8 and 0.9, respectively.

This explanation is applicable to the observation noticed in Kankara based as-synthesized zeolite. The presence of highly siliceous materials (i.e. RUB's, philipsite, ITQ's, Losod etc) in the products was attributed to both ***over and under alkaline treatment***; Al-O bonds are more readily attacked and broken than Si-O bonds. Accordingly, the probability of the formation of Al-O-Si bond is higher than that of Si-O-Si in aluminosilicate gel. This therefore favours

instantaneous incorporation of Al in the aluminosilicate gel formed and enrichment of silica in the liquor, on complete consumption of Al-O source (Fernandez-Jimenez et al, 2006). The immediate implication of this is that on completion of crystallization the liquor is saturated with silica and is in quasi-equilibrium with the evolving zeolite, whch equilibrium can shift, when disturbed.

Accordingly, it was observed that Kankara gave the prominent Y zeolite peak when treated with Na/Si ratio of 0.9.

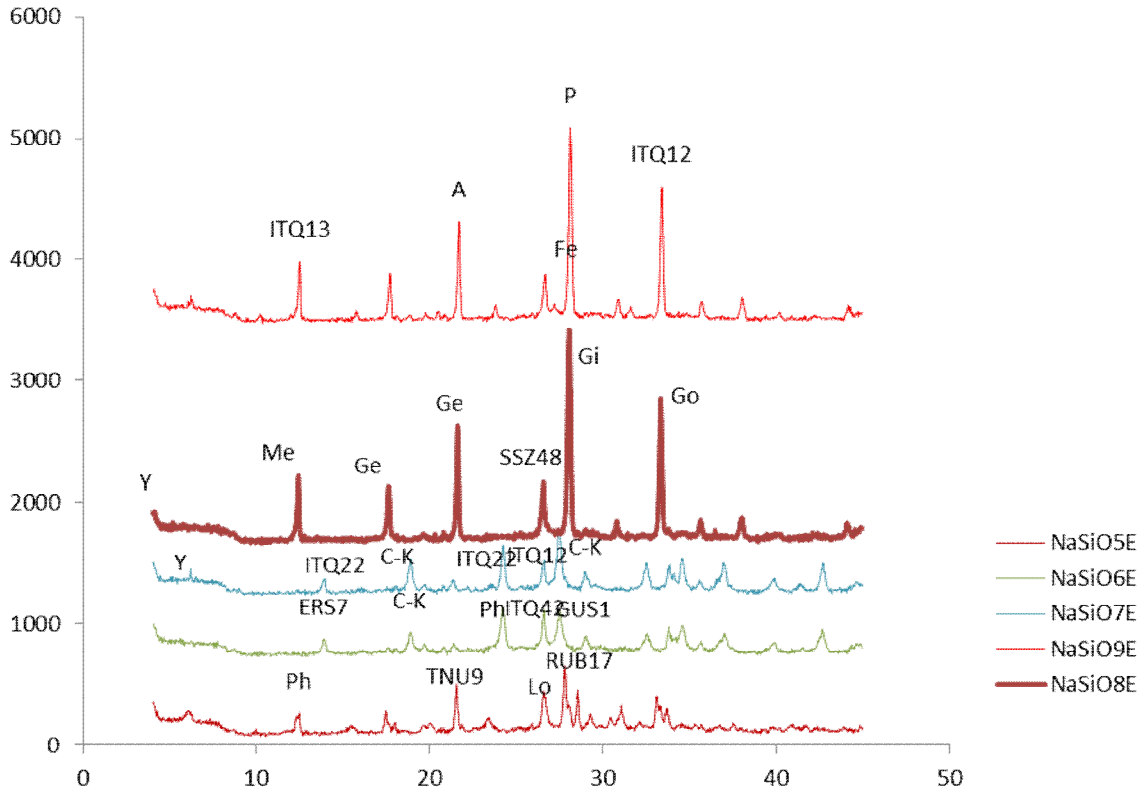


Figure 4.36: XRD patterns for zeolite from Elefun with different concentrations of NaOH.

The Elefun samples (with Na/Si=0.5 and 0.6) were observed to be made up of matrix materials, while a small peak for zeolite Y appeared for samples with the values of Na/Si, 0.7 and 0.9, as

shown in Figure 4.36. Higher NaOH concentration led to the disappearance of the most prominent peak at 2 theta value 6.21, though with less amorphous material and less highly siliceous phase, pointing to progressive digestion of the silica by the NaOH. Increase in NaOH concentration favoured formation of more crystalline phase, but not necessarily the desired zeolite phase. This may have resulted from the residual sodium hydroxide and unspent ingredient and inherent minerals, in the reaction mixture, which likely influenced the hydrothermal treatments (Alkan et al, 2005; Miao et al, 2009; Chandrasekhar and Pramada, 2001).

The higher the concentration of NaOH used for hydrothermal treatment, the lower the peak intensity of the unreacted quartz and inherent mineral phases in the starting gel. This indicates that with a higher concentration of NaOH, the proportion of unreacted crystalline starting materials in the powder product is smaller. Incidentally, the concentration of soluble Al species increase with treatment time, eventually going through a maxima and decreases to near-zero.

4.8.3.2 SEM and BET

The s.s.a for the two best samples (NaSi09K and NaSi09E) was determined to be 433m^2/g and 453m^2/g for Kankara and Elefun, respectively. The SEM (in Figure 4.37) shows the crystals shape for zeolite Y as-synthesized from Elefun and Kankara, indicated by arrow in white, while the rigid quartz material indicated by red arrow was observed to still remain undigested. From Figure 4.37, it was also observed that the size of quartz in Elefun seems to be bigger than in Kankara, but flaky in nature. This might be responsible for the observed more positive response of Elefun to alkaline treatment.

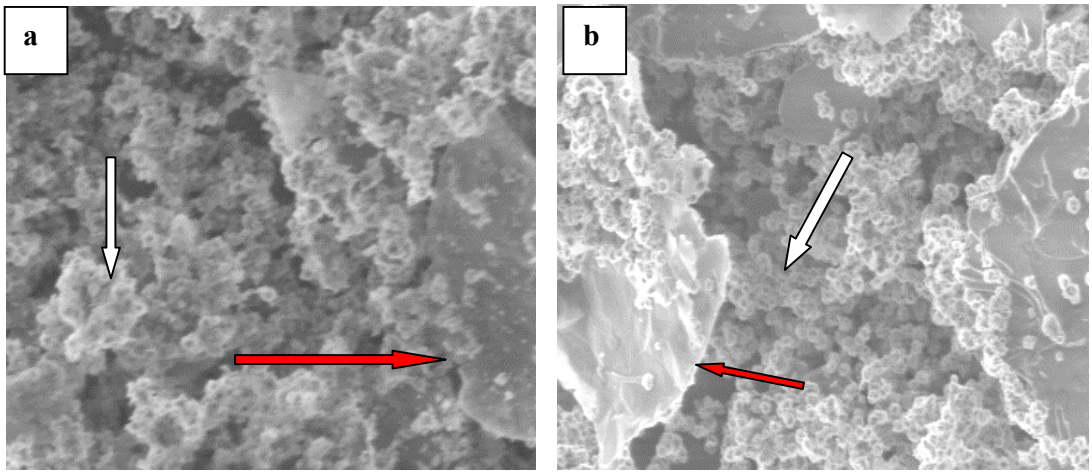


Figure 4.37: SEM images for zeolite Y (a) Kankara (NaSi09K) and (b) Elefun (NaSi09E)

4.8.4 pH effect

The XRD results for this sub-section represented in Appendix G, shows the effect of increase in pH of the reacting mixture on crystallization. This increase in pH is an indication that SiOH in colloidal state incorporates in the framework in the form of SiO_2 due to its acidic nature. The pH of the system is also very important to stabilize the sol, controls the particle size, but does not relate directly to the total OH content of the system. From the XRD results obtained pH adequate for depolymerization of silica and alumina and leading to synthesis of desired zeolite was gotten, which also correspond with the work of Lechert (2001). It is important to note that the XRD spectra (in Appendix G) were not very useful due to the limitations in the 2 theta range, lack of *ascii* file and poor peaks qualities. Despite this though, it was good enough to give an insight and assist in making necessary and decisive action, in our pursuit.

4.8.5 seeding effect

4.8.5.1 XRD Analysis

Seeding is an effective method for encouraging product formation in systems which are reluctant to nucleate, for controlling crystal size and for reducing the formation of crystalline impurity phase, by providing a surface on which crystallisation can occur.

The Kankara gel was not seen to respond positively to the added seeding material. Despite the added seeding agent, the products obtained were found to be rich in highly siliceous zeolite materials, like ITQ's, GUS, ERS, as shown in Figure 4.38.

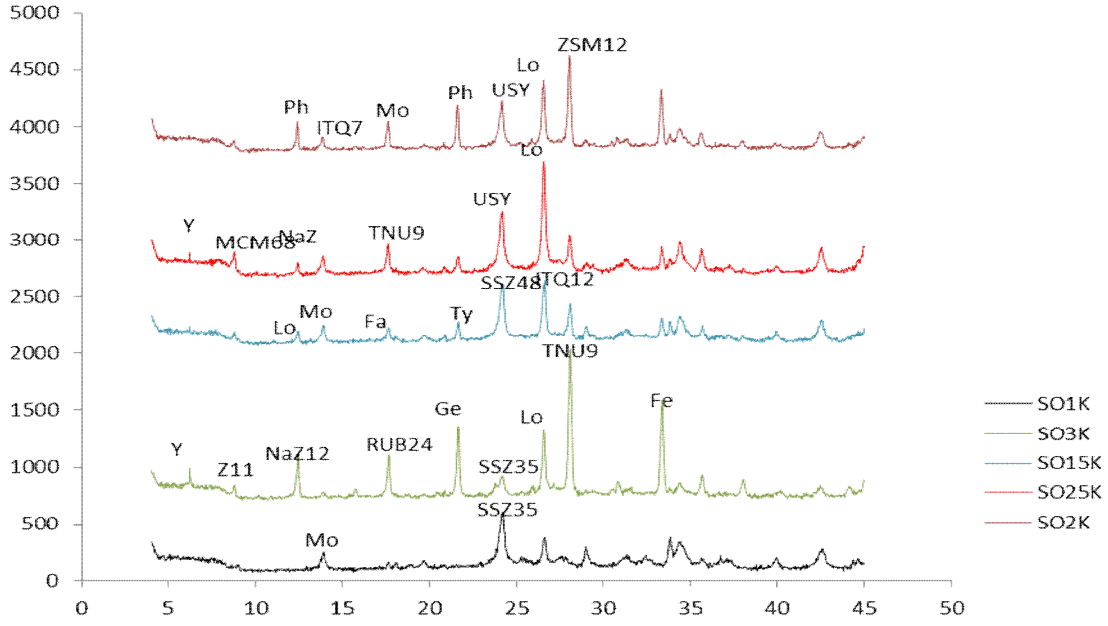


Figure 4.38: XRD patterns for zeolite from Kankara gel with different amount of seeding agent.

S01K, S015K, S02K, S025K, S03K-Kankara based gel seeded with 1, 1.5, 2, 2.5 and 3 wt% of metakaolin, respectively, with commercial NaY

The desired zeolite material was seen to be in trace for almost all the samples. The reason for this was partly blamed on the high content of SO_3, particle size and relative solubility of the inherent impure phase and also the competition for attainment of stable state between the re-constituitive species. Conclusively, seeding can cause perturbation in the local nutrient concentration that can have a large impact on the zeolite growth. Seeding can selectively induce the formation of zeolite Y without marked presence of other impurities and eliminate the processes of induction and nucleation. From the evidence shown one might speculate on the role of seeds in promoting zeolite crystallization rates. It seems apparent that the seed crystals do not *simply* grow. It would appear that in circumstances where surface nucleation or polycrystalline breeding occur, acceleration of the crystallization rate is due to the formation of new nuclei on the seed crystal surface. Subsequent growth of these new crystallites, of the same phase or a new phase, results in a dramatic increase in crystal surface area. Thus, any rate enhancement stems from this increased surface area.

Figure 4.39 depicts the XRD patterns for Elefun gel seeded with various proportion of commercial zeolite. It was observed that the added seed assisted in promoting the formation of desired zeolite only with small amount added and the product was seen to increase in intensity with increased seeded material. It is speculated that the added seeding agent (being an unstable phase) quickly dissolves in the synthesis mixture, providing the sufficient surface area, supersaturation and self-nucleation, needed for achievement of autocatalytic nucleation.

The Elefun based gel behaved positively to the seed material, since very little impure mineral phases were observed in the products obtained for samples treated with 2, 4 and 6 weight percentages. It was also seen that some less impure phases were noticed for that seeded with 6

wt%, meaning that the seeded material was enough to attain supersaturation and thereby enhance the conversion of peaks attributable to NaZ21, ZSM11, Z5 into desired faujasite zeolite. Despite the introduction of the seed, highly siliceous zeolitic phase were observed, this might be due to either improper homogeneousity of the synthesis mixture or re-silicalization resulting from the destruction of already formed zeolite and reconstitution of the newly extracted ingredients. This observation can be further clarified from the XRD peaks for sample treated with 8 weight percent.

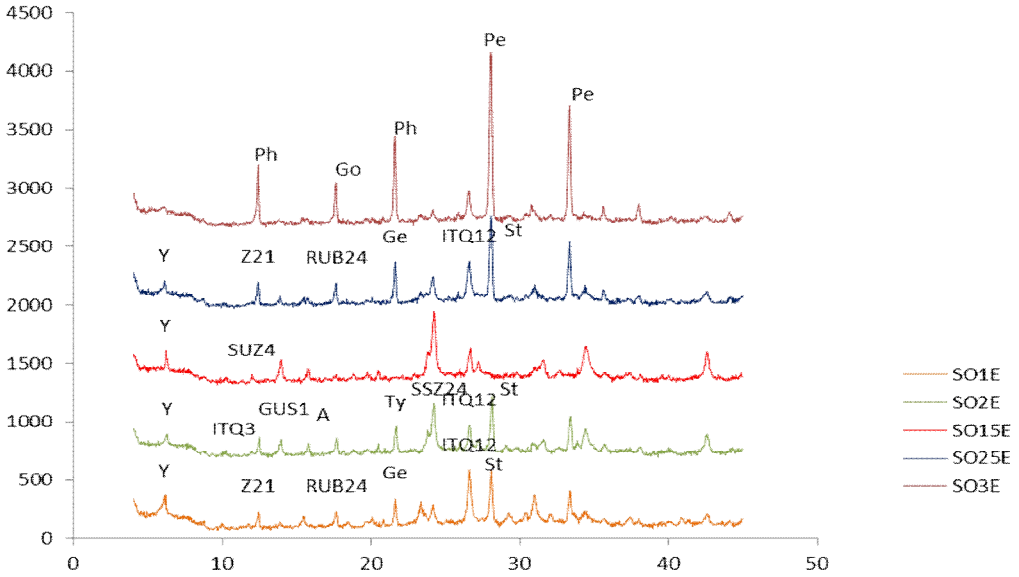


Figure 4.39: XRD patterns for zeolite from Elefun gel with different amount of seeding agent.

S01E, S015E, S02E, S025E, S03E- Elefun based gel seeded with 1, 1.5, 2, 2.5 and 3 wt% of metakaolin, respectively, with commercial NaY

4.8.5.2 SEM and BET

The SEM for zeolite synthesized from both Elefun and Kankara shown in Figure 4.40 gave a distinctive and more zeolite in Elefun, with fewer impurities compared to that from Kankara. The images in Figure 4.40 (a) had very little quartz-like material (arrow in red), while the one in

Kankara are not only much in number but even bigger (also arrowed in red) in Figure 4.40 (b). This observation only pave way for the speculation, that probably the ingredients in Kankara were not very responsive to seeding material, which is likely linked to the persistent quartz found more in Kankara.

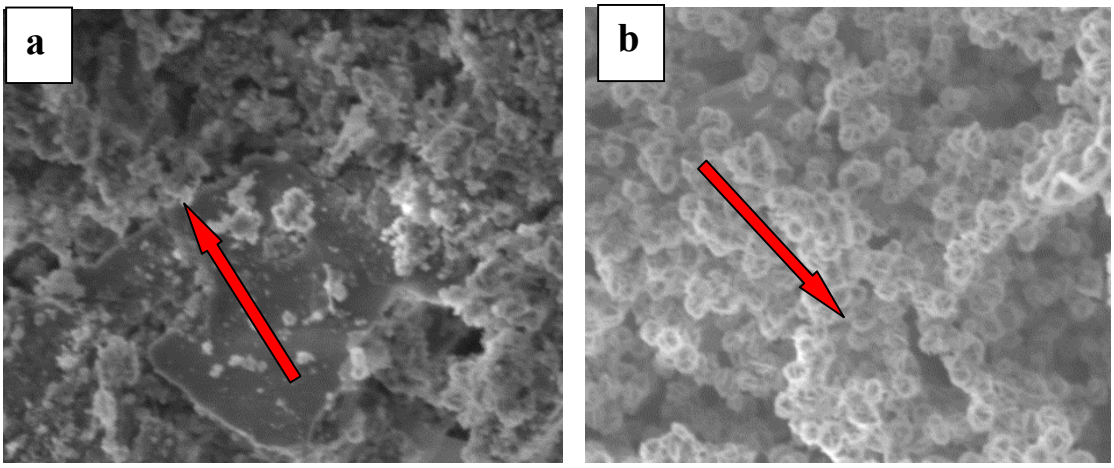


Figure 4.40: SEM images for zeolite formed from (a) Kankara (b) Elefun using seeding material

4.8.6 crystallization time and temperature

Temperature plays significant role in the synthesis of zeolitic material, so also is the crystallization time at which the synthesis mixture is subjected to. The XRD obtained for this parameter are depicted in Appendix H.

4.8.7 process improvement

The process improvement study was done to ascertain and most likely improve on the observed setbacks and reasons for inability to produce highly crystalline zeolite Y. The samples that were repeated are Elefun with Na_2O/SiO_2 ratio of 9 (NaSi09E now tagged sample A), Kankara with dye (KDY3 now sample B), Kankara seeded with 2wt% (sample C), sample D was prepared from soluble salts, Elefun seeded with 2wt% (sample E) and Elefun aged for 9days (Age9E-now

tagged as sample F). The XRD patterns for the re-synthesized products are given presented in Figures 4.41, 4.42, 4.43, 4.44 and 4.45, respectively for samples A, B, C, E and F.

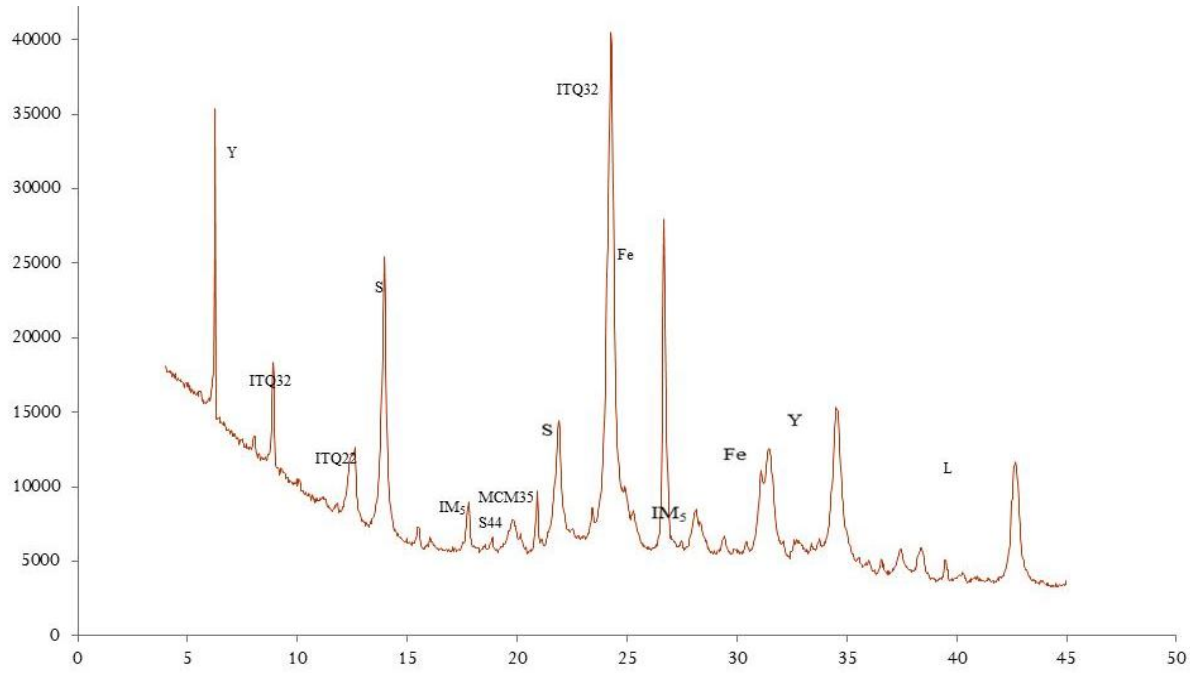


Figure 4.41: XRD patterns for reproduced zeolite from Elefun NaSi09E

It was observed that post dealumination calcination and increase in the NaOH for Kankara clay led to relative high intensity of zeolite Y and also formation of other highly silica zeolite phases. This might be due to the fact that the activity of inherent silica was improved in the presence of NaOH, which now serves as both mineralizer and buffering agent. A new important zeolite with very high pore size was observed along with zeolite Y, i.e. ITQ's zeolite family. Actually, ITQ's zeolite is being recognised as an alternative to most zeolite now in use, due to its property.

The Kankara dyed sample was also buffered with NaOH, by calculating the amount of SO_3 left unwashed in the synthesis mixture. About 3% of the sulphatic salt was left unaltered to allow activity of the dye used. The resulting XRD pattern for sample B, shown in Figure 4.42, gave a better crystalline material with the resulting increase in alkalinity of the mixture.

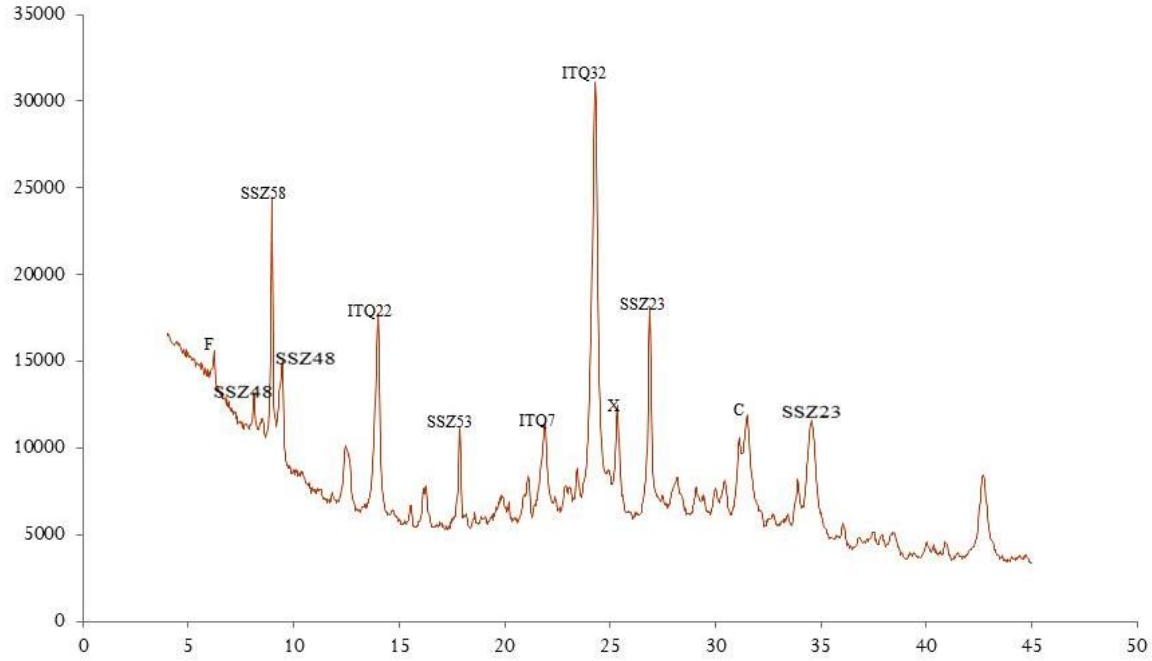


Figure 4.42 XRD patterns for reproduced zeolite from Kankara dye (Dye/Al_2O_3=0.001)

Despite the treatment, more stable zeolitic phase with higher pore-sizes was developed, namely, ITQ's and SSZ's family. This observation points to the conclusion that at higher alkalinity, synthesis of ITQ and SSZ families of zeolite are favoured.

The XRD pattern depicted in Figure 4.43 belongs to re-synthesized zeolite from Kankara kaolinite improved with 2wt% seeded commercial zeolite. It was observed that peaks attributable to zeolite Y emerges after the treatment and improvement steps taken. The most crystalline zeolite phase formed was SSZ family, and peaks earlier observed to belong to quartz and ITQ disappear and the evolvement of characteristic peaks for SSZ family.

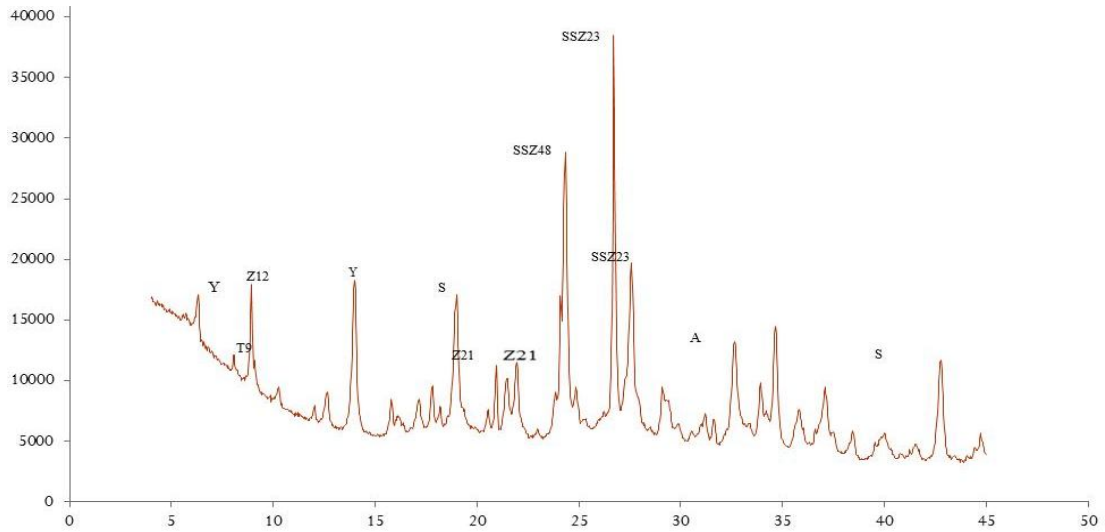


Figure 4.43: XRD patterns for reproduced zeolite from seeded Kankara gel (S03K)

Seeding under better alkaline condition was observed to favour the formation of zeolite Y from seeded Elefun sample. The intensity and number of peaks attributable to zeolite Y was observed to increase considerably with competitive phases like NaP and ITQ, as shown in Figure 4.43.

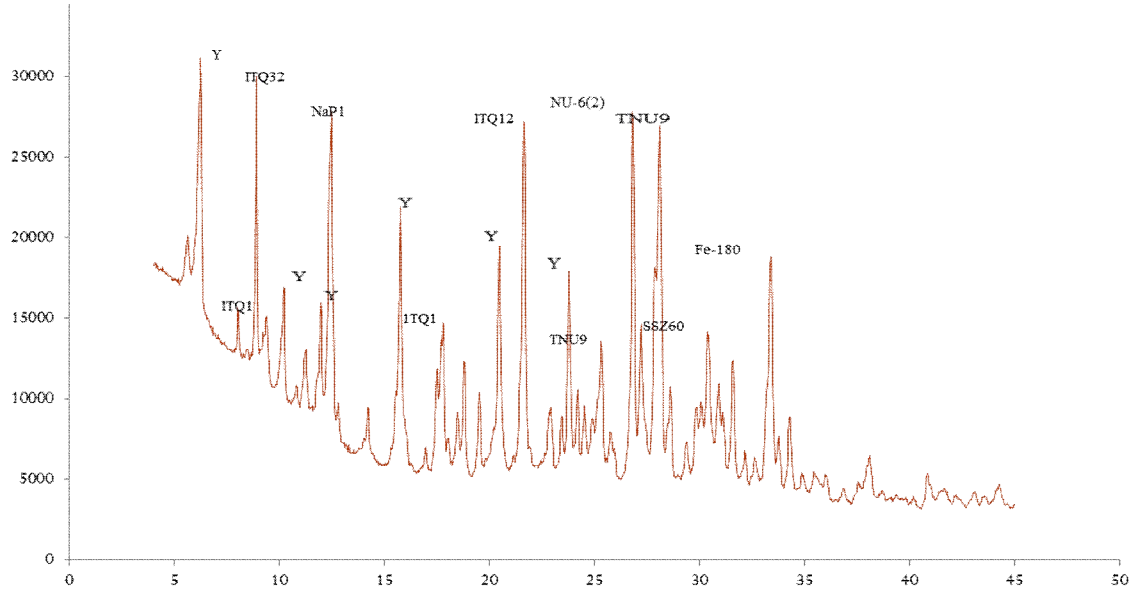


Figure 4.44: XRD patterns for reproduced zeolite from seeded Elefun gel (S01E)

This observation further confirmed our speculation that Elefun kaolin responded better to seeding treatment compared to Kankara. The XRD spectra were found to closely represent the XRD patterns for the commercial zeolite. The specific surface area for sample E was calculated to be 430.32m^2/g. It was observed to be smaller in value compared with that produced from soluble salt and very close to that of commercial zeolite Y. The reason for this could be attributed to less silica phases found in the product characterized and shown in Figure 4.43.

Aging Elefun kaolin under strong alkaline conditions led to formation of the following zeolitic materials: NaY, SSZ and ITQ's, as shown in Figure 4.44. These zeolites SSZ and ITQ formed from both Elefun and Kankara point to the conclusion that the sulphatic salts observed earlier could have served as a hindrance to the formation of this useful zeolites, on one hand. On the other hand, the 'stubborn' silica structure was almost completely destroyed and quickly recombined to form a relatively stable, high silica and enhanced pore-size and volume zeolite.

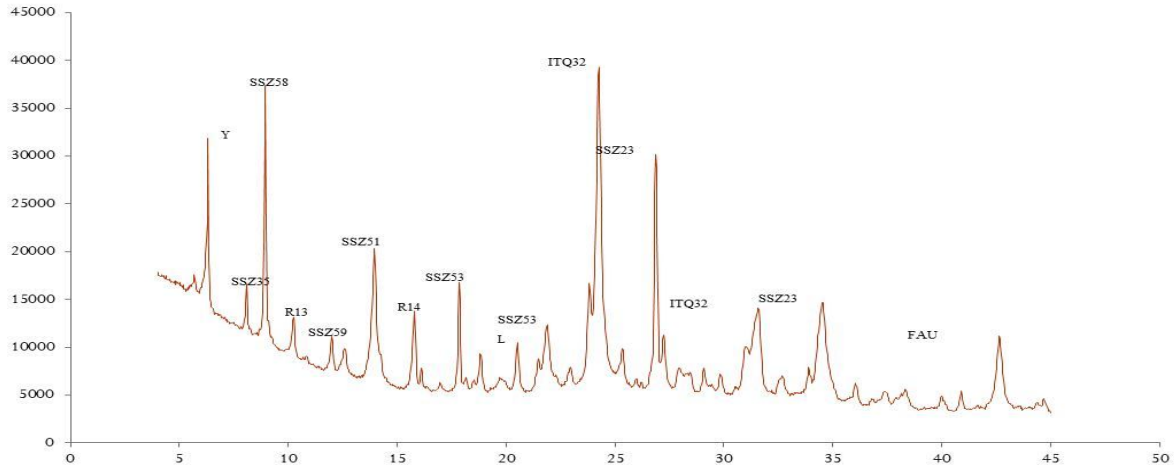


Figure 4.45: XRD patterns for reproduced zeolite from aged lefun gel (Age9E)

Additionally, ageing for a long period was found to also play significant role in formation of zeolite Y. In this case, we proposed that probably the as-synthesized zeolite Y might breakdown in the presence of the alkaline medium with the advantage of longer contact time.

CHAPTER FIVE

CONCLUSION AND RECOMMENDATION

5.1 CONCLUSION

The following conclusions were reached at the end of this project:

i. Zeolite Y was successfully synthesized from red kankara with good crystallinity in Category III, which later transformed into ZSM3 and the inherent quartz was observed to persist, despite 95days of post-synthesis aging.

ii. Zeolite Y was also produced from the improvement studies (Category V) with Elefun emerging as the best choice. Optimal ratios of Na_2O/SiO_2= 0.9, seeding/metakaolin=3wt%, dye/metakaolin=0.001, aging period is 9 days, crystallization time of 72hrs and temperature was established to be 105^0C.

iii. Other forms of zeolites namely SSZ, ITQ, ERS and ZSM family were observed to be formed along Y type zeolite.

iv. The presence of residual sulfatic salts were observed to influence zeolitization process. Its removal viz-a-viz reduction led to improved crystallinity of the desired product.

v. Zeolite Y with better crystallinity was formed from Elefun kaolinite clay, due to its relative initial purity.

vi. Nigerian kaolinite clay sourced from Kankara and Elefun serves as useable alternative sources for silica and alumina in zeolitization.

5.2 RECOMMENDATIONS

i. Better method of kaolin purification targeted at obtaining analytical grade be investigated.

ii. Need to understudy the concurrent activation of silica and alumina in kaolin

iii. Further study to be carried out on means of depolymerizing quartz, using ***multiple salt*** approach.

iv. Use of elevated temperature in gel aging to be investigated.

v. Use of Barium salt for testing the extent of sulphate salts removal after dealumination

vi. Further study to be conducted on role, chemistry and mechanism of dye/blanking in zeolite synthesis and also sourcing for alternatives

vii. Further studies on seeding using other types of zeolite as the agent, as well as seeding/aging using different mineralizer.

viii. Need to investigate means of removing already formed desire zeolite from the mother liquor

ix. Means of either producing locally pure grade soluble salts or upgrading the "locally procured chemicals".

x. ***Analytical equipment (XRD, XRF, SEM, NMR, BET, GC etc) needed***

xi. Procurement, installation and proper maintenance of an online XRD, XRF, ICP-MS, FTIR, BET, NMR, GC-MS, SEM/EDX and TEM

xii. Means of developing an absolutely pure grade kaolin from Nigerian kaolin and establishment of processing industry for the purpose

xiii. Need to understudy means of upgrading locally procured chemicals, i.e. H_2SO_4, NaOH, NaCl, dyes etc

xiv. Fund should be made available procurement of analytical grade chemicals

xv. Further work should be done on ageing at elevated temperature

xvi. Use of seawater should also be employed in this work.

xvii. Proper investigation should be carried out on removal of all forms of sulphatic salts formed during dealumination.

CHAPTER SIX

REFERENCES

Abrioux, C., B Coasne, G Maurin, F Henn, A. Boutin, A Di Lella, C Nieto-Draghi, A H Fuchs (2008). A molecular simulation study of the distribution of cation in zeolites. *Adsorption Journal of the International Adsorption Society* Volume: 14, Issue: 4-5, Pages: 743-754

Adefila, S.S., B.O. Aderemi, O.A.Ajayi and D.A.Baderin (2003), Comparative surface area determination using water adsorption method, *Nigerian Journal of Engineering,* vol.11, No1, 89-97.

Aderemi, B.O.(2000) Development of zeolite cracking catalyst from local raw materials, Ph.D Thesis, ABU, Zaria

Ahmed, K.S. and P.B. Onaji. (1986). The Effects of Beneficiation on the Properties of Some Nigerian Clay. *Journal of Nigerian Society of Chemical Engineering*. 6(2):119-129.

Ajayi, O.A., A.A.Atta, Aderemi, B.O and S.S.Adefila (2010). Novel method of metakaolin dealumination- preliminary investigation. *Journal of Applied Science Research*, 6(10), 1539-1546

Ajayi, O. A., Atta, A.Y., Aderemi, B.O., Ahmed, A.S., Ityokumbul, M.T., and S.S. Adefila (2011). Synthesis of Zeolite ZSM3 from Faujasite: Effects of Post-Synthesis Ageing and Insitu Seeding. A paper presented at the 1st International conference on Clays and Minerals in Africa and 2nd International (1st ICCCM) Conference on Geophagia in BoemfoteinSouth Africa (2nd ICGSA).

Akolekar, D., A. Chaffee, and R.F. Howe The transformation of kaolin to low-silica X zeolite. *Zeolites*, Volume 19, Issues 5–6, November–December 1997, Pages 359–365.

Alkan, M., Hopa, C., Yilmaz, Z., Guler, H (2005). The effect of alkali concentration and solid/liquid ratio on the hydrothermal synthesis of zeolite NaA from natural kaolinite. *Microporous Mesoporous Materials*, 86, 176–184.

Ambikadevi, V. R. and Lalithambika, M. (2000). Effect of organic acids on ferric iron removal from iron-stained kaolinite. *Applied Clay Sciences*, 16, 133–145.

Ambikadevi, V.R., Gopalakrishna, S.J., (1997). *Iron stain removal by bleaching and leaching techniques*. Proceeding 10th Kerala Science Congress, 445–448.

Andersson, K. R., Dent, G., Lesley, S., Smith, D. N. (1982). Polymerization and colloid formation in silicate solutions. *ACS Symposium series*, *194* (Soluble Silic.), 115-131.

Andersson, K.R., Dent, G., Lesley, S., Smith, D.N (1982). Polymerization and colloid formation in silicate solutions. ACS Symposium Series, 194 (Soluble Silicate), 115-131

Angell, C. L., Flank, W. H.(1970). Mechanism of zeolite A synthesis. *ACS Symposium series*,*40* (Mol. Sieves-2, Int. Conf., 4th), 194-206.

Anthony, G. D. and Garn, P. D (1974). Kinetics of kaolinite dehydroxylation. *Journal American Ceramic Society*, 57, N3, 132–135.

Arafat, A., Jansen, J. C., Ebaid A.R., van Bekkum, H. (1993). Microwave Preparation of Zeolite Y and ZSM 5. *Zeolites*, 13 (3), 162-165.

Argauer, R. J. and Landold, G. R. (1972). Crystalline Zeolite ZSM-5 and Method of Preparing the same. US 3,702,886. USA

Asmatulu, R., (2002). Removal of discoloring contaminants of east Georgia kaolin clay and its dewatering. Turk. J. *Engineering Environmental Sciences*. 26, 447–453.

Bailey, S.W (1980a) Structures of layer silicates. In: Brindley GW & Brown G ed. Crystal structures of clay minerals and their X-ray identification. London, Mineralogical Society, pp 1–123 (Monograph No. 5).

Barrer, R. M. and Denney, P., (1961). Hydrothermal Chemistry of the Silicates, Part IX Nitrogenous Aluminosilicates, Journal of *Chemical Society,* 971–1000

Barrer, R. M. (1982). Hydrothermal Chemistry of Zeolites. New York: Academic Press.

Barrer, R.M and Cole (1973) adapted from Molecular sieves W. M. Meier, J. B. Uytterhoeven, Eidgenössische Technische Hochschule Zürich - 1973 - 634

Barrer, R.M and Denny, P.J. (1961). *Journal of Chemical Society*, 971-982

Barrer, R.M., (1978). Zeolites and Clay Minernals as Sorbents and Molecular sieves, Academic Press, London.

Bartelmehs, KL, Gibbs GV, Boisen MB Jr (1989) Bond-length and bonded-radii variations in sulfide molecules and crystals containing main-group elements. *American Mineral* 74:620-626

Basaldella, E. I., Bonetto, R., Tara, J. C. (1993). Synthesis of NaY Zeolite on Preformed Kaolinite Spheres. Evolution of Zeolite Content and Textural Properties with the Reaction Time. *Industrial Engineering Chemical Research*, 32 (4), 751-752.

Basaldella, E.I, Kikot A, Tara J.C. (1995a). Effect of pellet pore size and synthesis conditions in the *in situ* synthesis of LSX zeolite. *Industrial Engineering Chemical Research* .34:2990-2996.

Basaldella, E.I, Tara JC. (1995b). Synthesis of LSX zeolite in the Na/K system. Influence of the Na/K ratio. *Zeolites* 11:243-248.

Belver, C., M.A.B. Munoz and M.A. Vicente (2002). Chemical Activation of a Kaolinite under Acid and Alkaline Conditions. *Chemical Material*. 14: 2033-2043.

Bhatia, S. (1990). *Zeolite Catalysis Principles and Applications*. Fla.: CRC Press Boca Raton.

Bibby, D.M and M.P. Dale (1985). Synthesis of silica-sodalite from non-aqueous systems. *Nature (London)*, 317, 157-158

Bodart, P., Nagy, J. B., Gabelica, Z., Derouane, E. G. (1986). Factors Governing the Synthesis of Zeolites From Silicoaluminate Hydrogels: A Comparative Study of the Crystallization Mechanisms of Zeolites Y, Mordenite, and ZSM-5. *Journal of Chim.Phys.Biol*.,83 (11-12),777-790.

Borggaard, O.K. (1979). Selective extraction of amorphous iron oxides by EDTA from a Danish sandy loam. *Journal of Soil Science* 30, 727– 734.

Breck, D. W. (1964). Crystalline molecular sieves. *Journal of Chemical Education*, 41 (12), 678-689.

Breck, D.W. (1974). Zeolite Molecular Sieves, John Wiley and Sons, New York.

Breck, W. D., Flanigen, E. M. (1967). Synthesis and Properties of Union Carbide Zeolites L, X, and Y. *Molecular Sieves Paper Conference*, 47-61.

Brent, M., Lok, Celeste A. Messina, R. Lyle Patton, Richard T. Gajek, Thomas R. Cannan, Edith M. Flanigen (1984**)**. Silicoaluminophosphate molecular sieves: another new class of microporous crystalline inorganic solids. *Journal of American Chemical Society*, 106 (20), pp 6092–6093

Brindley, G.W. Nakahira, M. (1959b), The kaolinite-mullite reaction series: II, Metakaolin. *Journal of American Ceramic Society*, 42, N7, 314–318.

Brindley, G.W. Nakahira, M. (1957), Kinetics of dehydroxylation of kaolinite and halloysite. *Journal of American Ceramic Society*, 40, N10, 346–350.

Brindley, G.W. Nakahira, M. (1959a): The kaolinite-mullite reaction series: I, A survey of outstanding problems. *Journal of American Ceramic Society*, 42, N7, 311–314.

Bronic, J., Subotic, B. (1995). Role of Homogeneous Nucleation in the Formation of Primary Zeolite Particles. *Microporous Mater.*, *4* (2-3), 239-242.

Bronic, J., Subotic, B., Skreblin, M. (1999). Investigation of the influence of seeding on thecrystallization of zeolite A in the membrane-type reactor. *Microporous Mesoporous Mater.*, *28* (1), 73-82.

Brunner, G. O. (1992). A proposal for a mechanism of nucleation in zeolite synthesis. *Zeolites*, 12 (4), 428-430.

Burkett, S. L., Davis, M. E. (1995a). Mechanism of Structure Direction in the Synthesis of Pure-Silica Zeolites. 2. Hydrophobic Hydration and Structural Specificity. *Chemistry of Materials, 7* (8), 1453-1463.

Burkett, S. L., Davis, M. E. (1995b). Mechanisms of Structure Direction in the Synthesis of Pure-Silica Zeolites. 1. Synthesis of TPA/Si-ZSM-5. *Chemistry of Materials*, *7* (5), 920-928.

Caballero, I., Colina, F.G., Costa, J. (2007). Synthesis of X-type zeolite from dealuminated kaolin by reaction with sulfuric acid at high temperature. *Industrial and Engineering Chemistry Research* 46, 1029–1038.

Carroll, D and Starkey, H. C. (197l). Reactivity of clay minerals with acids and alkalies. *Clays and Clay Minerals,* Vol. 19, 321-333

Chandrasekhar, S. (1996). Influence of metakaolinization temperature on the formation of zeolite 4A from kaolin. *Clay Minerals*. 31, 253–261.

Chandrasekhar, S., Pramada, P.N. (1999). Investigation on the synthesis of Zeolite NaX from kerala kaolin. *Journal of Porous Materials*, 6, 283– 297.

Chandrasekhar, S., Pramada, P.N.(2001). Sintering behaviour of ammonium exchanged low silica zeolites synthesised by two different routes. *Ceramics International* 27, 351–361.

Chandrasekhar, S. and P.N. Pramada (2004). Kaolin-Based Zeolite Y, a Precursor for Cordierite Ceramics, *Applied Clay Science*, 27(3): 187-198.

Chang, C. D., and Bell, A. T. (1991). Studies on the mechanism of ZSM-5 formation. *Catalysis Letters*, *8* (5-6), 305-316.

Chang, H.L., Shih, W.H. (1998). A General Method for the Conversion of Fly Ash into Zeolites as Ion Exchangers for Cesium. *Industrial Engineering Chemical Research*, 37 (1), 71-78.

Cheetham, A. K., Ferey G. and Loiseau, T (1999). Open-Framework Inorganic Materials, *Angewerson Chemical International* Ed. 38, 3268-3292.

Chen, N. Y., Miale, J. N., and Reagan, N. Y. (1978). Preparation of zeolites.(US Pat. No 4,112,056).

Cicel, B. Novák, I. Horváth, I. (1981). Mineralogy and crystallochemistry of clays. *SAV, Bratislava*.

Cocks, P.A. and Pope, C.G (1995). Salt effects on the synthesis of some aluminous zeolites. *Zeolites*, Volume 15, Issue 8, 701-707

Colina, F.G., Esplugas, S. and J. Costa (2002). High-temperature Reaction of Kaolin with Sulfuric Acid. *Industrial and Engineering Chemistry Research*, 41(17): 4168-4173.

Conley, R. F. and Lloyd, M. K.(1970). Improvement of iron leaching in clays: optimizing processing parameters in sodium dithionate reduction. *Industrial Engineering Chemical Process Design Development*, 9, 595–601.

Corma, A., Davis, M. E. (2004). Issues in the synthesis of crystalline molecular sieves: towards the crystallization of low framework-density structures. *Chemical Physics Chemistry*, 5 (3), 304-313.

Csicseri , S.M (1984). Shape-selective catalysis in zeolites. *Zeolites*. V.4. №3. P.202-213.

Culfaz, A., and Sand, L. B. (1973). Mechanism of nucleation and crystallization of zeolites from gels. *Advances Chemical Series*., 121 (Mol. Sieves, Int. Conf., 3rd), 140-151.

Cundy, C. S. (1998). Microwave Techniques in the Synthesis and Modification of Zeolite Catalysts. *A Review of Collection Czech. Chemical Community*. 63 (11), 1699-1723.

Cundy, C. S., Cox, P. A. (2003). The Hydrothermal Synthesis of Zeolites: History and Development from the Earliest Days to the Present Time. Chem.Rev. (Washington, DC,U.S.), 103 (3), 663-701.

Cundy, C. S., Cox, P. A. (2005). The hydrothermal synthesis of zeolites: Precursors, intermediates and reaction mechanism. *Microporous Mesoporous Material*., 82 (1-2), 1-78.

Cundy, C. S., Henty, M. S., Plaisted, R. J. (1995a). Zeolite Synthesis Using a Semicontinuous Reactor. Part 1. Controlled Nucleation and Growth of ZSM-5 Crystals Having Well-Defined Morphologies. *Zeolites*, *15* (4), 353-372.

Cundy, C. S., Henty, M. S., Plaisted, R. J. (1995b). Zeolites Synthesis Using a Semicontinuous Reactor. 2. Synthesis at High Nucleation Rates. *Zeolites*, *15* (2), 400-407.

Cundy, C. S., Lowe, B. M., Sinclair, D. M. (1990). Direct measurements of the crystal growth rate and nucleation behavior of silicalite, a zeolitic silica polymorph." *Journal of Crystalline Growth*, *100* (1-2), 189-202.

Davis M.E and Lobo R.F (1992). Zeolite and molecular sieve synthesis. *Chemistry of Materials* 4(4), 756-768.

de Mesquita, L. M. S., Rodrigues, T. and Gomes, S. S. (1996). Bleaching of Brazilian kaolins using organic acids and fermented medium. *Mineral Engineering*, 9, 965–971.

Deer, W. A., R. A. Howie, J. Zussman, (1997). *Rock-forming minerals*, Volume 4, Part 1

Degnan Jr. T.F. (2007). Recent progress in the development of zeolitic catalysts for the petroleum refining and petrochemical manufacturing industries. *Studies in Surface Science and Catalysis*, *Volume 170, Part 1*, *54-65*

Delhez, R., Th. H. Keijser and E. J. Mittemeijer (1982). Determination of crystallite size and lattice distortions through X-ray diffraction line profile analysis . *Fresenius' Journal of Analytical Chemistry*. Volume 312, Number 1 1-16, DOI: 10.1007/BF00482725

Den Ouden, C. J. J., Thompson, R. W (1991). Analysis of the Formation of Monodisperse Populations by Homogeneous Nucleation. *Journal of Colloid Interface Science*, *143* (1), 77-84.

Derouane, E. G., Detremmerie, S., Gabelica, Z., Blom, N. (1981). Synthesis and Characterization of ZSM-5 Type Zeolites. I. Physicochemical Properties of Precursors and Intermediates. *Applied. Catalysis*,*1* (3-4), 201-224.

Donahoe, R. J. and Liou, J. G. (1985). An experimental study on the process of zeolite formation: *Geochim. Cosmochim. Acta* 49, 2349-2360.

Dove, M. T.; Gambhir, M.; Hammonds, K. D.; Heine, V.; Pryde, A. K. A (1996). *Phase Transitions* 58, 121.

Dove, M. T.; Hammonds, K. D.; Heine, V.; Withers, R. L.; Xiao, Y.; Kirkpatrick, R. *Journal Physical Chemistry Minerals* (1995). 23, 55.

Dutta, P.K., J. Bronic, (1994). Mechanism of zeolite formation : seed gel interaction. *Zeolites*, 14, 250-255

Dwyer, F. G., Chu, P. (1979). "ZSM-4 crystallization via faujasite metamorphosis." *Journal of Catalysis.*, *59* (2), 263-271.

Dyer, A (1988). An Introduction to Zeolite Molecular Sieves John Wiley & Sons, Inc.

Dyer, A. and J. K. Abou-Jamous. (1994). Zeolites For Nuclear Waste Treatment: Co, Ni, Zn Uptake Into Synthetic Faujasites X & Y. I. Ph Effects, Calcination, Elution And Encapsulation Studies. *Journal of Radio analytical and Nuclear Chemistry, Articles*, Vol. 183, No. 2 225-233

Dypayan, J. (2007). Clinoptilolite – a promising pozzolan in concrete, http://www.cmcconcrete.com/CMC%20Seminars/2007%20ICMA%20Zeolite.pdf

Ekosse, G (2005). *X–Ray Powder Diffraction Patterns of Clay Minerals in Botswana*, Gaborone, Botswana, ISBN 99912-949-9-6, p.78.

Ekosse, Georges-Ivo E (*2010)*. Kaolin deposits and occurrences in Africa: Geology, mineralogy and utilization. *Applied Clay Science*, *Volume 50, Issue 2*, *212-236*

Elimbi, A., H.K. Tchakoute, D. Njopwouo (2011). Effects of calcination temperature of kaolinite clays on the properties of geopolymer cements. *Construction and Building Materials*, Volume 25, Issue 6, 2805-2812

Emofuriefa, W.O., A.A. Kayode and S.A. Coker,(1992). Mineralogy, Geochemistry and Economic Evaluation of the Kaolin Deposits near Ubulu-Uku, Awo-omama and Buan in Southern Nigeria, *Journal of Mining and Geology*, 28(2): 211-220.

Enjugu B. (2006) Personal Communication at Ahmadu Bello University, Zaria on 25th March, 2003

Erdem, A., Sand, L. B. (1979). Crystallization and Metastable Phase Transformations of Zeolite ZSM-5 in the $(TPA)_2O$-Sodium Oxide-Potassium Oxide-Aluminum Oxide-Silicon Dioxide-Water System. *Journal of Catalysis, 60* (2), 241-256.

Fahlke, B., Starke, P., Seefeld, V., Wieker, W., Wendlandt, K. P. (1987). On the intermediates in zeolite Y synthesis. *Zeolites*, 7 (3), 209-213.

Farhount, N., 1989. Beneficiation of kaolins of islands of Milos. PhD thesis, National Technical University, Athens.

Feng, P.Y., Bu, X.H. and Stucky, G.D. (1997). Hydrothermal syntheses and structural characterization of zeolite analogue compounds based on cobalt phosphate. *Nature*, 388, 735-741

Fernandez-Jimenez, A., Vallepu, R., Terai, T., Palomo, A. and Ikeda, K. (2006), Synthesis and Thermal Behavior of Different Aluminosilicate Gels. *Chemical Information*, Volume 37, Issue 42, doi: 10.1002/chin.200642211

Flanigen, E. M. (2001). Zeolites and molecular sieves: An historical perspective. *Studies in Surface Science Cataysis*, *137* (Introduction to Zeolite Science and Practice (2nd Edition)), 11-35.

Flanigen, E.M, Breck D.W, (1960).Crystalline Zeolites V-Growth of Zeolite Crystals from Gels, 137th Meet, ACS, Division of Inorganic Chemistry. Cleveland, OH, , Abstracts, p.33-M.

Flanigen, E.M., H.A. Szymanski and H. Khatami (1971). Infrared Structural Studies of Zeolite Frameworks, *Advances in Chemistry*, 101: 201-229.

Freund, E.F. (1976). Mechanism of the crystallization of zeolite X. *Journal of Crystal Growth*, Volume 34, Issue 1, 11-23

Freund, F. (1967). Kaolinite-metakaolinite, a model of a solid with extremely high lattice defect concentration. Ber. Deutsche Keram. Ges.,44,N4, 5–13.

Garn, P. D. and Anthony, G. D (1969). The questionable kinetics of kaolin dehydroxylation. *Journal of Thermal Analysis*, 1, N1, 29–33.

Ginter, D. M., Bell, A. T., Radke, C. J. (1992a). The Effects of Gel Aging on the Synthesis of NaY Zeolite from Colloidal Silica. *Zeolites*, *12* (6), 742-749.

Ginter, D. M., Went, G. T., Bell, A. T., Radke, C. J (1992b). A physicochemical study of the aging of colloidal silica gels used in zeolite Y synthesis. *Zeolites*, *12* (6), 733-741.

Ginter, D.M., Bell, A.T and C.T. Radke (1992c). Synthesis of Microporous Materials, vol. I, Molecular Sieves, ed. M.L. Occelli and H.E Robson, van Nostrand Reinhold, New York, 6.

Goldsmith, J.R (1953).The science of crystallization: Macroscopic phenomena and defect generation. *Journal of Geology,* 61:349 11.

Golemme, G., Crea, F., Nastro, A., Nagy, J. B., Subotic, B., Aiello, R.(1991). Kinetic Study on the Nucleation of (Na,TPA)ZSM-5 Zeolite. *Zeolites*, *11* (8), 776-783.

Gonthier, S., Gora, L., Guray, I., Thompson, R. W. (1993). Kinetic Study on the Nucleation of (Na,TPA)ZSM-5 Zeolite." *Zeolites*, *13* (6), 414-418.

Granizo, M. L., Blanco-Varela, M. T. and Palomo, A. (2000). "Influence of the starting kaolin on alkali-activated materials based on metakaolin. Study of the reaction parameters by isothermal conduction calorimetry." *Journal of Materials Science* 35(24): 6309-6315.

Grim, R.E (1968). Clay mineralogy, 2nd ed. New York, McGraw-Hill, p596.

Grimshaw, R.W. (1971). Physics and Chemistry of Clay, 4th ed. Ernest Benn, London, ISBN: 0510-47701-7.

Groudev, S. N. (1999). Biobeneficiation of mineral raw materials. *Mineral Metallurgical Process*, 16, 19–28.

Guggenheim, S., Koval PV, Müller G, Neiva AMR, Radoslovich EW, Robert J-L, Sassi FP, Takeda H, Weiss Z, & Wones DR (1998). Nomenclature of micas. *Clays and Clay Minerals*, 46: 586–595.

Guggenheim, S., Martin, R. T. (1995). Definition of clay and clay mineral: Journal report of the AIPEA nomenclature and CMS nomenclature committees. *Clays and Clay Minerals* 43 (2): 255–256, doi:10.1346/CCMN.1995.0430213

Hammond, C.; *"Introduction to Crystallography"*, Oxford University Press, Revised Edition (1992)

Hanykýř, V. and Kutzendoerfer, J. (2000). Technologie keramiky. Silis Praha a Vega Hradec Králové.

Haq, A., Iqbal,Y., Riaz Khan, M. (2009). Phase and Microstructural Characterization of Kaolin Clays from North Western Pakistan. *Journal of Pakistani Materials Society*. 3 (2)

Hay, R. L.; Sheppard, R. A. (2001). Occurrence of zeolites in sedimentary rocks: an overview. In: Bish; D.L., Ming, D. W. (eds), Natural zeolites: occurrence, properties, applications. *Reviews in Mineralogy and Geochemistry, volume 45. Mineralogical Society of America*, 217-234.

Hay, R.L. (1978). Geologic occurrence of zeolites. In: Sand, L.B.; Mumpton, FA. (eds), Natural zeolites - occurrence, properties, use, Pergamon Press, 135-143.

Hill, R.J. and Gibbs, G.V. (1979). Variation in d (T-O), d(T-O-T) and TOT in silica and silicate minerals, phosphates and aluminates. *Acta Crystallographica B*, 35, 25– 30.

Horvath, E., Frost, R.L., Makó, E., Kristof, J., Cseh, T. (2003). Thermal treatment of mechanochemically activated kaolinite. *Thermochimica Acta 404*, 227–234.

Horváth, I. and Kranz, G.(1980). Thermoanalytic study of the high-temperature dehydration of kaolins with different degree of the order. *Silikáty*, 24, N2, 149–160.

Horváth, I., Sedlec (1976). kaolinite dehydroxylation kinetics. In Book of Proceeding for the 7th Conference on Clay Mineral and Petrol. Karlovy Vary, 121–127.

Hosseini, M.R., Pazouki, M., Ranjbar, M., Habibian, M (2007). Bioleaching of iron from highly contaminated Kaolin clay by *Aspergillus niger*. *Applied Clay Science* 37, 251–257.

Howell, P.H., 1961. US Patent, No. 3,114, 603.

Howell, P.H., Acara, N.A., 1964. US Patent No. 3,119, 660.

Howell, P.H., Acara, N.A., Towne Jr., M.K., 1965. Br. Pat. No. 980, 891.

http://www.europa.eu.int (2007) accessed on 27th June, 2007

Hulbert, S. F., Huff, D. H., Kinetics of alumina removal from a calcined kaolin with nitric, sulphuric and hydrochloric acids, *Clay Minerals*, 8 (337) (1970).340–345

Iijima, A. (1980) Geology of natural zeolites and zeolitic rocks. In: Rees, L.V. (ed.), Proceedings, Fifth International Conference on Zeolites, Heyden Publishers, pp.103-117. Industrial Minerals 2000: Zeolites. Industrial Minerals, December 2000: 21.

Iler, R. K. (1979). The Chemistry of Silica: Solubility, Polymerization, Colloid and Surface Properties, and Biochemistry. Wiley, New York,

Ito, T., Fraissard, J., Nagy, J. B., Dewaele, N., Nastro, E. G., and Derouane, E. G. (1989). Zeolites: Facts, Figures, Future, *Studies in Surface Science and Catalysis*, 1989, Ed. Jacobs, P. A. and Van Santen, R. A. (49), 579.

Ivanova, I. I., Aiello, R., Nagy, J. B., Crea, F., Derouane, E. G., Dumont, N., Nastro, A.,Subotic, B., Testa, F. (1984). Influence of Cations on the Physicochemical and Structural Properties of Aluminosilicate Gel Precursors. II. Multinuclear Magnetic Resonance Characterization." *Microporous Materials*, *3* (3), 245-257.

Jacobs, P. A., Derouane, E. G., Weitkamp, J. (1981). Evidence for X-Ray-Amorphous Zeolites." *J.C.S.Chemical Communication*, (12), 591-593.

Jansen, J. C., Arafat, A., Barakat, A. K., and van Bekkum, H. (1992). Microwave techniques in zeolite synthesis. Synthesis of Microporous Materials: Molecular Sieves (1), 507-521. New York, Van Nostrand Reinhold.

Kacirek, H and H. Lechert (1975). Investigations on growth of zeolite type NaY. *Journal of Physical Chemistry*, 79, 1589-1593

Kacirek, H and H. Lechert (1976). Rate of crystallization and a model for growth of zeolite type NaY. *Journal of Physical Chemistry*, 80(12), 1291-1296

Kerr, G.T (1973) Hydrogen Y, ultrastable Y, and aluminum deficient zeolites: *Advanced Chemical Series* 121, American Chemical Society, 219-229

Koegler, J. H., and Yeh, C. (2002). Nanocrystalline inorganic based zeolite and method for making same. (ABB Lummus Global Inc. (2002)-67719(20030147805), 12. 8-7-2003. USA.

Komskaja, M., Dolin, A., Yatsunova, S., (1971). Enrichment of kaolin. Otkryt. *Izobret. Prom. Obraztsy Tovar*. Znaki 48 (5), 42–56.

Kozík, T. et al. (1992). The temperature dependence of the electric conductivity of unfired porcelain mixture. Ceramics-Silikáty, 36, N2, 69–72.

Krznaric, I., Antonic, T., Subotic, B., Babic-Ivancic, V. (1998). Results of thermal and hydrothermal treatment of the aluminosilicate gels prepared at different batch concentrations." *Thermochim.Acta*, *317* (1), 73-84.

Kühl, G (2001); in "Verified Syntheses of Zeolitic Materials", Robson, H. (Ed.) 2nd Edition Elsevier Science B.V. 19–20

Lechert, H., Kacirek, H. (1991) "Investigations on the Crystallization of X-Type Zeolites." *Zeolites* , 11 (7), 720-728.

Lechert. H. (1998). The pH Value and its Importance for the Crystallization of Zeolites, (H. Robson, ed.), *Microporous Macroporous Material*, 22:519–523, Karl Petter, Lillerud

Lee, S. R., Han, Y. S., Park, M., Park, G. S., Choy, J. H (2003). Nanocrystalline Sodalite from Al_2O_3 Pillared Clay by Solid-Solid Transformation. *Chemical Material*, *15* (25), 4841-4845.

Lee, S.R., Han, Y.S., Choy, J.H., (2002). 2DY3D transformation of layered aluminosilicate upon base treatment. *Solid State Ionics 151*, 343– 346.

Lee, W. K. W. and van Deventer, J. S. J. (2003). The use of infrared spectroscopy to study geopolymerization of heterogeneous amorphous aluminosilicates. *Langmuir* 19(21): 8726-8734.

Lenarda, M., L.Storaro, Talon, A., E.Moretti and Riello, P (2007). Solid acid catalysts from clays: Preparation of mesoporous catalysts by chemical activation of metakaolin under acid conditions. *Journal of Colloid and Interface Science* 311, 537-543

Li, Q., Creaser, D., Sterte, J (2002). An Investigation of the Nucleation/Crystallization Kinetics of Nanosized Colloidal Faujasite Zeolites. *Chemical Material*, 14 (3), 1319-1324.

Li, Q., Creaser, D., Sterte, J. (1999). The nucleation period for TPA-silicalite-1 crystallization determined by a two-stage varying-temperature synthesis." *J.Microporous Mesoporous Materials 31* (1-2), 141-150.

Li, W. C., Lu, A. H., Palkovits, R., Schmidt, W., Spliethoff, B. and Schuth, F. (2005). Hierarchically structured monolithic silicalite-1 consisting of crystallized nanoparticles and its performance in the Beckmann rearrangement of cyclohexanone oxime, *Journal of American Chemical Society*, 127, 12595–12600.

Loewenstein, W (1954). The distribution of aluminum in the tetrahedra of silicates and aluminates. *American Mineralogist* 39, pp. 92-96.

Lok, B. M., Cannan, T. R., and Messina, C. A. (1984). The Role of Organic Molecules in Molecular Sieve Synthesis, *Zeolites*, 3:282–291

Lowe, B.M.(1988).Synthesis Mechanisms for Zeolites and Molecular Sieves *Studies in Surface Science and Catalysis*, *Volume 37*, *Pages 1-12*

Mackenzie, R.C ed. IV. (1970). The smectite group, A. Dioctahedral smectites. In: Differential thermal analysis. London, Academic Press, 442–452 and 504–527.

Madani, A., Aznar A, Sanza J, Serratosa J.M. (1990). Si and Al NMR study of zeolite formation from alkali-leached kaolinites. Influence of thermal activation. *Journal of Physical Chemistry* 94:760-765.

Marcus, B.K and W.E. Cormier, (1999). Going Green with Zeolites. *Chemical Engineering. Progress*, 95(6), 47-53.

Marrot, B., C. Bebon, D. Colson, J.P. Klein. (2001). Influence of the Shear Rate during the Synthesis of Zeolites. *Crystal Research and Technology*. Volume 36, Issue 3, 269–281

McNicol, B. D., Pott, G. T., Loos, R. K., Mulder, N. (1973). Spectroscopic Studies of Zeolite Synthesis. Evidence for a Solid-State Mechanism." *Advanced Chemical Series*, *121* 152-161.

Meier, Olson (1970). Zeolite molecular sieves. *Advanced Chemical Series*, 101, 155

Meise, W. and Schwochow, F.E (1973). Molecular Sieves, ACS *Advanced Chemical Series* 121, American Chemical Society, Washington, DC, , p. 26 209

Mendioroz, S., Pajares, J., Benito, I., Pesquera, C., Gonzalez, F., Blanco, C (1987). Langmuir 3, 676

Meyer, W. C.and T. F. Yen (1974). Solubility of silica in basic organic solvent System. Accessed on *web.anl.gov/PCS/.../19_2_LOS%20ANGELES_04-74_0242.pdf*

Miao, Q., Zhou, Z., Yang, J., Lu, J., Yan, S., Wang, J. (2009). Synthesis of NaA zeolite from kaolin source. *Frontiers of Chemical Engineering in China* 3 (1 SPEC. ISS.), 8–11

Milton, R.M. (1959); US Patent No. 2,882,244

Mintova, S., Olson, N. H., Bein, T. (1999a). Electron Microscopy Reveals the Nucleation Mechanism of Zeolite Y from Precursor Colloids. *Angewerson Chemical Internationel Edition*, *38* (21), 3201-3204.

Mintova, S., Olson, N. H., Senker, J., Bein, T. (2002).Mechanism of the transformation of silica precursor solutions into Si-MFI zeolite." *Angewerson Chemical Internationel Edition*, *41* (14), 2558-2561.

Mintova, S., Olson, N. H., Valtchev, V., Bein, T (1999b). Mechanism of Zeolite a Nanocrystal Growth from Colloids at Room Temperature. *Science*, 283 (5404), 958-960.

Moolenaar, R. L., Evans, J. C., McKeever, L. D. (1970). Structure of the Aluminate Ion in Solutions at High pH." *J.Phy.Chem.*, *74* (20), 3629-3636.

Morey, G.W.and F.E. Ingerson (1937). The pneumatolytic and hydrothermal alteration and synthesis of silicates. *Economic Geology, v. 32, p. 607-761,*

Morris, R.E and S.J. Weigel (1997). The synthesis of molecular sieves from non-aqueous solvents. Chemical Society Rev., 26, 309-317

Mullin, J.W. (2001). Crystallization, 4th edition (Butterworth-Heinemann,Oxford, UK).

Murat, M., Amorkrane A, Bastide JP, Montanaro L. (1992). Synthesis of zeolites from thermally activated kaolinite: Some observations on nucleation and growth. *Clay Minerals* 27: 119-130.

Murray, H. H. (1951) *The structure of kaolinite and its relation to acid treatment.* Ph.D. thesis, University of Illinois, Urbana, lllinois.

Murrell, L. L., Overbeek, R. A., Chang, Y.-F., Puil, N. V. D., and Yeh, C. Y. (1999). Method for Making Molecular Sieves and Novel Molecular Sieve Compositions. US Patent 6,004,527. USA.

Nagy, J. B., Ivanova, I., Aiello, R., Crea, F., Nastro, A., Nesta, F. (1995). Multinuclear Magnetic Resonance Characterization of Various Aluminosilicate Gels in the Presence of Tetraalkylammonium Ions. *Zeolites*, *15* (5), 421-430.

Navrotsky, A., Petrovic, I., Hu, Y., Chen, C. Y., Davis, M. E. (1995). Little energetic limitation to microporous and mesoporous materials. *Microporous Materials, 4* (1), 95-98.

Nicolle, M. A., Di Renzo, F., Fajula, F., Espiau, P., and Des Courieres, T. (1993). A microporous tetraethylammonium permutite as synthesis intermediate of the zeolite beta. *Proceeding for International Zeolite Conference*, 9th, 1, 313-320.

Noreen, H., M.W. Anderson, V. Alfredsson and Osamu Terasaki. (2000).The effect of stirring on the synthesis of intergrowths of zeolite Y polymorphs. *Physical Chemstry.* 2, 3349-3357

Nutting, P.G (1943). The action of some aqueous solutions on clays of the montmorillonite group. *U.S.Geological Survey*. Prof. paper 197F, 219-235

Occelli, M. L., H. Robson (eds.),(1989). Zeolite Synthesis, ACS Symposium Series 398, Amer. Chem. Soc., Washington DCOgura, M.,Y. Kawazu, Z., H.Takahasi and T.Okubo (2003). Aluminosilicate species in the hydrogel phase formed during the aging process for the crystallization of FAU zeolite. *Chemistry of Material* 15, 2661-2667

Otterstedt, J. E., Ghuzel, M., Sterte, J. P. (1987). Colloidal components in solutions of alkali silicates. *Journal of Colloid Interface Sciences*, 1987, *115* (1), 95-103.

Panda, A. K., B.G. Mishra, D.K. Mishra, R.K. Singh (2010). Effect of sulphuric acid treatment on the physico-chemical characteristics of kaolin clay. *Colloids and Surfaces A: Physicochemical and Engineering Aspects*.Volume 363, Issues 1–3, 98–104

Park, S.E., Kim, D. S., Chang, J. S., and Kim, J. M (2001). Continuous Process and Apparatus for Preparing Inorganic Materials Employing Microwave. US Patent 2001054549, USA.

Piccione, P. M., Yang, S., Navrotsky, A., Davis, M. E. (2002). Thermodynamics of Pure-Silica Molecular Sieve Synthesis." *Journal of Physical Chemistry B*, *106* (14), 3629-3638.

Pinheiro, P.G., J.D. Fabris, Mussel, W.N., E. Murad, Scovzelli, R.B. and V.K.Garg (2005). Beneficiation of a commercial kaolin from Mar de Espanha, Minas Gerais, Brazil: Chemistry and Mineralogy. *Journal of South American Earth Sciences* 20, 267-271

Pradhan, N., Das, B., Gahan, C.S., Kar, R.N., Sukla, L.B (2006). Beneficiation of iron ore slime using Aspergillus niger and Bacillus circulans. *Bioresoures Technology* 97, 1876–1879.

Querol, X., A.Alastuey, J.L.Fernansez-Turiel and Lopez-Soler, A (1993). Synthesis of zeolites by alkaline activation of ferrous aluminous fly ash. *Fuel* 74, 1226-1231

R. M. Barrer (1981). Hydrothermal Chemistry of Zeolites, Academic Press, London,

Rees, L.V.C., Chandrasekhar, S.(1993). Formation of zeolite from the system Na_2O–Al_2O_3–SiO_2–H_2O in alkaline medium (pH>10). *Zeolites* 13, 524–533.

Regev, O., Cohen, Y., Kehat, E., Talmon, Y. (1994). Precursors of the zeolite ZSM-5 imaged by cryo-TEM and analyzed by SAXS. *Zeolites*, *14* (5), 314-319.

Rieder, M., Cavazzini G, D'yakonov YS, Frank-Kamenetskii VA, Gottardi G, Guggenheim S, Koval PV, Müller G, Neiva AMR, Radoslovich EW, Robert J-L, Sassi FP, Takeda H, Weiss Z, & Wones DR (1998). Nomenclature of micas. *Clays and Clay Minerals*, 46: 586–595.

Robson, H. E. (1998). Verified Syntheses of Zeolitic Materials, *Microporous and Mesoporous Materials* 22, H. Robson (ed.), Elsevier, Amsterdam, p. 495

Rollman, L. D. and E. W. Valyocsik, (1983a). Zeolite Molecular Sieves. *Inorganic Syntheses*, **22**, 61-68

Rollmann, L. D. and Valyocsik, E. W (1983b). Continuous-Stream Upflow Zeolite Crystallization Apparatus. US Patent 4,374,093, USA.

Saikia, N. J., Bharali, D. J., Sengupta, P., Bordolo, I. D., Goswamee, R. L., Saikia, P. C. and Borthakur, P. C. (2003). Characterization, beneficiation and utilization of a kaolinite clay from Assam, India. *Applied Clay Science*, 24, 93–103.

Sasaki, B., Bull (1952). Chemical Research Institute, Non aqueous solutions, Tehoku Univ., 2, 113.

Scherzer, J (1989). Octane-enhancing, zeolitic FCC catalysts: scientific and technical aspects. *Catalytic Reviews in Science and Engineering*, 31(3), 215-354.

Schmidt, I., Madsen, C., Jacobsen, C. J. H (2000). Confined space synthesis. A Novel Route to Nanosized Zeolites. *Inorganic Chemistry*,*39* (11), 2279-2283.

Schmitt, K. D. Casmer, S. G. (2005). Zeolite Synthesis with Directing Agents with Approximately Perpendicular Groups. Pub. No.: WO/2005/037713 International Application No.: PCT/US2004/034459 Publication Date: 28.04.2005 International Filing Date: 15.10.2004

Schoeman, B. J., Sterte, J., Otterstedt, J. E (1994). Colloidal Zeolite Suspensions. *Zeolites*, 14 (2), 110-116.

Sei, J., Morato, F., Kra, G., Staunton, S., Quiquampoix, H., Jumas,J.C., Olivier-Fourcade, J., Womes, M., 2006. Mineralogical,crystallographic and morphological characteristics of natural kaolin from the Ivory Coast (West Africa). *African Earth Science* 46, 245–252.

Senderov, E. E. and Khitarov, N. I. (1974). Synthesis of Thermodynamically Stable Zeolites in the Na_2O-Al_2O_3-SiO_2-H_2O System. *Molecular Sieve Zeolites-I*. Chapter 13, 149–154.

Sepulveda, M.J, Vallyathan V, Attfield M.D, Piacitelli L, & Tucker JH (1983) Pneumoconiosis and lung function in a group of kaolin workers. *Am Rev Respir Dis*, 127: 231–235.

Serrano, D. P., Van Grieken, R. (2001). Heterogeneous Events in the Crystallization of Zeolites." *Journal of Material Chemistry*, 11 (10), 2391-2407.

Sheppard, R. A.; Hay, R. L. (2001): Formation of zeolites in open hydrologic system. In: Bish; D.L., Ming, D. W. (eds), Natural zeolites: occurrence, properties, applications. *Reviews in Mineralogy and Geochemistry*, volume 45. Mineralogical Society of America, pp. 261-276.

Shih, W.H., Chang, H.L (1996). Conversion of Fly Ash into Zeolites for Ion-Exchange Applications. *Materials Letter* 28, 263.

Shoumkov, S., Dimitrov, Z., Brakalov, L. (1987). High-gradient magnetic treatment of kaolin. *Interceram* 6, 26–28.

Zheng, S., Sun,S., Z. Zhang, X. Gao, Xu, X (2005). Effect of Properties of Calcined Microspheres of Kaolin on the Formation of NaY Zeolite. *Bulletin of the Catalysis Society of India*, 4, 12-17

Siddiqui, M.A. and Z.Ahmed. (2005). Mineralogy of the Swat Kaolin Deposits, Pakistan. *The Arabian Journal for Science and Engineering*, 30(2A): 195-218.

Slangen, P. M., Jansen, J. C., van Bekkum, H. (1997a). Induction Heating: A Novel Tool for Zeolite Synthesis. *Zeolites* 18 (1), 63-66.

Slangen, P.M., J.C. Jansen, H. van Bekkum. (1997b). The effect of ageing on the microwave synthesis of zeolite NaA. *Microporous Materials*, Volume 9, Issues 5-6, 259-265

Sonuparlak, B., Sarikaya, M., Aksay, I.A. (1987). Spinel phase formation during the 980°C exothermic reaction in the kaolinite-to-mullite reaction series. *Journal of American Ceramic Society* 70: 837-842.

Subotic, B., Bronic, J., and Antonic, T (1999). On the real significance of the "induction period" of zeolite crystallization, Proc. Int. Conf. Zeolites, 12th, Baltimore, July 5-10, 3, 2057-2064.

Subotic, B., Graovac, A. (1985). Kinetic analysis of autocatalytic nucleation during crystallization of zeolites. *Studies in Surface Science and Catalysis*, 24 199-206.

Subotic, B., Skrtic, D., Smit, I., Sekovanic, L. (1980). Transformation of Zeolite A into Hydroxysodalite. I. An Approach to the Mechanism of Transformation and its Experimental Evaluation." *Journal of Crystal Growth*, *50* (2), 498-508.

Subotic, B., Tonejc, A. M., Bagovic, D., Cizmek, A., Antonic, T. (1994). Electron Diffraction and Infrared Spectroscopy of Amorphous Aluminosilicate Gels. *Studies in Surface Science and Catalysis*, *84* 259-266.

Suitch, P.R. (1986). Mechanism for the dehydroxylation of kaolinite, dickite, and nacrite from room temperature to 455^0C. *Journal of American Ceramic Society* 69, 61-65.

Szostak, R. (1998). Molecular sieves: principles of synthesis and identification. 2^{nd} edition, Blackie Academics and Professional, An imprint of Chapman and Hall, London.

Terres, E. (1996). Influence of the Synthesis Parameters on Textural and Structural Properties of MCM-41 Mesoporous Material. *Microporous and Mesoporous Materials*, 431, p.111-116

Thompson, R.W. (1992a). Comments of the Autocatalytic Nucleation of (Na, TPA)-ZSM 5. *Zeolites*, *12* (7), 837-840.

Thompson, R.W In: Catlow CRA (1992b). Modeling of structure and reactivity in zeolites, Academic Press, San Diego, 231-255.

Thompson, R. W.(1992c). Population balance analysis of zeolite crystallization. *Modell. Struct. React. Zeolites*, 231-255.

Thompson, R. W., Dyer, A. (1985a). A modified population balance model for hydrothermal molecular sieve zeolite synthesis. *Zeolites*, *5* (5), 292-301.

Thompson, R. W., Dyer, A. (1985b). Mathematical analyses of zeolite crystallization. *Zeolites*, *5* (4), 202-210.

Thompson, R. W., Dyer, A. "(1985c). Nucleation of zeolite Na-A crystals in hydrothermal systems. *Zeolites*, *5* (5), 302-308.

Toussaint F., Fripiat J.J. & Gastuche M.C. (1963). Dehydroxylation of Kaolinite. I. Kinetics. *Journal of Physical Chemistry* 67, 26-30.

Tsuruta, Y., Satoh, T., Yoshida, T., Okumura, O., Ueda, S. (1986).Studies on the initial product in the synthesis of zeolite A from concentrated solutions. *Studies in Surface Science and Catalysis, 28* (New Dev. Zeolite Sci. Technol.), 1001-1007.

Ueda, S., Murata, H., Koizumi, M., Nishimura, H. (1980). Crystallization of mordenite from Aqueous solutions. *American Mineralogy*, *65* (9-10), 1011-1018

Valyocsik, E. W. (1983). Apparatus for a continuous down-flow zeolite production. US Patent 4,368,174. USA.

Van Lier, J.A. quoted by Iler, R.K. (1979). The Chemistry of Silica, John Wiley & Sons, New York, 75

Van Santen, R. A., Ooms, G., Den Ouden, C. J. J., Van Beest, B. W., Post, M. F. M. (1989). Computational studies of zeolite framework stability. *ACS Symposium Series, 398* (Zeolite Synth.), 617-633.

Varga, G (2007). The structure of kaolinite and metakaolinite, Épít□anyag 59. évf.. 1. szám. Accessed on http://www.szte.mtesz.hu/06journal/2007_1/pdf/epa_1_2.pdf.

Veglio, F. and Toro, L. (1994). Process development of kaolin bleaching using carbohydrates in acid media. *International Journal on Mineral Process* 41, 239–255.

Veglio, F., Passariello, B., Toro, L. and Marabini, A. M. (1996), Development of a bleaching process for a kaolin of industrial interest by oxalic, ascorbic and sulphuric acids: Preliminary study using statistical methods of experimental design. *Industrial Engineering Chemistry Research*, 35, 1680–1687.

Venuto, P.B. (1994). *Microporous Materials*, 2, 297.

Verduijn, J. P. (1993). Manufacture of uniform MFI-type zeolites, and the adsorbents and catalysts obtained. (Exxon Chemical Patents, Inc. 92-EP2330 (9308124), 32 4-29-1993 WO 10-8-1992

Vučinić, D., Miljanović I., Rosić A., Lazić P. (2003). Effect of Na_2O/SiO_2 molar ratio on the crystal type of zeolite synthesized from coal fly ash. *Journal of Serbian Chemical Society*,68 (6) 471-478.

Walton, R. I., O'Hare, D. (2001). An X-ray absorption fine structure study of amorphous precursors of a gallium silicate zeolite. *Journal of Physical Chemistry of Solids*, *62* (8), 1469-1479

Warzywoda, J., Edelman, R. D., Thompson, R. W. (1989). Thoughts on the induction time in Zeolite crystallization. *Zeolites*, *9* (3), 187-192

Wells, M. A., Gilkes, R. J. and Fitzpatrick, R. W. (2001). Properties and acid dissolution of metal-substituted hematites. *Clays and Clay Minerals,* 49, 60–72.

Whittam, T. V. (1977) Preparation of synthetic zeolite molecular sieves. US Patent 4018870

Wilson, B. M. Lok, C. A. Messina, T. R. Cannan, and E. M. Flanigen (1982). *Journal of American Chemical Society* 104, 1146

Wilson, S.T., B.M.Lok, and E.M. Flanigen (1982), U.S. Patent 4, 310,440

Worrall, W.E. (1986). Clays and ceramic raw materials, Elsevier Applied Science Publishers, 2nd edition. New York.

www.chemicalland21.com (2007) accessed on 10th August, 2007

www.cnx.org accessed on 13th April, 2009

www.iza-structure.org/databases accessed on 14th May, 2007

www.rmrdc.com accessed on 17th May, 2003

Xu, R., Pang, W., Yu, J., Huo, Q and Chen, J (2007). Chemistry of zeolites and related porous materials: synthesis and structure. Jonh Wiley & Sons (Asia) Pte Ltd.

Xu, X.C., W.S. Yang, J. Liu, L.W. Lin (2000), Synthesis of a high-permeance NaA zeolite membrane by microwave heating. *Advanced Materials* 12, 195.

Yagi, S and Kunni, D. (1955). 5th Symposium (International) on combustion, Chemical Engineering (Japan) 19, 500 231. Reinhold, New York

Yagi, S and Kunni, D. (1961). Chemical Engineering Science 16, 364, 372, 380

Yang, H., Walton, R. I., Antonijevic, Sasa, Wimperis, Stephen, Hannon, Alex C. (2004). Local Order of Amorphous Zeolite Precursors from 29Si{1H} CPMAS and 27Al and 23Na MQMAS NMR and Evidence for the Nature of Medium-Range Order from Neutron Diffraction." *Journal of Physical Chemistry B*, *108* (24), 8208-8217.

Yoshida, A. (1995). The problems of identifications of phillipsite and gismondine: Crystal structures and X-ray diffraction patterns. *Clay Science* 9, 275–283.

Zhao, D., Kevan, L., Szostak, R. (1997). Hydrothermal synthesis of alkali cation heulandite aluminosilicate molecular sieves. *Zeolites*, Volume 19, Issues 5-6, 366-369

Zhdanov, (1971). Molecular Sieve Zeolites', American Chemical Society Washington, pp. 20-43.

Zhdanov, S. P. (1968) in 'Molecular Sieves', Society Chemical Industry, London, p.70

Zhdanov, S. P. and Samulevich, N. N. (1980) *"Nucleation and crystal growth of zeolites in crystallizing aluminosilicate gels",* Proceeding International Conference on Zeolites, 5th 75-84.

Živanovič, B. Janovič, O. (1978). Dehydroxylation of kaolinite. *Hem.Ind*. 32, N8, 512–516.

APPENDIX A

DEALUMINATION CALCULATION (KANKARA WHITE KAOLIN (CAT. I))

Basis 50g Metakaolin

Moles of silica content = $\frac{49.10}{60} = 0.8183mol$

molar mass of Al_2O_3 = 102g/mol

Number of moles of Al_2O_3 in 50g Metakaolin = $\frac{42g}{102g/mol} = 0.4118mol$

$\frac{0.8183}{0.4118} = 1.987$

The required Si/Al ratio for the desired is 10

Therefore,

$$\frac{number\ of\ moles\ of\ SiO_2}{number\ of\ moles\ of\ Al_2O_3} = 10$$

Number of moles of SiO_2 = (mass/molar mass) of SiO_2 in 50g Metakaolin $= \frac{0.8183}{x} = 10$

Number of moles of Al_2O_3 = 0.8183 / 10 =0.08183mol

The expected weight of Al_2O_3 to be left after dealumination is 0.08183 × 102 = 8.34666g

The weight of Al_2O_3 to be leached = 42 – 8.3467 = 33.6533g

The Dealumination reaction follows the equation

$Al_2O_3 + 3H_2SO_4 \longrightarrow Al_2(SO_4)_3 + 3H_2O$

From the equation of reaction, 102g aluminum oxide will require

$\left(\frac{3 \times 98 \times 100}{96}\right)$ of 96% H_2SO_4 = 306.25g of 96%H_2SO_4

So, 33.6533g Al_2O_3 will require $\frac{306.25 \times 33.6533}{102}$ = 101.042g of 96% H_2SO_4

For H_2SO_4 100% purity ≈ 98g of pure H_2SO_4

For 96% purity ≈ $\frac{100 \times 98}{102}$ = 102g of 96% pure H_2SO_4

From literature:

Density of 60% H_2SO_4 at 25°C = 1.494g/cm^3

Density of 96% H_2SO_4 at 25°C = 1.8305g/cm^3

Volume of acid required = (mass/density) of acid = 101.042/1.8305 = 55.20cm^3

Dilution Calculation

Taking component balance to obtain equivalent volume of 60% H_2SO_4 required.

$V_{60} \times \rho_{60} \times 60 = V_{96} \times \rho_{96} \times 96$

$V_{60} = \frac{V_{96} \times \rho_{96} \times 96}{60 \times \rho_{60}}$

$$V_{60} = \frac{55.20 \times 1.8305 \times 96}{60 \times 1.494} = 108.213cm^3$$

$V_{60} = 3 \times 108.213 = 324.639\ cm^3 \cong 323cm^3$

From dilution formula

$V_{60} \times \rho_{60} = V_{96} \times \rho_{96} + V_w \times \rho_w$

Where

V_w = volume of water

ρ_w= density of water = $1g/cm^3$

$V_w = \frac{V_{60}\rho_{60} - V_{96}\rho_{96}}{\rho_W}$

The volume of 96% H_2SO_4 (V_{96}) required is $\frac{324.639 \times 1.494 \times 60}{1.8305 \times 96} = 165.6cm^3 \cong 166\ cm^3$

Volume of water required is obtained as $V_{60} \times \rho_{60} = V_{96} \times \rho_{96} + V_w \times \rho_w$

V_w= (1.494×323.639) /(1.8305×166)/1= 483.52 / 303.863= $179.657cm^3 \cong 180\ cm^3$

DEALUMINATION CALCULATION (KANKARA RED KAOLIN (CAT IIa))

Basis 50g Metakaolin

Moles of silica content = $\frac{49.9}{60} = 0.8317mol$

molar mass of Al_2O_3 = 102g/mol

Number of moles of Al_2O_3 in 50g Metakaolin $= \frac{42g}{102g/mol} - 0.4118mol$

$$\frac{0.8317}{0.4118} = 2.02$$

The required Si/Al for our desired zeolite is 10

Therefore,

$$\frac{number\ of\ moles\ of\ SiO_2}{number\ of\ moles\ of\ Al_2O_3} = 10$$

Number of moles of SiO_2 = (mass/molar mass) of SiO_2 in 50g Metakaolin $= \frac{0.8317}{x} = 10$

Number of moles of Al_2O_3 = 0.8317 / 10 =0.08317mols

The expected weight of Al_2O_3 to be left after dealumination is 0.08317 × 102 = 8.4833g

The weight of Al_2O_3 to be leached = 42 – 8.4833 = 33.5167g

Dealumination equation

$Al_2O_3 + 3H_2SO_4 \longrightarrow Al_2(SO_4)_3 + 3H_2O$

From the equation of reaction, 102g aluminum oxide will require

$\left(\frac{3 \times 98 \times 100}{96}\right)$ of 96% H_2SO_4 = 306.25g of 96%H_2SO_4

So 33.5167g Al_2O_3 will require $\frac{306.25 \times 33.5167}{102} =$ 100.632g of 96% H_2SO_4

For H_2SO_4 100% purity ≈ 98g of pure H_2SO_4

For 96% purity ≈ $\frac{100 \times 98}{102}$ = 102g of 96% pure H_2SO_4

From literature:

Density of 60% H_2SO_4 at 25°C = 1.494g/cm^3

Density of 96% H_2SO_4 at 25°C = 1.8305g/cm^3

Volume of acid required = (mass/density) of acid = 100.632/1.8305 = 54.98cm^3

Dilution Calculation

Taking component balance to obtain equivalent volume of 60% H_2SO_4 required.

$V_{60} \times \rho_{60} \times 60 = V_{96} \times \rho_{96} \times 96$

$$V_{60} = \frac{V_{96} \times \rho_{96} \times 96}{60 \times \rho_{60}}$$

$$V_{60} = \frac{54.98 \times 1.8305 \times 96}{60 \times 1.494} = 107.781 cm^3$$

$V_{60} = 3 \times 107.781 = 323.343$ cm^3 $\cong 323 cm^3$

From dilution formula

$V_{60} \times \rho_{60} = V_{96} \times \rho_{96} + V_w \times \rho_w$

Where

V_w = volume of water

ρ_w= density of water = 1g/cm^3

$V_w = \frac{V_{60}\rho_{60} - V_{96}\rho_{96}}{\rho_w}$

The volume of 96% H_2SO_4 (V_{96}) required is $\frac{323\times1.494\times60}{1.8305\times96} = 164.764cm^3 \cong 165cm^3$

Volume of water required is obtained as $V_{60} \times \rho_{60} = V_{96} \times \rho_{96} + V_w \times \rho_w$

V_w= (1.494×323)/ (1.8305×165)/1 = 482.562 /302.0325 = 180.5295 $cm^3 \cong 181cm^3$

DEALUMINATION CALCULATION (KANKARA RED KAOLIN (CAT III))

Basis 100g metakaolin for MK 6

Basic composition of metakaolin ($Al_2O_3.2SiO_2$) mole of silica content in 50gm would be

$54.6/60 = 0.91mol$ (1)

Mole of alumina content in 50gm metakaolin would be

$32.8/102 = 0.351mol$ (2)

The expected mole ratio for pure metakaolin is 2, but from (1) and (2) one gets 2.5926, an indication of higher content of impurities.

The targeted mole ratio of Si/Al = 10, therefore let the new mole be x.

$0.91/x = 10 \rightarrow x = 0.091mol$

Accordingly the weight of Al_2O_3 in the dealuminated sample would be 0.091 x 102 = 9.282gm.

Hence, the amount of alumina to be removed would be 35.8 – 9.282= 26.518gm

Dealumination reaction is given as:

$Al_2O_3 + 3H_2SO_4 \longrightarrow Al_2(SO_4)_3 + 3H_2O$

102gm of Al_2O_3 = 294gm of H_2SO_4 (100% H_2SO_4)

102gm of Al_2O_3 = Xgm of H_2SO_4 (96% H_2SO_4)

$294 * 100 / 96 = 306.25g$

Therefore,

26.518gm Al_2O_3 will requires $((306.25 + 26.518)/102) of\ 96\% H_2SO_4 = 83g$ 96% H_2SO_4

Density of 96% H_2SO_4 @ 25^0C = 1.8305gm/cm^3

$V = m/\rho = 83/1.8305 = 45.34288\ cm^3$

For the dealumination reaction, 60% acid strength is required, hence the need for conversion from 96% to 60% to find the component balance:

$V_{60}.\ \rho_{60}.60 \quad = \quad V_{96}.\ P_{96}.96$

The density of 60% H_2SO_4 at 25^0C = 1.494gm/cm^3

Therefore, $V_{60} = 45.3428 * 1.8305 * 96/1.494 * 60 = 88.8889\ cm^3 of\ 60\% H_2SO_4$

To avoid formation of slurry, three folds volume of acid was used, then

$V_{60} = 3 * 88.8889\ cm^3 of\ 60\% H_2SO_4 = 266.667 \approx 267 cm^3$

The volume of 96% H_2SO_4 required is $V_{60} = 267 * 1.494 * 60/1.8305 * 96 = 136.1984\ cm^3 \cong 136 cm^3$

Volume of H_2O required is determined as follows: $\rho_{60} * V_{60} = \rho_{96} * V_{96} + \rho_w * V_w$

$V_w = (\rho_{60} * V_{60} - \rho_{96} * V_{96})/\rho_w = (1.494 * 267 - 1.8305 * 136)/1 = 149.95\ cm^3 \cong 150 cm^3$

DEALUMINATION CALCULATION (KANKARA RED KAOLIN (CAT IV))

Basic composition of 100g metakaolin ($Al_2O_3.2SiO_2$) mole of silica content in 50gm would be

$49.79/60 = 0.83 mol$ (1)

Mole of alumina content in 50gm metakaolin would be

$36.65/102 = 0.359mol$ (2)

The expected mole ratio for pure metakaolin is 2, but from (1) and (2) one gets 2.312, an indication of higher content of impurities

The targeted mole ratio of Si/Al = 10, therefore let the new mole be x.

$0.83/x = 10 \rightarrow x = 0.083mol$

Accordingly the weight of Al_2O_3 in the dealuminated sample should be 0.083x 102 = 8.466g.

Hence, the amount of alumina to be removed would be

36.65 – 8.466= 28.184g

Dealumination reaction is given as:

$Al_2O_3 + 3H_2SO_4 \longrightarrow Al_2(SO_4)_3 + 3H_2O$

102gm of Al_2O_3 = 294gm of H_2SO_4 (100% H_2SO_4)

102gm of Al_2O_3 = Xgm of H_2SO_4 (96% H_2SO_4)

$294*100/96 = 306.25g$

Therefore, 28.184gm Al_2O_3 requires $((306.25 + 28.184)/102)of\ 96\%H_2SO_4 = 92g$ 98% H_2SO_4

Density of 96% H_2SO_4 @ 25^0C = 1.8305gm/cm^3

$V = m/\rho = 92/1.8305 = 50.2595\ cm^3$

For the dealumination reaction, we need the acid strength to be 60%, hence the need for conversion from 96% to 60% to find the component balance:

$V_{60}.\ \rho_{60}.60 = V_{96}.\ \rho_{60}.96$

The density of 60% H_2SO_4 at 25^0C = 1.494gm/cm^3

Therefore, $V_{60} = 50.2595 * 1.8305 * 96 / 1.494 * 60 = 98.5275\ cm^3 of\ 60\%\ H_2SO_4$

To avoid formation of slurry, three folds acid strength was used,

$V_{60} = 3 * 98.5275\ cm^3 of\ 60\%\ H_2SO_4 = 295.583 \approx 269 cm^3$

The volume of 96% H_2SO_4 required is $V_{60} = 296 * 1.494 * 60 / 1.8305 * 96 = 150.9915\ cm^3 \cong 151 cm^3$

Volume of H_2O required is determined as $\rho_{60} * V_{60} = \rho_{96} * V_{96} + \rho_w * V_w$

$V_w = (\rho_{60} * V_{60} - \rho_{96} * V_{96}) / \rho_w = (1.494 * 296) - (1.8305 * 151) / 1 = 165.819\ cm^3 \cong 166 cm^3$

DEALUMINATION CALCULATION (KANKARA WHITE KAOLIN (CAT IV))

100g basic composition of metakaolin ($Al_2O_3.2SiO_2$) mole of silica content in 50gm would be

$52.08 / 60 = 0.868 mol$ (1)

Mole of alumina content in 100g metakaolin would be

$41.01 / 102 = 0.402 mol$ (2)

The expected mole ratio for pure metakaolin is 2, but from (1) and (2) one gets 2.16, an indication of higher content of impurities

The targeted mole ratio of Si/Al = 10, therefore let the new mole be x.

$0.868/x = 10 \rightarrow x = 0.0868 mol$

Accordingly the weight of Al_2O_3 in the dealuminated sample should be 0.0868 x 102 = 8.8536g.

Hence, the amount of alumina to be removed would be 41.01 – 8.8536= 32.1564g

Dealumination reaction is given as:

$Al_2O_3 + 3H_2SO_4 \longrightarrow Al_2(SO_4)_3 + 3H_2O$

102gm of Al_2O_3 = 294gm of H_2SO_4 (100% H_2SO_4)

102gm of Al_2O_3 = x gm of H_2SO_4 (96% H_2SO_4)

$294 * 100/96 = 306.25 g$

Therefore, 32.1564g Al_2O_3 require $((306.25 + 32.156)/102)\,96\%\, H_2SO_4 = 106.69 g$ 98% H_2SO_4

Density of 96% H_2SO_4 @ 25^0C = 1.8305gm/cm^3

$V = m/\rho = 106.69/1.8305 = 58.2846\ cm^3$

For the dealumination reaction, the acid strength needed is 60%, hence the need for conversion from 96% to 60% to find the component balance:

$V_{60}.\ \rho_{60}.60 = V_{96}.\ \rho_{96}.96$

The density of 60% H_2SO_4 at 25^0C = 1.494g/cm^3

Therefore, $V_{60} = 58.2846 * 1.8305 * 96/1.494 * 60 = 114.2597\ cm^3 of$ 60% H_2SO_4

To avoid formation of slurry, three folds acid was used,

$V_{60} = 3 * 114.2597\ cm^3 of\ 60\%\ H_2SO_4 = 342.7791 \approx 343\, cm^3$

The volume of 96% H_2SO_4 required is $V_{60} = 343 * 1.494 * 60 / 1.8305 * 96 = 174.967\, cm^3 \cong 175 cm^3$

Volume of H_2O required is determined as $\rho_{60} * V_{60} = \rho_{96} * V_{96} + \rho_w * V_w$

$V_w = (\rho_{60} * V_{60} - \rho_{96} * V_{96}) / \rho_w = (1.494 * 343) - (1.8305 * 175) / 1 = 192.11\, cm^3 \cong 192 cm^3$

DEALUMINATION CALCULATION (ELEFUN KAOLIN (CAT IV))

100g metakaolin for EKC

100g basic composition of metakaolin ($Al_2O_3.2SiO_2$) mole of silica content in 50gm would be

$47.6 / 60 = 0.793 mol$ (1)

Mole of alumina content in 100g metakaolin would be

$44.1 / 102 = 0.432 mol$ (2)

The expected mole ratio for pure metakaolin is 2, but from (1) and (2) one gets 1.84, an indication of lower crystallinity

The targeted mole ratio of Si/Al = 10, therefore let the new mole be x.

$0.793 / x = 10 \rightarrow x = 0.0793 mol$

Accordingly the weight of Al_2O_3 in the dealuminated sample should be 0.0793 x 102 = 8.0886g.

Hence, the amount of alumina to be removed would be 44.1– 8.0886= 32.0114g

Dealumination reaction is given as:

$Al_2O_3 + 3H_2SO_4 \longrightarrow Al_2(SO_4)_3 + 3H_2O$

102gm of Al_2O_3 = 294gm of H_2SO_4 (100% H_2SO_4)

102gm of Al_2O_3 = x gm of H_2SO_4 (96% H_2SO_4)

$294 * 100/96 = 306.25g$

Therefore, 32.0114g Al_2O_3 require $((306.25 + 32.011)/102)96\% H_2SO_4 = 106.15g$ 98% H_2SO_4

Density of 96% H_2SO_4 @ 25^0C = 1.8305gm/cm^3

$V = m/\rho = 106.15/1.8305 = 57.9896\ cm^3$

For the dealumination reaction, the acid strength needed is 60%, hence the need for conversion from 96% to 60% to find the component balance:

$V_{60}.\ \rho_{60}.60 = V_{96}.\ \rho_{96}.96$

The density of 60% H_2SO_4 at 25^0C = 1.494g/cm^3

Therefore, $V_{60} = 57.9896 * 1.8305 * 96/1.494 * 60 = 113.6814\ cm^3 of\ 60\% H_2SO_4$

To avoid formation of slurry, three folds acid was used,

$V_{60} = 3 * 113.6814\ cm^3 of\ 60\% H_2SO_4 = 341.0442 \approx 341 cm^3$

The volume of 96% H_2SO_4 required is $V_{60} = 341 * 1.494 * 60/1.8305 * 96 = 173.946\ cm^3 \cong 174 cm^3$

Volume of H_2O required is determined as $\rho_{60} * V_{60} = \rho_{96} * V_{96} + \rho_w * V_w$

$V_w = (\rho_{60} * V_{60} - \rho_{96} * V_{96})/\rho_w = (1.494 * 341) - (1.8305 * 174)/1 = 190.947\ cm^3 \cong 191 cm^3$

APPENDIX B

GELATION CALCULATION FOR DMK 5

Basis: 20 gram of dealuminated metakaolin

Molar mass of SiO_2 = 60g/mol

Molar mass of Al_2O_3 = 102g/mol

Molar mass of Na_2O = 62g/mol

Number of moles % of SiO_2 = 63.86/60 = 1.0643

Number of moles % of Al_2O_3 = 11.01/102 = 0.1079

Number of moles % of SO_3 = 11.4/80 = 0.1425

Number of moles % of Na_2O = 0.06/62 = 0.001

Number of moles % of K_2O = 5.89/94 = 0.0627

Silica :Alumina ratio = 1.0643/0.1079 = 9.8638

Mass of dealuminated metakaolin = (60 x 9.8638) +102 + 80 + 94 + 62 = 929.828 g/mol

Moles of dealuminated metakaolin in 20g of sample = 20/929.828 = 0.0215 moles

Moles of silica in 20g of sample = 0.0215 x 9.8638 = 0.2121 moles

For $Na_2O/SiO_2 = 0.6$

$Na_2O = 0.6 \times SiO_2 = 0.6 \times 0.2121 = 0.1273$ moles

Considering the reaction,

$2NaOH \longrightarrow Na_2O + H_2O$

2 moles of NaOH requires 1 mole of Na_2O.

Therefore 0.1273 moles of Na_2O gives 2*(0.1273) moles of NaOH which is equal to 0.2546 moles of NaOH.

Also molar mass of NaOH = 40g/mol

Therefore mass of NaOH needed = 40 x 0.2546 = 10.18g

For $Na_2O/SiO_2 = 0.7$

$Na_2O = 0.7 \times SiO_2 = 0.7 \times 0.2121 = 0.1485$ moles

Considering the reaction,

$2NaOH \longrightarrow Na_2O + H_2O$

2 moles of NaOH requires 1 mole of Na_2O.

Therefore 0.1485 moles of Na_2O gives 2(0.1485) moles of NaOH which is equal to 0.297 moles of NaOH.

Also molar mass of NaOH = 40g/mol

Therefore mass of NaOH needed = 40 x 0.297 = 11.88g

For $Na_2O/SiO_2 = 0.8$

$Na_2O = 0.8 \times SiO_2 = 0.8 \times 0.2121 = 0.1697$ moles

Considering the reaction,

$2NaOH \longrightarrow Na_2O + H_2O$

2 moles of NaOH requires 1 mole of Na_2O.

Therefore 0.1697 moles of Na_2O gives 2*(0.1697) moles of NaOH which is equal to 0.3394 moles of NaOH.

Also molar mass of NaOH = 40g/mol

Therefore mass of NaOH needed = 40 x 0.297 = 11.88g

For $Na_2O/SiO_2 = 0.9$

$Na_2O = 0.7 \times SiO_2 = 0.9 \times 0.2121 = 0.1909$ moles

Considering the reaction,

$2NaOH \longrightarrow Na_2O + H_2O$

2 moles of NaOH requires 1 mole of Na_2O.

Therefore 0.1909 moles of Na_2O gives 2(0.1909) moles of NaOH which is equal to 0.3818 moles of NaOH.

Also molar mass of NaOH = 40g/mol

Therefore mass of NaOH needed = 40 x 0.3818 = 15.27g

For H_2O/Na_2O =30

Moles of water needed = 30 x Na_2O = 30 x 0.1485 = 4.455 moles of H_2O

Molar mass of water = 18g/mol

Mass of water required = 18 by 4.455 = 80.19g

Volume of H_2O required = 80.19cm^3 (since density = 1g/cm^3).

Gelation Calculation for DAK 3

Basis: 20 gram of dealuminated metakaolin

Molar mass of SiO_2 = 60g/mol

Molar mass of Al_2O_3 = 102g/mol

Molar mass of Na_2O = 62g/mol

Number of moles % of SiO_2 = 66.56/60 = 1.1093

Number of moles % of Al_2O_3 = 18.98/102 = 0.1861

Number of moles % of SO_3 = 1.93/80 = 0.0241

Number of moles % of Na_2O = 0.51/62 = 0.0082

Number of moles % of K_2O = 7.35/94 = 0.0782

Silica :Alumina ratio = 1.1093/0.1861 = 5.9608

Mass of dealuminated metakaolin = (60 x 5.9608) +102 + 80 + 94 + 62 =695.648 g/mol

Moles of dealuminated metakaolin in 20g of sample = 20/695.648 = 0.0288 moles

Moles of silica in 20g of sample = 0.0288 x 5.9608 = 0.1717 moles

For $Na_2O/SiO_2 = 0.7$

Na_2O = 0.7 x SiO_2 = 0.7x 0.1717 = 0.1202 moles

Considering the reaction,

$2NaOH \longrightarrow Na_2O + H_2O$

2 moles of NaOH requires 1 mole of Na_2O.

Therefore 0.1202 moles of Na_2O gives 2(0.1202) moles of NaOH which is equal to 0.2404 moles of NaOH.

Also molar mass of NaOH = 40g/mol

Therefore mass of NaOH needed = 40 x 0.2404 = 9.616g

For H_2O/Na_2O =30

Moles of water needed = 30 x Na_2O = 30 x 0.1202 = 3.606 moles of H_2O

Molar mass of water = 18g/mol

Mass of water required = 18 x3.606 = 64.908g

Volume of H_2O required = 64.908cm^3 (since density = 1g/cm^3).

GELATION CALCULATION FOR DMK 82

Basis: 20 gram of dealuminated metakaolin

Molar mass of SiO_2 = 60g/mol

Molar mass of Al_2O_3 = 102g/mol

Molar mass of Na_2O = 62g/mol

Number of moles % of SiO_2 = 76.5/60 = 1.275

Number of moles % of Al_2O_3= 14.5/102 = 0.142

Number of moles % of SO_3 = 0.18/80 = 0.0023

Number of moles % of Na_2O = 0.11/62 = 0.0018

Number of moles % of K_2O = 1.55/94 = 0.0165

Silica : Alumina ratio = 1.275/0.142 = 8.9789

Mass of dealuminated metakaolin = (60 x 8.9789) +102 + 80 + 94 + 62 = 876.734 g/mol

Moles of dealuminated metakaolin in 20g of sample = 20/876.734 = 0.0228 moles

Moles of silica in 20g of sample = 0.0228 x 8.9789 = 0.2047 moles

For $Na_2O/SiO_2 = 0.6$

$Na_2O = 0.6 \times SiO_2 = 0.6 \times 0.2047 = 0.1228$ moles

Considering the reaction,

$2NaOH \longrightarrow Na_2O + H_2O$

2 moles of NaOH requires 1 mole of Na_2O.

Therefore 0.1228 moles of Na_2O gives 2*(0.1228) moles of NaOH which is equal to 0.2456 moles of NaOH.

Also molar mass of NaOH = 40g/mol

Therefore mass of NaOH needed = 40 x 0.2456 = 9.83g

For $Na_2O/SiO_2 = 0.7$

$Na_2O = 0.7 \times SiO_2 = 0.7 \times 0.2047 = 0.1433$ moles

Considering the reaction,

$2NaOH \longrightarrow Na_2O + H_2O$

2 moles of NaOH requires 1 mole of Na_2O.

Therefore 0.1433 moles of Na_2O gives 2(0.1433) moles of NaOH which is equal to 0.2866 moles of NaOH.

Also molar mass of NaOH = 40g/mol

Therefore mass of NaOH needed = 40 x 0.2866 = 11.64g

For $Na_2O/SiO_2 = 0.8$

$Na_2O = 0.8 \times SiO_2 = 0.8 \times 0.2047 = 0.1638$ moles

Considering the reaction,

$2NaOH \longrightarrow Na_2O + H_2O$

2 moles of NaOH requires 1 mole of Na_2O.

Therefore 0.1638 moles of Na_2O gives 2*(0.1638) moles of NaOH which is equal to 0.3275 moles of NaOH.

Also molar mass of NaOH = 40g/mol

Therefore mass of NaOH needed = 40 x 0.3275 = 13.10g

For $Na_2O/SiO_2 = 0.9$

$Na_2O = 0.9 \times SiO_2 = 0.9 \times 0.2047 = 0.1842$ moles

Considering the reaction,

$2NaOH \longrightarrow Na_2O + H_2O$

2 moles of NaOH requires 1 mole of Na_2O.

Therefore 0.1842 moles of Na_2O gives 2*(0.1842) moles of NaOH which is equal to 0.3684 moles of NaOH.

Also molar mass of NaOH = 40g/mol

Therefore mass of NaOH needed = 40 x 0.3684 =14.74g

For $H_2O/Na_2O = 30$

Moles of water needed = 30 x Na_2O = 30 x 0.1433 = 4.299 moles of H_2O

Molar mass of water = 18g/mol

Mass of water required = 18 x 4.299 = 77.382g

Volume of H_2O required = 77.382cm3 (since density = 1g/cm^3).

GELATION CALCULATION FOR KD 3

Basis: 20 gram of dealuminated metakaolin

Molar mass of SiO_2 = 60g/mol

Molar mass of Al_2O_3 = 102g/mol

Molar mass of Na_2O = 62g/mol

Number of moles % of SiO_2 = 64.7/60 = 1.0783

Number of moles % of Al_2O_3 = 12.08/102 = 0.118

Number of moles % of SO_3 = 13.7/80 = 0.1713

Number of moles % of Na_2O = 0/62 = 0

Number of moles % of K_2O = 1.64/94 = 0.0174

Silica : Alumina ratio = 1.0783/0.118 = 9.1381

Mass of dealuminated metakaolin = (60 x 9.1381) +102 + 80 + 94 + 62 = 886.286 g/mol

Moles of dealuminated metakaolin in 20g of sample = 20/886.286 = 0.0226 moles

Moles of silica in 20g of sample = 0.0226 x 9.1381 = 0.2065 moles

For $Na_2O/SiO_2 = 0.6$

$Na_2O = 0.6 \times SiO_2 = 0.6 \times 0.2067 = 0.1240$ moles

Considering the reaction,

$2NaOH \longrightarrow Na_2O + H_2O$

2 moles of NaOH requires 1 mole of Na_2O.

Therefore 0.1240 moles of Na_2O gives 2*(0.1240) moles of NaOH which is equal to 0.2480 moles of NaOH.

Also molar mass of NaOH = 40g/mol

Therefore mass of NaOH needed = 40 x 0.2480 = 9.92g

For $Na_2O/SiO_2 = 0.7$

$Na_2O = 0.7 \times SiO_2 = 0.7 \times 0.2067 = 0.1447$ moles

Considering the reaction,

$2NaOH \longrightarrow Na_2O + H_2O$

2 moles of NaOH requires 1 mole of Na_2O.

Therefore 0.1447 moles of Na_2O gives 2*(0.1447) moles of NaOH which is equal to 0.2894 moles of NaOH.

Also molar mass of NaOH = 40g/mol

Therefore mass of NaOH needed = 40 x 0.2894 = 11.58g

For $Na_2O/SiO_2 = 0.8$

$Na_2O = 0.8 \times SiO_2 = 0.8 \times 0.2067 = 0.1654$ moles

Considering the reaction,

$2NaOH \longrightarrow Na_2O + H_2O$

2 moles of NaOH requires 1 mole of Na_2O.

Therefore 0.1654 moles of Na_2O gives 2*(0.1654) moles of NaOH which is equal to 0.3308 moles of NaOH.

Also molar mass of NaOH = 40g/mol

Therefore mass of NaOH needed = 40 x 0.3308 = 13.23g

For $Na_2O/SiO_2 = 0.9$

$Na_2O = 0.9 \times SiO_2 = 0.9 \times 0.2067 = 0.1860$ moles

Considering the reaction,

$2NaOH \longrightarrow Na_2O + H_2O$

2 moles of NaOH requires 1 mole of Na_2O.

Therefore 0.1860 moles of Na_2O gives 2*(0.1860) moles of NaOH which is equal to 0.372 moles of NaOH.

Also molar mass of NaOH = 40g/mol

Therefore mass of NaOH needed = 40 x 0.372 = 14.88g

For $H_2O/Na_2O = 30$

Moles of water needed = 30 x Na_2O = 30 x 0.1447 = 4.341 moles of H_2O

Molar mass of water = 18g/mol

Mass of water required = 18 x 4.341 = 78.138g

Volume of H_2O required = 78.138cm3 (since density = 1g/cm3).

GELATION CALCULATION FOR ED 3

Basis: 20 gram of dealuminated metakaolin

Molar mass of SiO_2 = 60g/mol

Molar mass of Al_2O_3 = 102g/mol

Molar mass of Na_2O = 62g/mol

Number of moles % of SiO_2 = 75.68/60 = 1.2613

Number of moles % of Al_2O_3 = 13/102 = 0.1275

Number of moles % of SO_3 = 2.4/80 = 1.2613

Number of moles % of Na_2O = 0/62 = 0

Number of moles % of K_2O = 1.29/94 = 0.0137

Silica : Alumina ratio = 1.2613/0.1275 = 9.8925

Mass of dealuminatedmetakaolin = (60 x 9.8925) +102 + 80 + 94 + 62 = 931.55 g/mol

Moles of dealuminatedmetakaolin in 20g of sample = 20/931.55 = 0.0214 moles

Moles of silica in 20g of sample = 0.0214 x 9.8925 = 0.2117 moles

For Na_2O/SiO_2 = 0.6

Na_2O = 0.6 x SiO_2 = 0.6 x 0.2117 = 0.1270 moles

Considering the reaction,

$2NaOH \longrightarrow Na_2O + H_2O$

2 moles of NaOH requires 1 mole of Na_2O.

Therefore 0.1270 moles of Na_2O gives 2*(0.1270) moles of NaOH which is equal to 0.2540 moles of NaOH.

Also molar mass of NaOH = 40g/mol

Therefore mass of NaOH needed = 40 x 0.2540 = 10.16g

For $Na_2O/SiO_2 = 0.7$

$Na_2O = 0.7 \times SiO_2 = 0.7 \times 0.2117 = 0.1482$ moles

Considering the reaction,

$2NaOH \longrightarrow Na_2O + H_2O$

2 moles of NaOH requires 1 mole of Na_2O.

Therefore 0.1482 moles of Na_2O gives 2(0.1482) moles of NaOH which is equal to 0.2964 moles of NaOH.

Also molar mass of NaOH = 40g/mol

Therefore mass of NaOH needed = 40 x 0.2964 = 11.856g

For $Na_2O/SiO_2 = 0.8$

$Na_2O = 0.8 \times SiO_2 = 0.8 \times 0.2117 = 0.1694$ moles

Considering the reaction,

$2NaOH \longrightarrow Na_2O + H_2O$

2 moles of NaOH requires 1 mole of Na_2O.

Therefore 0.1694 moles of Na_2O gives 2*(0.1694) moles of NaOH which is equal to 0.3388 moles of NaOH.

Also molar mass of NaOH = 40g/mol

Therefore mass of NaOH needed = 40 x 0.3388 = 11.856g

For $Na_2O/SiO_2 = 0.9$

$Na_2O = 0.9 \times SiO_2 = 0.9 \times 0.2117 = 0.1905$ moles

Considering the reaction,

$2NaOH \longrightarrow Na_2O + H_2O$

2 moles of NaOH requires 1 mole of Na_2O.

Therefore 0.1905 moles of Na_2O gives 2*(0.1905) moles of NaOH which is equal to 0.3811 moles of NaOH.

Also molar mass of NaOH = 40g/mol

Therefore mass of NaOH needed = 40 x 0.3811 = 15.24g

For $H_2O/Na_2O = 30$

Moles of water needed = 30 x Na_2O = 30 x 0.1482 = 4.446 moles of H_2O

Molar mass of water = 18g/mol

Mass of water required = 18 x 4.446 = 80.028g

Volume of H_2O required = 80.028cm3 (since density = 1g/cm3).

APPENDIX C

DYE APPLICATION CALCULATIONS (CATEGORY I)

a. Toluidine dye

The target is to obtain toluidine blue/ Al_2O_3 = 0.005, 0.01, 0.015, corresponding to TD1, TD2 and TD3 samples. The SiO_2 / Al_2O_3 ratio of 10, was attained through dealumination.

Toluidine/ Al_2O_3 = 0.01

(Toluidine/ Al_2O_3)×(Al_2O_3/ SiO_2) = 0.01× (1/10)

Toluidine/ SiO_2 = 0.001

Toluidine/(79.05/60) = 0.001

Hence, amount of toluidine needed per gram,

Toluidine = 1.3175×0.001 = 0.0013175g

As such, for 50g of dealuminated metakaolin,

Toluidine blue= 0.0013175×50 = 0.06588g of toluidine blue

Toluidine/ Al_2O_3 = 0.005

=0.06588/2 = 0.03294g of toluidine blue

Toluidine/ Al_2O_3 = 0.015

= (0.015/0.01)× 0.06588 = 0.09881g of toluidine blue

b. Malachite green

The target is to obtain malachite green/ Al_2O_3 = 0.005, 0.01, 0.015, corresponding to MD1, MD2 and MD3 samples. The SiO_2 / Al_2O_3 ratio of 10, was attained through dealumination.

Malachite green/ Al_2O_3 = 0.01

The dealuminated metakaolin contains 0.052mols Al_2O_3

Therefore, Malachite green = 0.01*0.052 = 0.00052moles

Hence, amount of Malachite green needed per gram = 364×0.0052 = 0.1893g

Malachite green/ Al_2O_3 = 0.005

The dealuminated metakaolin contains 0.052mols Al_2O_3

Therefore, Malachite green = 0.005*0.052 = 0.000026moles

Hence, amount of Malachite green needed per gram = 364×0.000026 = 0.0095g

Malachite green/ Al_2O_3 = 0.001

The dealuminated metakaolin contains 0.052mols Al_2O_3

Therefore, Malachite green = 0.001*0.052 = 0.000052moles

Hence, amount of Malachite green needed per gram = 364×0.00052 = 0.01893g

c. Methylene blue

The required amount of methylene blue is given by the relationship

$$\frac{moles\ of\ methylene\ blue}{moles\ of\ Al_2O_3} = y, \quad where \quad y = 0.005, 0.01, 0.015$$

Methylene blue/ Al_2O_3 = 0.01

The dealuminated metakaolin contains 0.052mols Al_2O_3

Therefore, Malachite green = 0.01*0.052 = 0.00052moles

Hence, amount of Malachite green needed per gram = 320×0.00052 = 0.1664g

Malachite green/ Al_2O_3 = 0.015

The dealuminated metakaolin contains 0.052mols Al_2O_3

Therefore, Malachite green = 0.015*0.052 = 0.00078moles

Hence, amount of Malachite green needed per gram = 320×0.000026 = 0.2496g

Malachite green/ Al_2O_3 = 0.005

The dealuminated metakaolin contains 0.052mols Al_2O_3

Therefore, Malachite green = 0.005*0.052 = 0.000052moles

Hence, amount of Malachite green needed per gram = 364×0.000026 = 0.0832g

DYE APPLICATION CALCULATIONS (CATEGORY IV-ELEFUN)

Basis of 20g delaminated metakeolin

Mass of SiO_2 = $\frac{75.68}{150} \times 15 = 11.352g$

Mass of Al_2O_3 = $13 \times \frac{20}{150} = 1.95g$

Mass of K_2O = $1.29 \times \frac{20}{150} = 0.194g$

Mass of Na_2O = $0.08 \times \frac{20}{150} = 0.012g$

No. of moles of:

$SiO_2 \equiv \frac{11.352}{60} = 0.1892mole$

$Al_2O_3 \equiv \frac{1.95}{102} = 0.0191mole$

$K_2O \equiv \frac{0.199}{94} = 0.0021moles$

$Na_2O \equiv \frac{0.016}{62} = 0.00034$

$SiO_2/Al_2O_3 = 9.89moles$

$M_2O/SiO_2 = 0.00274 + \frac{0.000268}{0.282} = 0.0129 mole$

From iteration

$M_2O/SiO_2 = 0.295\ (desired)$

$M_2O = 0.295 * SiO_2 = 0.0558$mole

$M_2O = K_2O + Na_2O$

$Na_2O = M_2O - K_2O = 0.0537$mole

$2NaOH \rightarrow H_2O + Na_2O$

2moles of NaOH $\equiv 1 mole\ of\ Na_2O$

2*0.0537mole of NaOH $\equiv 0.1074 mole$

Mass of NaOH = 40*0.1074 = 4.297 $\approx 4.3g$

$Na_2O/M_2O = \frac{0.0537}{0.0558} = 0.96\ (in\ range)$

$H_2O/M_2O = 60$

H_2O= 60*M_2O = 60*0.0558= 3.348moles

Mass of H_2O = 3.348*18 = 60.26g

Water for NaOH= 18*0.00034 = 0.000612g

Total volume of H_2O = 60.27cm^3

Sodium metasilicate/Al_2O_3 = 0.4

Na-metasilicate = 0.4*0.0191=0.00764mole

Mass of Na-metasilicate = 83*0.00764= 0.637g

The target is to obtain crystal violet/ Al_2O_3 = 0.0001, 0.005, 0.0005, 0.001, 0.01, corresponding to EDY1, EDY2, EDY3, EDY4 and EDY5 samples. The SiO_2 / Al_2O_3 ratio of 10, was attained through dealumination.

i. Crystal violet/Al_2O_3 = 0.0005
   Crystal violet = Al_2O_3*0.0005 =0.00191*0.0005= 0.00001275mole

   Mass of crystal violet = 0.0039g

ii. Crystal violet/Al_2O_3 = 0.0001
   Mass of crystal violet = 0.00078g

iii. Crystal violet/Al_2O_3 = 0.005
   Mass of crystal violet = 0.039g

iv. Crystal violet/Al_2O_3 = 0.001
   Mass of crystal violet = 0.0078g

v. Crystal violet/Al_2O_3 = 0.01
   Mass of crystal violet = 0.078g

DYE APPLICATION CALCULATIONS (CATEGORY IV-KANKARA)

Mass of SiO_2 = 64.70 *$\frac{15}{100}$ = 9.705g

Mass of AlO_3 = 12 * $\frac{15}{100}$ = 1.8g

Mass of K_2O = 1.64 *$\frac{20}{100}$ = 0.246g

Mass of Na_2O = 0.09* $\frac{20}{100}$ = 0.0135g

No of moles:

$SiO_2 \equiv \frac{12.94}{60} = 0.1618$ mole

$Al_2O_3 \equiv \frac{2.4}{102} = 0.0176$ mole

$K_2O \equiv \frac{0.328}{94} = 0.00262$ gm

$Na_2O \equiv \frac{0.018}{62} = 0.00029$ mole

$\frac{SiO2}{Al2O3} = 9.19$ moles

$\frac{M2O}{SiO2} = \frac{0.000262 + 0.00022}{0.1618} = 0.0176$ mole

Desired $\frac{M2O}{SiO2} = 0.295$ mole

$M_2O = 0.295 * SiO_2$

$M_2O = K_2O + Na_2O$

$Na_2O = M_2O - K_2O = 0.0477 - 0.00262 = 0.0451$ mole

$2NaOH \rightarrow Na_2O + H_2O$

2 mole of NaOH $\equiv$ 1 mole of Na_2O

2 *0.0451 mole of NaOH = 0.0902 mole

Mass of NaOH = 40 *0.0902 = 3.609g

$\frac{Na2O}{M2O} = \frac{0.0451}{0.0477} = 0.95$ (in range)

$\frac{H2O}{M2O} = 60$

$H_2O = 60 * M_2O = 60*0.0477 = 2.862$

Mass of $H_2O = 18*2.862 = 51.516g$

Water in NaOH = 18*0.000022 = 0.00396g

Total water content = 51.52g

$\frac{Na-metasilicate}{Al2O3} = 0.4$

Mass of Na-metasilicate = 0.4*0.0176*83 = 0.584g

The target is to obtain crystal violet/ Al_2O_3 = 0.0001, 0.005, 0.0005, 0.001, 0.01, corresponding to KDY1, KDY2, KDY3, KDY4 and KDY5 samples. The SiO_2 / Al_2O_3 ratio of 10, was attained through dealumination.

i. Crystal violet = Al_2O_3*0.0005 = 0.0176*0.0005 mole
   Mass of crystal violet = 0.0176*0.0005*409 = 0.0036g

ii. Crystal violet = Al_2O_3*0.0001 = 0.0176*0.0001 mole
   Mass of crystal violet = 0.0176*0.0001*409 = 0.00072g

iii. Crystal violet = Al_2O_3*0.005 = 0.0176*0.005 mole
   Mass of crystal violet = 0.0176*0.0005*409 = 0.0036g

iv. Crystal violet = Al_2O_3*0.001 = 0.0176*0.001 mole
   Mass of crystal violet = 0.0176*0.001*409 = 0.0072g

v. Crystal violet = Al_2O_3*0.01 = 0.0176*0.01 mole
   Mass of crystal violet = 0.0176*0.01*409 = 0.072g

APPENDIX D

SURFACE AREA CALCULATION

To determine the specific surface area using water adsorption method, the following computations were made using the Brunauer-Emmet-Teller (BET) method.

The BET equation is given as

$$\frac{P}{V(P_o - P)} = \frac{1}{V_m C} + \frac{(C-1)}{V_m C}\left(\frac{P}{P_o}\right) \ldots\ldots\ldots\ldots\ldots\ldots\ldots\ldots\ldots\ldots 1$$

Rearranging Equation 1, gives

$$\frac{P/P_o}{V\left(1 - P/P_o\right)} = \frac{1}{V_m C} + \frac{(C-1)}{V_m C}\left(\frac{P}{P_o}\right) \ldots\ldots\ldots\ldots\ldots\ldots\ldots\ldots\ldots\ldots 2$$

Where,

V = Amount of water vapour adsorbed per gram of sample

V_m = Amount of water vapour adsorbed per gram of sample for monolayer capacity

P = pressure (atm)

P_o = Saturation vapour pressure

P/P_o = Relative humidity of saturated salt at room temperature

From Equation 2, a plot of $\frac{P/P_o}{V\left(1-P/P_o\right)}$ against $\frac{P}{P_o}$ yields a straight line from which

Intercept (I) = $\frac{1}{V_m C}$ ……...…..3

Slope (S) = $\frac{(C-1)}{CV_m}$ ……..4

Mathematical manipulation of Equation 3 and 4 gives

$V_m = \frac{1}{(I+S)}$ ……5

From ideal gas Equation, (i.e., assuming ideality)

PV = nRT ……6

Where n = $\frac{Mass\ of\ Water\ Vapour}{Molar\ mass\ of\ water\ vapour} = \frac{V_m}{M}$

Hence, $V_{ml} = \frac{V_m RT}{MP}$ 7

R = 8.314J/(gmol.K)

T = Room temperature = 298K

M = molar mass of water = 18g/gmol

P = atmospheric pressure = $1.01325 \times 10^5 N/m^2$

V = standard volume at STP = $22400cm^3$

$\alpha = 1.09 \times \left(\frac{M}{N_a \rho}\right)^{\frac{2}{3}}$ ……...8

Where

$N_a = 6.02 \times 10^{23}$ molecules/mole
$\rho = 1.0 g/cm^3$

Therefore,

$$\alpha = 1.09 \times \left[\frac{18}{(6.02\times10^{23})\times1}\right]^{\frac{2}{3}} = 1.05\times10^{-15} cm^2/molecule$$

But

$$S_g = \left(\frac{V_{ml} N_a}{V}\right)\alpha$$

$$S_g = \frac{V_{mi}\times6.02\times10^{23}\times1.05\times10^{-15}}{22400} = 28218.75 V_{ml} (cm^2/g)$$

But $V_m = \frac{1}{(1+S)}$ g of H_2O per gram of sample

From Equation 7,

$$V_{ml} = \frac{V_{ml}\times8.314\times298}{18\times1.01325\times10^5} = 1.3584\times10^{-3} V_m m^3/g \text{ of sample}$$

$V_{ml} = 1358.4 V_m \ cm^3/g$

Therefore,

$S_g = 28218.75 \times 1358.4 V_m$

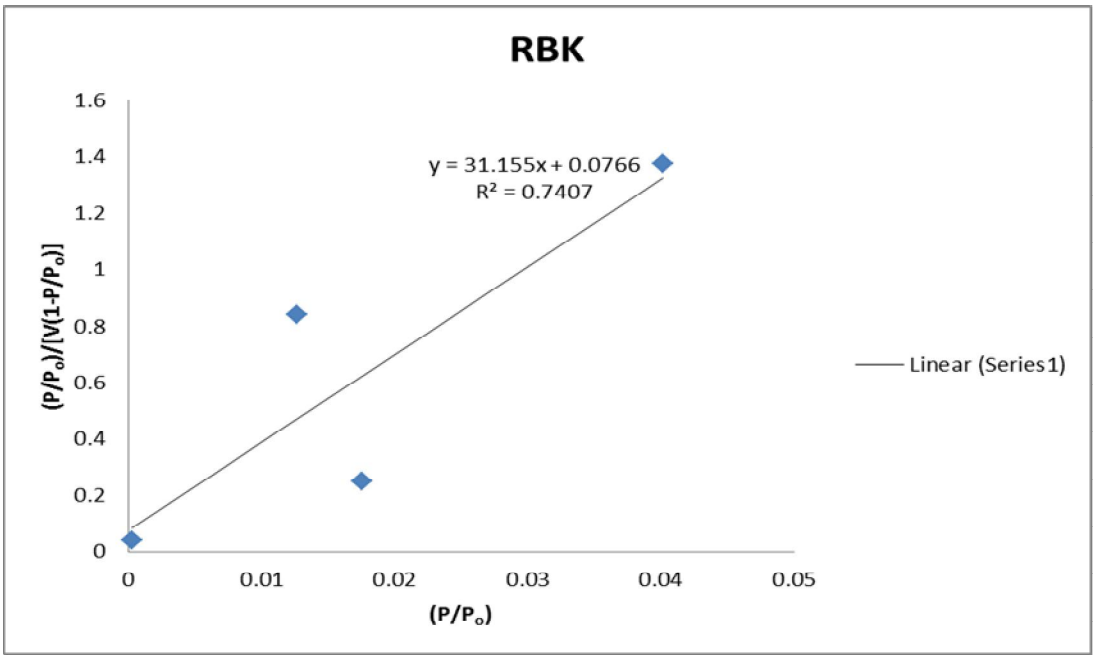
$= 38333196.56V_m cm^2/g$ of sample $= 3833.32V_m(m^2/g)$ of sample

Hence, the relation used for surface area calculation is $S_g = 3833.32V_m m^2/g$

The results obtained are shown in Table D1 to Table D7

Table D1: Surface area result for RBK

Salt Sample	P/P_o	V	$(P/P_o)/[V(1-P/P_o)]$
$LiCl_2$	0.000234478	0.0099	0.023690159
$CaCl_2$	0.040135523	0.0218	1.918061413
CH_3COOK	0.017597248	0.0366	0.489411418
$CaSO_4$	0.012623762	0.4612	0.027721507

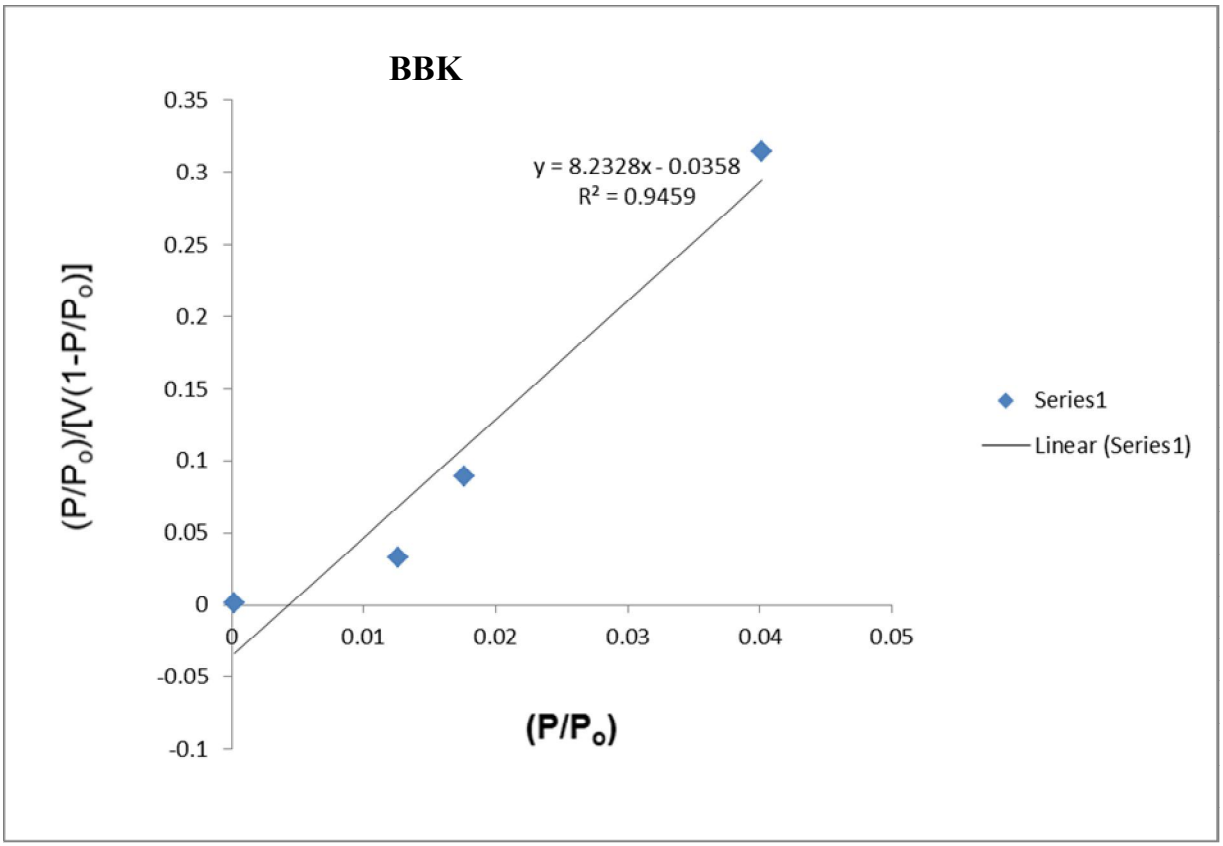


$V_m = 0.03200$ Specific surface area $= 122.74 m^2/g$

Figure D1: Water adsorption isotherm for RBK

Table D2: Surface area result for BBK

Salt Sample	P/P_o	V	$(P/P_o)/[V(1-P/P_o)]$
$LiCl_2$	0.000234478	0.0945	0.002481826
$CaCl_2$	0.040135523	0.0238	1.756879782
CH_3COOK	0.017597248	0.2304	0.077745043
$CaSO_4$	0.012623762	0.1946	0.065699688

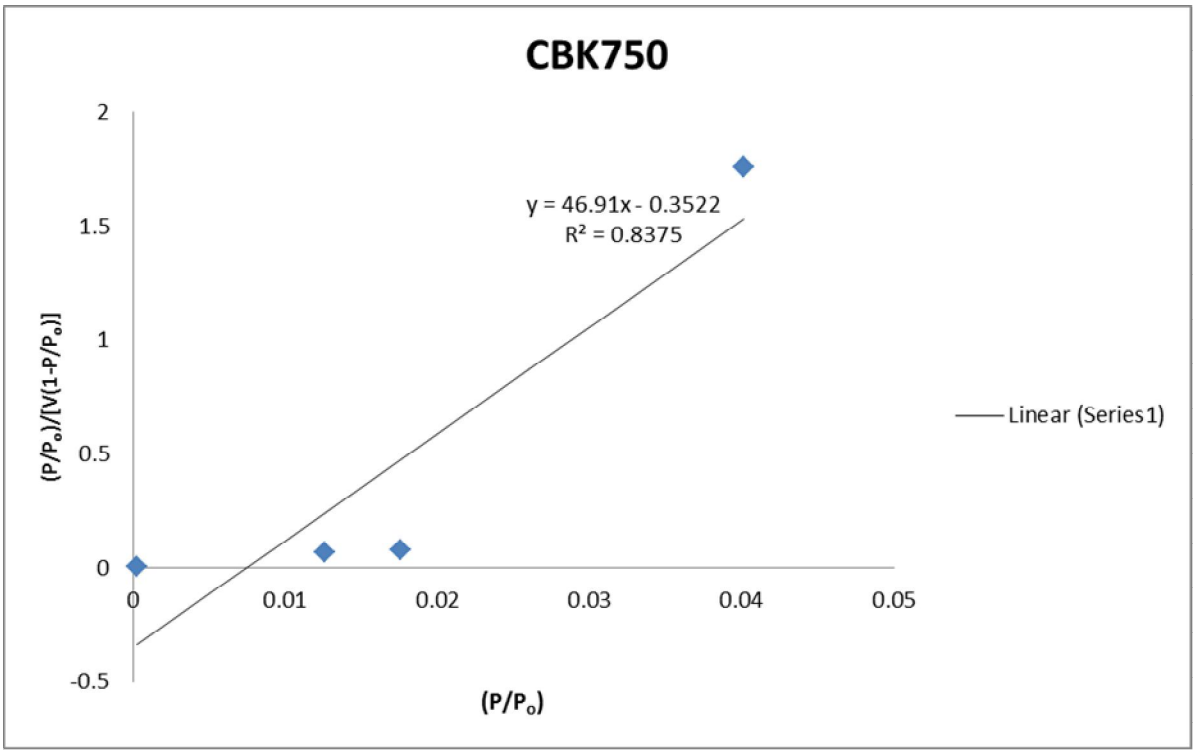


$V_m = 0.12199$ Specific surface area = $467.62 m^2/g$

Figure D2: Water adsorption isotherm for BBK

Table D3: Surface area result for CBK750

Salt Sample	P/P_o	V	$(P/P_o)/[V(1-P/P_o)]$
$LiCl_2$	0.000234478	0.0058	0.040436651
$CaCl_2$	0.040135523	0.0304	1.375451934
CH_3COOK	0.017597248	0.072	0.248784138
$CaSO_4$	0.012623762	0.2193	0.058299859

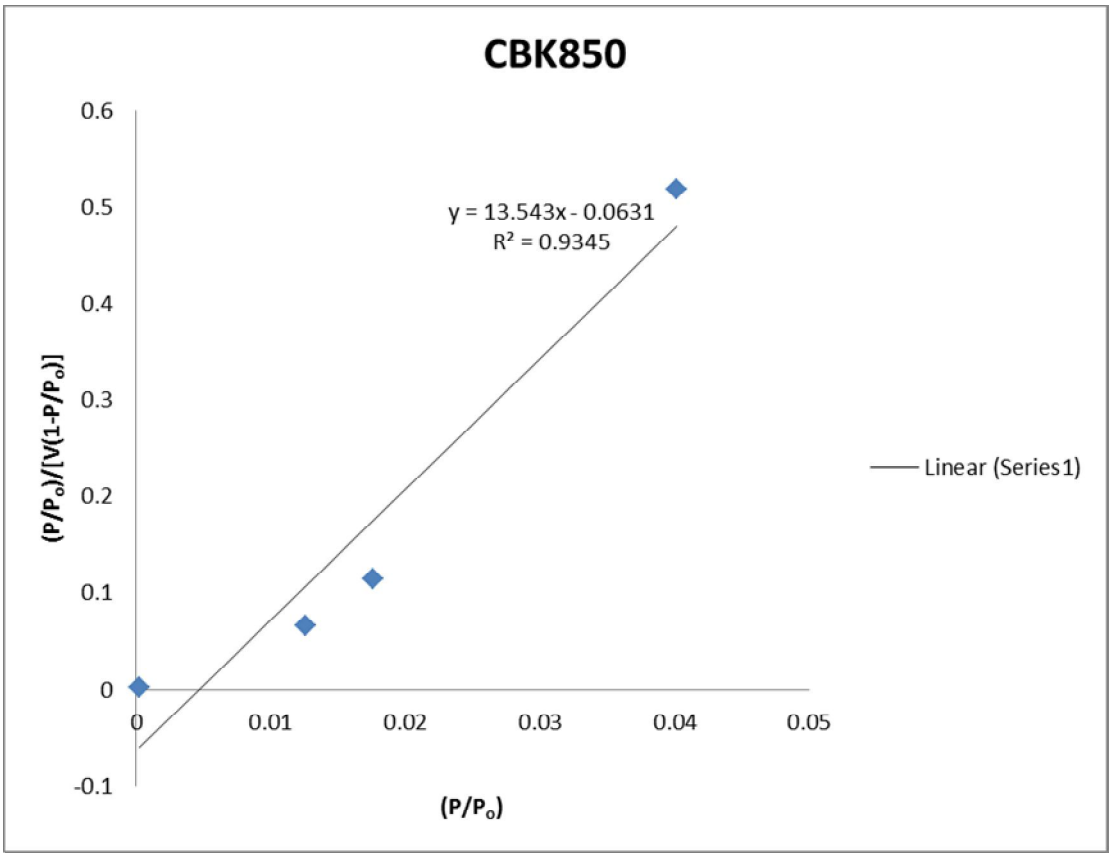


$V_m = 0.02148$ Specific surface area = $82.34 m^2/g$

Figure D3: Water adsorption isotherm for CBK750

Table D4: Surface area result for CBK850

Salt Sample	P/P_o	V	$(P/P_o)/[V(1-P/P_o)]$
$LiCl_2$	0.000234478	0.0931	0.002519147
$CaCl_2$	0.040135523	0.0805	0.519425327
CH_3COOK	0.017597248	0.1554	0.115266782
$CaSO_4$	0.012623762	0.1922	0.066520079

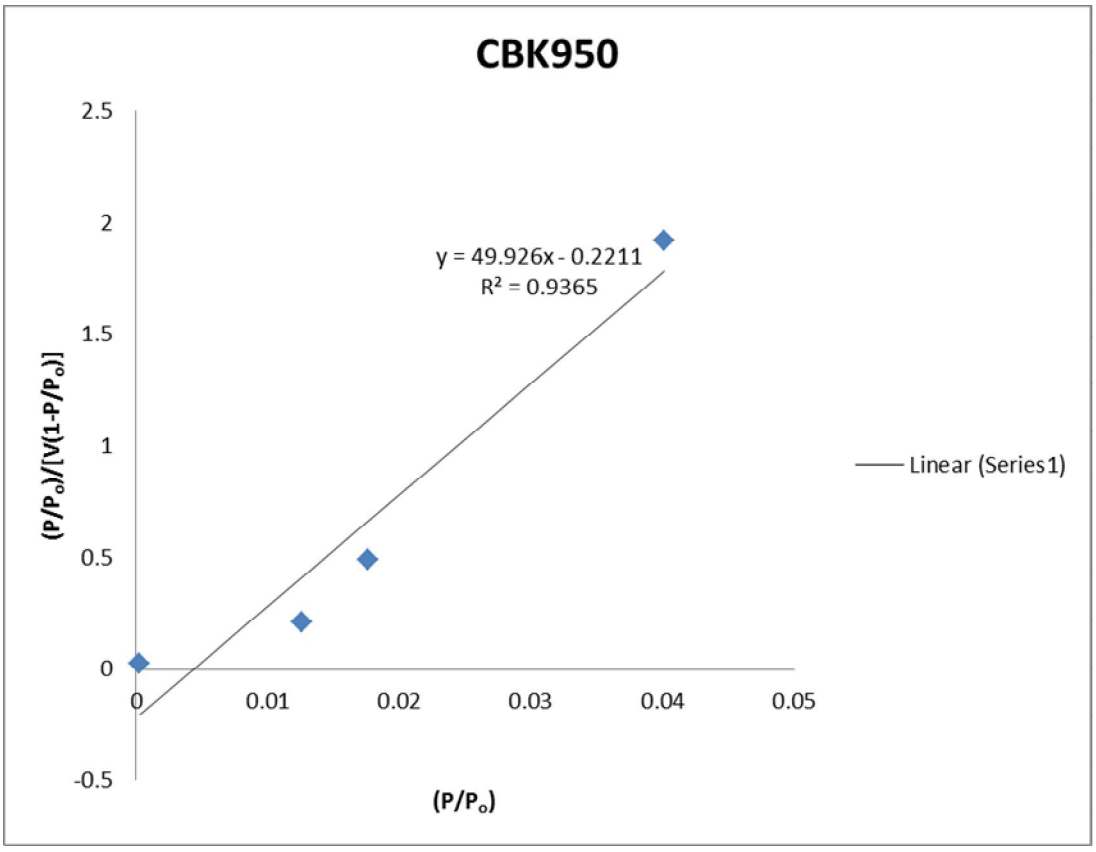


$V_m = 0.07418$ Specific surface area = $284.37 m^2/g$

Figure D4: Water adsorption isotherm for CBK850

Table D5: Surface area result for CBK950

Salt Sample	P/P_o	V	$(P/P_o)/[V(1-P/P_o)]$
$LiCl_2$	0.000234478	0.0095	0.02468764
$CaCl_2$	0.040135523	0.0954	0.438299149
CH_3COOK	0.017597248	0.1618	0.110707404
$CaSO_4$	0.012623762	0.0435	0.293911705

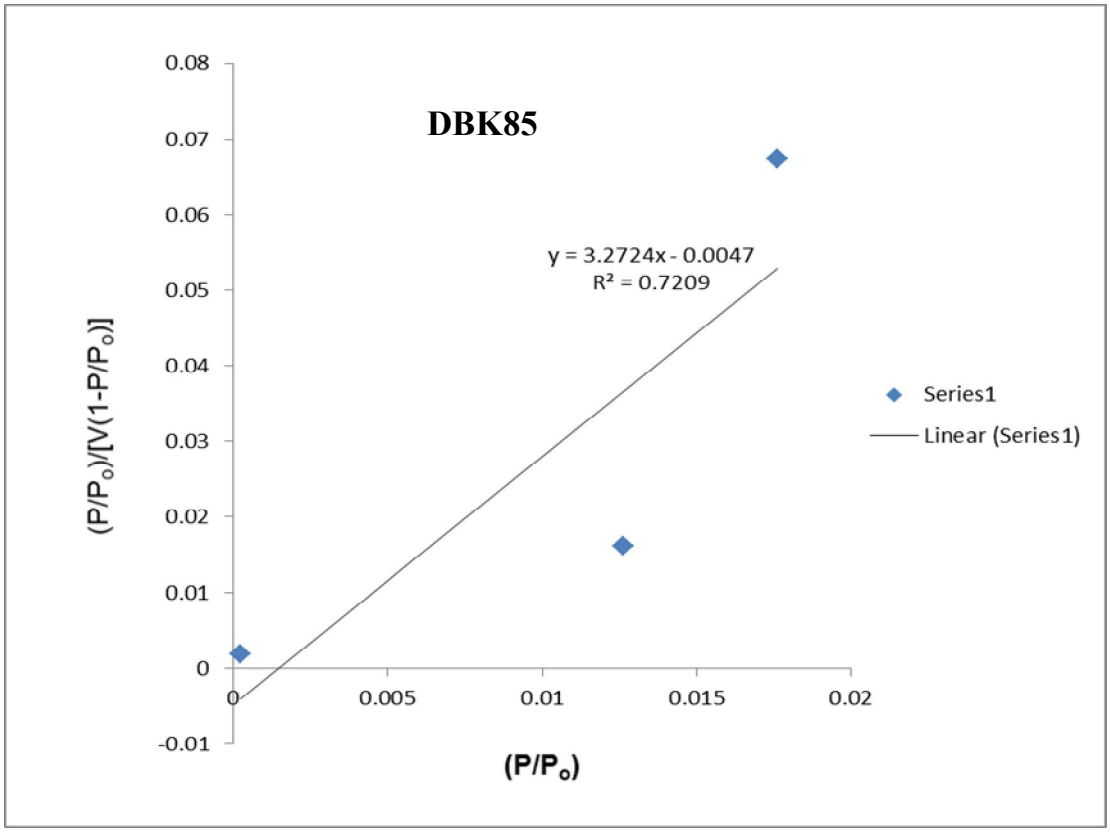


$V_m = 0.02012$ Specific surface area = $77.12 m^2/g$

Figure D5: Water adsorption isotherm for CBK950

Table D6: Surface area result for DBK85

Salt Sample	P/P_o	V	$(P/P_o)/[V(1-P/P_o)]$
$LiCl_2$	0.000234478	0.1247	0.000188078
CH_3COOK	0.017597248	0.2657	0.067416100
$CaSO_4$	0.012623762	0.7908	0.016167373

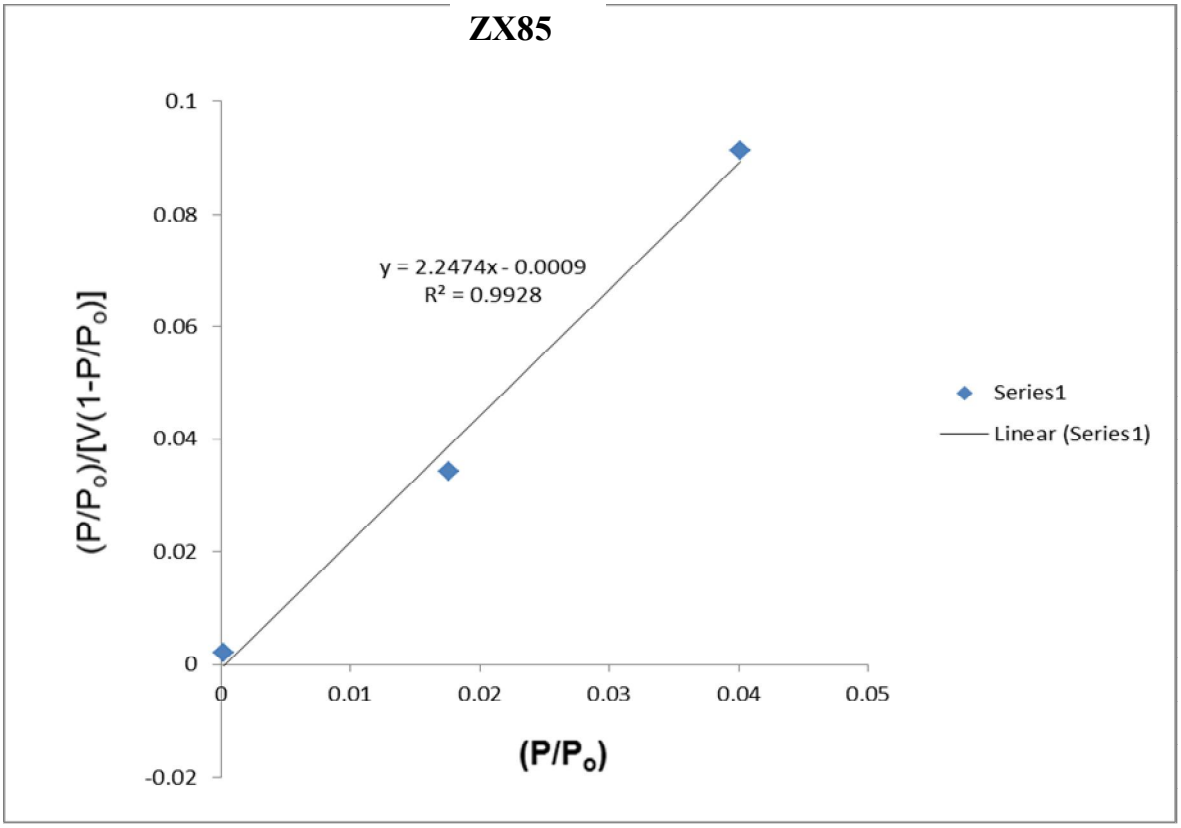


$V_m = 0.3060$ Specific surface area = $1173.09 m^2/g$

Figure D6: Water adsorption isotherm for DBK85

Table D7: Surface area result for ZX85

Salt Sample	P/P_o	V	$(P/P_o)/[V(1-P/P_o)]$
$LiCl_2$	0.000234478	0.1099	0.002134045
CH_3COOK	0.017597248	0.5227	0.034269099
$CaCl_2$	0.040135523	0.4583	0.091236611



$V_m = 0.4448$ Specific surface area = $1704.98 m^2/g$

Figure D7: Water adsorption isotherm for ZX85

APPENDIX E

XRD SPECTRA FOR CATEGORIES I AND II

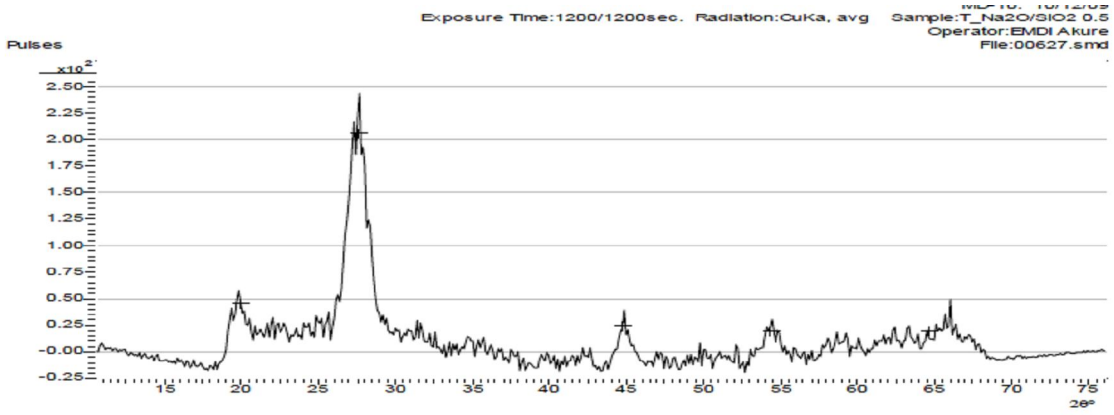


Figure E1: XRD pattern for TNa/Si0.5

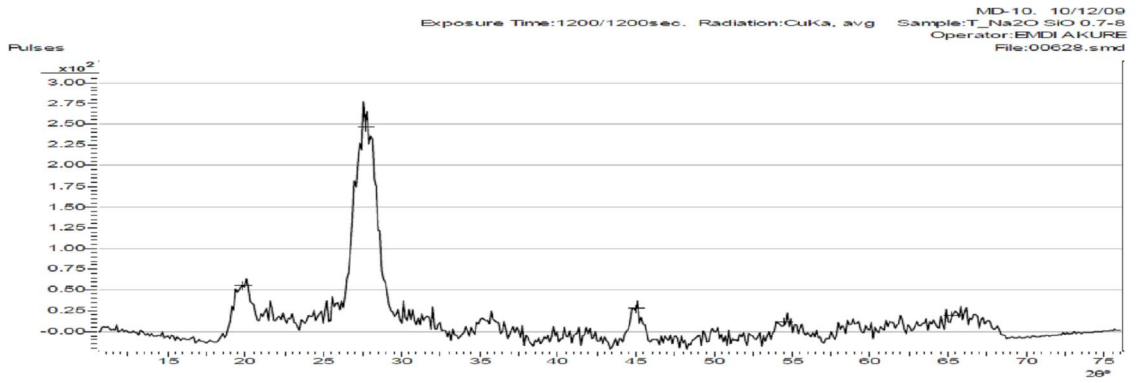


Figure E2: XRD pattern for TNa/Si0.7

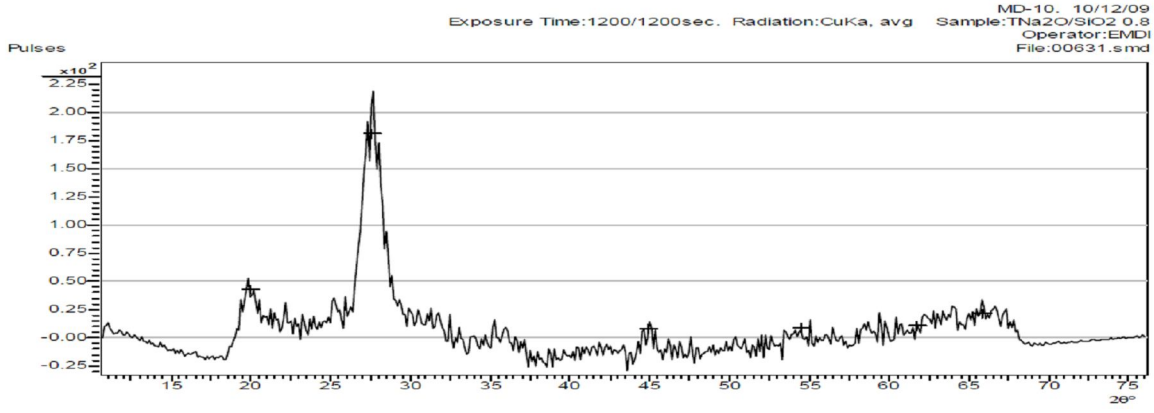


Figure E3: XRD pattern for TNa/Si0.8

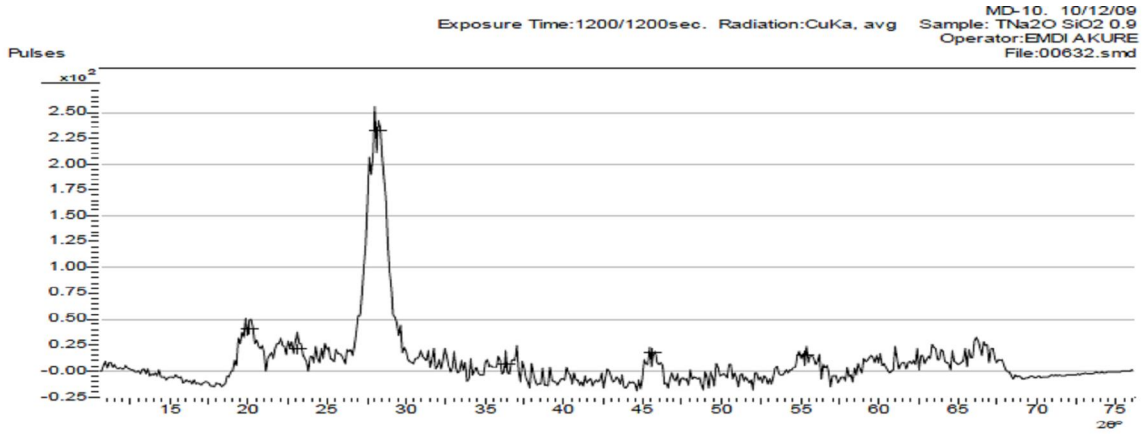


Figure E4: XRD pattern for TNa/Si0.9

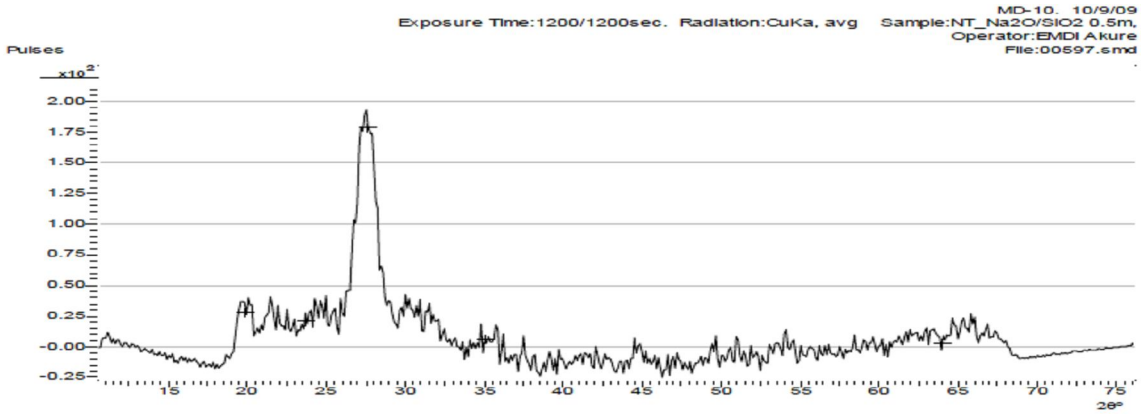


Figure E5: XRD pattern for NTNa/Si0.5

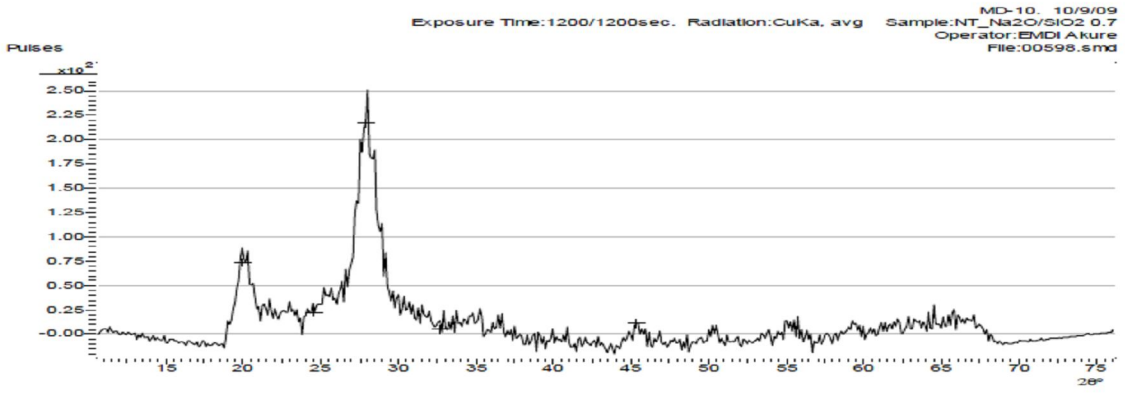


Figure E6: XRD pattern for NTNa/Si0.7

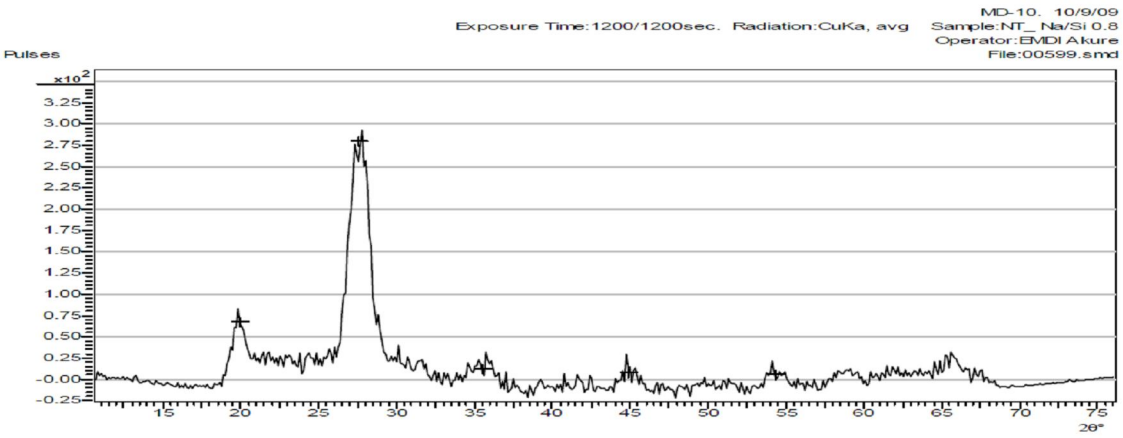


Figure E7: XRD pattern for NTNa/Si0.8

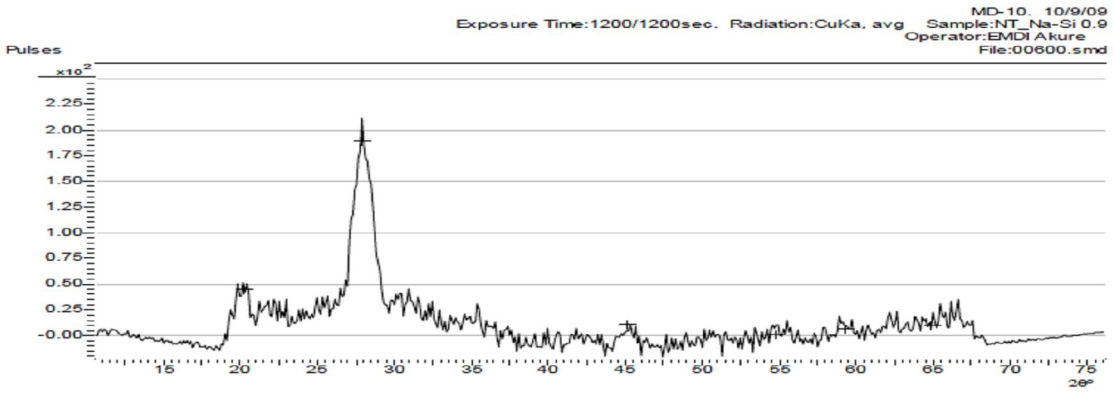


Figure E8: XRD pattern for NTNa/Si0.9

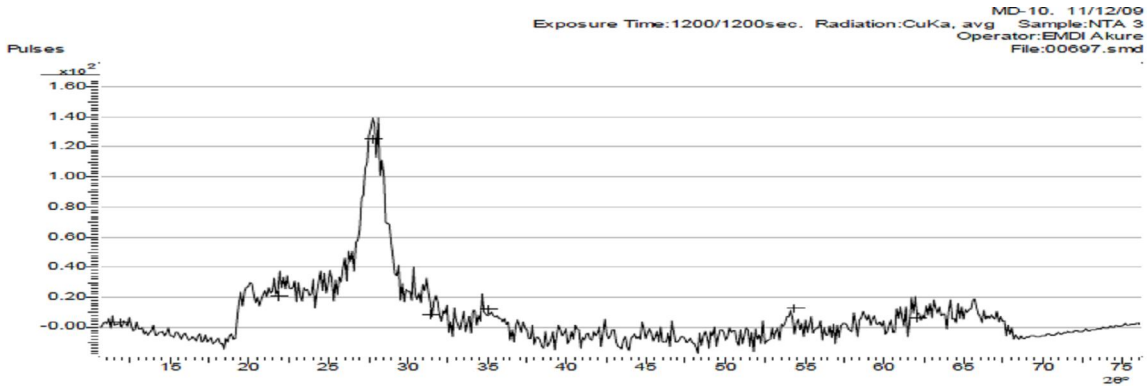


Figure E9: XRD pattern for NTA3

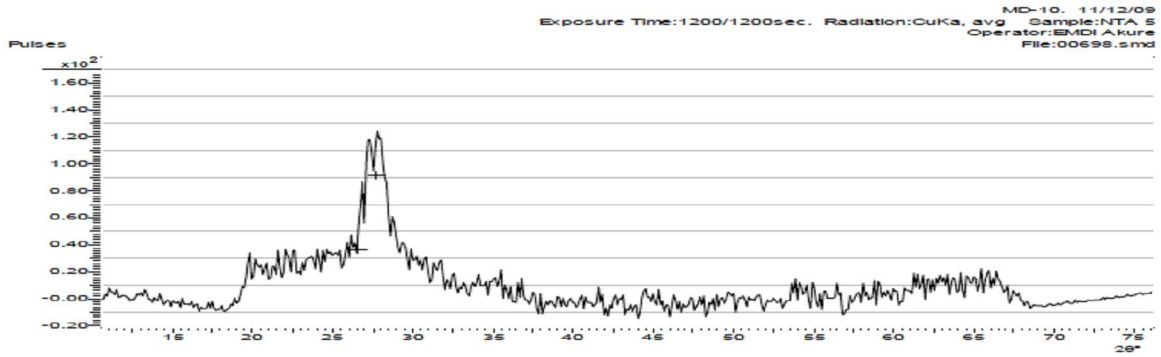


Figure E10: XRD pattern for NTA5

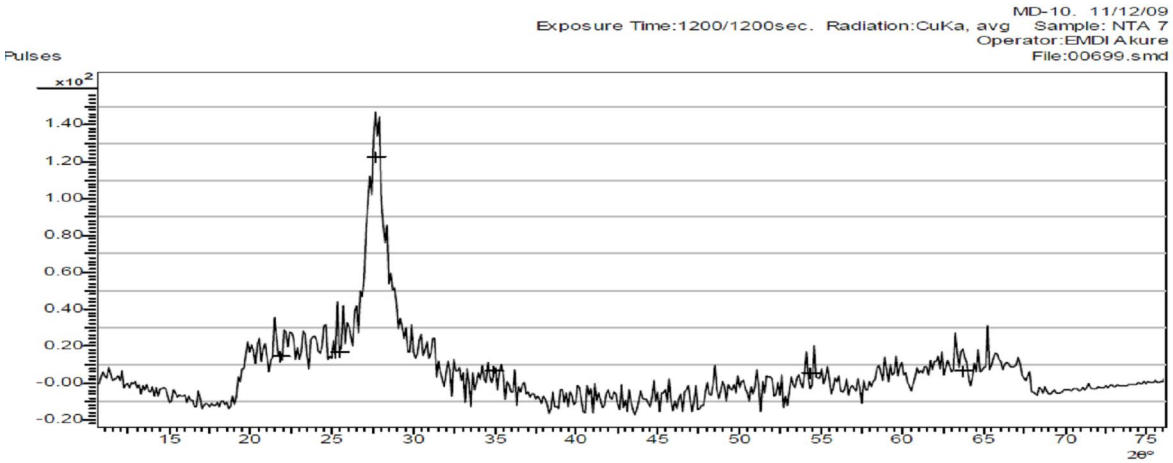


Figure E11: XRD pattern for NTA7

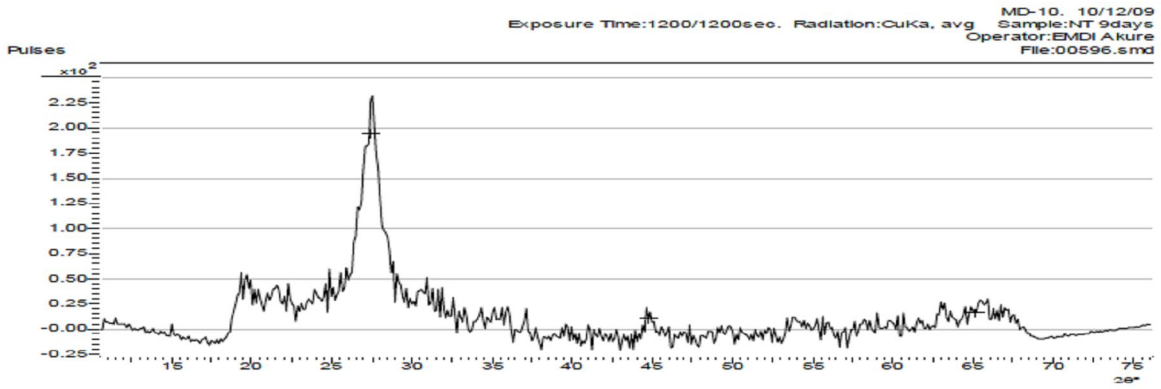


Figure E12: XRD pattern for NTA9

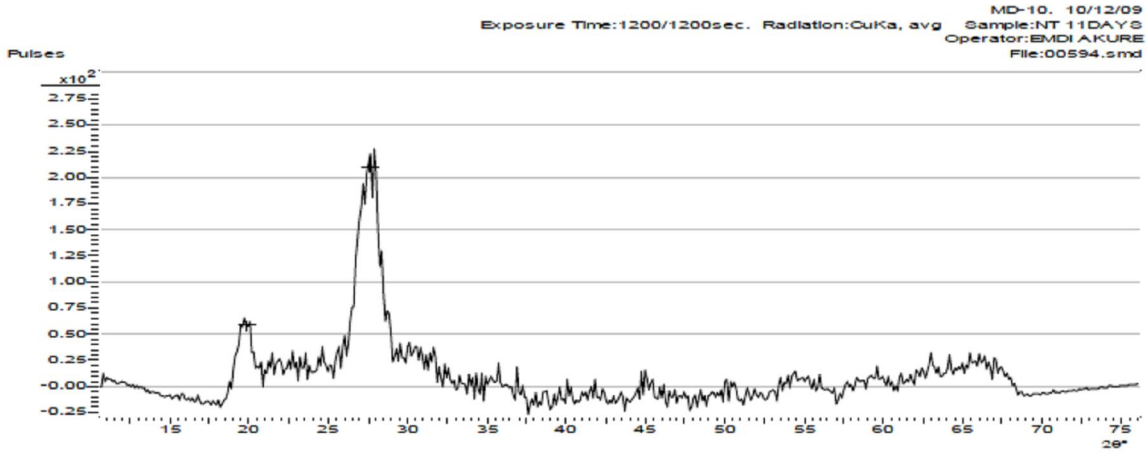


Figure E13: XRD pattern for NTA11

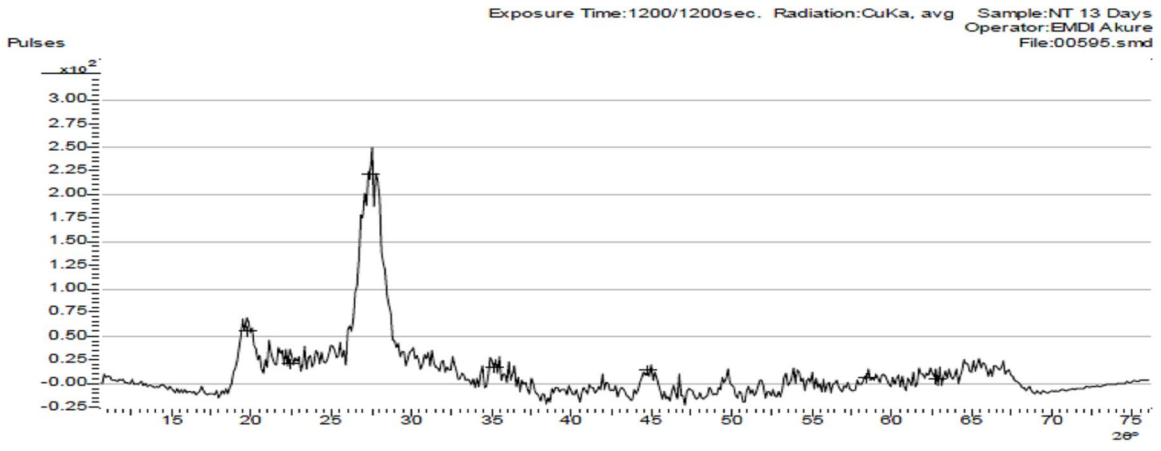


Figure E14: XRD pattern for NTA13

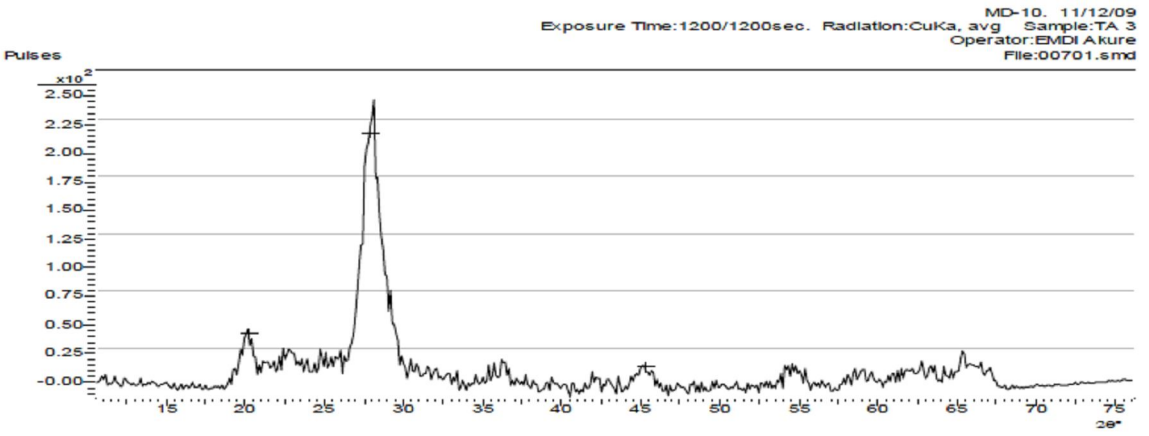


Figure E15: XRD pattern for TA3

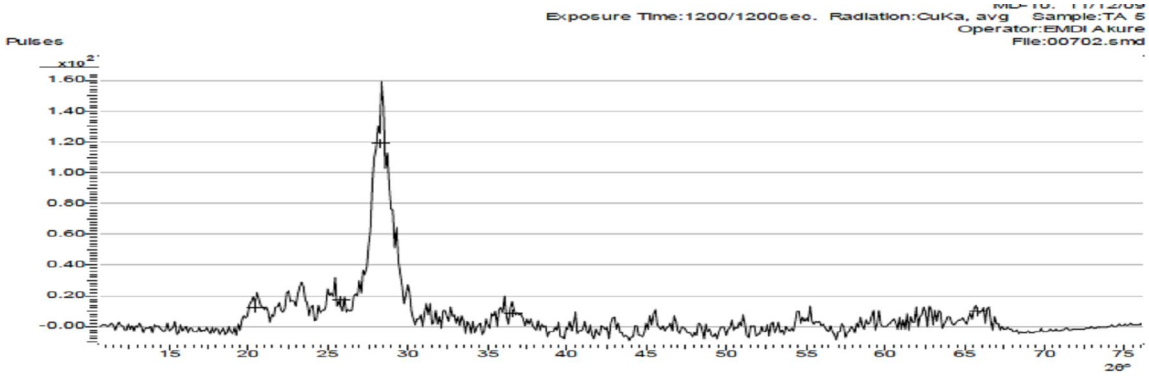


Figure E16: XRD pattern for TA5

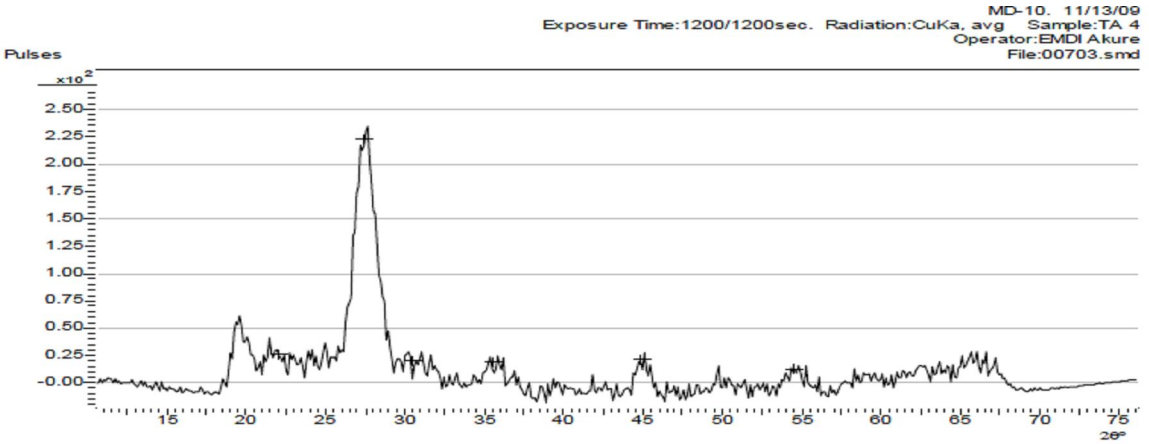


Figure E17: XRD pattern for TA7

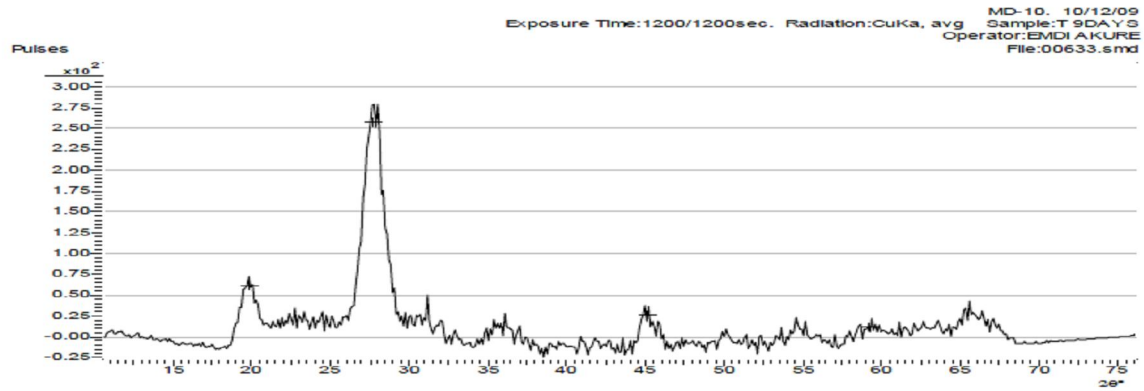


Figure E18: XRD pattern for TA9

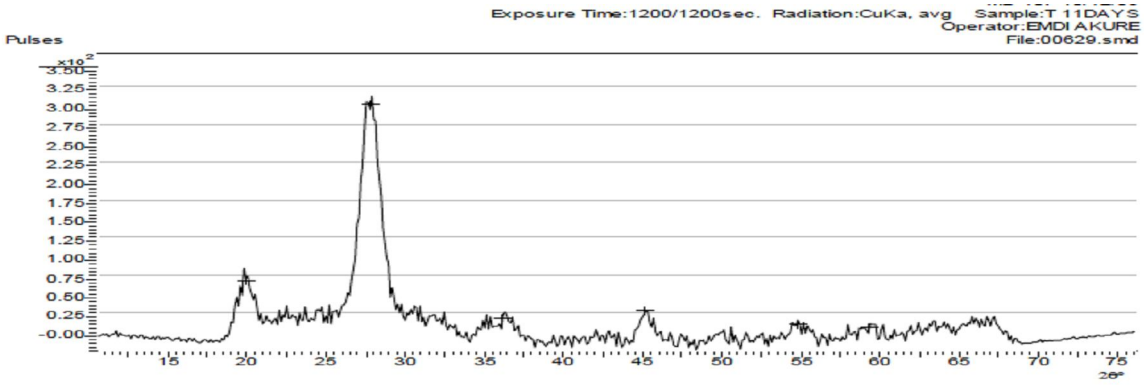


Figure E19: XRD pattern for TA11

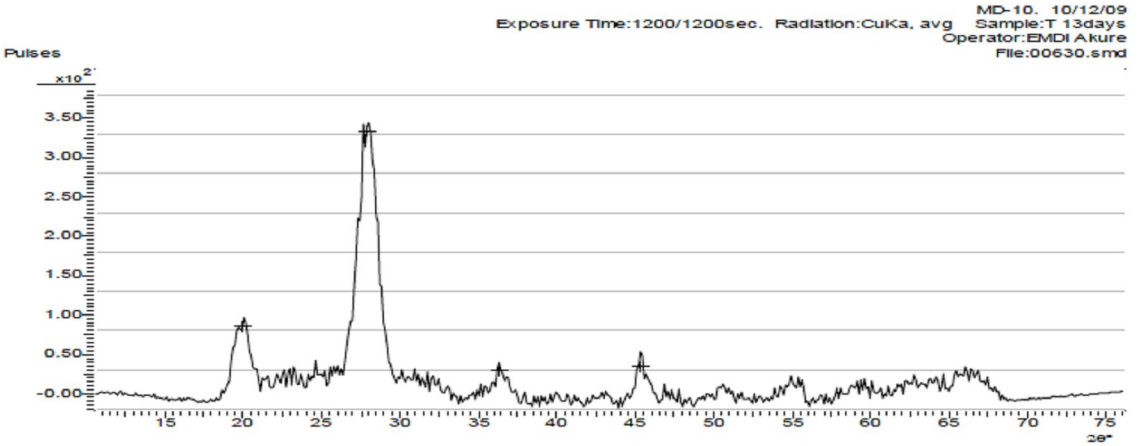


Figure E20: XRD pattern for TA13

APPENDIX F

XRD SPECTRA FOR DYED SAMPLE

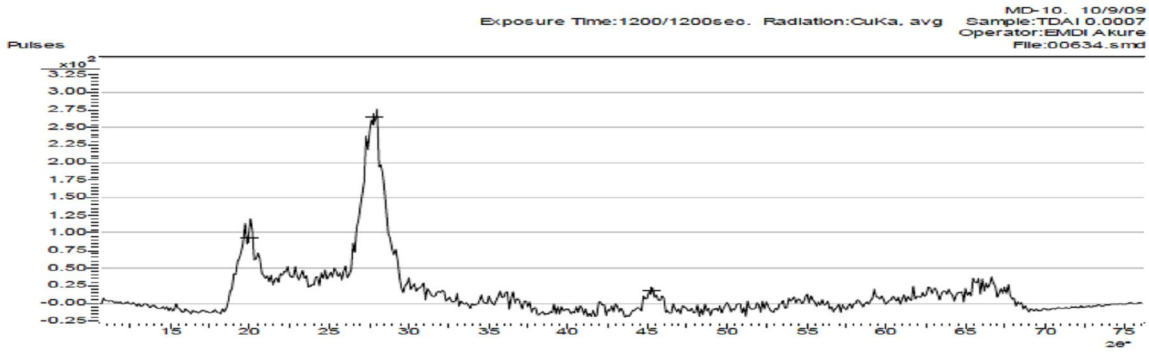


Figure E1: XRD pattern for TDAL0.0007

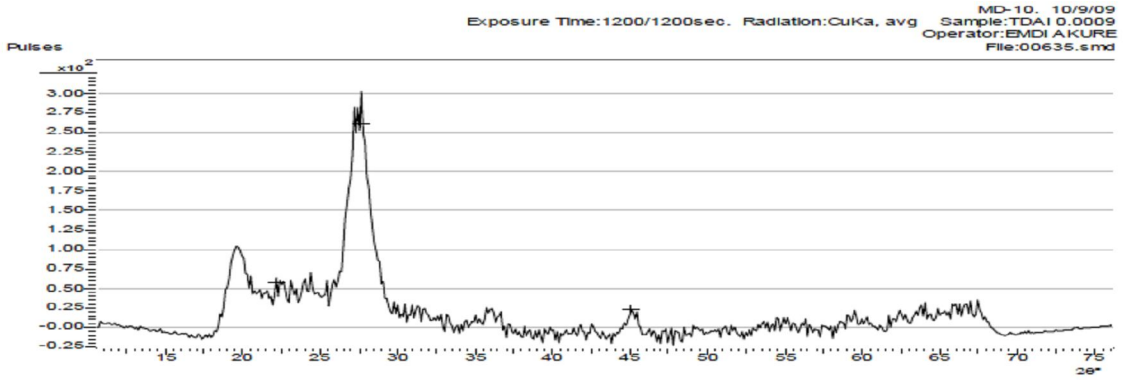


Figure E2: XRD pattern for TDAL0.0009

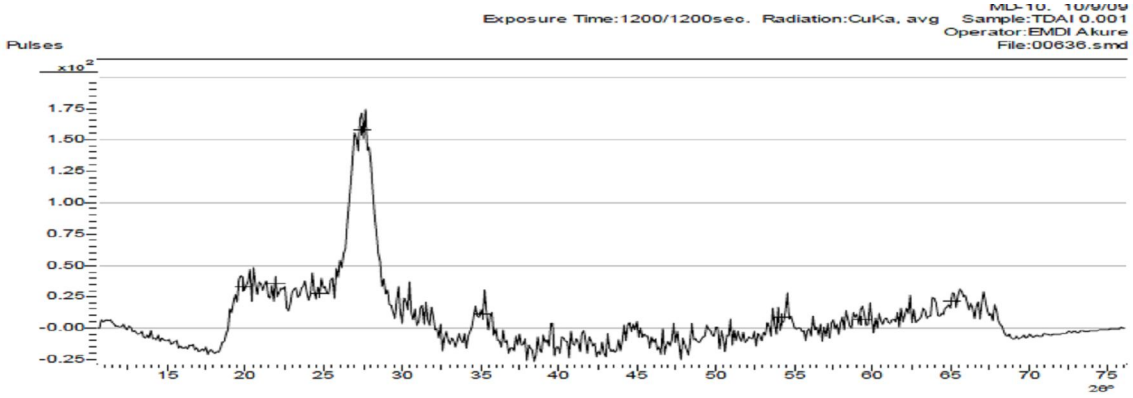


Figure E3: XRD pattern for TDAL0.001

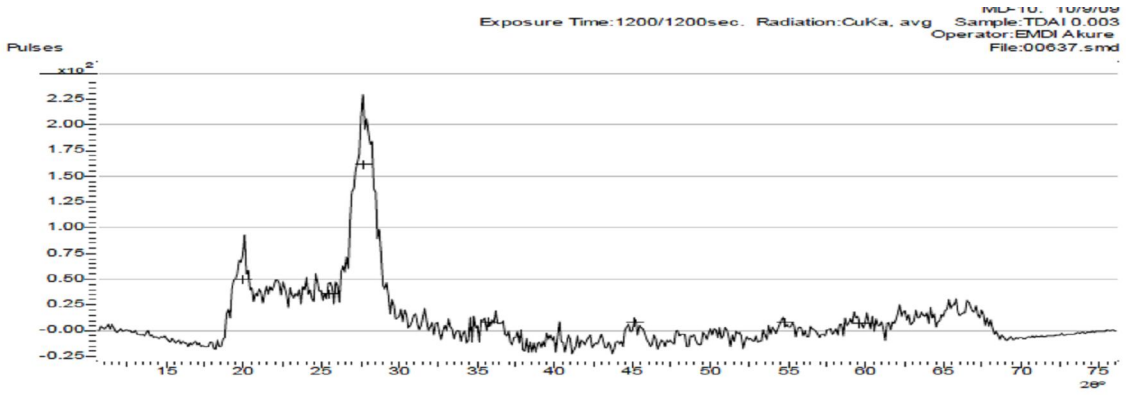


Figure E4: XRD pattern for TDAL0.003

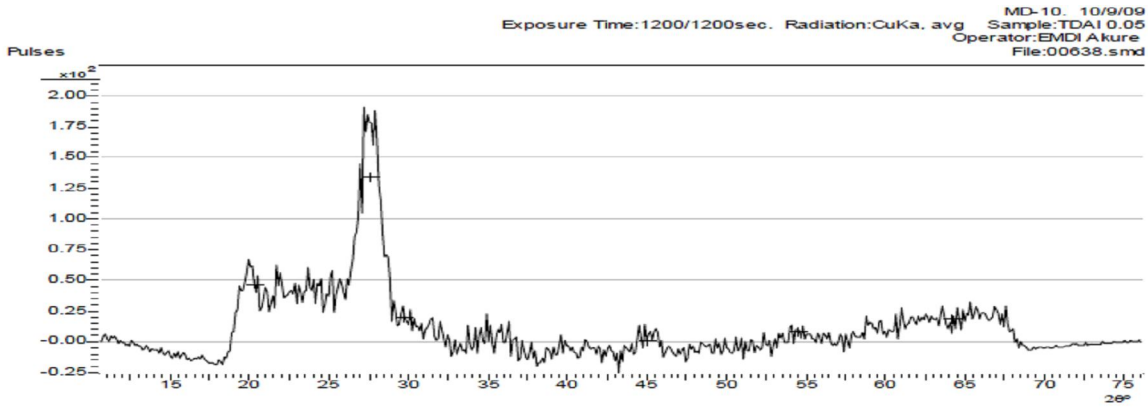


Figure E5: XRD pattern for TDAL0.005

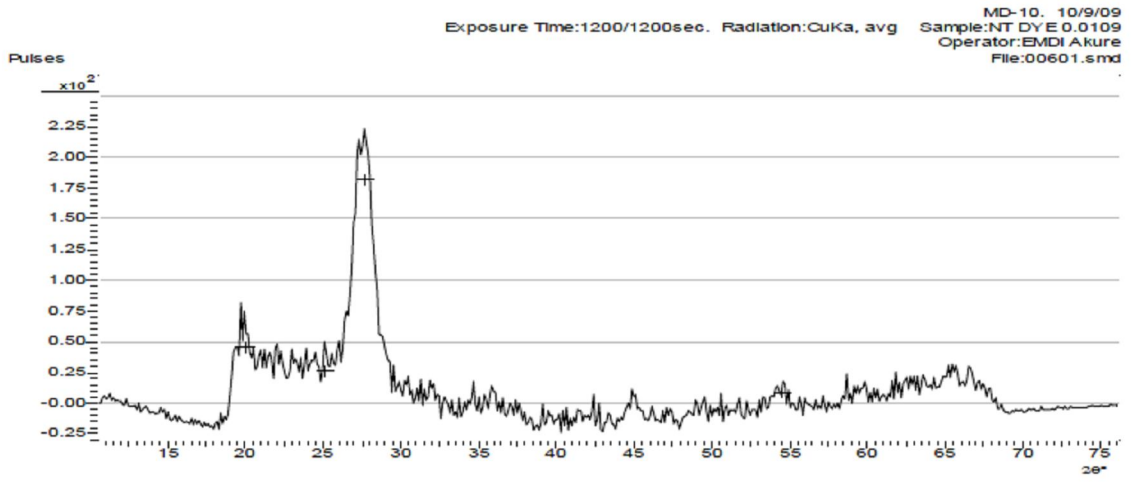


Figure E6: XRD pattern for NTDYE0.0109

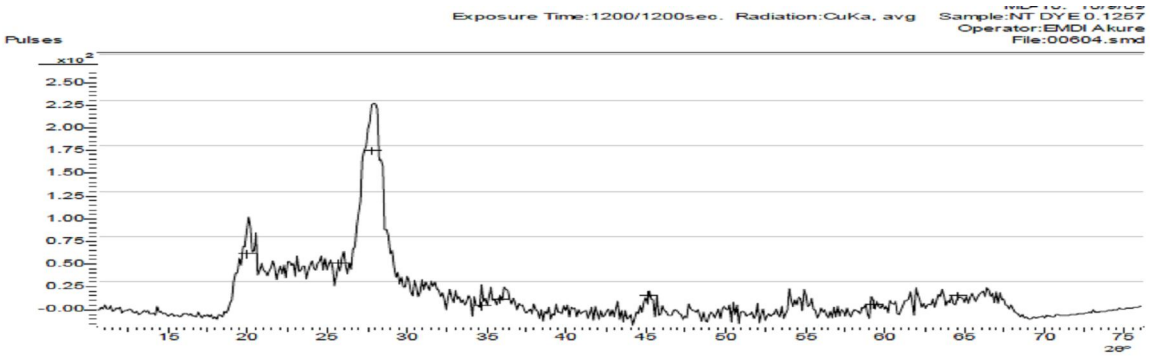


Figure E7: XRD pattern for NTDYE0.1257

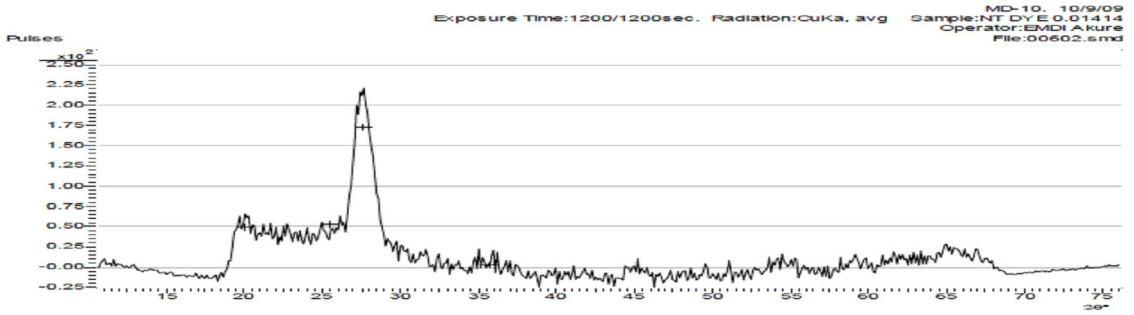


Figure E8: XRD pattern for NTDYE0.01414

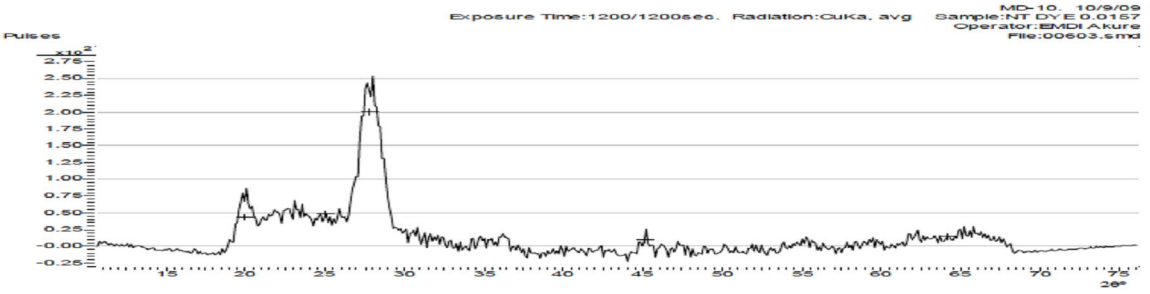


Figure E9: XRD pattern for NTDYE0.0157

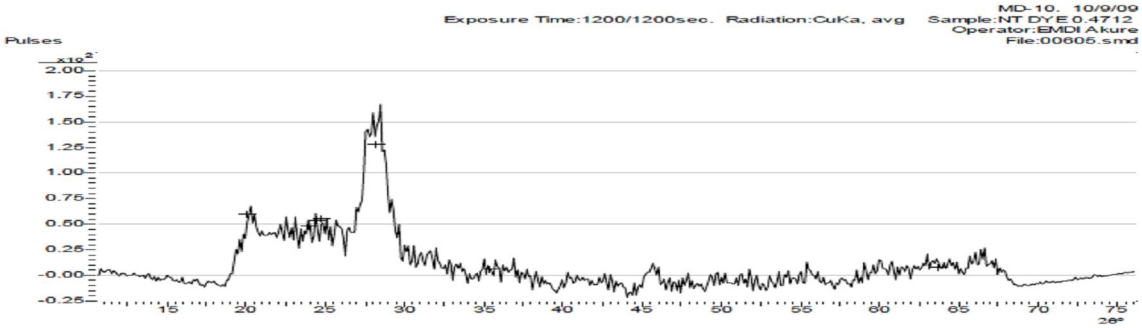


Figure E10: XRD pattern for NTDYE0.4712

APPENDIX G

XRD SPECTRA FOR EFFECT OF pH ON ZEOLITIZATION (CATEGORY II)

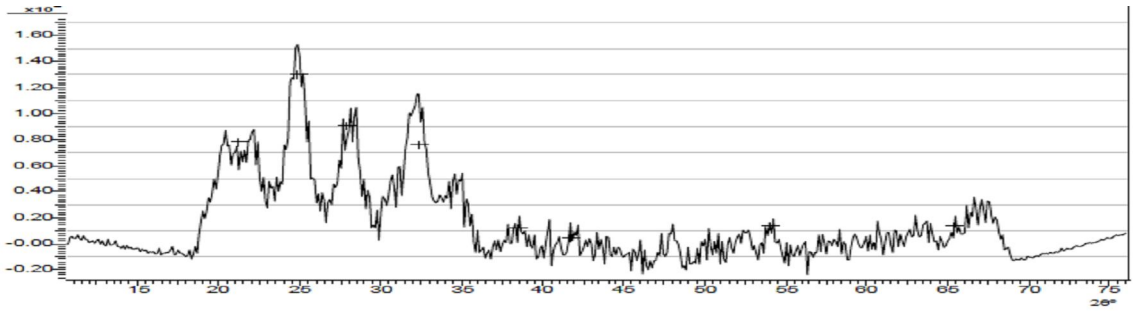


Figure G1: XRD Patterns of Commercial Zeolite Y

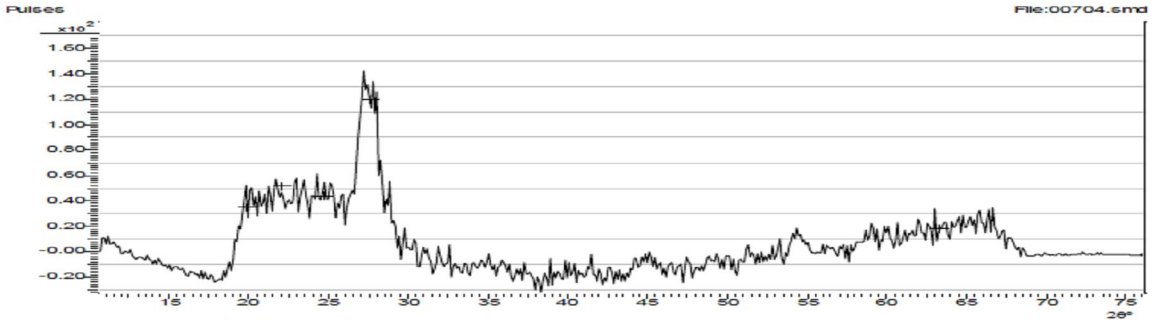


Figure G2: XRD Patterns of Product PHTH 11.03

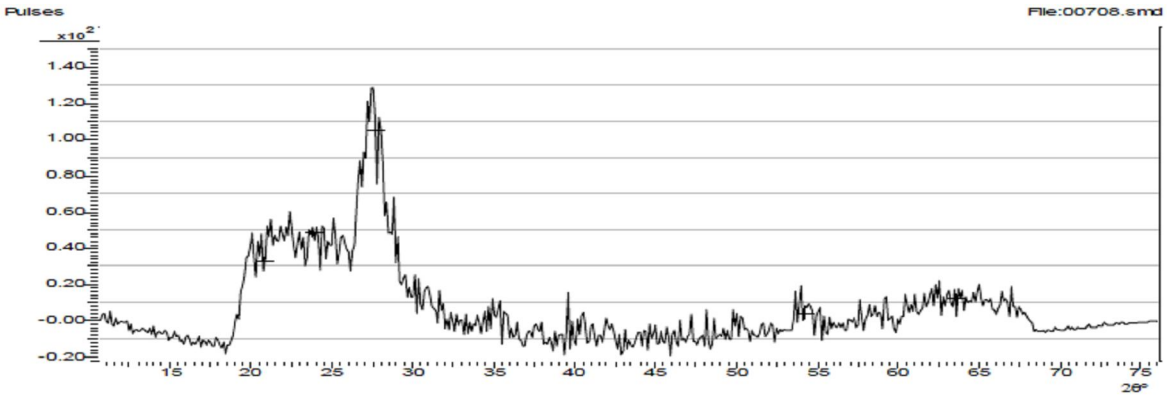


Figure G3: XRD Patterns of Product PHTH 11.54

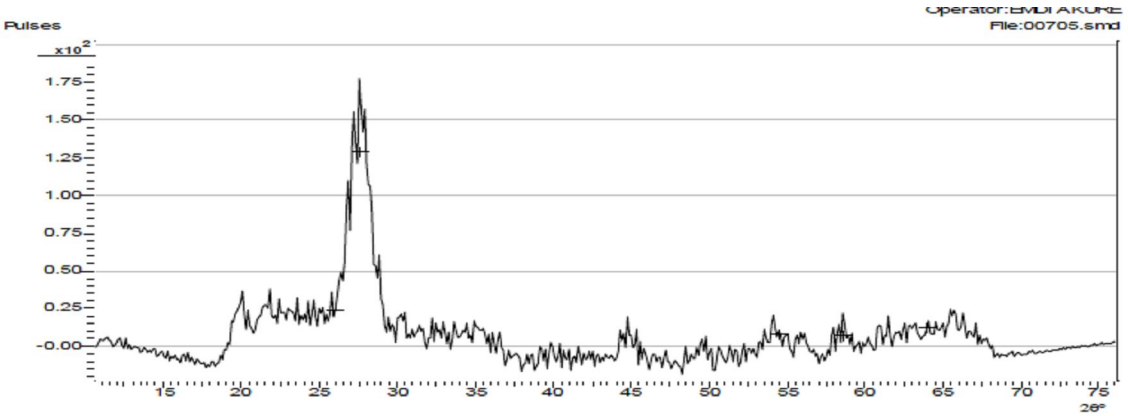


Figure G4: XRD Patterns of Product PHTH 12.23

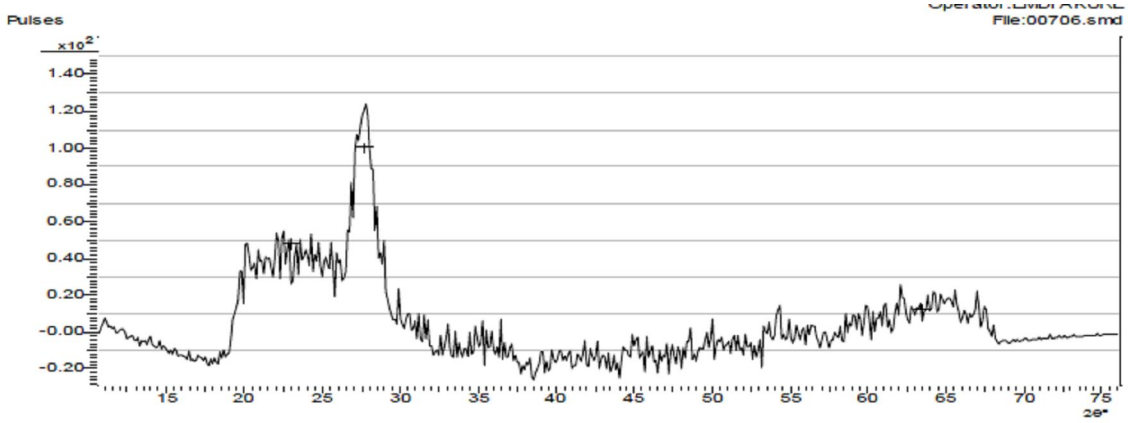


Figure G5: XRD Patterns of Product PHTH 12.89

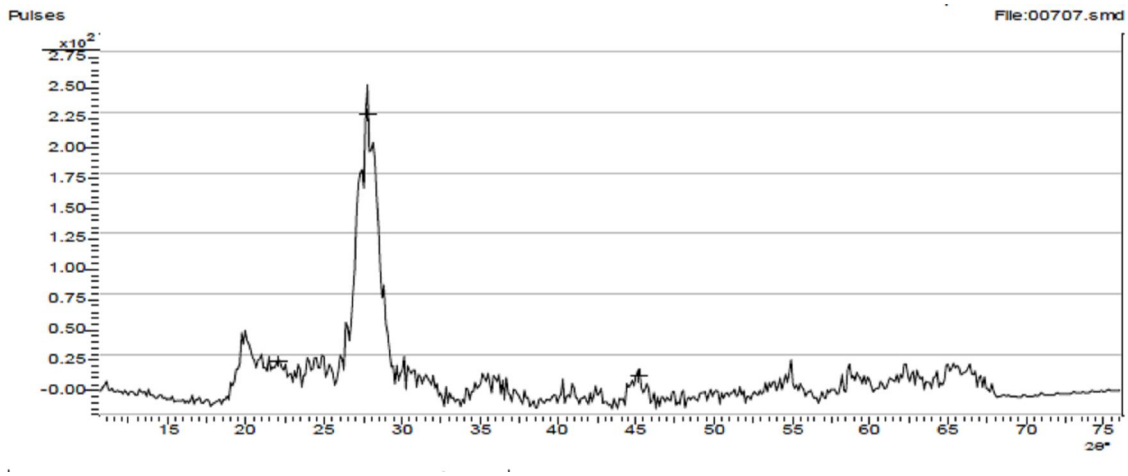


Figure G6: XRD Patterns of Product PHTH 13.10

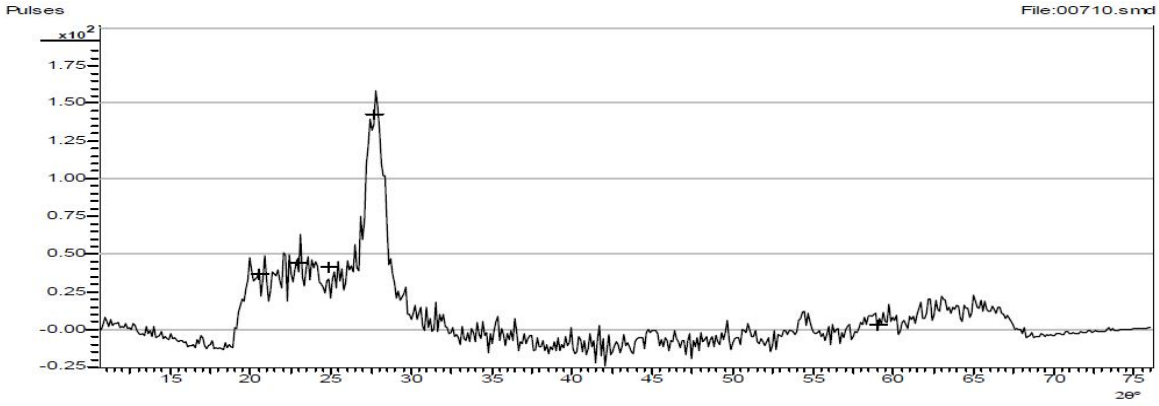


Figure G7: XRD Patterns of Product PHNT 9.97

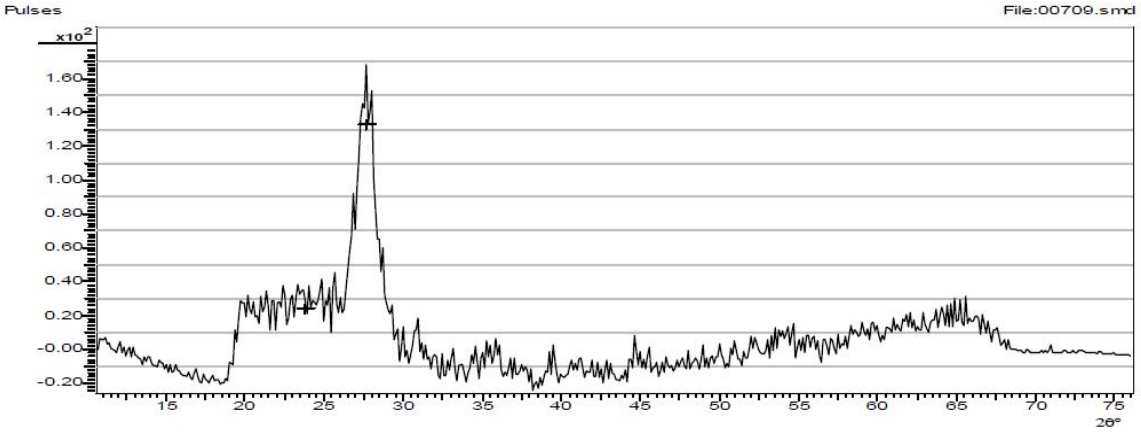


Figure G8: XRD Patterns of Product PHNT 10.57

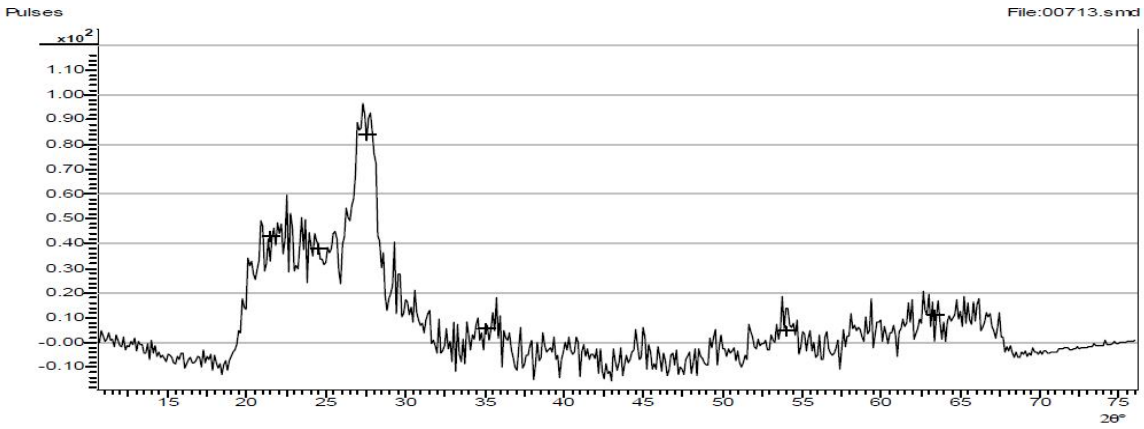


Figure G9: XRD Patterns of Product PHNT 11.03

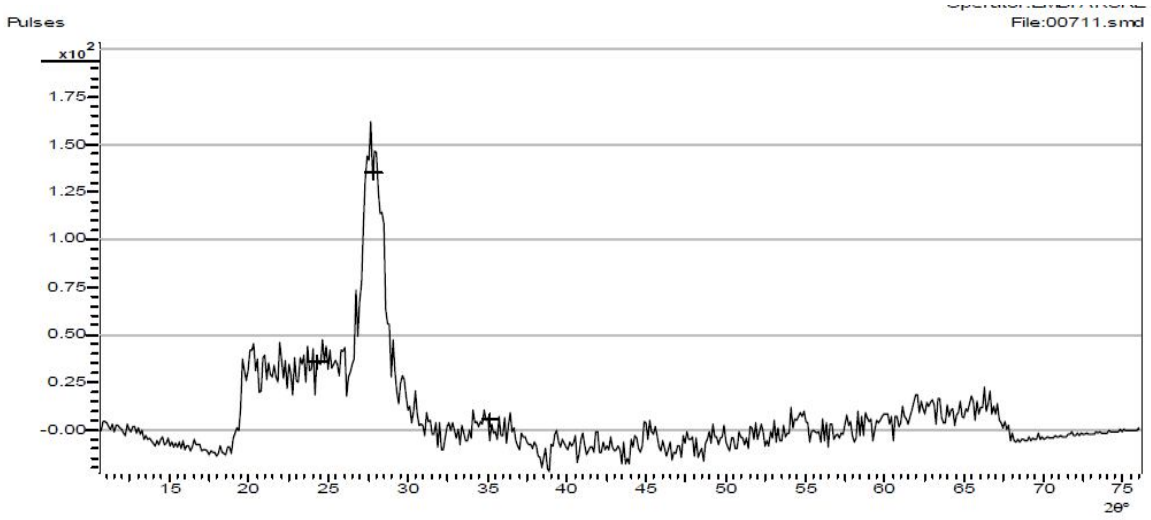


Figure G10: XRD Patterns of Product PHNT 11.58

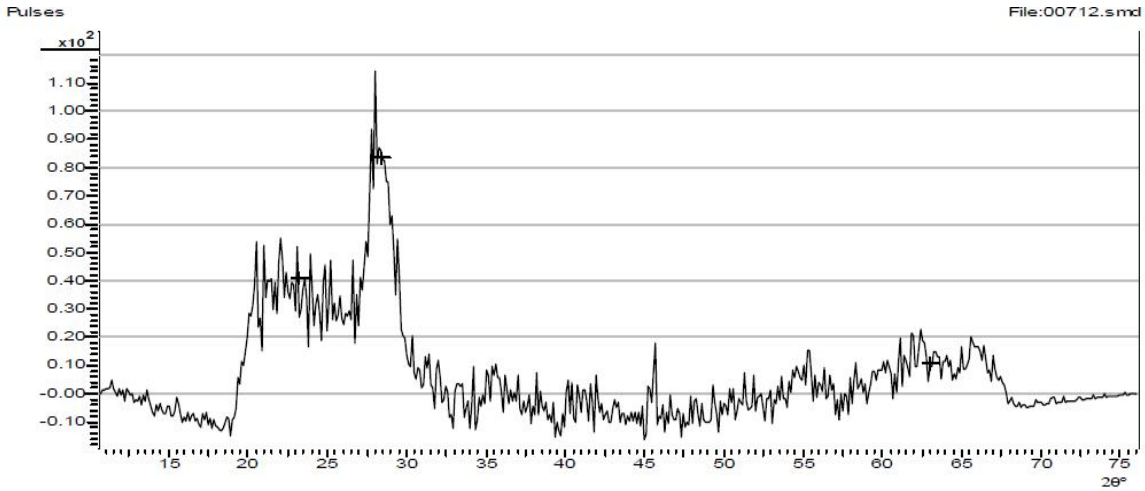


Figure G11: XRD Patterns of Product PHNT 11.98

APPENDIX H

XRD SPECTRA ON CRYSTALLIZATION TIME AND TEMPERATURE (CAT I)

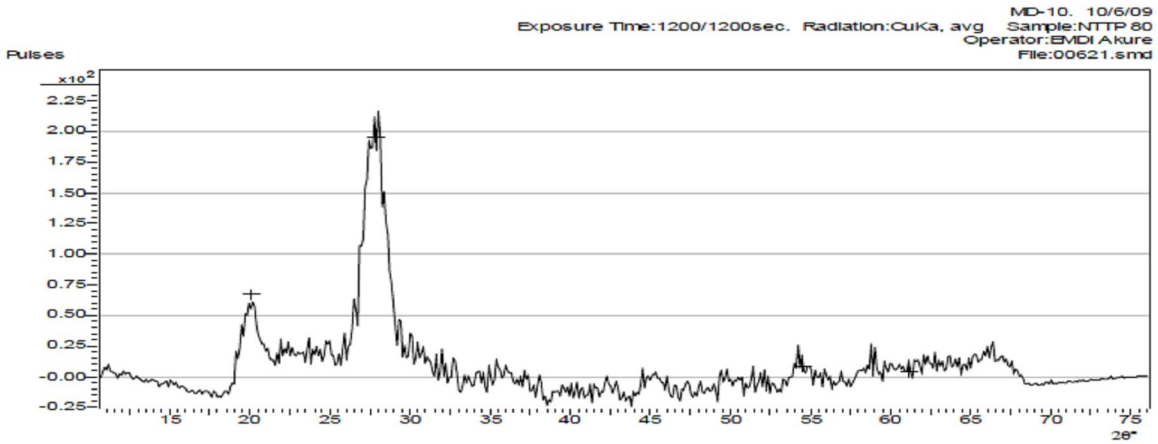


Figure H1: XRD patterns for NTTP80

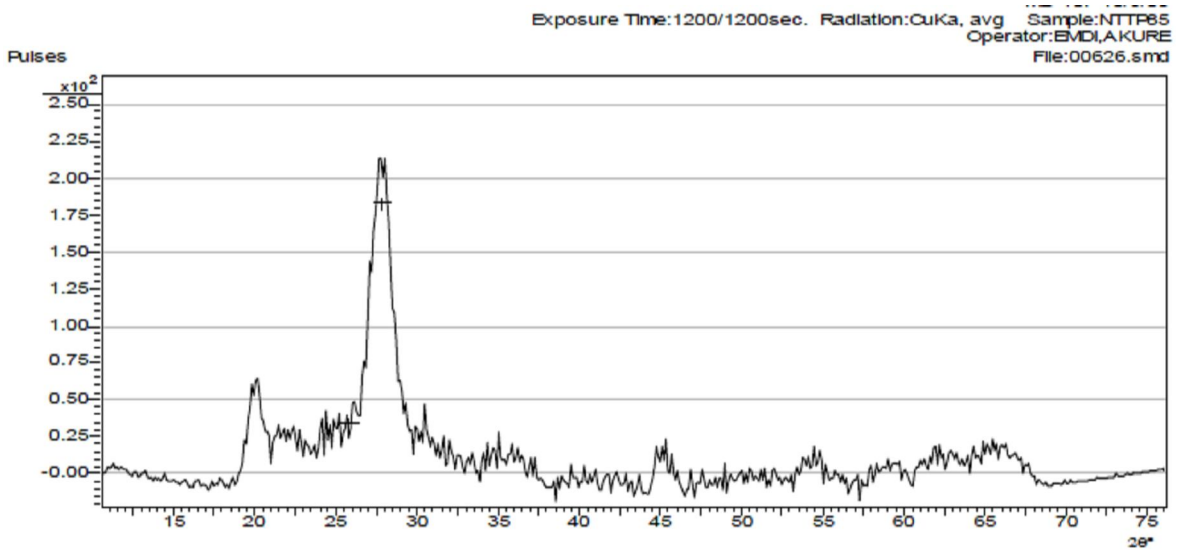


Figure H2: XRD patterns for NTTP85

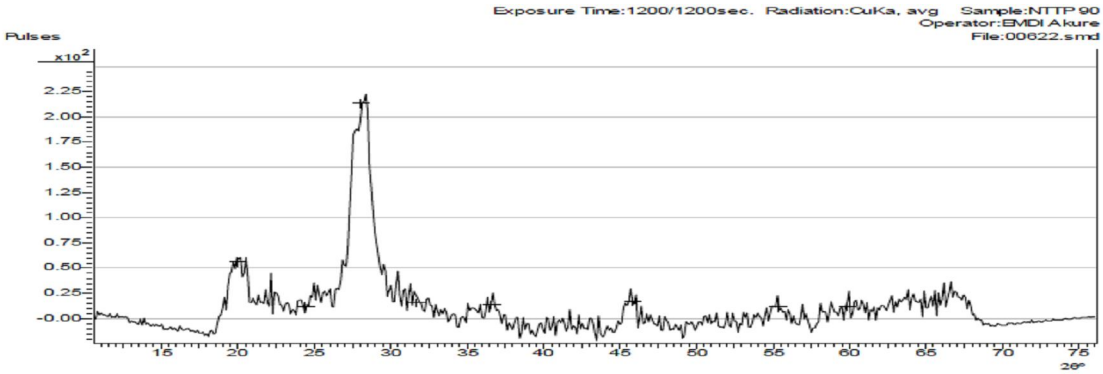


Figure H3: XRD patterns for NTTP90

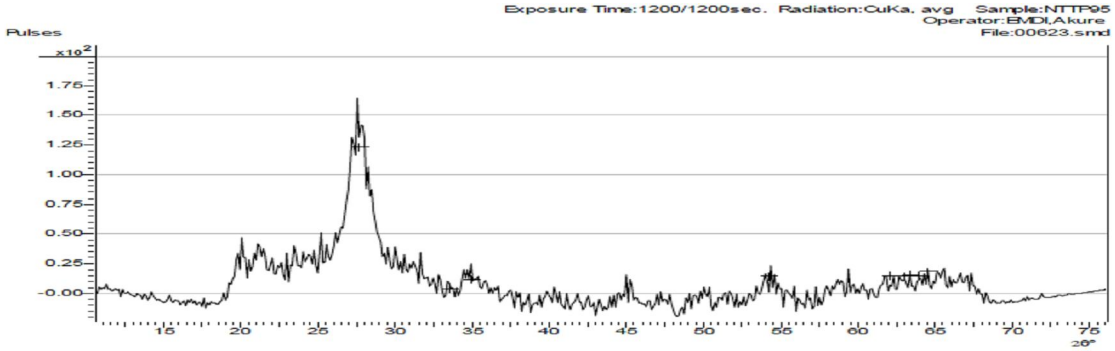


Figure H4: XRD patterns for NTTP95

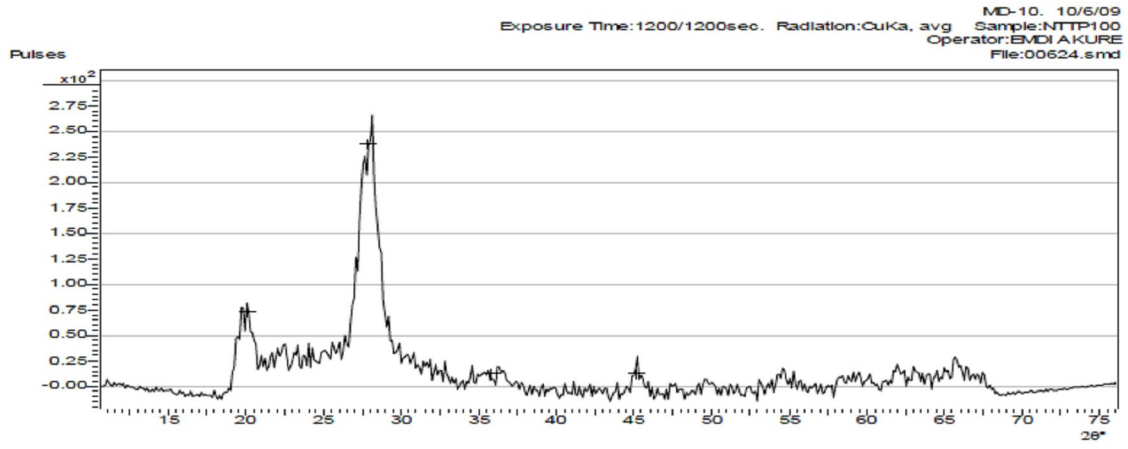


Figure H5: XRD patterns for NTTP100

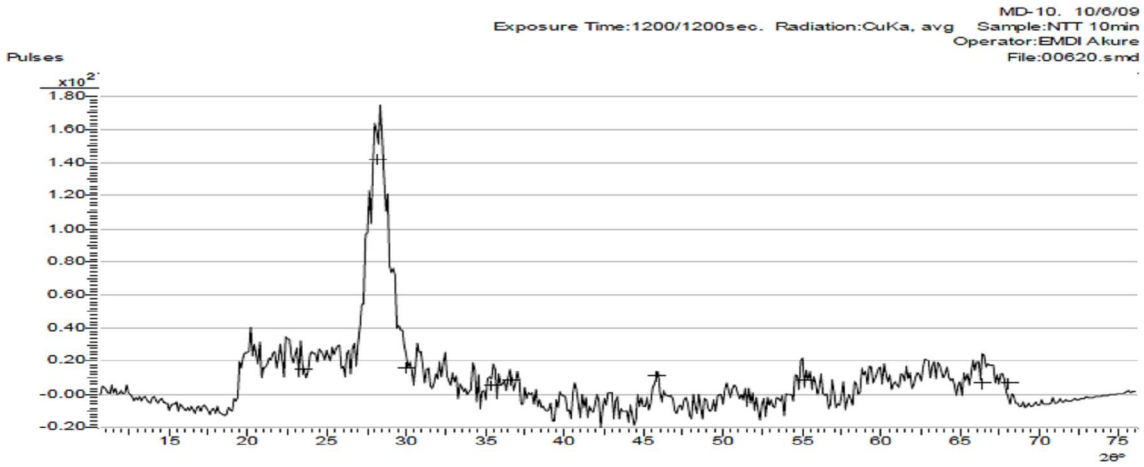


Figure H6: XRD patterns for NTT10

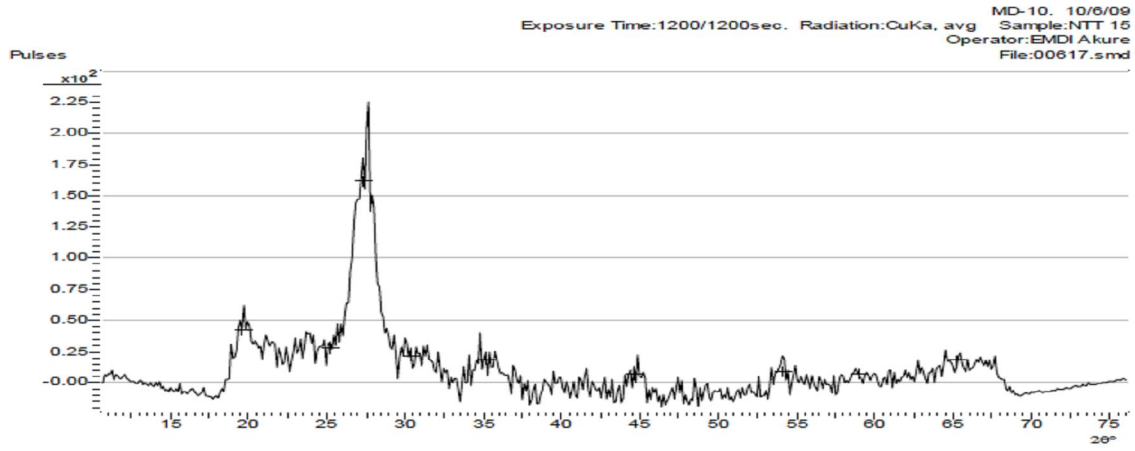


Figure H7: XRD patterns for NTT15

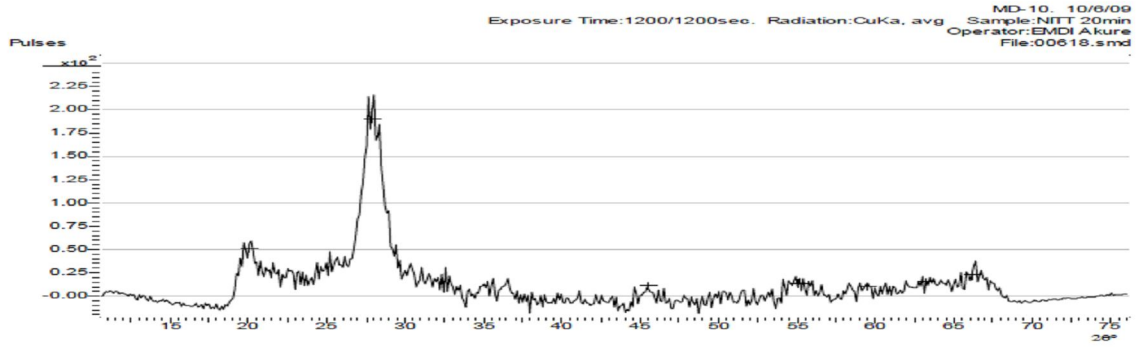


Figure H8: XRD patterns for NTT20

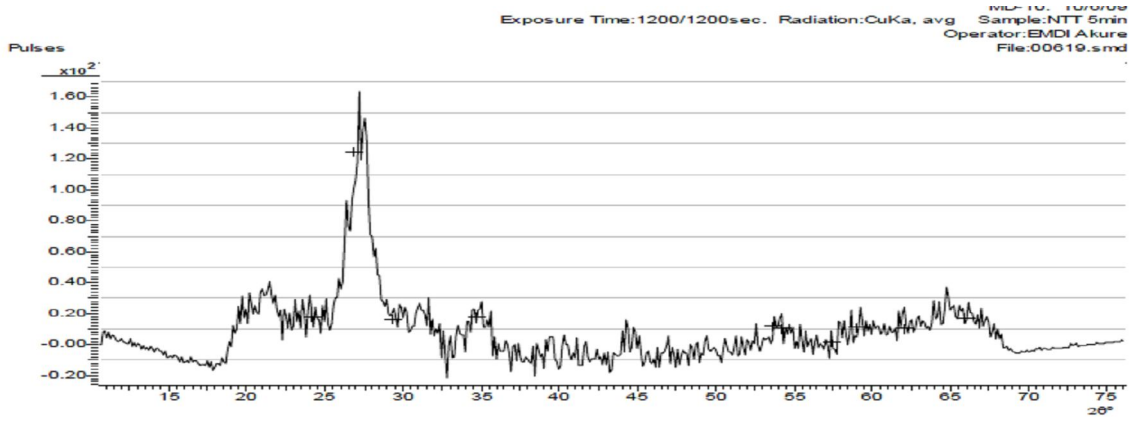


Figure H9: XRD patterns for NTT5

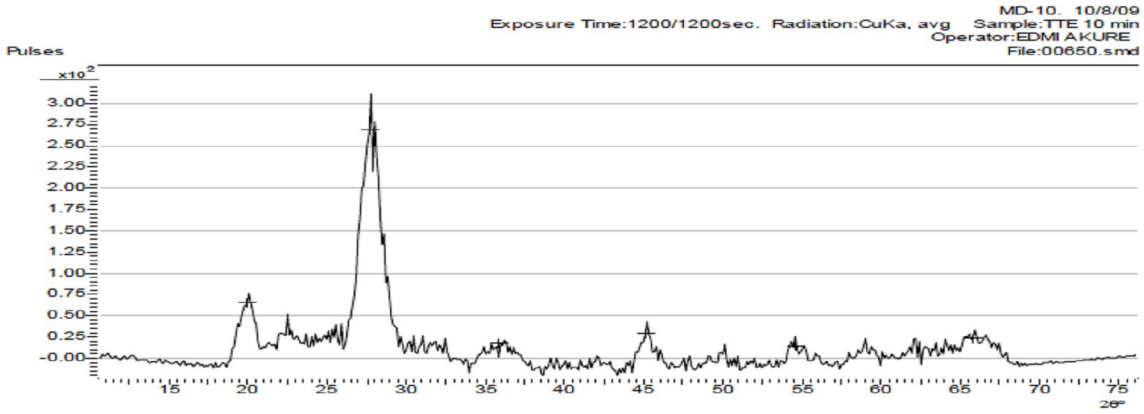


Figure H10: XRD patterns for TTE10

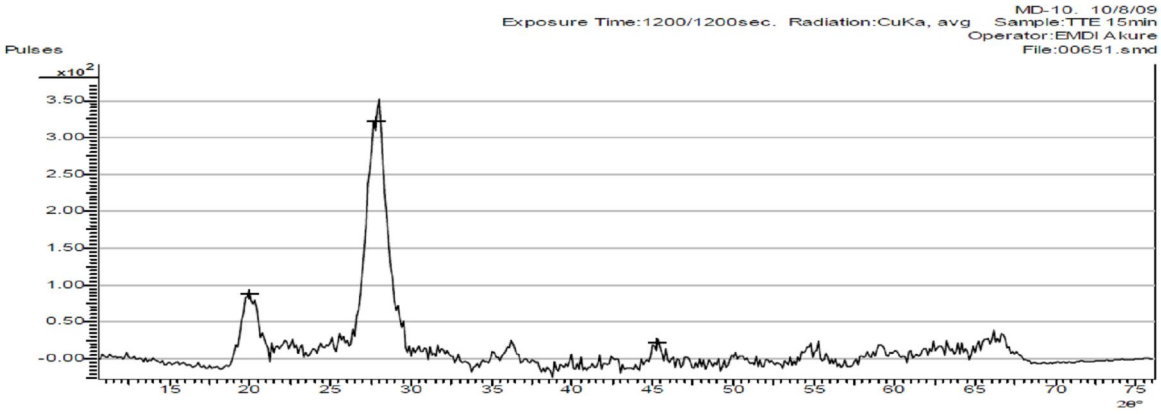


Figure H11: XRD patterns for TTE15

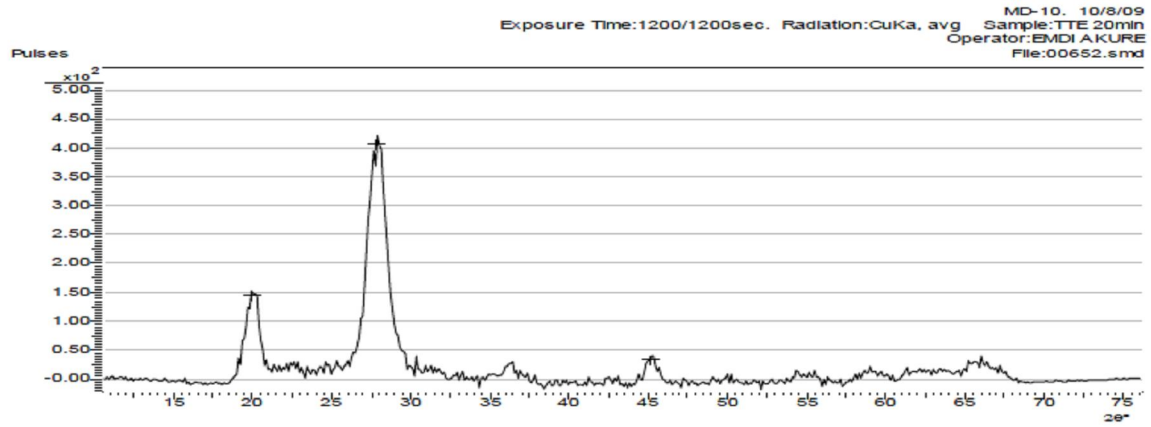


Figure H12: XRD patterns for TTE20

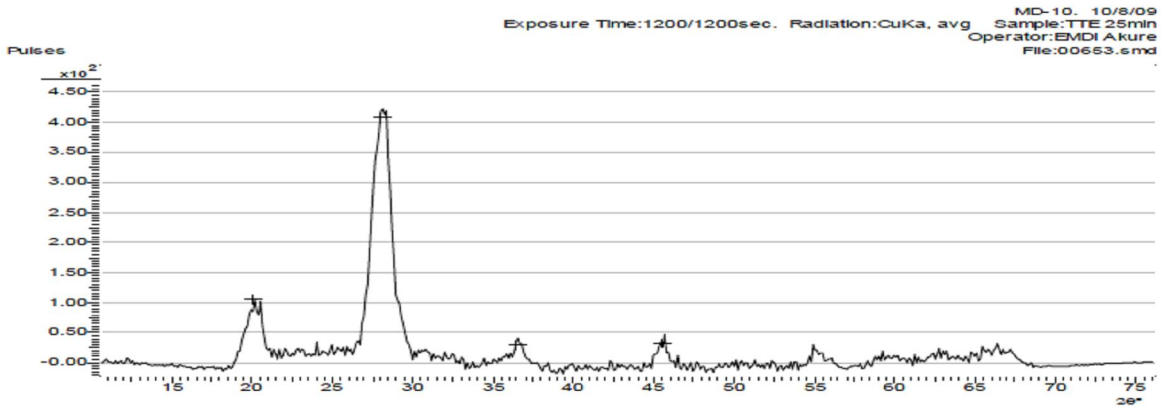


Figure H12: XRD patterns for TTE25

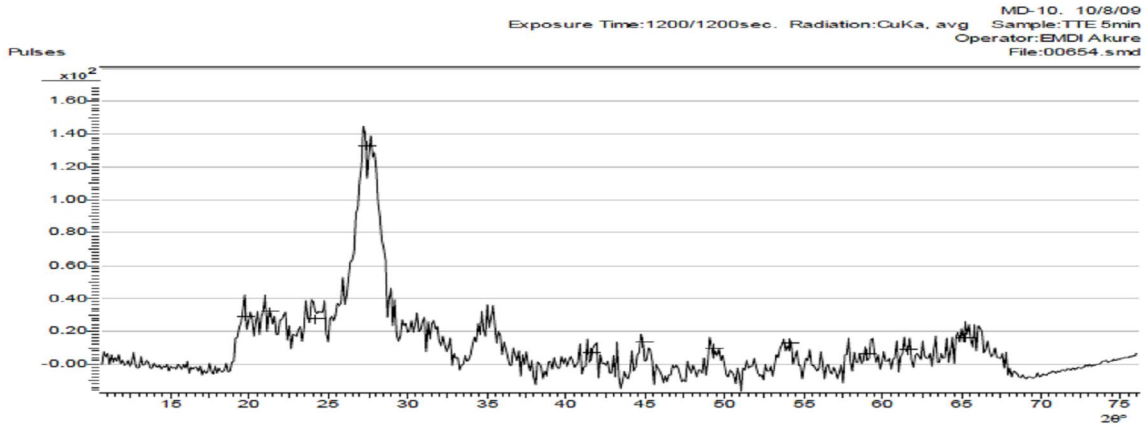


Figure H13: XRD patterns for TTE5

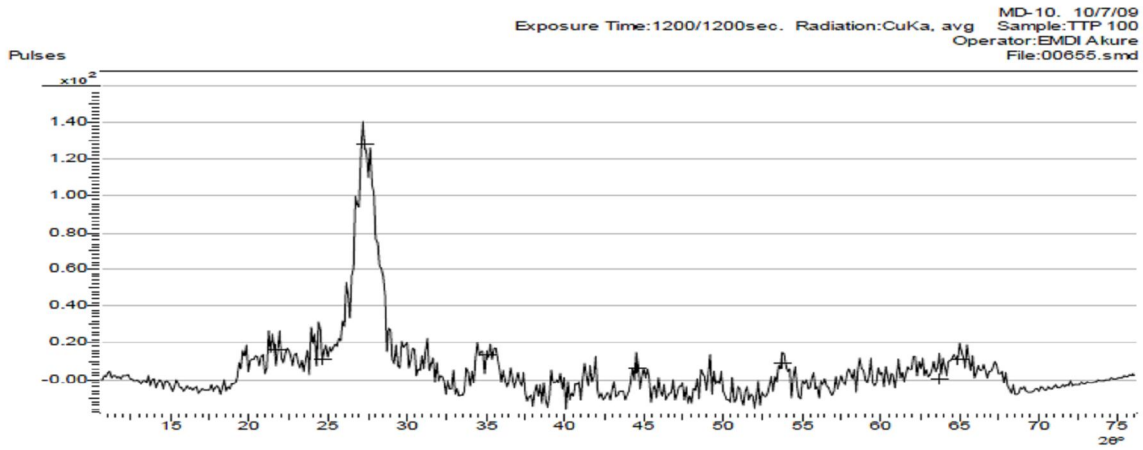


Figure H14: XRD patterns for TTP100

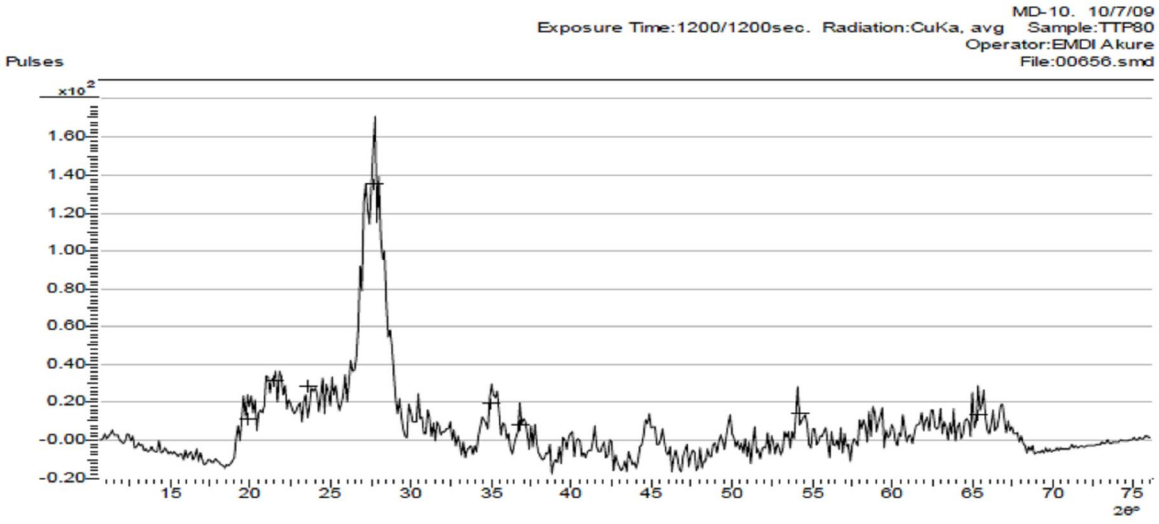


Figure H15: XRD patterns for TTP80

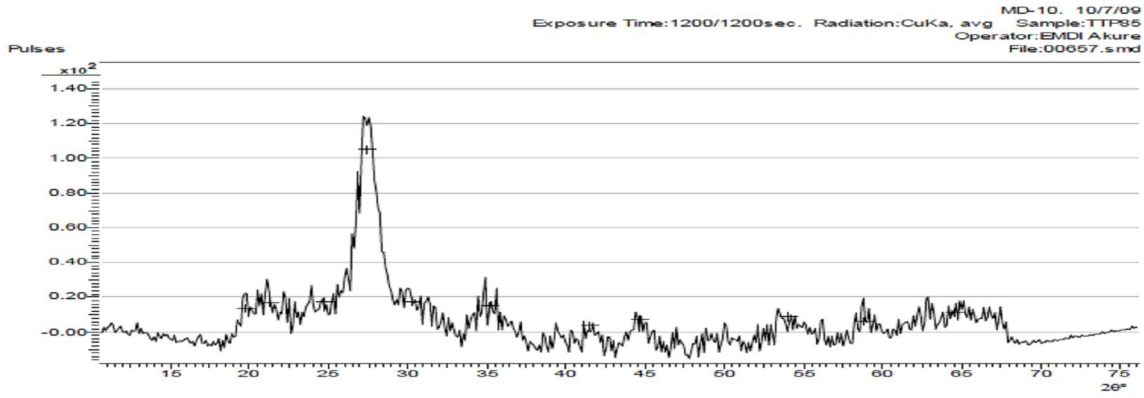


Figure H16: XRD patterns for TTP85

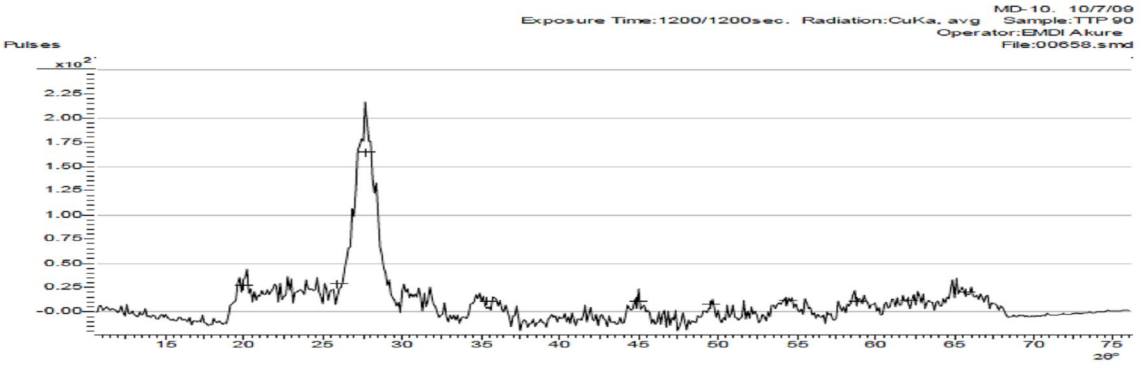


Figure H17: XRD patterns for TTP90

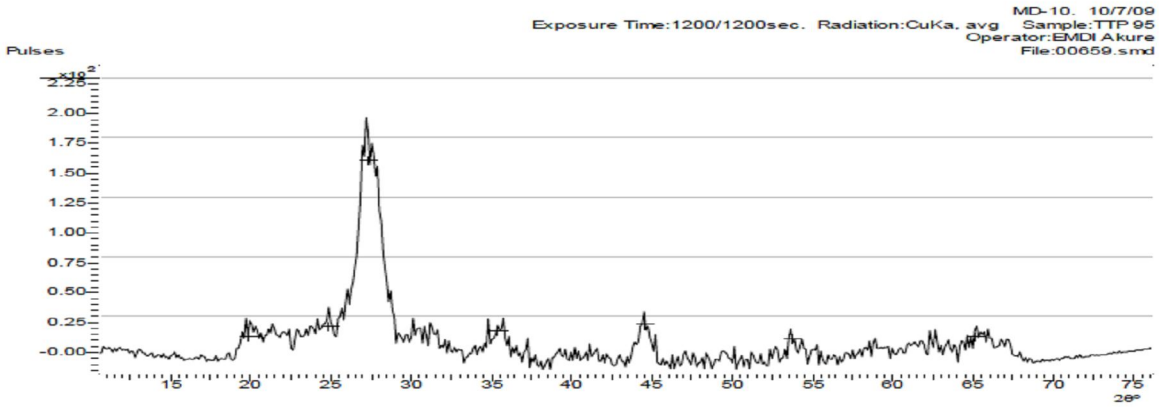


Figure H18: XRD patterns for TTP95